

The meiotic progression of *Arabidopsis thaliana* under elevated temperatures and towards an understanding of translational control in plant meiosis

Joke De Jaeger-Braet

Dissertation with the aim of achieving a doctoral degree
at the Faculty of Mathematics, Informatics and Natural Sciences
Department of Developmental Biology
Universität Hamburg

Hamburg, October 2021

The meiotic progression of *Arabidopsis thaliana* under elevated temperatures and towards an understanding of translational control in plant meiosis

Joke De Jaeger-Braet

Dissertation with the aim of achieving a doctoral degree
at the Faculty of Mathematics, Informatics and Natural Sciences
Department of Developmental Biology
Universität Hamburg

Supervisor: Prof. Dr. Arp Schnittger

Examiners: Prof. Dr. Arp Schnittger

Prof. Dr. Stefan Hoth

Disputation date: January 21st 2022

Hamburg, October 2021

Table of Content

Table of Content	II
List of Figures and Tables	V
List of Abbreviations	VII
List of Publications and Presentations	X
Abstract	XI
Zusammenfassung	XII
INTRODUCTION	1
1. <i>The meiotic division</i>	1
2. <i>The molecular mechanisms behind sister chromatid cohesion, synapsis and recombination</i> ..	3
2.1. Sister chromatid cohesion	3
2.2. Synapsis of the homologs	4
2.3. Meiotic recombination	5
3. <i>The regulation of the meiotic progression by cyclin-CDK complexes</i>	7
4. <i>The male reproductive organs in Arabidopsis thaliana and Zea mays</i>	7
5. <i>My research topics</i>	10
CHAPTER I. Heat stress reveals the existence of a specialized variant of the pachytene checkpoint in meiosis of Arabidopsis thaliana	11
1. INTRODUCTION TO CHAPTER I	12
2. RESULTS	14
2.1. <i>A cytological sensor of heat stress in meiocytes</i>	14
2.2. <i>Heat stress affects microtubule configurations during meiosis in a quantitative but not qualitative manner</i>	17
2.3. <i>Duration of meiosis under heat stress</i>	20
2.4. <i>Duration of individual meiotic phases under heat stress</i>	22
2.5. <i>Exposure to high temperature causes chromosomal defects during meiosis</i>	25
2.6. <i>Synaptonemal complex formation is defective at 34°C</i>	26
2.7. <i>Defects in early prophase I cause an elongation of pachytene/diakinesis</i>	28
2.8. <i>Loss of recombination per se does not cause the elongation of pachytene/diakinesis</i>	29
2.9. <i>Prolongation of MT array state 5-6 is largely recombination-dependent</i>	32
2.10. <i>A specialized pachytene checkpoint in Arabidopsis</i>	34
3. DISCUSSION	36
3.1. <i>Formation of stress granules during meiosis</i>	36
3.2. <i>Heat and meiotic progression</i>	38
3.3. <i>Heat and meiotic recombination</i>	39
3.4. <i>A specialized pachytene checkpoint in Arabidopsis</i>	41
4. MATERIAL AND METHODS	43
4.1. <i>Plant materials and growth conditions</i>	43
4.2. <i>Plasmids and plant transformation</i>	43

4.3.	<i>Confocal microscopy and intensity plots</i>	43
4.4.	<i>Live cell imaging and data processing</i>	44
4.5.	<i>Quantitative analysis of the meiotic phases</i>	44
4.6.	<i>Statistical methods</i>	44
4.7.	<i>Cytology</i>	45
4.8.	<i>Accession numbers</i>	45
5.	SUPPLEMENTAL DATA CHAPTER I	46
	CHAPTER II. The characterization of the translational landscape of Arabidopsis and Maize meiocytes	53
1.	INTRODUCTION TO CHAPTER II	54
1.1.	<i>General overview of eukaryotic translation</i>	54
1.2.	<i>Translation regulation mechanisms</i>	57
1.3.	<i>Translation regulation during meiosis</i>	58
2.	RESULTS	62
2.1.	<i>Ribosome profiling of maize male reproductive organs - a genome wide approach to investigate the meiotic translome</i>	62
2.1.1.	<i>Optimization of the RNA-seq and Ribo-seq from maize male reproductive organs</i> ...	62
2.1.2.	<i>The detection of meiotic genes in the libraries generated from spikelets</i>	65
2.1.3.	<i>Anther collection and meiotic staging</i>	69
2.1.4.	<i>Quality control of the libraries generated from isolated anthers</i>	70
2.1.5.	<i>The expression of meiotic genes during meiosis</i>	73
2.2.	<i>The gene specific approach- A TRICKy system in Arabidopsis</i>	80
2.2.1.	<i>The principle of the MS2-system and TRICK</i>	80
2.2.2.	<i>The mRNA reporters of the MS2-system</i>	84
2.2.3.	<i>The RNA biosensors</i>	90
2.2.4.	<i>The MS2-system in Arabidopsis male meiocytes</i>	92
3.	DISCUSSION	94
3.1.	<i>The identification of maize meiotic orthologs in inbred line A188</i>	94
3.2.	<i>Towards a high-resolution atlas of meiotic translation in maize</i>	95
3.3.	<i>Tapetum-dependent male meiosis</i>	97
3.4.	<i>MS2-system and TRICK, tricky systems to follow translation in Arabidopsis</i>	99
4.	MATERIAL AND METHODS	103
4.1.	<i>Plant materials and growth conditions</i>	103
4.2.	<i>Maize meiocyte staging</i>	103
4.3.	<i>Total RNA and polysome isolation</i>	103
4.4.	<i>Digestion and isolation of RPFs</i>	104
4.5.	<i>Preparation of RPF and total mRNA libraries</i>	104
4.6.	<i>RNA-seq and Ribo-seq data processing</i>	106
4.7.	<i>Genotyping</i>	107
4.8.	<i>Plasmids and plant transformation</i>	107

4.9.	<i>RT-PCR</i>	112
4.10.	<i>Confocal microscopy</i>	113
4.11.	<i>Propidium iodide (PI) staining</i>	113
4.12.	<i>Phenotypic analysis</i>	113
4.13.	<i>Accession numbers</i>	113
5.	SUPPLEMENTAL DATA CHAPTER II	114
	REFERENCES	137
	DECLARATION OF OATH	XIII
	CONFIRMATION OF ENGLISH	XIV
	ACKNOWLEDGMENT	XV

List of Figures and Tables

Figure 1. A general overview of meiosis and its key processes.	2
Figure 2. The localization of male meiocytes in <i>Arabidopsis thaliana</i>	8
Figure 3. The localization of male meiocytes in <i>Zea Mays</i>	9
Figure 1.1. Localization of CDKA;1 in male meiocytes under control and stress conditions.	16
Figure 1.2. Duration of meiotic phases based on MT array states.	18
Figure 1.3. Microtubule array in the wild type in control and heat stress conditions.	20
Table 1.1. Overview of the duration of the meiotic phases based on the MT array states.	23
Figure 1.4. Localization of the synaptonemal complex elements ASY1 and ZYP1b upon heat stress.	27
Figure 1.5. Effect of early and late heat shock on the duration of MT array state 5-6.	29
Figure 1.6. Duration of prophase in the recombination mutants <i>spo11-1</i> , <i>dmc1</i> , <i>msh4</i> and <i>atm</i> at 21°C and HS34°C.	31
Supplemental Figure S1.1. Microtubule array states upon heat stress.	46
Supplemental Figure S1.2. Meiotic defects in the wild type upon heat stress.	47
Supplemental Figure S1.3. Duration of meiotic phases in the recombination mutants <i>spo11-1</i> , <i>dmc1</i> , <i>msh4</i> and <i>atm</i> at 21°C and HS34°C.	48
Supplemental Table S1.1. Detailed overview of the sample sizes.	49
Supplemental Table S1.2. Pairwise comparison of the meiotic phases.	50
Supplemental Table S1.3. Genotyping primers.	51
Figure 2.1. Overview of eukaryotic gene expression.	54
Figure 2.2. Overview of the three phases of eukaryotic translation.	56
Figure 2.3. Optimization of the protocol for RNA-seq and Ribo-seq.	63
Table 2.1. Meiotic genes detected in the total RNA and RPF libraries from spikelets.	67
Figure 2.4. Read coverage of <i>CDKB2;1</i> , <i>TAM</i> , <i>DMC1</i> and <i>SWI1/DYAD</i>	68
Figure 2.5. The developmental gradient of a tassel branch in <i>Zea mays</i>	69
Figure 2.6. Quality control of the libraries from anthers.	71
Figure 2.7. K-means clustering of genes expressed during meiosis.	73
Figure 2.8. Expression plots of genes displaying the same pattern for mRNA and RFP counts during meiosis.	75
Figure 2.9. Expression plots of genes with the highest RPF at leptotene.	76
Figure 2.10. Expression plots of genes displaying a decrease of RNA levels and an increase of RPFs at MII.	78
Figure 2.11. Expression plots of additional genes with potential for translational regulation.	79
Figure 2.12. Scheme of the principle of the MS2-system.	81
Figure 2.13. Scheme of the principle of TRICK.	83
Figure 2.14. The ASY3 mRNA reporters.	85
Figure 2.15. The TAM mRNA reporters.	87
Figure 2.16. The REC8 mRNA reporters.	89

Figure 2.17. The RNA biosensors.....	91
Figure 2.18. The MS2-system in Arabidopsis male meiocytes.....	93
Table 2.2. Primers library generation and amplification.....	105
Table 2.3. PCR-program for library amplification using Pfu DNA polymerase.	105
Table 2.4. PCR-program using Taq and PrimeSTAR MAX DNA polymerase.....	107
Table 2.5. Genotyping primers.....	107
Table 2.6. SLiCE primers.	108
Table 2.7. Colony PCR primers.	110
Table 2.8. Sequencing primers.	111
Table 2.9. RT-PCR primers.....	112
Supplemental Figure S2.1. The TAM reporter.	114
Supplemental Figure S2.2. Quality of the extracted total RNA.....	116
Supplemental Figure S2.3. Optimization of polysome digestion into monosomes.....	117
Supplemental Figure S2.4. Quality of the RNA and RPF libraries of the spikelet test run and first anther replicate.	122
Supplemental Figure S2.5. The quality control of the mRNA and RPF libraries from anthers.....	123
Supplemental Figure S2.6. GO analysis of the clusters for GO category Biological Process (BP)....	124
Supplemental Figure S2.7. GO analysis of the clusters for GO category Cellular Component (CC). 125	
Supplemental Figure S2.8. GO analysis of the clusters for GO category Molecular Function (MF). .126	
Supplemental Table S2.1. Meiotic genes detected in the RNA and RPF libraries of anthers during meiosis.	127
Supplemental Figure S2.9. Quality of the RNA and RPF libraries of the second anther replicate.	135
Supplemental Figure S2.10. Confirmation of MS2-loops in the ASY3 and TAM mRNA reporters.....	136

List of Abbreviations

43S PIC	43S pre-initiation complex
AIC	Akaike Information Criterion
<i>ap1</i>	<i>apetala 1</i>
ASY3/1	ASYNAPTIC 3/1
ATM	ATAXIA TELANGIECTASIA MUTATED
BF	bright field
BiFC	bimolecular fluorescence complementation
BrdU	5'-bromo-2'-deoxyuridine
BRU	BRUNO
<i>BUBR1</i>	<i>BUDDING UNINHIBITED BY BENZYMIDAZOL RELATED 1</i>
<i>cal</i>	<i>cauliflower</i>
CDC28	Cell Division Cycle 28
<i>CDC6</i>	<i>CELL DIVISION CYCLE 6</i>
CDKA;1	CYCLIN DEPENDENT KINASE A;1
CDKs	CYCLIN DEPENDENT KINASES
cDNA	complementary DNA
CDS	coding DNA sequence
CI	confidence interval
<i>CLB3</i>	<i>CYCLIN B3</i>
CO	cross-over
CPE	cytoplasmic polyadenylation element
DAPI	4',6-diamidino-2-phenylindole
DAZL	Deleted in azoospermia-like
DMC1	DISRUPTED MEIOTIC cDNA1
DSB	double stranded break
<i>eat1</i>	<i>eternal tapetum1</i>
eIFs	eukaryotic initiation factor complexes
eRFs	eukaryotic release factors
ESP	SEPARASE
FEST	WURSTFEST
Gbp	giga base pairs
gDNA	genomic DNA
<i>GEN2</i>	<i>XPG-LIKE ENDONUCLEASE 2</i>
GFP	green fluorescent protein
GO	Gene Ontology
<i>GR</i>	<i>GLUCOCORTICOID RECEPTOR</i>
HR	homologous recombination
HS	heat shock
IME1/2	INDUCER OF MEIOSIS 1/2
IRES	internal ribosomal entry sites
<i>JAS</i>	<i>JASON</i>
LEP	leptotene
LT	long-term
Mbp	million base pairs
MCP	MS2-coat protein
MII	diakinesis to tetrad formation
MIP6	MEX67-INTERACTING PROTEIN 6
miRNA	microRNAs
<i>ML1/4</i>	<i>MEI2-LIKE 1/4</i>

mORF	main open reading frame
MPK3	MITOGEN ACTIVATED PROTEIN KINASE 3
MRE11	MEIOTIC RECOMBINANT 11
mRNA	messenger RNA
MS	Murashige and Skoog
<i>MS44</i>	<i>MALE STERILE44</i>
MSH4	MUTS HOMOLOG 4
MT	microtubule
MUS81	MMS AND UV SENSITIVE 81
NBS1	NIJMEGEN BREAKAGE SYNDROME 1
NCOs	non-crossovers
ncRNAs	noncoding RNAs
<i>NDC80</i>	<i>NUCLEAR DIVISION CYCLE 80</i>
NDT80	NON-DITYROSINE 80
NEB	nuclear envelope breakdown
NLS	nuclear localization signal
PABP	poly(A)-binding proteins
PACH	pachytene
PBs	processing bodies
PCA	principal component analysis
PCH2	Pachytene checkpoint protein homolog 2
PCP	PP7 bacteriophage coat proteins
PES4	POLYMERASE EPSILON SUPPRESSOR 4
<i>PGK1</i>	<i>PHOSPHOGLYCERATE KINASE 1</i>
phasiRNAs	phased secondary small interfering RNA
<i>PHYC</i>	<i>PHYTOCHROME C</i>
PI	propidium iodide
PMCs	pollen mother cells
PP2A	Protein phosphatase 2A
PRE	premeiosis
<i>PSY</i>	<i>PHYTOENE SYNTHASE</i>
<i>ptc1</i>	<i>persistent tapetal cell 1</i>
<i>PTD</i>	<i>PARTING DANCERS</i>
pUBQ10	Promoter UBIQUITIN 10
<i>PUM</i>	<i>PUMILIO 1</i>
QC	quality control
qRT-PCR	quantitative RT-PCR
RAD50	RADIATION 50
RBP	RNA binding proteins
REC8	RECOMBINANT PROTEIN 8
RFP	red fluorescent protein
RIM4	REGULATOR OF INDUCER OF MEIOSIS 2 (IME2) 4
RIN	RNA Integrity Number
RNase	ribonuclease
RPFs	ribosome protected fragments
RPKM	reads per kilobase of transcript, per million mapped reads
RPs	ribosomal proteins
rRNA	ribosomal RNA
SAC	spindle assembly checkpoint
SC	synaptonemal complex
SCC3	SISTER CHROMATID COHESION 3
<i>sds</i>	<i>solo dancers</i>

SG	stress granules
SGO1	SHUGOSHIN 1
siRNAs	small interfering RNAs
<i>SKS14</i>	<i>SKU5 SIMILAR 14</i>
<i>SLD2</i>	<i>SYNTHETICALLY LETHAL WITH DPB11-1 2</i>
SMC1	STRUCTURAL MAINTENANCE 1/3
smFISH	single molecule fluorescence in situ hybridisation
SPO11-1	SPORULATION 11-1
<i>SPS1/2</i>	<i>SPORULATION SPECIFIC 1/2</i>
<i>SSP2</i>	<i>SPORULATION SPECIFIC 2</i>
<i>SWI1</i>	<i>SWITCH 1</i>
TAIR	The Arabidopsis Information Resource
TAM	TARDY ASYNCHRONOUS MEIOSIS
<i>tdr</i>	<i>tapetum degeneration retardation</i>
TE	translation efficiency
TF	transcription factor
TORC1	TARGET OF RAPAMYCIN COMPLEX 1
TRICK	Translating RNA Imaging by Coat Protein Knock-off
Trip13	Thyroid Hormone Receptor Interactor 13
tRNAs	transfer RNAs
TSS	transcription start site
TTS	transcription termination site
TUA5	TUBULIN ALPHA-5
uORF	Upstream open reading frame
UTR	untranslated region
WAPL	WINGS APART-LIKE
WHI8	WHISKEY 8
ZMM	acronym from <i>Saccharomyces cerevisiae</i> Zip, Mer and Msh
ZYG	zygotene
ZYP1	ZIPPER 1

List of Publications and Presentations

Publications

- (accepted, The Plant Cell) **Heat stress reveals the existence of a specialized variant of the pachytene checkpoint in meiosis of *Arabidopsis thaliana*.** Joke De Jaeger-Braet, Linda Krause, Anika Buchholz and Arp Schnittger
- (under revision, The Plant Journal) **Knock-down of gene expression throughout meiosis and pollen formation by virus-induced gene silencing in *Arabidopsis thaliana*.** Vanesa Calvo-Baltanás, Joke De Jaeger-Braet, Wei Yuan Cher, Nils Schönbeck, Eunyoung Chae, Arp Schnittger and Erik Wijnker

Poster presentations

- Annual Maize Genetics Conference, Saint-Louis (USA), 2017 - **Analysis of meiosis in maize**
- European Maize Meeting, Ghent (BELGIUM), 2017 - **Analysis of meiosis in maize**
- Biology Conference of Doctoral Candidates, Hamburg (GERMANY), 2017 - **Analysis of meiosis in maize**
- EMBO Conference Protein Synthesis and Translation Control, Heidelberg (GERMANY), 2017 - **Identification of the translational landscape of *Arabidopsis* and Maize meiocytes**
- Annual Maize Genetics Conference, Saint-Malo (FRANCE), 2018 - **Identification of the translational landscape of *Arabidopsis* and Maize meiocytes**
- International Conference on Arabidopsis Research, Wuhan (CHINA), 2019 - **Challenges of imaging translational control during meiosis**

Oral presentations

- SPP 1935 Meeting, Mainz (GERMANY), 2017 - **Deciphering the translational landscape of *Arabidopsis* and maize meiocytes**
- MOLBAR Workshop, Digital (ONLINE), 2020 - **Meiotic progression under elevated temperatures reveals to be recombination dependent in *Arabidopsis thaliana***

Abstract

Plant growth and fertility strongly depend on environmental conditions and previous work has demonstrated that meiosis is highly sensitive to temperature changes. To counteract the detrimental effects of high temperatures and adjust breeding programs, it is vital to comprehend the changes imposed by heat stress on yield-related traits at a cellular and molecular level. Thus, to better understand the impact of temperature on meiosis, I followed male meiocytes in *Arabidopsis thaliana* under three different temperature conditions using live cell imaging. This work led to a cytological framework of meiotic progression at elevated temperatures. A sudden increase to 34°C leads to a faster overall progression of meiosis compared to 21°C. However, the phase in which cross-overs mature is prolonged at 34°C and I could further show that this delay is recombination-dependent, since mutants in genes involved in meiotic recombination proceed faster through this phase at 34°C than wild type. Further analysis revealed that the DNA damage sensor kinase ATM is also involved in this heat stress induced prolongation, indicating the existence of a previously unrecognised pachytene checkpoint in plants.

Recent studies in yeast revealed that translational regulation is crucial in the control of protein abundance during meiosis. However, little is known about meiotic gene regulation at translational level in plants. To bridge this gap, I aimed at revealing evidence for meiotic translational control in dicotyledonous and monocotyledonous species, *Arabidopsis thaliana* and *Zea mays*, respectively. To this end, transcriptome and translome analysis using isolated maize reproductive organs, *i.e.* spikelets and anthers, were conducted. This resulted in the establishment of a functional protocol to perform RNA-sequencing and ribosome profiling from these tissues and led to the discovery that whole anthers have distinct transcriptomes and translomes at defined meiotic time points. Preliminary results of the first sequencing analysis suggest that several meiotic genes undergo translational regulation, as their mRNA levels and translation profiles significantly differ. In addition, to visualize temporal differences between the onset of transcription and translation at a cellular level in *Arabidopsis thaliana*, the meiotic genes *ASY3*, *TAM* and *REC8* were analyzed using fluorescent mRNA and protein reporter based systems, *i.e.* MS2-system and TRICK. While these methods have been used in several species, they appear to be challenging for studying translational regulation during meiosis in *Arabidopsis thaliana*. However, a careful analysis of the encountered problems was carried out, which facilitates how and where this strategy can be used for future research.

Zusammenfassung

Das Wachstum sowie die Fertilität von Pflanzen hängt von äußeren Einflüssen ab. So haben vorangegangene Studien gezeigt, dass beispielsweise die Meiose sensitiv gegenüber Temperaturänderungen ist. Um schädlichen Effekten durch zu hohe Temperaturen entgegenzuwirken und ggf. Züchtungs-Programme anzupassen, ist es essentiell durch Hitzestress verursachte Veränderungen, die den Ertrag beeinflussen auf Zellulärer sowie molekularer Ebene zu verstehen. Aus diesem Grund habe ich den Ablauf der Meiose in lebenden männlichen Meiozyten in *Arabidopsis thaliana* bei drei verschiedenen Temperaturbedingungen mittels konfokaler Mikroskopie analysiert. Im Zuge dieser Arbeit konnte ein zytologisches Modell erarbeitet werden, das den Ablauf der Meiose bei erhöhten Temperaturen beschreibt. So induziert ein plötzlicher Temperaturanstieg auf 34 °C ein generell schnelleres Fortschreiten der Meiose als bei 21 °C. Allerdings ist die Phase, in der sich Crossover entwickeln bei 34 °C signifikant verlängert und ich konnte durch die Analyse von Rekombinationsmutanten zeigen, dass diese Verlängerung rekombinationsabhängig ist, da die Mutanten die Phase bei 34°C schneller durchlaufen als der Wildtyp. Weitere Analysen ergaben, dass die DNA-Schaden Sensor Kinase ATM in diesem Prozess involviert ist und somit ein bis dahin unentdeckter „Pachytene Checkpoint“ in Pflanzen existent sein könnte.

Kürzlich konnte in Hefen gezeigt werden, dass die Translationsregulation essentiell für die Proteinmenge während der Meiose ist. Allerdings ist über die Regulation der Translation während der pflanzlichen Meiose nur wenig bekannt. Um diese Wissenslücke zu schließen, habe ich untersucht, ob meiotische Gene auch in dikotylen und monokotylen Pflanzen (z.B. in *Arabidopsis thaliana* und *Zea mays*) auf translationaler Ebene reguliert werden. In diesem Zusammenhang habe ich Transkriptions- und Translationsanalysen von Ährchen und Antheren von Maispflanzen durchgeführt und ein robustes Protokoll etabliert, das die Analyse der Gesamt-RNA sowie ein Ribosome-Profiling dieser Gewebe erlaubt. Die Ergebnisse meiner Experimente haben zu der Erkenntnis geführt, dass Antheren zu verschiedenen meiotischen Zeitpunkten deutlich unterschiedliche Transkriptome und Translatome aufweisen. Erste Auswertungen der RNA Sequenzierungen und des ribosomalen Profiling deuten außerdem daraufhin, dass auch pflanzliche meiotische Gene auf der Ebene der Translation reguliert werden, da ihr mRNA Level und ihr Translationsprofil signifikant unterschiedlich sind. Zusätzlich zu den Maisexperimenten sollten eventuelle zeitliche Unterschiede zwischen Transkription und Translation der Gene *ASY3*, *TAM* und *REC8* auf zellulärer Ebene in *Arabidopsis thaliana* visualisiert werden. Hierfür habe ich die Systeme MS2 und TRICK getestet, die auf Fluoreszenzreportern zum Nachweis spezifischer mRNAs und Proteine basieren. Obwohl diese Systeme bereits erfolgreich in anderen Organismen verwendet werden, zeigten sich beide Ansätze als wenig geeignet für die Untersuchung der Translationsregulation während der Meiose in *Arabidopsis thaliana*. Allerdings kann die hier durchgeführte sorgfältige Analyse der

aufgetretenen Probleme helfen zu entscheiden, wie und wo diese Systeme dennoch für bestimmte Forschungsfragen eingesetzt werden könnten.

INTRODUCTION

1. The meiotic division

Meiosis is a specialized cell division during which DNA replication is followed by two rounds of chromosome segregation (meiosis I and meiosis II), resulting in the reduction of the DNA content by half as a prerequisite for a subsequent fusion between gametes and restoration of the full genome size. Furthermore, meiosis I plays an important role for the generation of genetic diversity via a process called recombination, through cross-over (CO) formation during prophase I and the resulting new assortment of chromosome sets. COs are not only important for the generation of new allelic combinations but also ensure physical connections between homologous chromosomes (homologs) that are needed for their balanced segregation (Harrison et al., 2010; Hillers et al., 2017; Ma, 2006; Mercier et al., 2015).

Meiosis I and meiosis II can be further subdivided into several stages, which can be characterized by chromosome appearance, e.g. chromosome pairing, condensation and segregation. After DNA replication, cells enter meiosis in prophase I, during which several important meiotic events take place, *i.e.* chromosome pairing and meiotic recombination. Prophase I can be further subdivided into five phases: leptotene, zygotene, pachytene, diplotene and diakinesis (Ma, 2006).

During leptotene, chromosomes start to condense, visible as thin thread-like structures, and recombination is initiated by the formation of double stranded breaks (DSBs) (**Figure 1A**). As chromosome condensation continues, cells enter zygotene (**Figure 1B**). Homologs start to pair, which coincides with synapsis via the formation of the synaptonemal complex (SC) (Capilla-Perez et al., 2021; Higgins et al., 2005). The partially synapsed chromosomes can be visualized as thicker thread-like stretches, as they become tightly connected. During pachytene, chromosomes are visible as thick thread-like structures, as they reach a fully synapsed state with the homologs fully connected via the SC (**Figure 1C**). The SC then disassembles and chromosomes decondense during diplotene. A subsequent recondensation results in the formation of highly condensed and paired chromosomes in diakinesis (**Figure 1D**). In addition, as COs have been formed, with a minimum of one CO per pair of

homologs required, they become now visible as chiasmata, resulting in structures which are called bivalents.

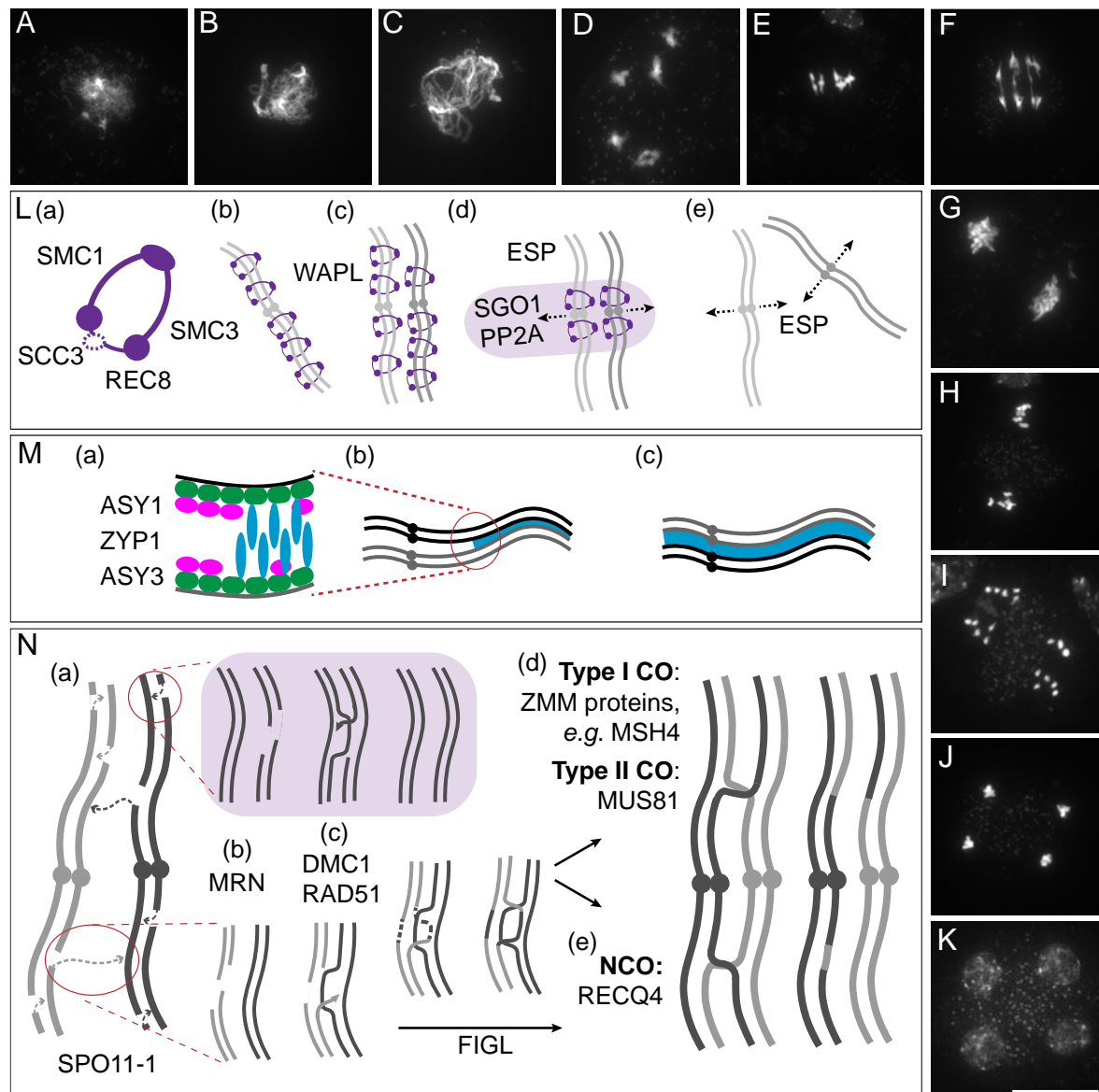


Figure 1. A general overview of meiosis and its key processes.

Chromosome spreads of *Arabidopsis* male meiocytes: (A) leptotene, (B) zygotene, (C) pachytene, (D) diakinesis, (E) metaphase I, (F) anaphase I, (G) telophase I, (H) metaphase II, (I) anaphase II, (J) telophase II and (K) tetrad. Scale bar, 20 μ m. (L) Schematic representation of sister chromatid cohesion. (a) The meiotic cohesion complex (purple), consists of SMC1, SMC3, REC8 and SCC3. (b,c,d) Cohesin embraces the sister chromatids from premeiosis until anaphase I onset. (c) During prophase I, WAPL-mediated removal of cohesion takes place and (d) at anaphase I onset the remaining arm cohesin gets cleaved by ESP, but centromeric cohesin is protected by SGO1 and PP2A (light purple box). (e) Finally, at anaphase II onset centromeric cohesin is cleaved by ESP. (M) Schematic representation of chromosome synapsis. (a) axis proteins ASY1 (magenta) and ASY3 (green) and central element ZYP1 (blue). During zygotene (b), the synaptonemal complex starts to be formed (blue), in detail (a) ZYP1 is loaded and ASY1 gets partially removed. (c) At pachytene, all chromosomes are fully synapsed (blue). (N) Schematic representation of meiotic recombination. (a) Recombination is initiated with the formation of DSBs by SPO11-1. (b) The DSBs first undergo resection with the help of MRN complex, (c) followed by strand invasion mediated by DMC1 and

RAD51, into the sister chromatids which leads to inter-sister repair (light purple box), or into the homolog which leads to NCO (mediated by FIGL and (e) RECQ4), (d) Type I CO (mediated by ZMM proteins, e.g. MSH4) or Type II CO (mediated by MUS81).

After prophase I, the bivalents align at the metaphase plate and the microtubules form the first meiotic spindle during metaphase I (**Figure 1E**). To assure proper segregation of the homologs, a control mechanism, called spindle assembly checkpoint (SAC), ensures that the spindle microtubules are correctly attached to the chromosomes at the kinetochores, which are protein structures assembled on the centromeres of the duplicated chromatids. The SAC remains active until all kinetochores are properly attached to the meiotic spindle and the homologs are then pulled to the opposite poles during anaphase I (**Figure 1F**) (Gorbisky, 2015; Jones and Franklin, 2008; Marston and Wassmann, 2017). When the homologs are successfully separated, the nuclei reform at telophase I and the chromosomes temporarily decondense during interkinesis (**Figure 1G**).

During the second meiotic division, the sister chromatids recondense during prophase II and align at the metaphase plate in metaphase II (**Figure 1H**). In contrast to the first meiotic division, where sister chromatids moved to the same pole, the kinetochores of the sister chromatids now attach to the spindle microtubules deriving from the opposite poles. Subsequently, the sister chromatids are separated during anaphase II and the nuclei reform during telophase II (**Figure 1I,J**). At the end of meiosis II, four daughter cells are formed, which are haploid in case of diploid organisms, like *Arabidopsis thaliana* (*Arabidopsis*) (**Figure 1K**) (De Storme and Geelen, 2013a).

2. The molecular mechanisms behind sister chromatid cohesion, synapsis and recombination

2.1. Sister chromatid cohesion

Key to a successful meiotic division is the proper segregation of chromosomes during meiosis I and II. In order to prevent premature segregation of the sister chromatids during anaphase I, the sister chromatids of each homolog are embraced by cohesin, a highly conserved proteinaceous ring-shaped complex (**Figure 1L(b)**) (Nasmyth and Haering, 2009). The meiotic cohesin complex consists of four subunits: STRUCTURAL MAINTENANCE 1 (SMC1), SMC3, SISTER CHROMATID COHESION 3 (SCC3) and the meiosis specific α -kleisin RECOMBINANT PROTEIN

8 (REC8) (**Figure 1L(a)**) (Ishiguro, 2019; Roig et al., 2014; Schubert, 2009; Skibbens, 2019). The central role of REC8 during meiosis was deduced from *rec8* mutant analysis, which showed that REC8 is not only important for sister chromatid cohesion, but is also involved in axis formation and synapsis (Cai et al., 2003).

Cohesion is established during DNA replication at S-phase prior to meiosis along the whole length of the chromosomes and is partially maintained until the onset of anaphase II. From prophase I onwards, sister chromatid cohesion gets gradually removed. The stepwise loss of cohesion along the chromosome arms relies on two mechanisms. First, arm cohesin gets partially detached by a conserved WINGS APART-LIKE (WAPL)-dependent pathway until late prophase I (**Figure 1L(c)**). In addition, a SEPARASE (ESP)-dependent proteolytic cleavage of phosphorylated REC8 takes place at anaphase I onset. This leads to the removal of the remaining arm cohesion (**Figure 1L(d)**) (Bolanos-Villegas et al., 2017; Makrantonis and Marston, 2018; Yang et al., 2019). During meiosis I centromeric cohesin is protected from cleavage by SHUGOSHIN 1 (SGO1) and PROTEIN PHOSPHATASE 2A (PP2A), which enforce the dephosphorylation of REC8 around the centromeres. This is needed for the proper segregation of sister chromatids to the same cell pole and the separation of the homologs to opposite cell poles (**Figure 1L(d)**) (Clift and Marston, 2011; Watanabe, 2005).

At the onset of anaphase II, centromeric cohesin is no longer protected by SGO1 and PP2A, which leads to the phosphorylation of REC8 and cleavage by ESP (Clift and Marston, 2011). The removal of centromeric cohesion allows the separation of the sister chromatids to opposite cell poles (**Figure 1L(e)**). The above described stepwise loss of cohesion mediated by ESP is largely conserved among eukaryotes (Luo and Tong, 2018).

2.2. Synapsis of the homologs

Another prominent feature of meiosis is the tight connection between co-aligned homologs, mediated by the formation of the SC (**Figure 1M**) (Mercier et al., 2015).

At early prophase, the chromosome axis, which is a proteinaceous structure that organizes chromosomes as loop arrays, is formed. Its main components are a coiled-coil domain-containing protein ASYNAPTIC 3 (ASY3) and a HORMA domain-containing protein ASYNAPTIC 1 (ASY1) (Armstrong et al., 2002; Ferdous et al., 2012; Lee et al., 2015). The recruitment of ASY1 to the chromosome axis is

dependent on ASY3 and is regulated via the phosphorylation by CYCLIN DEPENDENT KINASE A;1 (CDKA;1) (Yang et al., 2020).

From zygotene onwards, when homologs start to recognize each other, the formation of the SC is initiated by the loading of the transverse filament ZIPPER 1 (ZYP1) proteins, as the central elements of the SC (Higgins et al., 2005; Osman et al., 2006). This process brings the chromosome axes of the homologs in close proximity (**Figure 1M(a,b)**). The axis proteins are then considered as lateral elements of the SC. As the SC assembles, ASY1 gets partially removed from the chromosomes, which is required for a successful synapsis (Lambing et al., 2015). The SC installation starts at multiple sites along the chromosomes, developing into a continuous SC along the entire length of the homologs, resulting in fully synapsed homologs at pachytene (**Figure 1M(c)**) (Osman et al., 2006).

Both *asy1* and *asy3* mutant plants show a reduced CO frequency. In addition, for ASY1 it was shown that it plays a role in the initiation of synapsis and DSB repair via the homolog as a template, rather than the inter-homolog (Armstrong et al., 2002; Caryl et al., 2000; Sanchez-Moran et al., 2007). The importance of the SC is revealed by the mutant analysis of ZYP1. In a *ZYP1* RNAi knock down line of *Arabidopsis*, homologs fail to synapse and show an increase of non-homologous recombination, which results in the formation of multivalents (Higgins et al., 2005). It was further shown that ZYP1 is necessary for CO interference but not for recombination per se (Capilla-Perez et al., 2021; France et al., 2021). The fact that the SC is not needed for recombination can also be deduced from *Saccharomyces pombe*, a species that lacks an SC but is still able to perform homologous recombination in meiosis (Brown et al., 2018).

2.3. Meiotic recombination

The control and execution of meiotic recombination is highly conserved and as in other eukaryotes, meiotic recombination in plants is initiated by the conserved topoisomerase complex subunit SPORULATION 11-1 (SPO11-1), and together with associated proteins catalyzes DSBs in early meiosis (**Figure 1N(a)**) (Grelon et al., 2001; Hartung et al., 2007; Keeney et al., 1997; Stacey et al., 2006). Subsequently, DSBs are processed by the MRN protein complex, comprising of MEIOTIC RECOMBINANT 11 (MRE11), RADIATION 50 (RAD50) and NIJMEGEN BREAKAGE SYNDROME 1 (NBS1), and are recognized by the recombinases

DISRUPTED MEIOTIC cDNA1 (DMC1) (Bishop et al., 1992; Couteau et al., 1999) and RecA homolog RAD51 (**Figure 1N(b,c)**) (Jachymczyk et al., 1981; Li et al., 2004). They mediate the invasion of the processed single stranded DNA into the DNA double strand of the homolog. In the absence of DMC1, DSBs are repaired by inter-sister recombination resulting in the absence of COs and hence causing the formation of unconnected homologs, called univalents. In *rad51* mutants, DSBs are not repaired resulting in severely fragmented chromosomes and complete sterility of the mutant plants.

Towards the end of prophase I, all DSBs are resolved into either non-crossovers (NCOs) or COs (**Figure 1N(d,e)**). COs can be divided into two classes: Type I and Type II. Type I COs rely on the ZMM proteins (acronym from *Saccharomyces cerevisiae* Zip, Mer and Msh proteins), including MUTS HOMOLOG 4 (MSH4), and they occur at a minimal distance from each other due to a phenomenon called CO interference (Higgins et al., 2004; Su and Modrich, 1986). In contrast, Type II CO formation relies on a protein called MMS AND UV SENSITIVE 81 (MUS81) and is not subjected to interference (Berchowitz et al., 2007; Interthal and Heyer, 2000).

Successful execution of meiotic recombination, *i.e.* equally segregate homologs and ensuring genetic diversity, is controlled by the pachytene checkpoint or meiotic recombination checkpoint in animals and yeast (Roeder and Bailis, 2000). This checkpoint delays meiotic progression until recombination defects are resolved. Consequently, several mutants, especially in the recombination pathway, *e.g.* *dmc1* mutants, trigger this checkpoint which lead to a prolonged meiotic arrest, potentially leading to apoptosis in several species, including mouse (Barchi et al., 2005; Bishop et al., 1992; Lange et al., 2011; Rockmill et al., 1995).

A master regulator of the pachytene checkpoint is ATAXIA TELANGIECTASIA MUTATED (ATM), a kinase activated by DNA damage, which triggers checkpoint signaling, promotes DSB repair, and also controls the number of DSBs by regulating SPO11-1 activity via a negative feedback loop (Lange et al., 2011). While ATM is present in plants and fulfills several important functions during meiosis, it was believed that a pachytene checkpoint did not exist in plants since mutants like *dmc1* do not arrest at pachytene and instead complete meiosis, leading

to aneuploid gametes (Caryl et al., 2003; Couteau et al., 1999; Jackson et al., 2006; Jones and Franklin, 2008; Muylt et al., 2009).

3. The regulation of the meiotic progression by cyclin-CDK complexes

The progression through meiosis is tightly coordinated and among the major regulators are CYCLIN DEPENDENT KINASES (CDKs), typical proline dependent serine-threonine kinases. As their name implies, their activity relies on the binding of a cyclin. Mammals and plants contain multiple CDKs and cyclins, which are highly dynamic in the formation of CDK-cyclin complexes, acting in specific combinations at different moments throughout the meiotic division. Furthermore, the progression through meiosis correlates with the oscillating activity of CDKs and it has been hypothesized that the CDK activity decreases to medium levels after meiosis I, which allows for a second meiotic division without an intervening S-phase. (Dissmeyer et al., 2007; Wijnker and Schnittger, 2013).

In *Arabidopsis*, the main mitotic kinase CDKA;1 is shown to be expressed throughout meiosis and to be involved in synapsis and recombination, e.g. CDKA;1 phosphorylates ASY1, which is required for the formation of the chromosome axis (Bulankova et al., 2010; Dissmeyer et al., 2007; Sofroni et al., 2020; Wijnker et al., 2019; Yang et al., 2020).

Cyclins define the activity level and the specificity of CDKs and cyclin mutants often manifest severe defects, e.g. the mutation of *solo dancers* (*sds*), coding for a meiosis-specific cyclin, causes the formation of univalents, which results in sterile plants. It was further shown that SDS is involved in CO formation (Azumi et al., 2002; Wu et al., 2015). Another meiosis-specific cyclin is the A-type cyclin TARDY ASYNCHRONOUS MEIOSIS (TAM, CYCA1;2). In *Arabidopsis tam* mutants, meiosis is prematurely terminated due to cytokinesis after meiosis I, resulting in the formation of diploid microspores (Bulankova et al., 2010; d'Erfurth et al., 2010; Wang et al., 2004).

4. The male reproductive organs in *Arabidopsis thaliana* and *Zea mays*

In this study, two plant species were used, *Arabidopsis thaliana* (*Arabidopsis*) and *Zea mays* (maize). The dicot *Arabidopsis* is the most broadly used plant model organism for research, in part due to its relatively short lifespan of 8-12 weeks and its easy transformability (**Figure 2A**). The *Arabidopsis* genome is distributed over five

chromosomes and has a total length of 120 million base pairs (Mbp). It was first sequenced in 2000 and has reached a very reliable level of sequence annotation fidelity (Arabidopsis Genome, 2000).

At the top of inflorescences of an Arabidopsis plant, a set of flower buds, harbouring the male and female organs, can be found (**Figure 2B**). The developmental stage of those buds can be determined according to their size and position on the inflorescence (Smyth et al., 1990). Inside the flower, six stamens (male) are grouped around one central pistil (female) (**Figure 2C,D**). A stamen consists of a filament and an anther. The cells of interest, the male meiocytes, are located inside the anther and are well protected by multiple layers of somatic cells, e.g. epidermis and tapetum (**Figure 2E**) (Goldberg et al., 1993).

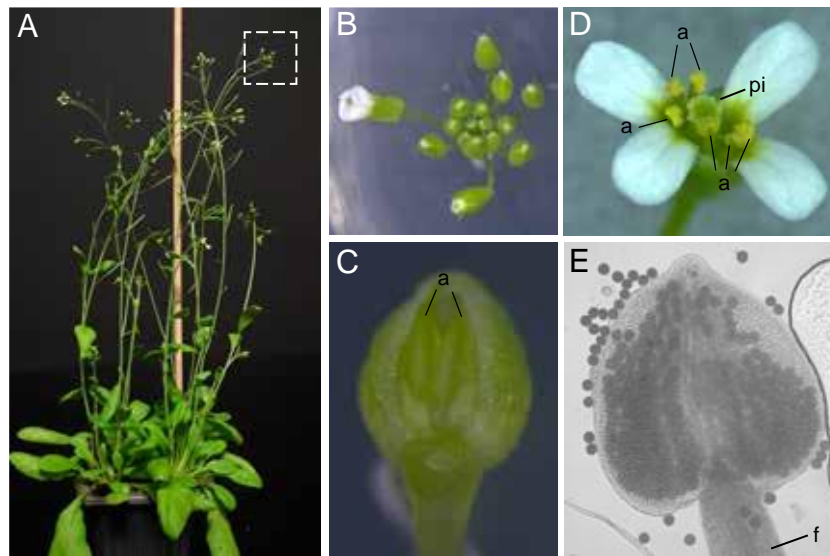


Figure 2. The localization of male meiocytes in *Arabidopsis thaliana*.

(A) On a flowering Arabidopsis plant, at the top of an inflorescence (dotted white box), (B) a set of flower buds can be found. (C) The flower bud with one sepal removed, showing two anthers (a). (D) The flower contains one pistil (pi) and six stamens, a stamen consists of a filament (f) and an anther (a). (E) Inside the anther the male meiocytes are located, which develop into microspores (stained using Peterson staining solution (Peterson et al., 2010)).

Maize not only serves as a model system for monocots but is also one of the most economically important crops in the world (**Figure 3A**). Maize has become significant for research, even though it has a relatively long lifespan of 12-28 weeks and was not easily transformable at first. The maize genome has ten chromosomes and a total length of 2.4 giga base pairs (Gbp). Despite its enormous genome size, annotated reference genomes for several inbred lines are available, i.e. B104,

CML247, Mo17, PH207 and W22. The first maize genome that was fully sequenced and annotated was from the inbred line B73 (Schnable et al., 2009).

In maize, the male and female inflorescences are located in different organs, the tassel and ear, respectively. When male meiosis takes place, the immature tassel is still inside the stalk (**Figure 3A,B**). A tassel consists of hundreds of paired spikelets containing each two florets, with 3 stamens inside (**Figure 3C-E**). As in *Arabidopsis*, a stamen consists of an anther and a filament and the male meiocytes can be found inside the anther (Bommert et al., 2005; Laudencia-Chingcuanco and Hake, 2002). While the size of an *Arabidopsis* meiocyte is about 20 μm , the maize meiocytes are significantly larger, namely around 40-50 μm in diameter.

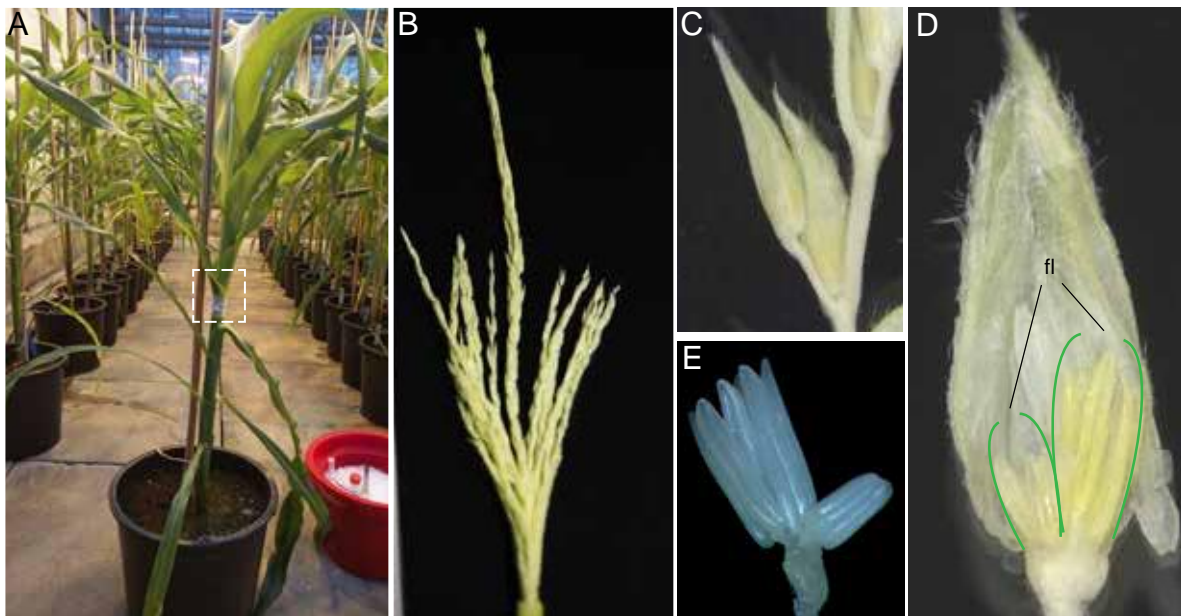


Figure 3. The localization of male meiocytes in *Zea Mays*.

(A) A 6-8 week-old maize plant (inbred line A188) contains inside the stalk (dotted white box) (B) the male inflorescence, called tassel. The immature tassel consists of (C) spikelets organized in pairs. (D) A spikelet includes two florets (fl, highlighted between the green lines) with (E) each three anthers inside.

5. My research topics

For my dissertation, two different aspects of meiosis were studied. First, the effect of heat on the meiotic progression in *Arabidopsis* was investigated using live cell imaging. Additionally, the question if there is translational control during meiosis was tackled using maize and *Arabidopsis*. Currently these analyses are considered as independent, however they may converge in future research, as the regulation of heat stress possibly also occurs at translational level.

Chapter 1, entitled “Heat stress reveals the existence of a specialized variant of the pachytene checkpoint in meiosis of *Arabidopsis thaliana*”, includes the manuscript of this study which has been accepted for publication in *The Plant Cell*.

In chapter 2, entitled “The characterization of the translational landscape of *Arabidopsis* and maize meiocytes”, the ongoing work to investigate translational regulation during maize meiosis using a genome-wide approach, *i.e.* ribosome profiling, as well as the challenges of using gene-specific approaches, *i.e.* the MS2-system and TRICK, to visualize the temporal differences between transcription and translation in *Arabidopsis* meiocytes are described.

**CHAPTER I. Heat stress reveals the existence of a
specialized variant of the pachytene checkpoint in meiosis
of *Arabidopsis thaliana***

1. INTRODUCTION TO CHAPTER I

Ambient temperature is one of the key environmental parameters that determines plant growth and fertility and has been the focal interest of many plant researchers. Understanding plant responses to temperature is further boosted by the ongoing climate change (Anderson et al., 2016; Collins, 2014; Couteau et al., 1999), during which crops are expected to be exposed to very high temperatures in the near future, threatening to sharply reduce crop yield (Hatfield and Prueger, 2015; Yue et al., 2019). For example, a drop in yield of up to 22% for maize can be observed with a 1°C increase in temperature (Kukal and Irmak, 2018). To counteract these detrimental effects and adjust breeding programs, it is vital to understand the changes imposed by temperature stress on yield-related traits at the cellular and molecular levels.

Meiosis and in particular meiotic recombination are highly sensitive to environmental conditions, leading to meiotic failure in many different organisms, such as the nematode *Caenorhabditis elegans* (Bilgir et al., 2013), mice (Nebel and Hackett, 1961), wheat (*Triticum aestivum*) (Pao and Li, 1948), and rose (*Rosa hybrida*) (Pecrix et al., 2011). Elevated temperatures also affect the meiotic microtubule cytoskeleton, resulting in irregular spindle orientation, aberrant cytokinesis and the production of unreduced gametes, polyads and micronuclei in poplar (*Populus pseudo-simoni*), rose and Arabidopsis (De Storme and Geelen, 2020; Hedhly et al., 2020; Pecrix et al., 2011; Wang et al., 2017).

Furthermore, while DSB numbers are reported to be unaffected at elevated temperatures in several organisms, e.g. yeast and Arabidopsis (Brown et al., 2020; Modliszewski et al., 2018), other aspects of the recombination pathway were found to be altered by temperature, leading to diverse effects that differ depending on the environmental conditions and species. Chiasma frequency was shown to be highly sensitive to environmental conditions. At high temperatures, chiasma frequency decreases in some species, such as in barley (*Hordeum vulgare*, female meiosis), spiderwort (*Tradescantia bracteata*), perfoliate bellwort (*Uvularia perfoliate*) and wild garlic (*Allium ursinum*) (Dowrick, 1957; Lloyd et al., 2018; Loidl, 1989; Modliszewski et al., 2018; Phillips et al., 2015), while it increases in other species, for instance in barley (male meiosis), Arabidopsis and the fungus *Sordaria fimicola* (Lamb, 1969;

Lloyd et al., 2018; Modliszewski et al., 2018; Phillips et al., 2015). In *Arabidopsis*, the increase in CO frequency at high temperatures was shown to be due to elevated numbers of type I COs (Lloyd et al., 2018; Modliszewski et al., 2018). In addition, CO distribution is also altered by heat stress (Dowrick, 1957; Higgins et al., 2012). In barley (male meiosis), high temperatures (30°C) cause an increase in chiasmata at the interstitial/proximal region of chromosomes but an overall decrease in chiasmata per cell (Higgins et al., 2012). At very high temperatures (35°C and above), in many species, such as wheat, barley and wild garlic, synapsis of the homologs fails, resulting in the formation of univalents (Higgins et al., 2012; Loidl, 1989; Pao and Li, 1948).

To obtain further insights into the effects of temperature on meiosis, I followed *Arabidopsis* male meiocytes under three different temperature regimes via live cell imaging using a recently established setup (Prusicki et al., 2019). I obtained a detailed picture of meiotic progression under heat stress. While meiocytes progressed through meiosis much faster at higher temperatures than at 21°C in general, a key discovery was that the length of pachytene/diakinesis is prolonged at 34°C. An extension of pachytene/diakinesis was not observed when recombination was abolished. Since this extension was also eradicated in *atm* mutants, I conclude that *Arabidopsis* and likely other plants have a specialized form of the pachytene checkpoint that is only triggered by recombination intermediates, but not by the complete absence of recombination as is the case in other species. Here, the manuscript of this work, which has been accepted for publication by *The Plant Cell*, is included.

2. RESULTS

2.1. A cytological sensor of heat stress in meiocytes

To analyze the effects of increased temperatures on meiosis, we applied three different heat conditions reflecting possible environmental stress scenarios and matching conditions used in previous studies. Arabidopsis is typically grown between 18 and 24°C, with our standard growth conditions being 21°C during the day and 18°C during the night (hereafter called 21°C). As a first stress condition, we used a heat shock of 30°C (HS30°C) and analyzed the effects on meiosis immediately. In parallel, we allowed plants to acclimatize to 30°C (during both day and night) in highly controlled growth chambers for one week (long-term, LT30°C) before analyzing meiosis. The third condition consisted of an even more severe heat stress of 34°C (HS34°C) that was also applied immediately and analyzed.

However, the proper and reliable application of heat stress to multicellular structures, such as anthers, can be challenging when the focus is on particular cells, like meiocytes, which are surrounded by many different cell layers, such as the tapetum layer and the epidermis. The multicellular environment and the size of these structures have the capacity to buffer temperatures, hence making it difficult to exactly time the moment when the heat stress will reach the cells of interest. To resolve this problem, we took advantage of the observation that stress granules (SGs) form at elevated temperatures in different plant tissues, e.g. roots, leaves and hypocotyls (Chodasiewicz et al., 2020; Dubiel et al., 2020; Hamada et al., 2018; Kosmacz et al., 2019; Modliszewski et al., 2018). These SGs were previously shown in Arabidopsis seedlings to contain the cell cycle regulator CDKA;1 (Kosmacz et al., 2019). CDKA;1 is a major regulator of meiotic progression as well as recombination and its encoding gene is highly expressed in Arabidopsis male meiocytes (Bulankova et al., 2010; Dissmeyer et al., 2007; Sofroni et al., 2020; Wijnker et al., 2019; Yang et al., 2020; Zhao et al., 2017; Zhao et al., 2012). To test whether CDKA;1 might change its homogenous cytosolic and nuclear localization pattern during meiosis upon heat stress, we applied the different temperature regimes to male meiocytes from plants carrying the *CDKA;1-mVenus* and the *TagRFP-TUA5* (encoding a fusion protein between the red fluorescent protein [RFP] and TUBULIN ALPHA-5 [TUA5]) reporters, and followed the localization pattern of CDKA;1:mVenus during meiosis (Sofroni et al., 2020).

Under our standard *Arabidopsis* growth conditions (21°C) and in agreement with previous analyses, CDKA;1-mVenus uniformly localized to both the cytoplasm and the nucleus. This localization shifted from preferentially cytosolic to predominantly nuclear in late leptotene to early pachytene, followed by an increased cytosolic accumulation in pachytene and diakinesis. After anaphase I and anaphase II, CDKA;1-mVenus accumulated again in the reforming nuclei (Yang et al., 2020) (**Figure 1.1A**).

At the elevated temperatures HS30°C and HS34°C, we observed the same cytosolic-nuclear localization dynamics for CDKA;1 (**Figure 1.1B,C**). At HS34°C, we detected no SGs in early meiotic stages (n=0/89 in G2-early leptotene; n=0/105 from late leptotene to early pachytene), when CDKA;1 preferentially localized to the nucleus of meiocytes (**Figure 1.1C,D**). Notably, SGs readily formed at HS34°C in all meiocytes from pachytene to diakinesis (n=81/81), from metaphase I to interkinesis (n=82/82), and from metaphase II to telophase II (n=72/72), *i.e.* the period when CDKA;1 starts to locate predominantly to the cytoplasm. These granules were visible about 15 min after the heat stress was applied, which was also the time required to set up the acquisition for live cell imaging at the microscope. Thus, the formation of SGs occurred within the first 15 min of heat stress.

By contrast, CDKA;1 granules rarely formed at HS30°C, *i.e.* in only 9% and 14% of the meiocytes in pachytene/diakinesis (n=16/165) and from metaphase I to interkinesis (n=4/24), respectively (**Figure 1.1B,D**). In addition, the number of SGs per meiocyte was also lower at HS30°C compared to granule-containing meiocytes at HS34°C. These findings are consistent with the previous observation that the temperature threshold for the formation of SGs is around 34°C (Hamada et al., 2018).

Taken together, monitoring the formation of SGs allows the visualization of temperature stress in the tissue of interest. Importantly, this optical marker indicated that the ambient temperature reaches meiocytes in a short time, *i.e.* less than 15 min, paving the road for the faithful application of different heat treatments and their comparisons by live cell imaging.

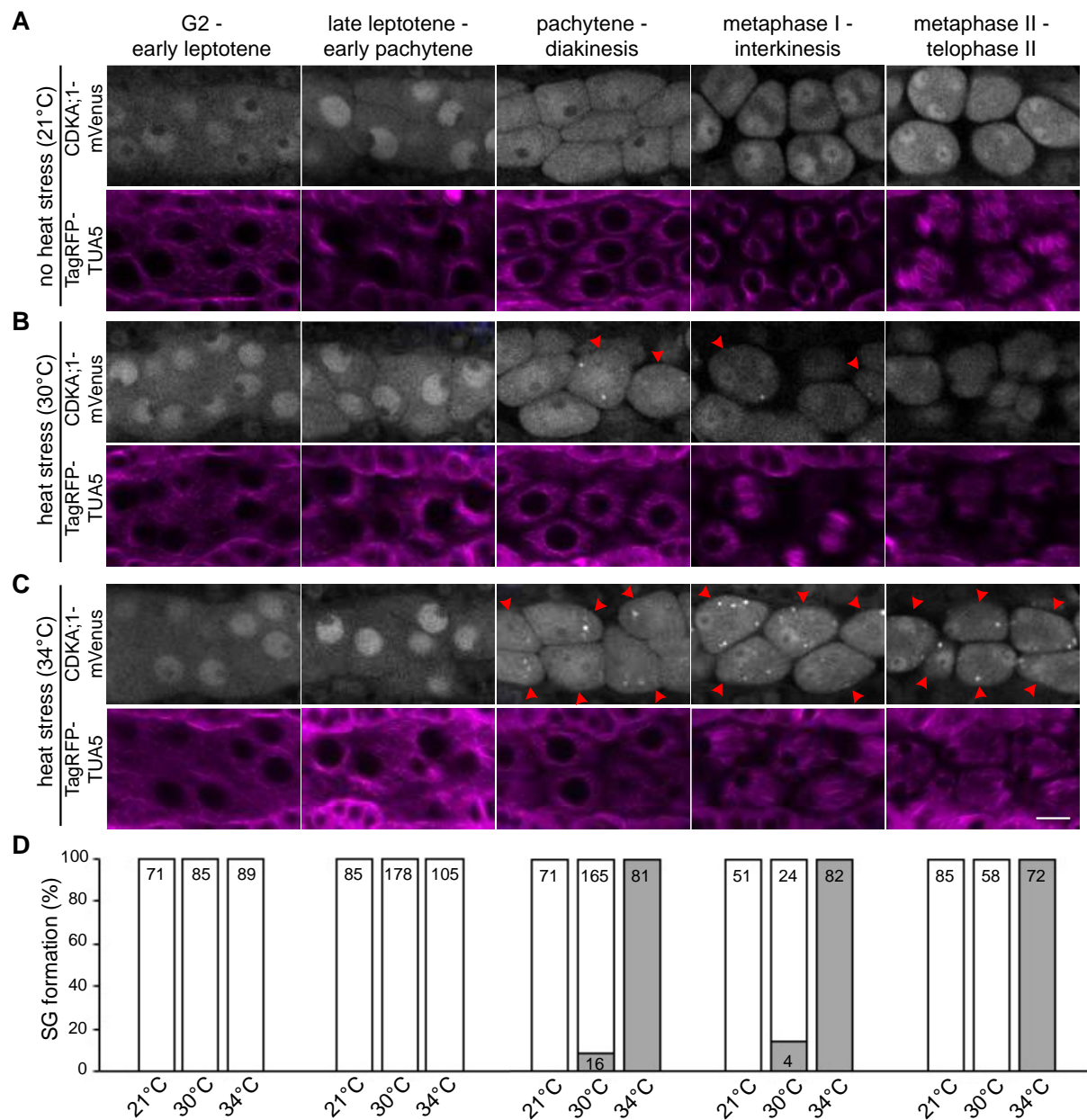


Figure 1.1. Localization of CDKA;1 in male meocytes under control and stress conditions.

(A-C) CDKA;1-mVenus (first row; white) and TagRFP-TUA5 (second row; magenta) localization under the control conditions of 21°C (A), heat stress of 30°C (B) or 34°C (C) at different meiotic stages: G2-early leptotene (column 1), late leptotene-early pachytene (column 2), pachytene-diakinesis (column 3), metaphase I-interkinesis (column 4) and metaphase II-telophase II (column 5). Red arrowheads highlight cells with CDKA;1 localization at SGs. Scale bar, 10 μ m. (D) Quantification of CDKA;1 SG formation on the cellular level per stage in percent; white bar, cells without SGs; gray bar, cells with at least one SG. The absolute sample size is given in the corresponding bar.

2.2. Heat stress affects microtubule configurations during meiosis in a quantitative but not qualitative manner

After having confirmed that the applied temperature regime reached male meiocytes fast and faithfully, we turned to addressing the general aim of this study, *i.e.* how increased temperature affects the dynamics of meiosis. To tackle this question, we used a previously established live cell imaging method for meiosis (Prusicki et al., 2019). A crucial finding of this approach was the observation that meiosis can be dissected by so-called landmarks that occur in a predictable order and that reflect highly defined cytological stages, for instance using fluorescently labeled microtubules (MTs, TagRFP-TUA5). Thus, these landmarks not only allow the staging of meiocytes but also provide means to reveal the dynamics of meiosis by determining the time between landmarks.

In brief, MTs have the following dynamics during male meiosis: During G2-early leptotene, MTs are first homogeneously distributed in meiocytes with the nucleus in the center, for what is called MT array state 1 (**Supplemental Figure S1.1A**). MTs then will gradually polarize into a half moon-like structure on one side of the nucleus, which defines MT array state 2-3-4, from late leptotene to early pachytene (**Figure 1.2A, Supplemental Figure S1.1B**). This structure develops further into a full moon-like assembly entirely surrounding the nucleus, marking MT array state 5-6, during pachytene, diplotene and diakinesis (**Figure 1.2B, Supplemental Figure S1.1C**). After nuclear envelope breakdown (NEB), the pre-spindle transforms into the first meiotic spindle at MT array state 7-8-9, from metaphase I to anaphase I (**Figure 1.2C, Supplemental Figure S1.1D**). Next, MTs reorganize around the two newly formed nuclei and central MTs form a phragmoplast-like structure for MT array state 10-11 at telophase I and interkinesis (**Figure 1.2D, Supplemental Figure S1.1E**). The second division is characterized by the formation of two pre-spindles, followed by two spindles, at MT array state 12-13, from metaphase II to anaphase II (**Figure 1.2E, Supplemental Figure S1.1F**). Phragmoplast-like structures, which appear at MT array state 14, are visible at telophase II (**Figure 1.2F, Supplemental Figure S1.1G**) until cytokinesis, resulting in tetrads, the four meiotic products.

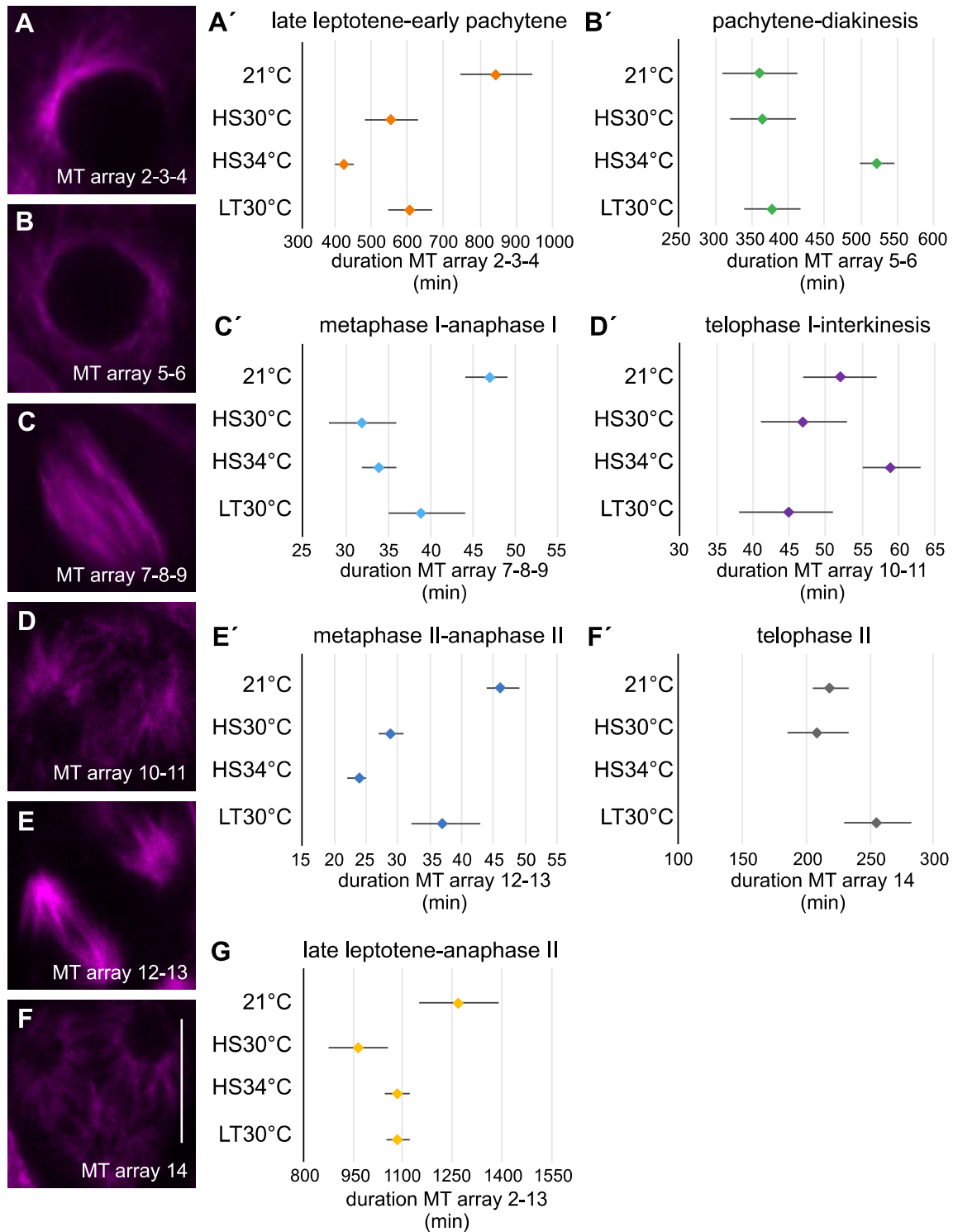


Figure 1.2. Duration of meiotic phases based on MT array states.

Confocal images of MT array states (A-F) and the corresponding predicted median times (in min) with 95% confidence intervals in control (21°C) and heat conditions (HS30°C, HS34°C and LT30°C) (A'-F'); (A,A'; orange) MT array state 2-3-4, late leptotene-early pachytene; (B,B'; green) MT array state 5-6, pachytene-diakinesis; (C,C'; light blue) MT array state 7-8-9, metaphase I-anaphase I; (D,D'; purple) MT array state 10-11, telophase I-interkinesis; (E,E'; dark blue) MT array state 12-13, metaphase II-anaphase II; (F,F'; grey) MT array state 14, telophase II. Scale bar, 10 μ m. (G)

Predicted median time (in min) of MT array states 2-13 with the 95% confidence interval in control (21°C) and heat conditions (HS30°C, HS34°C and LT30°C) (yellow).

By analyzing meiosis at HS30°C, HS34°C and LT30°C, we confirmed that meiosis does not arrest upon exposure to these temperature regimes, consistent with previous studies (De Storme and Geelen, 2020; Lei et al., 2020). Importantly, in all movies taken at higher temperatures (46 in total), the meiocytes progressed through the same MT array states as previously seen at 21°C (**Movies 1-4, Supplemental Figure S1.1**, (Prusicki et al., 2019)).

MT stability and polymerization are known to be temperature-sensitive, (Bannigan et al., 2007; Li et al., 2009a; Liu et al., 2017; Song et al., 2020; Wu et al., 2010). Consistently, we observed quantitative changes in some MT structures, confirming that meiocytes were exposed to elevated temperatures. As revealed by pixel intensity quantification of meiocytes in MT array state 6, in which MTs fully surround the nucleus (**Figure 1.3A-D**), we determined that the intensity of the fluorescence signal measured for TagRFP-TUA5 drops upon both HS30°C (**Figure 1.3B'**, n=17) and HS34°C (**Figure 1.3D'**, n=32) in comparison to 21°C (**Figure 1.3A'**, n=14), indicating that MT density decreases. However, high temperatures can have an influence on the emission intensity of fluorescent proteins (Toca-Herrera et al., 2006). Hence, we cannot exclude that this reduction in emission intensity partially accounts for the decrease in pixel intensity seen here. Notably, the reduction in pixel intensity largely reverted at LT30°C (**Figure 1.3C'**, n=31), implying that the biophysical emission reduction caused by heat does not have such a great impact in our setup, at least at 30°C. Moreover, the restoration of pixel intensities suggests the existence of an adaptation mechanism for MT bundling in response to heat. Further confirming an effect of heat on MTs, we specifically observed irregular spindle structures at 34°C but not at lower temperatures (**Figure 1.3E**), consistent with previous analyses (De Storme and Geelen, 2020; Lei et al., 2020).

Taken together, the quantitative but not qualitative changes of the typical meiotic MT configurations allow the adoption of characteristic MT arrays for staging of meiosis during live cell imaging. At the same time, the quantitative effects on the MT arrays corroborate the previous finding that meiocytes successfully receive the heat treatment in our experimental set up.

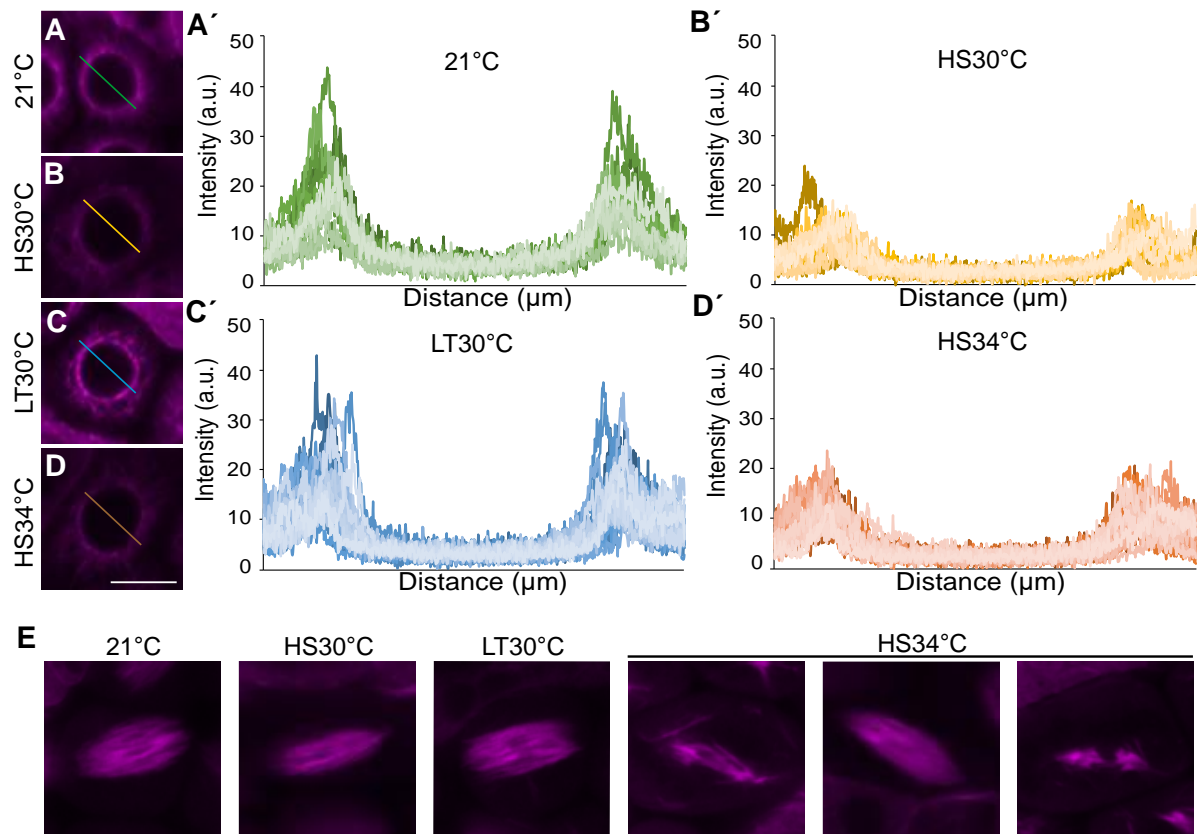


Figure 1.3. Microtubule array in the wild type in control and heat stress conditions.

(A-D) Confocal images of meiocytes expressing *TagRFP-TUA5* (magenta) at MT array state 6 in control conditions of 21°C (A), heat shock conditions of HS30°C (B), LT30°C (C) and HS34°C (D). (A'-D') Pixel intensity plot of a section crossing through the middle of the cell (distance in μm) in MT array state 6 in 21°C (A', green, n=14), HS30°C (B', yellow, n=17), LT30°C (C', blue, n=31) and HS34°C (D', brown, n=32), section lines also highlighted in (A-D). (E) Confocal images of meiocytes expressing *TagRFP-TUA5* (magenta) at MT array state 8-9 at 21°C, HS30°C, LT30°C and HS34°C. Scale bar, 10 μm.

2.3. Duration of meiosis under heat stress

The next challenge to overcome for the evaluation of meiotic progression at elevated temperatures was how to statistically compare the MT-based dissection of the different heat stress experiments with the control growth conditions. This was not a trivial question, since the analyses of meiocytes within one anther-sac cannot be regarded as statistically independent measurements but represent clustered data. In addition, the above-mentioned nature of defined meiotic stages gives rise to a multi-state nature of our dataset. Moreover, our measurements occasionally did not capture the exact start and/or end point (left, right and/or interval censored data) of a MT array state, since the observed anthers sometimes move out of the focal plane (but also occasionally move into focus again).

Including the combination of the three characteristics of our data, *i.e.* clustered data, left/right and/or interval censoring, as well as having a multistate nature, was not possible in one statistical model. Therefore, we reduced the multistate complexity of the analysis and built a separate model for each meiotic state, as defined by the MT configuration (see above) which also allowed us to simplify the mixture of left/right and/or interval censored data with respect to the duration of each state to interval and right censoring. For detailed description of the models, please see the Materials and Methods section on Statistical Methods. With the imaging and evaluation system in hand, we then addressed the effect of HS30°C, HS34°C and LT30°C treatments on the total length of meiosis.

The determination of the meiotic duration relied on defined start and end points of MT states (events). Since this is not possible for MT array state 1 (no start point), the first stage that could be temporally evaluated was thus MT array state 2-3-4. From a total of 59 movies, we first selected movies that covered all MT array states (2-14) under the four temperature regimes. Unfortunately for HS34°C, we were unable to reliably determine the end point of MT array state 14, as the fluorescent signal of the MTs became very poor, possibly due the fact that MTs are more diffusely organized at high temperature versus control conditions (described above, **Figure 1.3**), photobleaching after long time lapses as well as possible effects on fluorescence emission at high temperatures.

To compare the overall meiotic duration at all heat conditions, we excluded MT array state 14 for this analysis and only considered movies capturing MT array states 2-13 (23 movies). We then built a separate parametric survival model for the complete duration (as described in Materials and Methods), resulting in the total predicted median time, together with the 95% confidence interval (CI).

We determined that the duration of MT array states 2-13 at 21°C has a predicted median time of 1,271 min (or 21.2 h, CI 1,151-1,390 min, **Figure 1.2G**, **Supplemental Table S1.1**). This value matched very well with previous analyses of the duration of male meiosis in *Arabidopsis* by pulse-chase experiments and live cell imaging, underscoring the robustness of our analysis and the reproducibility of meiotic progression at 21°C (Armstrong et al., 2003; Prusicki et al., 2019; Sanchez-Moran et al., 2007; Stronghill et al., 2014).

Next, we analyzed the duration of meiosis under the heat conditions, resulting in a predicted median time of 966 min (16.1 h, CI 876-1,056 min) upon HS30°C; 1,086 min (18.1 h, CI 1,048-11,24 min) upon HS34°C; and 1,086 min (18.1 h, CI 1,050-1,122 min) upon LT30°C (**Figure 1.2G, Supplemental Table S1.1**). Since the confidence intervals did not overlap, these data confirm previous observations that meiosis progresses faster under elevated temperatures in comparison to control conditions, also demonstrating that our experimental system can be faithfully used to study the effect of heat on meiosis (Bennett et al., 1972; Draeger and Moore, 2017; Stefani and Colonna, 1996; Wilson, 1959).

2.4. Duration of individual meiotic phases under heat stress

The live cell imaging approach, together with the model-based calculation of the duration of the MT array states, allowed us then to target the main aim of this study, that was to obtain a detailed and phase-specific assessment of meiotic progression under elevated temperatures.

At 21°C, we observed a total of 206 meiocytes from 23 anther sacs and calculated the predicted median time per MT array state from those cells of which we could observe at least one time point in that specific state (**Movie 1, Table 1.1, Supplemental Table S1.1**). All reported median times were predictions from the respective parametric survival models (see Materials and Methods). The predicted median time in MT array state 2-3-4 was 845 min (CI 746-944 min, **Figure 1.2A**), followed by MT array state 5-6, with a predicted median time of 360 min (CI 309-412 min, **Figure 1.2B**). MT array state 7-8-9 took place over 47 min (CI 44-49 min, **Figure 1.2C**) while MT array state 10-11 spanned 52 min (CI 47-57 min, **Figure 1.2D**). The second meiotic division then followed with a predicted median time of 46 min for MT array state 12-13 (CI 44-49 min, **Figure 1.2E**), finishing the meiotic division with 219 min for MT array state 14 (CI 205-234 min, **Figure 1.2F**).

Table 1.1. Overview of the duration of the meiotic phases based on the MT array states.

Predicted median times and 95% confidence intervals (in min) of MT array state 2-3-4 (late leptotene-early pachytene), MT array state 5-6 (pachytene-diakinesis), MT array state 7-8-9 (metaphase I- anaphase I), MT array state 10-11 (telophase I- interkinesis), MT array state 12-13 (metaphase II- anaphase II) and MT array state 14 (telophase II) of the wildtype at 21°C, HS30°C, HS34°C, LT30°C; recombination mutants *spo11*, *dmc1* and *msh4* at 21°C and HS34°C and *atm* mutant at 21°C and HS34°C. (n= number of cells/anther sacs observed). NA: not analysed.

MT array state Meiotic stage	2-3-4 late leptotene- early pachytene			5-6 pachytene- diakinesis			7-8-9 metaphase I- anaphase I			10-11 telophase I- interkinesis			12-13 metaphase II- anaphase II			14 telophase II		
	Median	95% Conf. Interval		Median	95% Conf. Interval		Median	95% Conf. Interval		Median	95% Conf. Interval		Median	95% Conf. Interval		Median	95% Conf. Interval	
Treatment (n)																		
21°C (206/23)	845	746	944	360	309	412	47	44	49	52	47	57	46	44	49	219	205	234
HS30°C (133/22)	556	485	628	365	319	411	32	28	36	47	41	53	29	27	31	209	185	233
HS34°C (188/26)	428	403	453	522	498	546	34	32	36	59	55	63	24	22	25	NA	NA	NA
LT30°C (211/25)	609	550	667	378	340	416	39	35	44	45	38	51	37	32	43	256	230	282
<i>spo11</i> 21°C (224/27)	1119	1031	1206	374	349	399	72	67	76	63	58	67	48	45	52	356	326	385
<i>dmc1</i> 21°C (157/24)	1056	929	1184	343	331	355	67	63	71	63	59	67	47	45	49	281	262	301
<i>msh4</i> 21°C (193/26)	951	861	1040	314	299	329	67	63	71	59	56	63	49	46	52	274	253	294
<i>spo11</i> HS34°C (198/25)	626	572	681	412	393	431	35	32	38	54	49	58	23	21	26	NA	NA	NA
<i>dmc1</i> HS34°C (160/19)	565	526	605	383	362	403	30	28	32	57	54	60	22	21	23	NA	NA	NA
<i>msh4</i> HS34°C (116/17)	571	536	606	398	346	450	32	30	34	49	43	55	24	22	26	NA	NA	NA
<i>atm</i> 21°C (228/28)	834	761	908	295	270	321	45	42	49	60	55	66	43	40	46	245	230	260
<i>atm</i> HS34°C (172/23)	702	640	764	350	330	370	31	29	33	55	50	60	26	23	28	NA	NA	NA

Next, we analyzed male meiosis subjected to the three different temperature regimes in the same way. Accordingly, we observed a total of 133, 188 and 211 meiocytes from 22, 26 and 25 anther sacs were observed for HS30°C, HS34°C and LT30°C, respectively. Again, we calculated the predicted median time per state from those cells of which we could observe at least one time point in that specific state (**Movies 2-4, Table 1.1, Supplemental Table S1.1**). The duration of MT array state 2-3-4 upon higher temperature was shorter compared to 21°C (845 min), with a predicted median time of 556 min upon HS30°C (CI 485-628 min), 428 min upon HS34°C (CI 403-453 min) and 609 min upon LT30°C (CI 550-667 min, **Figure 1.2A**). The predicted median time in MT array state 2-3-4 at 21°C was therefore 289 min (CI 167-410 min) longer compared to HS30°C, 417 min (CI 315-519 min) longer compared to HS34°C and 236 min (CI 122-351 min) longer compared to LT30°C (**Supplement Table S1.2**). These results demonstrated that the rise in temperature generally decreases the duration of this phase.

In the next phase, MT array state 5-6 exhibited a strikingly different behavior. While upon exposure to HS30°C and LT30°C, the predicted median time was 365 min (CI 319-411 min) and 378 min (CI 340-416 min), respectively, HS34°C resulted in a predicted median of 522 min (CI 498-546 min, **Figure 1.2B**). The duration of this phase at HS34°C was thus longer compared to 21°C (360 min), with a difference of 162 min (CI 104-219 min, **Supplemental Table S1.2**), presenting a prolongation of ~2.7 h.

After NEB, the meiocytes undergo the first round of chromosome segregation, *i.e.* MT array state 7-8-9, with a predicted median time of 32 min (CI 28-36 min) upon HS30°C, 34 min (CI 32-36 min) upon HS34°C and 39 min (CI 35-44 min) upon LT30°C, which is shorter compared to 21°C (47 min, **Figure 1.2C**, for details on differences see **Supplemental Table S1.2**).

The following MT array state 10-11 spanned 47 min (CI 41-53 min) upon HS30°C, 59 min (CI 55-63 min) upon HS34°C and 45 min (CI 38-51 min) upon LT30°C (**Figure 1.2D**), with only the duration at HS34°C being longer by 7 min (CI 0.6-13 min) than at 21°C (**Supplemental Table S1.2**).

Upon HS30°C, HS34°C and LT30°C, the second round of chromosome segregation, MT array state 12-13, spanned 29 min (CI 27-31 min), 24 min (CI 22-25 min) and 37 min (CI 32-43 min), respectively (**Figure 1.2E**). These durations were

shorter compared to 21°C (46 min, for details on differences see **Supplemental Table S1.2**).

We estimated the end of the meiotic division upon heat treatment by using MT array state 14, which spanned 209 min (CI 185-233 min) upon HS30°C and 256 min (CI 230-282 min) upon LT30°C (**Figure 1.2F**). Notably, the pairwise comparison of 21°C and LT30°C showed an increase of 9 min (CI 3-15 min, **Supplemental Table S1.2**).

Currently, the underlying reasons for the above-identified alterations in meiotic durations under different temperatures are not clear and await further investigations. In the following, we focused on one of the most striking and unexpected observations: the temporal increase of late prophase at HS34°C.

2.5. Exposure to high temperature causes chromosomal defects during meiosis

To investigate the prolongation of late prophase at 34°C (**Figure 1.2B**) in more detail, we first performed chromosome spreads from fixed flower buds exposed to the different temperature regimes. At control growth conditions, decondensed chromatin becomes organized into chromosomes that will gradually condense during early prophase I and reach a fully paired state at pachytene. The paired homologs condense further, where chiasmata hold homologs together, finally reaching the highest condensed state at diakinesis with the formation of five bivalents that align at the metaphase plate during metaphase I (**Supplemental Figure S1.2A**). At both HS30°C (n=136) and LT30°C (n=130), homologs condensed and fully paired. Occasionally, two or more bivalents appeared to be entangled at diakinesis (n=36/73 and n=52/81, respectively) and metaphase I, forming chromosome bridges (n=26/65 and n=11/25, respectively), suggesting interconnected non-homologous chromosomes. In addition, we infrequently observed chromosome fragments (n=3/81 at LT30°C) and univalents (at diakinesis: n=2/73 and n=1/81, at metaphase n=4/65 and n=2/25, respectively; **Supplemental Figure S1.2B,C**). In contrast to 21°C and 30°C, we failed to detect fully paired homologs at 34°C (n=115). Furthermore, chromosome spreads of cells in diakinesis and metaphase I at 34°C revealed the formation of mainly 10 univalents (n=64 and n=17, respectively). In addition, chromosome bridges were visible between both homologs and non-

homologous chromosomes (n=33/64 and n=11/17, respectively) (**Supplemental Figure S1.2D**).

Thus, consistent with previous analyses in fission yeast (*Saccharomyces pombe*), barley and Arabidopsis, high temperature caused recombination defects that increase with rising temperatures (Bombliès et al., 2015; Brown et al., 2020; De Storme and Geelen, 2020; Higgins et al., 2012; Modliszewski et al., 2018; Morgan et al., 2017; Phillips et al., 2015).

2.6. Synaptonemal complex formation is defective at 34°C

Given the central role of the formation of the chromosome axis for pairing and meiotic recombination, we next analyzed the localization of the previously generated reporters ASY1 fused to RFP (ASY1-RFP) and ZYP1b fused to the green fluorescent protein (ZYP1b-GFP) upon 30°C and 34°C (Yang et al., 2019; Yang et al., 2020). ASY1 is a chromosome axis-associated protein that plays a major role in the initiation of synapsis and recombination (Armstrong et al., 2002; Caryl et al., 2000; Sanchez-Moran et al., 2007). ZYP1b is a component of the transversal filament of the SC (Capilla-Perez et al., 2021; France et al., 2021; Higgins et al., 2005; Osman et al., 2006).

Under the standard growth conditions of 21°C, ASY1 localized to the chromosome axis from early leptotene to pachytene. During zygotene, when the formation of the SC is initiated, ASY1 became largely depleted from the chromosome axis, while the ZYP1b signal started to appear on chromosomes and gradually expanded to form a linear structure (n=99), resulting in the labeling of the entire chromosome axis at pachytene (n=39) (**Figure 1.4A**).

At the high temperatures of 30°C and 34°C, the localization of ASY1 at the chromosome axis was unaffected and ZYP1b started to form short linear stretches at the chromosome axis during zygotene (n=84 and n=93, respectively) (**Figure 1.4B,C**). At 30°C, ZYP1b continued to label the full length of the axis (n=40), in contrast to 34°C, at which temperature we only detected small stretches of ZYP1b signal (n=68), suggesting that ZYP1b loading is initiated properly but discontinues (**Figure 1.4B,C**). This result was in accordance with previous findings in nematodes, barley and wild garlic showing that synapsis is obstructed upon high temperature exposure, leading to the formation of abnormal structures called polycomplexes (Bilgiri et al., 2013; Higgins et al., 2012; Loidl, 1989).

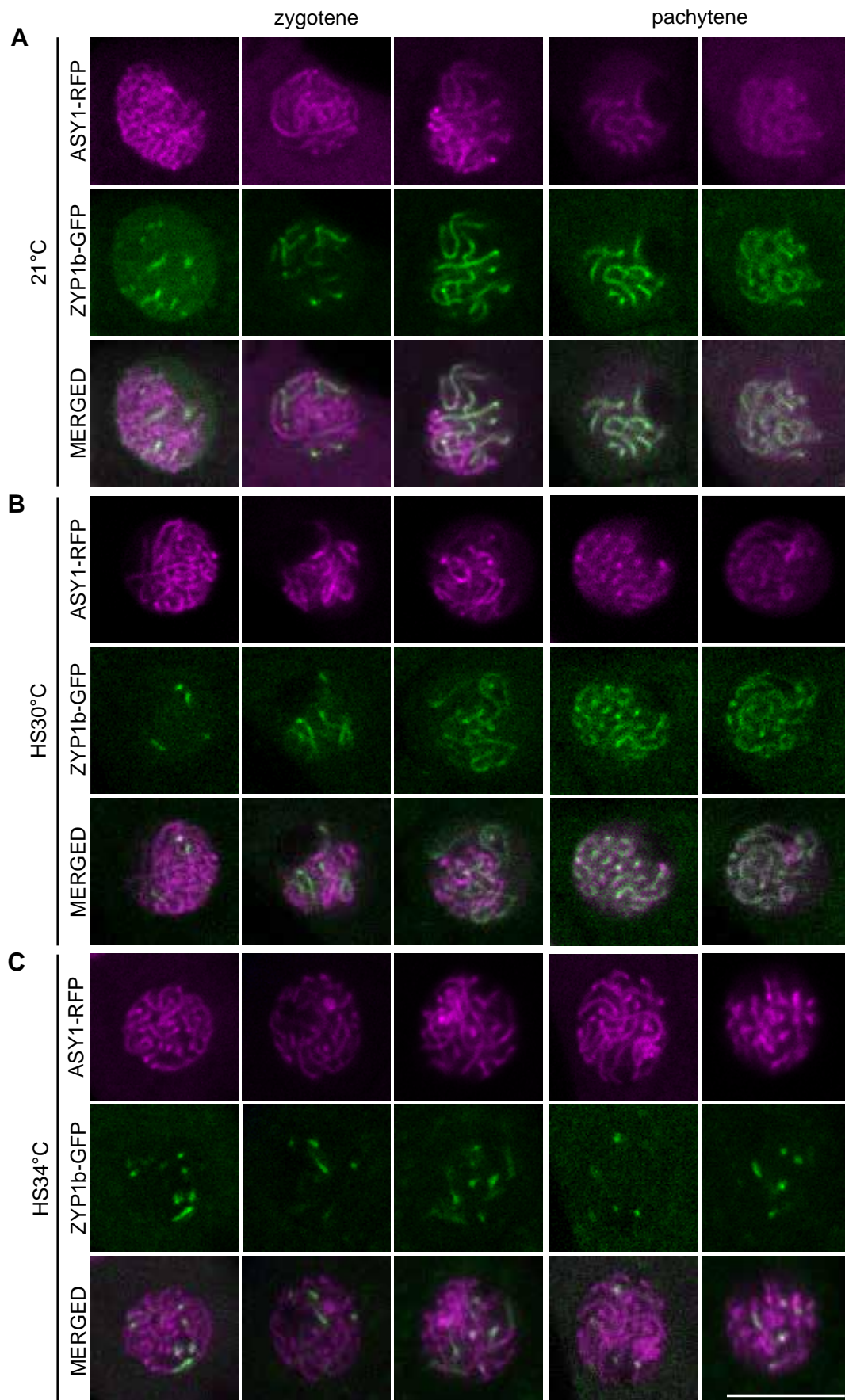


Figure 1.4. Localization of the synaptonemal complex elements ASY1 and ZYP1b upon heat stress.

Confocal images of the nucleus of meiocytes at 21°C (A), HS30°C (B) and HS34°C (C) of SC elements ASY1-RFP (magenta, first row) and ZYP1b-GFP (green, second row) separately and merged (third row) at zygotene (columns 1-3) and pachytene (columns 4-5). Scale bar, 10 µm.

2.7. Defects in early prophase I cause an elongation of pachytene/diakinesis

Seeing defective SC formation at 34°C, we asked whether events between zygotene and pachytene were particularly sensitive to heat stress and hence, responsible for the delay of NEB. Therefore, we specifically applied heat stress only from MT state 2-3-4 (zygotene) onward (called late HS) and compared the effect of this treatment to the previously applied heat shock before MT state 1, *i.e.* from pre-meiosis-leptotene onward (referred to as early HS), by live cell imaging. Since we showed above that male meiocytes perceive heat stress in less than 15 min, we were confident that a late heat shock would allow us to distinguish the temperature effects on early versus late prophase faithfully.

We calculated the predicted median time of MT array state 5-6 as described above and performed a comparison between early and late HS. We did not observe a difference between HS30°C applied early or late (difference of 52 min [CI -11-115 min]), with a predicted median time of 313 min for MT array state 5-6 at late HS30°C (CI 270-355 min, **Figure 1.5, Supplemental Table S1.1, Supplemental Table S1.2**). Remarkably, the MT array state 5-6 was not extended when we applied HS34°C late in prophase I, since we obtained a predicted median time of 393 min (CI 349-437 min, **Figure 1.5, Supplemental Table S1.1**, for details on differences see **Supplemental Table S1.2**). This observation suggested that the prolongation of MT array state 5-6 is predominantly due to temperature-sensitive events in early steps in prophase I, *e.g.* the initiation of meiotic recombination, that subsequently affect the duration of pachytene/diakinesis.

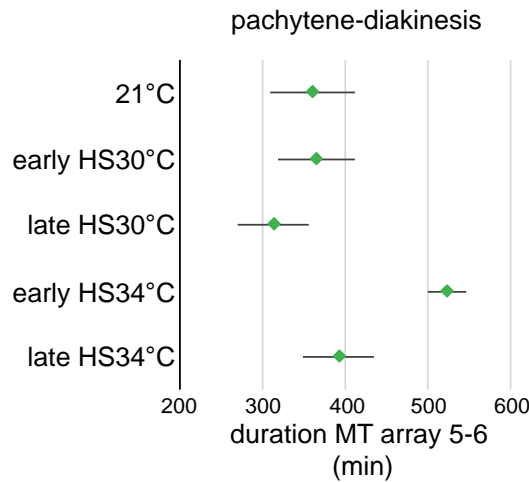


Figure 1.5. Effect of early and late heat shock on the duration of MT array state 5-6.

Predicted median time (in min) with 95% confidence intervals of pachytene-diakinesis (MT array state 5-6; green) at 21°C, early HS30°C versus late HS30°C and early HS34°C versus late HS34°C. 21°C, early HS30°C and early HS34°C, as shown in Figure 2B'.

2.8. Loss of recombination per se does not cause the elongation of pachytene/diakinesis

To address to what degree a failure of recombination causes a pachytene/diakinesis delay, as observed in animals (Crichton et al., 2018), we first made use of the well-characterized *spo11-1* mutant, in which recombination is completely abolished due to a failure to form DSBs (Grelon et al., 2001; Hartung et al., 2007). We introduced the *TagRFP-TUA5* reporter in *spo11-1*, allowing us to follow meiotic progression by using live cell imaging and MT state-based determination of meiotic phases from 27 anther sacs with a total of 224 observed meiocytes (**Supplemental Movie S1, Table 1.1, Supplemental Table S1.1**).

Interestingly and not previously recognized, early prophase (MT array state 2-3-4, late leptotene to early pachytene) was clearly extended in *spo11-1* mutants, with a predicted median time of 1,119 min (CI 1,031-1,206 min, **Figure 1.6A**), *i.e.* a difference of 274 min (CI 143-405 min) with the wild type (**Supplemental Table S1.2**).

Important for this study, the duration of MT array state 5-6 in *spo11-1* (predicted median time of 374 min [CI 349-399 min], **Figure 1.6B**) was not relevantly different compared to the wild type (with a difference of 14 min [CI -36-64 min], **Supplemental Table S1.2**). This result suggested that the complete loss of

recombination caused by the absence of DSBs in the *spo11-1* mutant does not lead to a prolongation of MT array state 5-6 at 21°C.

After prophase I, the meiotic division in *spo11-1* mutants continued with a predicted median time of 72 min (CI 67-76 min) for MT array state 7-8-9, followed by MT array state 10-11 with 63 min (CI 58-67 min), MT array state 12-13 with 48 min (CI 45-52 min) and finally MT array state 14 with 356 min (CI 326-385 min) (**Supplemental Figure S1.4**). Of note, the durations of MT array state 7-8-9, MT array state 10-11, and MT array state 14 in the *spo11-1* mutant were slightly longer compared to the wild type (for details on differences see **Supplemental Table S1.2**).

Next, we asked whether a prolongation of MT array state 5-6 depend on homologous recombination (HR) repair by following meiosis in *dmc1* mutants in which we introduced the *TagRFP-TUA5* reporter and observed a total of 157 meiocytes from 24 anther sacs (**Supplemental Movie S2, Table 1.1, Supplemental Table S1.1**). In *dmc1* mutants, DSBs are repaired through the sister chromatid of the same chromosome in an HR-dependent manner (Kurzbauer et al., 2012). We calculated the predicted median time per state, which returned a duration of 1,056 min for MT array state 2-3-4 (CI 929-1,184 min, **Figure 1.6A**), which was longer relative to the wild type (with a difference of 211 min [CI 36-386 min], **Supplemental Table S1.2**) and resembling the extension of this phase seen in *spo11-1*. Thus, loss of early recombination steps appeared to trigger a prolongation of early meiosis in Arabidopsis, although it is currently not clear whether the extensions in *spo11-1* and *dmc1* have the same underlying reason. For MT array state 5-6 in *dmc1*, we determined a similar duration of 343 min (CI 331-355 min, **Figure 1.6B**) compared to the wild type (360 min, **Figure 1.2B'**); hence, we also did not observe a temporal extension of MT array state 5- 6 for *dmc1* mutants (for details on differences see **Supplemental Table S1.2**). The meiotic division continued with a predicted median time of 67 min (CI 63-71 min) for MT array state 7-8-9. MT array state 10-11 took 63 min (CI 59-67 min), MT array state 12-13 lasted 47 min (CI 45-49 min) and MT array state 14 spanned 281 min (CI 262-301 min, **Supplemental Figure S1.4**). All these subsequent phases had durations similar to those in *spo11-1* (for details on differences see **Supplemental Table S1.2**).

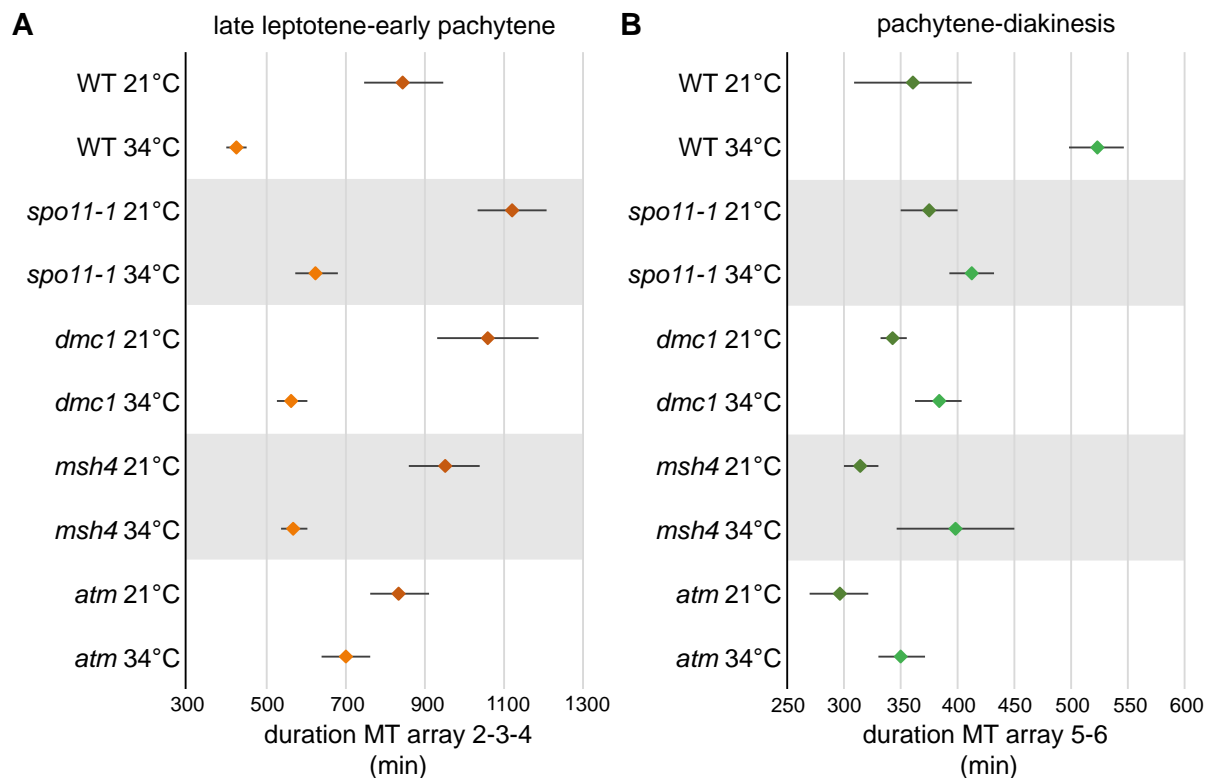


Figure 1.6. Duration of prophase in the recombination mutants *spo11-1*, *dmc1*, *msh4* and *atm* at 21°C and HS34°C.

(A, B) Predicted median times (in min) with 95% confidence intervals of (A) late leptotene-early pachytene (MT array state 2-3-4; orange) and (B) pachytene-diakinesis (MT array state 5-6; green) in the wild type (as shown in Figure 2A',B') and recombination mutants *spo11-1*, *dmc1*, *msh4* and *atm* at 21°C and HS34°C.

Finally, we tested whether a failure to resolve recombination intermediates as Type I COs might be responsible for the delayed onset of NEB, using *msh4* mutants harboring the *TagRFP-TUA5* reporter (**Supplemental Movie S3**). Accordingly, we observed a total of 193 meicytes from 26 anther sacs and calculated the predicted median time for every stage (**Table 1.1, Supplemental Table S1.1**). In *msh4*, MT array state 2-3-4 took 951 min (CI 861-1040 min, **Figure 1.6A**). This duration was not relevantly different from that of the wild type (with a difference of 106 min [CI -18-230 min], **Supplemental Table S1.2**) but lied in between the CI for the wild type and the CI for *spo11-1* and *dmc1* mutants. Hence, it was difficult at this point to judge from this dataset whether this extension was biologically relevant in comparison to the wild type and resembled the situation found in the other two recombination mutants.

Subsequently, we determined a duration of 314 min (CI 299-329 min) in *msh4* for MT array state 5-6 (**Figure 1.6B**). The meiotic division continued with an

extended MT array state 7-8-9 for 67 min (CI 65-72 min, **Supplemental Figure S1.3A**) compared to the wild type (with a difference of 21 min [CI 16-25 min], **Supplemental Table S1.2**), which was similar to the extension seen in *spo11-1* and *dmc1*. Next, MT array state 10-11 in *msh4* lasted 59 min (CI 56-63 min), MT array state 12-13 took 49 min (CI 46-52 min) and finally, MT array state 14 spanned 274 min (CI 253-294 min, **Supplemental Figure S1.3B-D**). Thus, all recombination mutants tested displayed a similar duration of MT array states 5-6 and 12-13, compared to the wild type (for details on differences see **Supplemental Table S1.2**).

Yet, *msh4* mutants progressed through pachytene/diakinesis as wild-type plants at 21°C. Previous 5'-bromo-2'-deoxyuridine (BrdU) labeling experiments in Arabidopsis had shown a delay of 8 h for S-phase to the end of prophase I in *msh4* mutants that we did not see in our experiments. Notably, our time predictions did not include meiotic S-phase and early leptotene, where MSH4 is known to start appearing as numerous foci on the axes (Higgins et al., 2004). Thus, considering all data, it is likely that Arabidopsis *msh4* mutants are particularly delayed in the pre-meiotic S-phase given its known role in repairing DNA base-pair mismatches, which take place during DNA replication (Santucci-Darmanin et al., 2002).

Taken together, these results indicated that the loss of recombination *per se* does not cause the elongation of the MT array state 5-6 seen in wild-type meiocytes at 34°C.

2.9. Prolongation of MT array state 5-6 is largely recombination-dependent

To then investigate the role of the recombination pathway on the elongation of MT array state 5-6 upon very high temperature heat stress, we characterized a total of 198 meiocytes from 25 anther sacs and analyzed the duration of this phase in *spo11-1* mutants at HS34°C (**Supplemental Movie S4, Table 1.1, Supplemental Table S1.1**). As with heat shock treatments of wild-type meiocytes, we only used only flower buds in MT array state 1 to model the duration of the different meiotic states at HS34°C.

The MT array state 2-3-4 of *spo11-1* had a predicted median time of 626 min (CI 572-681 min, **Figure 1.6A**), which was shorter in duration compared to *spo11-1* at 21°C (with a difference of 492 min [CI 389-595 min], **Supplemental Table S1.2**), showing a similar reduction of 417 min (CI 315-519 min, **Supplemental Table S1.2**) as described for wild-type meiocytes. Notably, the elongation of MT array state 5-6

seen in the wild type at HS34°C (a difference of 162 min [CI 104-219 min] compared to 21°C, **Figure 1.2B'**, **Supplemental Table S1.2**) was not found in *spo11-1* mutant at HS34°C, with a predicted median time of 412 min (CI 393-431 min, **Figure 1.6B**), compared to *spo11-1* at 21°C (a difference of 38 min [CI 6-70 min], **Supplemental Table S1.2**). Further, MT array state 7-8-9 took 35 min (CI 32-38 min), MT array state 10-11 spanned 54 min (CI 49-58 min) and MT array state 12-13 lasted 23 min (CI 21-26 min, **Supplemental Figure S1.3A-C**). All these states, with the exception of MT array states 2-3-4 and 5-6, were not relevantly different compared to the wild type at HS34°C (**Supplemental Table S1.2**). Furthermore, all these states showed a reduction similar in length to that described for the wild type at HS34°C versus 21°C. For MT array state 14 in *spo11-1* at HS34°C, we did not calculate median time, as we did not for the wild type at HS34°C.

This result suggested that the delay in the wild type at the very high temperature of 34°C is not due to the absence of recombination, but rather due to aberrant recombination intermediates; in their absence, as in *spo11-1* mutants, meiosis progresses without delay. To further explore this possibility, we next observed a total of 160 *dmc1* and 116 *msh4* meiocytes from 19 and 17 anther sacs, respectively, and measured the duration of MT array state 5-6 at HS34°C (**Supplemental Movies S5-6, Table 1.1, Supplemental Table S1.1**). The predicted median time of MT array state 2-3-4 upon HS34°C was 565 min (CI 526-605 min) for *dmc1* mutants and 571 min (CI 536-606 min) for *msh4* mutants, representing a decrease relative to their median time at 21°C (**Figure 1.6A**, (for details on differences see **Supplemental Table S1.2**). The predicted median time of MT array state 5-6 of *dmc1* and *msh4* at HS34°C was 383 min (CI 362-403 min) and 398 min (CI 346-450 min), respectively (**Figure 1.6B**).

Finally, *dmc1* and *msh4* mutant plants continued meiosis at HS34°C, with MT array state 7-8-9 of 30 min (CI 28-32 min) and 32 min (CI 30-34 min); MT array state 10-11 lasting 57 min (CI 54-60 min) and 49 min (CI 43-55 min); and MT array state 12-13 taking 22 min (CI 21-23 min) and 24 min (CI 22-26 min), respectively (**Supplemental Figure S1.3A-C**). Similar to the wild type and *spo11-1* at HS34°C, we were unable to obtain a predicted median time for the MT array state 14.

In summary, the analyses of *dmc1* and *msh4* together with the data obtained for *spo11-1* strongly suggested that aberrant recombination structures are largely

responsible for the delay of pachytene/diakinesis observed in the wild type. However, compared to the timing of these three mutants at 21°C, their durations at 34°C were also slightly longer (**Figure 1.6B, Supplemental Table S1.2**). Thus, it is also likely that an unknown and recombination-independent component appears to contribute to the observed elongation.

2.10. A specialized pachytene checkpoint in Arabidopsis

Our results illustrating the prolongation of pachytene/diakinesis was reminiscent of the pachytene checkpoint of animals and yeast. However, the observation that mutants devoid of recombination nevertheless go through meiosis in plants (as quantified above) has previously raised the hypothesis that plants do not have a pachytene checkpoint (Caryl et al., 2003; Couteau et al., 1999; Grelon et al., 2001; Higgins et al., 2004; Jones and Franklin, 2008; Li et al., 2004; Li et al., 2009b). A central executor of the pachytene checkpoint in yeast and animals is the checkpoint kinase ATM (Lange et al., 2011; Pacheco et al., 2015; Penedos et al., 2015). ATM is highly conserved and also plays a major role in meiosis in Arabidopsis, for instance for the repair of DSBs (Garcia et al., 2003; Kurzbauer et al., 2021; Lange et al., 2011; Li et al., 2004; Yao et al., 2020).

We hypothesized that if the observed extension of MT array state 5-6 in the wild type is due to a pachytene checkpoint, *atm* mutants should also suppress this extension. To test this idea, we introduced the *TagRFP-TUA5* reporter in the *atm* mutant and followed meiotic progression at 21°C and HS34°C using live cell imaging by observing a total of 228 and 172 meiocytes from 28 and 23 anther sacs, respectively. We then determined the duration of the MT array states as described before (**Supplemental Movies S7-8, Table 1.1, Supplemental Table S1.1**).

At 21°C, MT array state 2-3-4 lasted 834 min (CI 761-908 min) while MT array state 5-6 took 295 min (CI 270-321, **Figure 1.6**) in the *atm* mutant. Thus, *atm* meiocytes progressed even faster than the wild type through MT array state 5-6 (with a difference of 65 min [CI 7-123 min], **Supplemental Table S1.2**), hinting at a possible role in prolonging pachytene/diakinesis even under control conditions. Next, we measured the duration of MT array state 7-8-9 at 45 min (CI 42-49 min), MT array state 10-11 at 60 min (CI 55-66 min), MT array state 12-13 at 43 min (CI 40-46 min) and MT array state 14 at 245 min (CI 230-260 min, **Supplemental Figure S1.3**). Thus, MT array state 10-11 and 14 were slightly longer than in the wild type

(for details on differences see **Supplemental Table S1.2**). The reason for this extension is not clear at the moment.

Upon exposure to HS34°C, MT array state 2-3-4 had a predicted median time of 702 min (CI 640-764 min); strikingly, the prolongation of MT array state 5-6 seen in the wild type was largely abolished, as the difference between *atm* mutants HS34°C and 21°C was only 55 min (CI 22-87 min) versus a difference of 162 min (CI 104-219 min) between the wild type at HS34°C and 21°C (**Figure 1.6, Supplemental Table S1.2**).

The durations of the other MT array states were not relevantly different compared to the wild type at HS34°C, *i.e.* MT array state 7-8-9 lasted 31 min (CI 29-33 min), MT array state 10-11 took 55 min (CI 50-60 min) and MT array state 12-13 spanned 26 min (CI 23-28 min) (**Supplemental Figure S1.3A-C**, for details on differences see **Supplemental Table S1.2**). The duration of MT array state 14 at HS34°C could not be determined as before.

These results implicated ATM in the prolongation of pachytene/diakinesis at HS34°C. Given the similarities in extension of pachytene/diakinesis, *i.e.* dependency on recombination and the involvement of ATM, we conclude that Arabidopsis and likely other plants do have a specialized variant of the pachytene checkpoint that relies on the action of ATM and possibly other regulators to monitor aberrant recombination intermediates at high temperatures but, in contrast to animals, not the absence of recombination itself.

3. DISCUSSION

More than 50 years ago, the consequences of high temperature on plant development in general and on meiosis in particular were already being studied (Dowrick, 1957; Pao and Li, 1948; Wilson, 1959). Due to the dire outlook caused by climate change, research on the influence of temperature on meiosis has been revived. Previous and current studies have relied on the analysis of fixed samples and obtained important insights into the duration of meiosis and meiotic recombination patterns at elevated temperatures (Brown et al., 2020; De Storme and Geelen, 2020; Modliszewski et al., 2018). Here, we followed a complementary approach by following meiosis by time-lapse live cell imaging. This method allowed us to obtain a highly temporally resolved dissection of meiotic progression in which we compared the effects of three heat stress treatments, *i.e.* a heat shock at 30°C and 34°C and a long-term (one week) treatment at 30°C in comparison to the control temperature of 21°C. Notably, this work provided novel insights into the effects of temperature on recombination as well as meiotic progression and set the stage for revising a current dogma in the field.

3.1. Formation of stress granules during meiosis

Heat stress induces a multitude of cellular responses, including the inhibition of general translation and the formation of SGs, which are proposed to function as transient places for both storage and degradation of proteins and mRNAs during stress resulting in translational re-programming. The formation of SGs is thought to be especially important for the re-initiation of translation upon recovery from the stress condition, as reviewed previously (Anderson and Kedersha, 2002, 2008; Buchan and Parker, 2009). In mice spermatocytes, SGs were previously shown to be formed after heat treatment (42°C) and these SGs contained for instance Deleted in azoospermia-like (DAZL), an RNA-binding protein that interacts with the SC, is involved in mRNA transport and is proposed to function as a translational activator (Kim et al., 2012).

By fluorescently labeling the major cell cycle regulator of Arabidopsis CDKA;1, we showed here that meiocytes in Arabidopsis also form SGs at 30°C and 34°C. CDKA;1 was previously demonstrated along with several other proteins, like MITOGEN ACTIVATED PROTEIN KINASE 3 (MPK3) and the TARGET OF

RAPAMYCIN COMPLEX 1 (TORC1), to be present in SGs of heat-stressed seedlings (Kosmacz et al., 2019). The presence of CDKA;1 in SGs was hypothesized to allow a cell to resume cell division activity in Arabidopsis after attenuation of the stress (Kosmacz et al., 2019). CDKs typically require a co-factor, called cyclin, for their activity; in budding yeast, the RNA-binding protein WHISKEY 8 (WHI8) was shown to bind to and recruit the mRNA of the cyclin CLN3 to SGs upon heat stress, causing the inhibition of *CLN3* mRNA translation (Yahya et al., 2021). Interestingly, Cell Division Cycle 28 (CDC28), the homolog of CDKA;1 in budding yeast, is itself also recruited to SGs by WHI8 and has been found to play an important role in SG dissolution and the translation of SG-recruited mRNAs, such as for *CLN3*, upon release from stress.

Might Arabidopsis CDKA;1 also be a mediator of SG dissolution and subsequent re-initiation of translation? Interestingly, many proteins related to translation were previously identified as putative CDKA;1 substrates (Pusch et al., 2011). A pivotal role of translational control for the abundance of proteins in meiosis has been established in several organisms including budding yeast (Brar et al., 2012)., raising the possibility that translational regulation of meiosis in Arabidopsis is also present and likely controlled by CDK activity.

The appearance of CDKA;1 in SGs allowed us to faithfully confirm the application of the heat stress in meiocytes. On the one hand, we were able to show that the heat stress reaches meiocytes relatively fast, *i.e.* in less than 15 min. Thus, all our imaging started when meiocytes are already exposed to the desired applied temperature in our set-up. On the other hand, we observed that SGs are not regularly found at 30°C. Thus, the appearance of SGs highlights meiocytes experiencing temperature stress above 30°C. Since SGs formed rapidly at 34°C, we hypothesize that the heat stress at 30°C also reaches meiocytes in a similar time frame, offering us the confidence that we are looking at an immediate effect of the high temperature rather than a ramping effect over a long period. We anticipate that the formation of CDKA;1-containing SGs may be used as a general readout to study heat stress in other plant tissues and possibly other plant species as well.

Interestingly, the localization of CDKA;1 to SGs was stage-specific and its SG localization was only observed from pachytene onward but not earlier in meiosis. Notably, DAZL also shows a stage-specific localization to SGs in mice

spermatocytes and is recruited to SGs only during pachytene in response to heat, coinciding with its highest accumulation level (Kim et al., 2012). In comparison, CDKA;1 dynamically localized to the nucleus and the cytoplasm and the formation of CDKA;1-positive SGs appeared when its cytoplasmic portion was the highest. Therefore, whether the formation of CDKA;1-positive SGs is dependent on its high cytoplasmic concentration or whether the presence of CDKA;1 in SGs relies on other meiotic stage-specific parameters needs to be determined. Conversely, it is also not clear whether non-CDKA;1-containing SGs form prior to pachytene.

3.2. Heat and meiotic progression

The changes in duration for meiosis upon high temperatures were studied in several plant species including *Arabidopsis*, barley, wheat, *Dasypyrum villosum* (L.) P. candargy and bluebell (*Hyacinthoides non-scripta*) (Bennett et al., 1972; Draeger and Moore, 2017; Higgins et al., 2012; Stefani and Colonna, 1996; Wilson, 1959). These studies have relied on static analyses of fixed material, e.g. anther fixation and staging before and after a certain time interval or BrdU pulse labeling followed by the analysis of meiotic chromosome figures (Armstrong et al., 2003; Bennett et al., 1972). These studies concluded that the duration of meiosis hastens at high temperatures. Here, we confirmed this general trend of increased meiotic speed at high temperatures. However, our live cell imaging approach allowed us to follow meiotic progression with great depth, generating quantitative data that can be statistically analyzed, which led to the finding that not all meiotic phases respond equally to an increase in temperature. For instance, the progression into interkinesis in the wild type was considerably delayed at 34°C. The underlying reasons for this delay are currently unclear, but it is an interesting speculation that there are several as yet recognized control point/checkpoints during meiosis.

Most strikingly, we discovered that pachytene/diakinesis are in particular extended at 34°C when compared to control conditions at 21°C, as seen by a considerable prolongation of the time of NEB. This observation opens the door to study which regulators and/or processes are sensitive to heat, for instance with respect to controlling NEB. However, how NEB is controlled in plants is still an enigma, especially since lamins do not appear to be conserved in plants (Ciska and Moreno Diaz de la Espina, 2013; Fiserova and Goldberg, 2010). Notably, NEB likely represents a gate in meiotic progression. Chromosomes are strong microtubule

organizing structures in plants (Lee and Liu, 2019), and once the nuclear envelope is broken down, the MT array that is enriched around the nucleus quickly connects to the chromosomes and organizes itself into a spindle (Prusicki et al., 2019). Thus, a delay of NEB represents a physical barrier that provides additional time to complete and/or correct processes in the reaction environment of the nucleus before chromosomes start to be moved in the cell.

3.3. Heat and meiotic recombination

The observed extension of pachytene/diakinesis under heat stress prompted us to genetically and temporally dissect this effect. An obvious cause for the observed prolongation was altered meiotic recombination, supported by this study and previous analyses in *Arabidopsis* and barley of meiotic chromosome configurations (De Storme and Geelen, 2020; Hedhly et al., 2020; Higgins et al., 2012). Using mutants in genes that control different steps in the meiotic recombination process, like *spo11-1*, *dmc1*, and *msh4*, we showed that the extension of pachytene/diakinesis is recombination-dependent, *i.e.* the extension of pachytene/diakinesis was lost in these mutants at 34°C. Notably, these mutants, when grown under non-stress conditions at 21°C, did not display a relevant prolongation of late pachytene (MT array state 5-6) in a detectable manner with our assays. This result stands in contrast to animals where loss of recombination, *e.g.* in *dmc1* mutant mice, triggers meiotic arrest and subsequently induces cell death (Barchi et al., 2005; de Rooij and de Boer, 2003; Roeder and Bailis, 2000).

To further narrow down the origin of the elongation of pachytene/diakinesis, we applied heat stress only around zygotene, *i.e.* up to 17 h later than in our first sets of experiments. Importantly, this late heat stress did not cause a prolongation, suggesting that recombination appears to be affected prior to SC formation. This observation is interesting, since earlier work in barley and *A. ursinum* indicated that the SC is severely affected by heat, leading to so-called polycomplexes in which transverse filaments become laterally connected; a study in *C. elegans* suggested that ZYP1 aggregation upon high temperature primarily reflects a failure of SC assembly (Bilgir et al., 2013; Higgins et al., 2012; Loidl, 1989). In addition, temporal dissection of heat stress on spermatocytes of the desert locust (*Schistocerca gregaria*) revealed that heat-induced chiasma frequency changes are most likely the consequence of the completeness or efficiency of pairing (Henderson, 1988). Thus,

we conclude that already very early recombination processes, such as pairing of homologs, are affected by heat and that these aberrant processes likely cause the formation of polycomplexes.

From our mutant analysis and chromosome spreads at elevated temperatures, it is likely that recombination intermediates cause this delay. What the structure of these intermediates is and how they cause a delay needs to be investigated in the future. Possibly, the delay is triggered by non-homologous recombination caused by mispairing and hence partially interconnected chromosomes. Analysis of a *zmm* mutant in yeast revealed that a specific block in progression of CO formation occurs at high temperatures, resulting in the formation of intermediates and/or interactions with sister chromatids (Borner et al., 2004). Further, it is well known from yeast that unresolved recombination intermediates can cause nuclear division defects (Kaur et al., 2015; Kaur et al., 2019; Tang et al., 2015).

Notably, our work also revealed a previously unrecognized delay of the recombination mutants *spo11-1* and *dmc1* in early meiosis of Arabidopsis, i.e. in late leptotene/early pachytene, at both high and low temperatures with respect to the wild type. A similar extension was clearly seen for *msh4* at HS34°C, with a corresponding tendency for a delay at 21°C. Matching our observations, mutants in *dmc1* in yeast are delayed, too, which was explained by the absence of axial associations between homologs (Rockmill et al., 1995). However, nearly complete synapsis can be detected in *dmc1* mutants in yeast after a substantial delay, while in Arabidopsis *dmc1* mutants stay strictly asynaptic (Couteau et al., 1999). Possibly, this difference is also due to the differently acting pachytene checkpoints in both species (see below).

Another difference between yeast and Arabidopsis concerns *spo11* mutants, which progress faster through prophase I in the yeast mutant than its wild-type strain, whereas, as shown in this study, Arabidopsis *spo11* mutants are delayed in early prophase in meiosis (Cha et al., 2000; Jiao et al., 1999; Klapholz et al., 1985). The different behavior of these mutants cannot currently be resolved, but possibly hints at different mechanisms of homolog interaction in yeast versus Arabidopsis.

3.4. A specialized pachytene checkpoint in Arabidopsis

Aberrant recombination structures and the absence of recombination trigger an arrest in late prophase I in animals and yeast, executed by the so-called pachytene checkpoint (Barchi et al., 2005; Bishop et al., 1992; Rockmill et al., 1995). Since in plants mutants in which recombination is abolished, such as *dmc1*, are not arrested in meiosis, it has been proposed that plants do not possess a pachytene checkpoint (Caryl et al., 2003; Couteau et al., 1999; Grelon et al., 2001; Higgins et al., 2004; Jones and Franklin, 2008; Li et al., 2004; Li et al., 2009b).

A major regulator of the pachytene checkpoint in animals and yeast is the checkpoint kinase ATM (Barchi et al., 2005; Lange et al., 2011; Pacheco et al., 2015; Penedos et al., 2015; Roeder and Bailis, 2000). Removing ATM in mutants that trigger the pachytene checkpoint in mice spermatocytes, for instance in weak loss-of-function mutants for Trip13 (Thyroid Hormone Receptor Interactor 13, also known as PCH2 [Pachytene checkpoint protein homolog 2]), restores progression through pachytene, indicating that the early arrest is under control of this checkpoint kinase (Pacheco et al., 2015).

In budding yeast, *atm* mutants undergo the first meiotic division before all recombination events are complete (Lydall et al., 1996; Stuart and Wittenberg, 1998). Correspondingly, we found that the pachytene/diakinesis extension is lost in Arabidopsis *atm* mutants, implicating ATM in this checkpoint and the execution of the observed meiotic delay, e.g. by sensing aberrant recombination structures. Together with our finding that the prolongation of pachytene/diakinesis is recombination-dependent, we conclude that Arabidopsis and likely other plants do have a pachytene checkpoint. However, this checkpoint appears to be less stringent than in animals, since it does not respond to the absence of meiotic recombination. Moreover, the extension is temporally restricted and typically after 2.7 h meiosis continues. After the nature of the presumptive aberrant recombination intermediates becomes better understood, it should be determined whether they are resolved during this time or whether the checkpoint erodes, i.e. meiosis progresses even though checkpoint conditions are not fulfilled. An erosion has been observed for another checkpoint in plants, i.e. the spindle assembly checkpoint, which ensures that all chromosomes are connected to microtubule fibers of the spindle. Triggering this checkpoint was only able to delay the onset of anaphase by at most less than 2

h (Komaki and Schnittger, 2017). Notably, the spindle assembly checkpoint can also erode in mammals and yeast, although typically only after several hours (Rieder and Maiato, 2004; Rossio et al., 2010).

It is an interesting discussion point whether less stringent cell division checkpoints (pachytene and SAC) represent an evolutionary strategy in plants. Genome mutations, especially polyploidization events, are more prominent in plants than in animals and are suspected to be a major driving force of their evolution (Brownfield and Kohler, 2011; De Storme and Geelen, 2013b; Li et al., 2009b; Wijnker and Schnittger, 2013). Moreover, hybridization events are very frequent in plants. An alien genome would likely affect recombination by either reducing it or causing aberrant recombination structures. Less stringent checkpoints would pave the road for hybridization events since by chance viable combinations of chromosomes are generated. Especially an interplay between a relaxed pachytene checkpoint and a relaxed SAC may promote rapid genome evolution, as often found in plant species.

4. MATERIAL AND METHODS

4.1. Plant materials and growth conditions

All *Arabidopsis* (*Arabidopsis thaliana*) plants used in this study were in the Columbia (Col-0) accession. The *CDKA;1-mVenus TagRFP:TUA5* double reporter line, *KINGBIRD reporter line 2* (*REC8pro:REC8-GFP RPS5Apro:TagRFP-TUA5*) and the *ASY1-RFP ZYP1b-GFP* double reporter line have been previously described (Prusicki et al., 2019; Sofroni et al., 2020; Yang et al., 2019; Yang et al., 2020). Seeds for T-DNA insertion mutants for *DMC1* (GABI_918E07), *SPO11-1* (SALK_146172), *MSH4* (SALK_136296) and *ATM* (SALK_006953) were obtained from the GABI-Kat T-DNA mutation collection and the collection of T-DNA mutants of the Salk Institute Genomic Analysis Laboratory (<http://signal.salk.edu/cgi-bin/tdnaexpress>) via NASC (<http://arabidopsis.info/>) (for genotyping primers see **Supplemental Table S1.3**).

Seeds were surface sterilized with chlorine gas and germinated on 1% (w/v) agar containing half-strength Murashige and Skoog (MS) salts and 1% (w/v) sucrose, pH 5.8. When required, antibiotics were added for seed selection. All plants were grown under long-day conditions (16-h light at 21°C (+/- 0.5°C)/ 8-h dark at 18°C (+/- 0.5°C), with 60% humidity). For short-term heat treatment, plants were first grown under standard long-day conditions until flowering. Flower buds were then harvested and cultured on agar in petri plates *ex vivo* as previously described (Prusicki et al., 2020). These plates were then exposed to heat shock by transfer to a preheated incubation chamber (30°C or 34°C) mounted on the microscope stage, where meiotic progression was followed in real time.

For the cytology analysis and protein localization studies, plants were transferred to a climate chamber under a long-day photoperiod with constant temperature (30°C/34°C (+/- 0.5°C)) for 24/16 h prior to fixation/observation, respectively. For long-term heat treatment, healthy plants at the bolting stage were transferred to a climate chamber under a long-day photoperiod with constant temperature of 30°C (+/- 0.5°C) with 60% humidity for 7 d.

4.2. Plasmids and plant transformation

The reporter constructs *RPS5Apro:TagRFP-TUA5* and *KINGBIRD reporter line 2*, previously described (Prusicki et al., 2019), were transformed into the T-DNA insertion mutants by floral dipping. T₁ seeds were selected on half-strength MS medium containing the antibiotics hygromycin. All observations were carried out with T₂ lines.

4.3. Confocal microscopy and intensity plots

For protein localization experiments, healthy flower buds were dissected exposing two anthers and carefully positioned in a petri plate filled with half-strength MS medium, pH 5.8 solidified with 0.8% (w/v) agar, and meiocytes of different meiotic stages were imaged using a Zeiss LSM880 confocal microscope.

For pixel intensity plots, flower buds were dissected and the anthers in MT array state 6 were imaged using a Zeiss LSM880 confocal microscope with the exact same settings for the different heat conditions. The pixel brightness was measured through a region of interest using ImageJ (Schindelin et al., 2012; Schneider et al., 2012) and plotted against the X dimension, which is the distance of the region of interest.

4.4. Live cell imaging and data processing

Live cell imaging was performed as described previously (Prusicki et al, 2019). In short, up to six flower buds of 0.2-0.6 mm were carefully positioned in a petri plate filled with half-strength MS medium, pH 5.8 and solidified with 0.8% (w/v) agar. Time lapse was performed using an upright Zeiss LSM 880 confocal microscope with ZEN 2.3 SP1 software (Carl Zeiss AG, Oberkochen, Germany) and a W-plan Apochromat 40X/ 1.0 DIC objective (Carl Zeiss AG, Oberkochen, Germany). GFP and TagRFP were excited at $\lambda = 488$ nm and 561 nm, respectively, and detected between 498-560 nm and 520-650 nm, respectively. Auto-fluorescence was detected between 680-750 nm. With a time interval of 10 min, a series of six Z-stacks with 50 μ m distance was acquired under a thermally-controlled environment (21°C/30°C/34°C (+/- 0.15%)) in an incubation chamber. Due to sample movement, the Z-planes were manually selected using the review multi-dimensional data function of the software Metamorph Version 7.8 and the XY movement was corrected using the Stack Reg plugin of Fiji.

4.5. Quantitative analysis of the meiotic phases

The analysis of the duration was based on the *TagRFP-TUA5* reporter. Meiocytes were manually assigned to defined MT states (**Supplemental Data Set S1.1 and S1.2**). The data were collected from a minimum of three independent set-ups, with a minimum of eight anthers per genotype per heat treatment. The durations of the meiotic phases were extracted from at least 65 meiocytes.

4.6. Statistical methods

Parametric models for interval-censored survival time data with a clustered sandwich estimator of variance were applied to address the clustering of meiocytes within anther-sacs, including effects of the heat treatment, genotype and their interaction. The underlying distribution of the parametric model was chosen based on the Akaike Information Criterion (AIC) with exponential, Gompertz, log-logistic, Weibull and log-normal distribution as candidates.

The models used information from all cells of which we observed at least one time point in the respective state. The event of interest is the transition of a cell from one state to the next. Each cell for which the exact beginning and end of the state were known was modeled as having an event, with the event time calculated as the difference between the start of the next state and the end of the previous state. Cells where the exact time points of either the transition from the previous state to the state of interest or to the next state were not known were modeled as

interval-censored data points, with the lower limit of the interval being the time where the cell was observed in this specific state and the upper limit of the interval being one time unit after/before the cell was observed in the previous/next state, respectively. If for a cell the state before or after the current state of interest was not observed at all, the cell was modeled as right-censored with the censoring time being the maximum observed time (i.e. the minimum actual time in this state) for this cell in the state of interest. In addition to the individual states, we also calculated a model for the duration from MT array states 2- 13 in an analogous fashion. In specific models, some combinations of heat treatment and genotype had to be excluded because no (or hardly any) events had been observed.

The chosen distributions underlying our parametric model were log-normal for MT array states 7-8-9, 10-11, 12-13 and 14, while a Weibull distribution was selected for MT array states 2-3-4 and 5-6 and the model for the complete duration of MT array states 2-13. Estimation results are presented as predicted marginal median times (or corresponding contrasts), together with 95% confidence intervals (CI). Since the analysis is of an exploratory nature, no adjustment for multiplicity was applied. The statistical analysis was performed with R version 3.5.1 and Stata SE version 16.1. Scripts available at https://github.com/linda-kr/Heatstress_Meiosis.

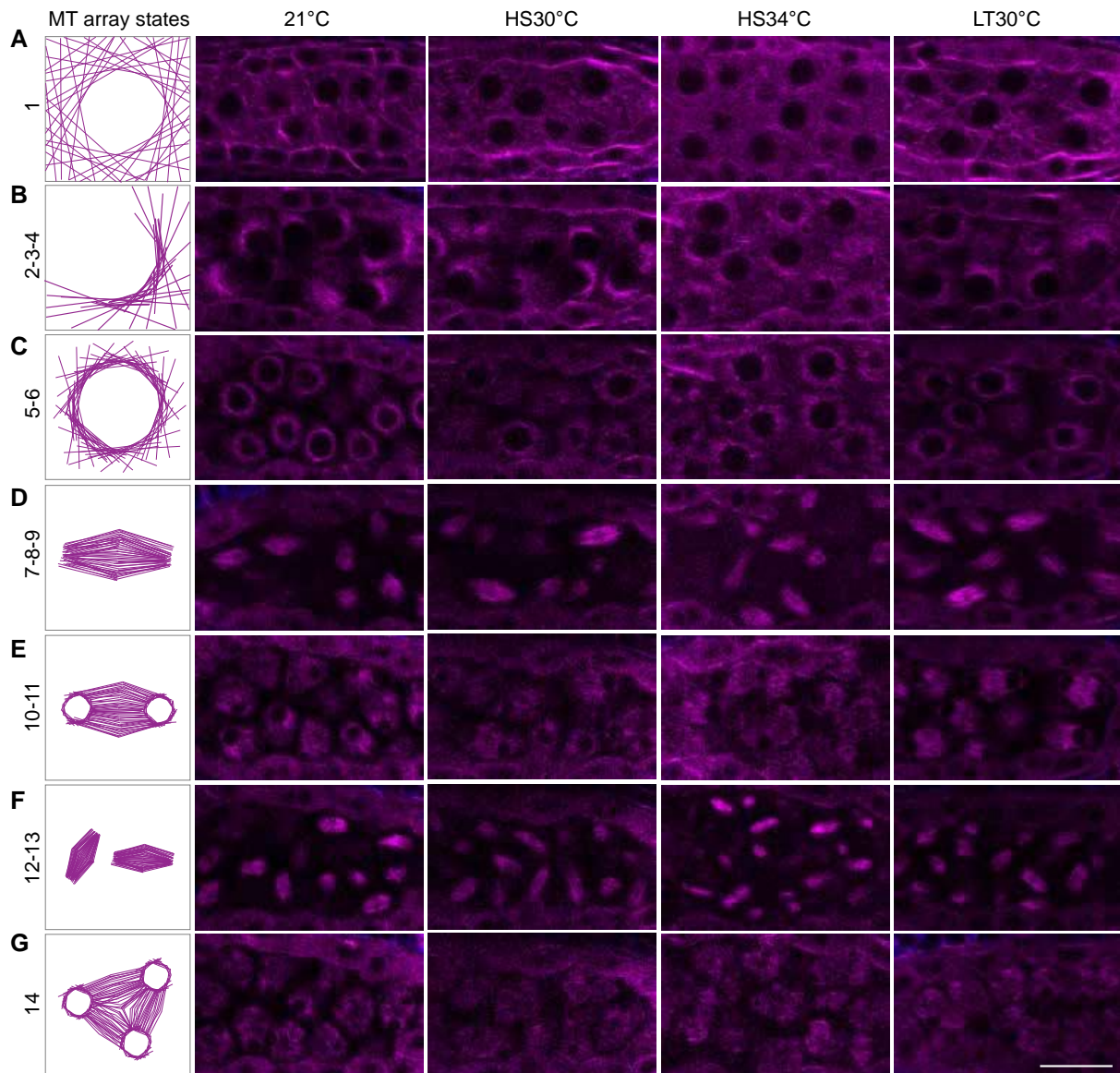
4.7.Cytology

The cytological analysis of the meiocytes under short and long heat treatment was conducted by performing chromosome spreads, as previously described (Sofroni et al., 2020). Briefly, healthy flower buds were fixed in ethanol:acetic acid (3:1, v/v) for a minimum of 24 h at 4°C, following washing steps with 70% (v/v) ethanol and stored at 4°C. Next, flower buds were washed in water and in 10 mM citrate buffer, pH 4.5 and digested in an enzyme mix (10 mM citrate buffer containing 0.5% [w/v] cellulase, 0.5% [w/v] pectolyase and 0.5% [w/v] cytohelicase) for 2.5 h at 37°C. Digested flower buds were squashed and spread onto a glass slide in 45% (v/v) acetic acid on a 46°C hot plate. Finally, the slides were washed in cold ethanol:acetic acid (3:1, v/v) and mounted in Vectashield medium with 4',6-diamidino-2-phenylindole (DAPI, Vector Laboratories).

4.8.Accession numbers

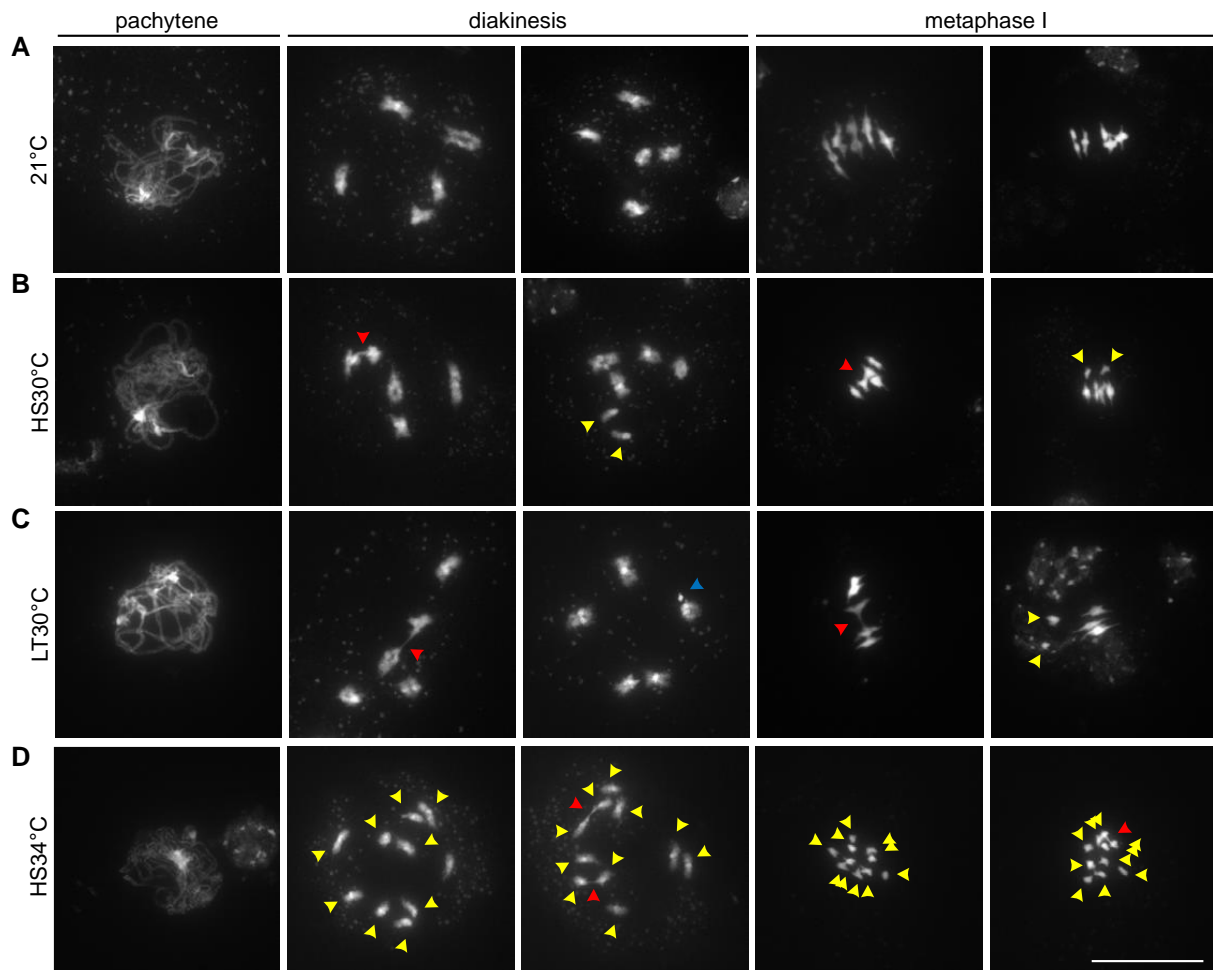
Accession numbers based on The Arabidopsis Information Resource (TAIR) (<https://www.arabidopsis.org>) for all genes examined in this study are *DMC1* (At3g22880), *SPO11-1* (At3g13170), *MSH4* (At4g1738) and *ATM* (At3g48190).

5. SUPPLEMENTAL DATA CHAPTER I



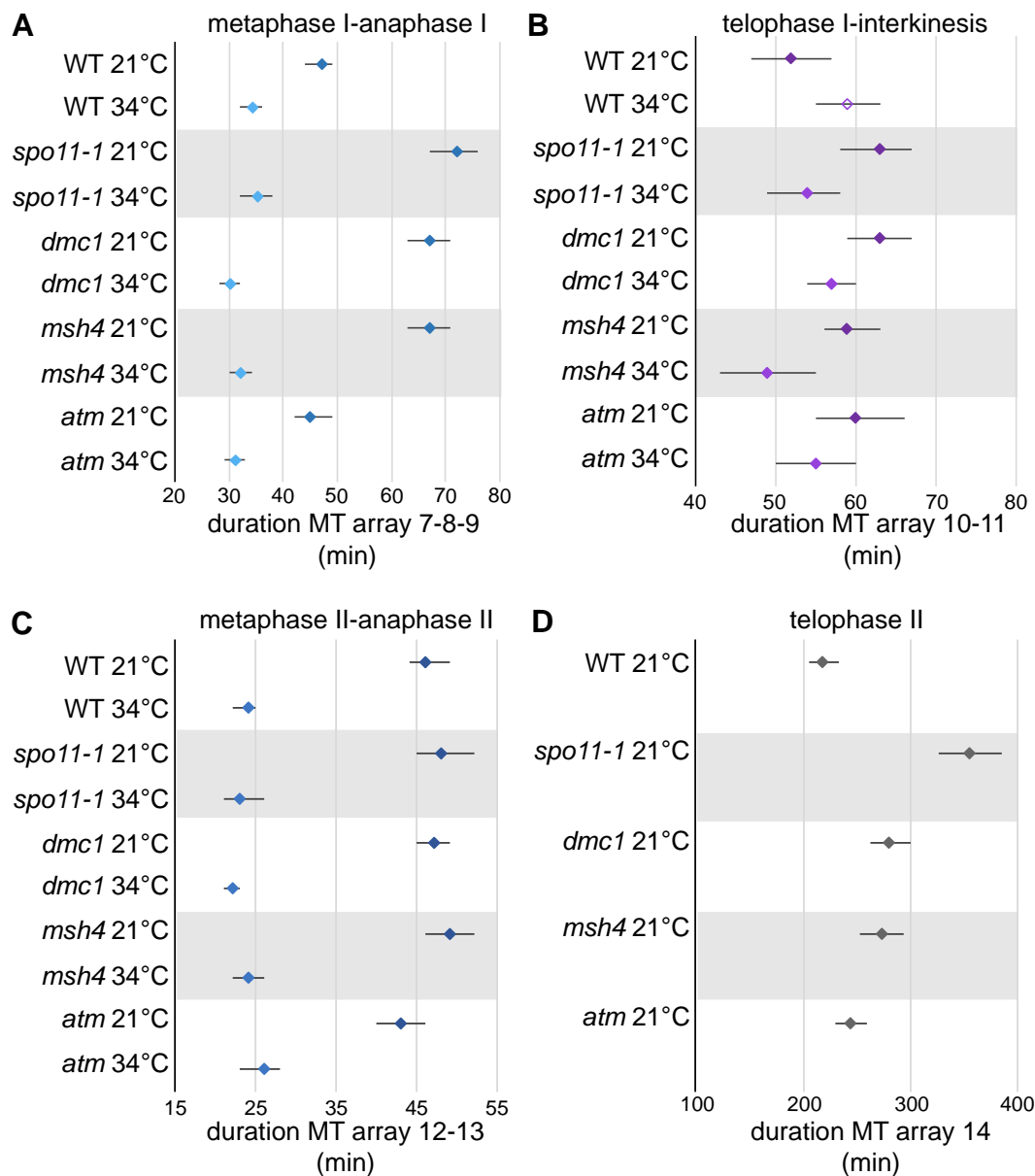
Supplemental Figure S1.1. Microtubule array states upon heat stress.

Images from live cell imaging of TagRFP-TUA5 (magenta) at different temperature regimes, 21°C (column 1), HS30°C (column 2), HS34°C (column 3) and LT30°C (column 4) showing the different MT array states and schematic representation (column 4). (A) MT array state 1. (B) MT array state 2-3-4. (C) MT array state 5-6. (D) MT array state 7-8-9. (E) MT array state 10-11. (F) MT array state 12-13. (G) MT array state 14. Scale bars, 20 μm . (Supports Figure 2)



Supplemental Figure S1.2. Meiotic defects in the wild type upon heat stress.

Cell spreads of wild-type meiocytes at the different temperature regimes: (A) 21°C, (B) HS30°C, (C) LT30°C and (D) HS34°C showing a selection of the meiotic defects from pachytene till metaphase I. Red arrowheads highlight chromosome bridges (B, n=36/73 and 26/65; C, n=52/81 and 11/25; D, n=33/64 and 11/17 for diakinesis and metaphase I, respectively); Blue arrowheads highlight chromosome fragments (n=3/81); Yellow arrowheads highlight univalents (B, n= 2/73 and 4/65; C, n=1/81 and 2/25; D, n=64 and 17 for diakinesis and metaphase I, respectively). Scale bar, 20 μ m. (Supports Figure 2)



Supplemental Figure S1.3. Duration of meiotic phases in the recombination mutants *spo11-1*, *dmc1*, *msh4* and *atm* at 21°C and HS34°C.

Predicted median times (in min) with 95% confidence intervals at control (21°C, as shown in Figure 2C-F) and HS34°C of the MT array states 7-14; (A; light blue) MT array state 7-8-9, metaphase I-anaphase I; (B; purple) MT array state 10-11, telophase I-interkinesis; (C; dark blue) MT array state 12-13, metaphase II-anaphase II; (D; gray) MT array state 14, telophase II. (Supports Table 1)

Supplemental Table S1.2. Pairwise comparison of the meiotic phases.

The pairwise difference in median times and the 95% confidence intervals (in min) of MT array state 2-3-4 (late leptotene-early pachytene), MT array state 5-6 (pachytene- diakinesis), MT array state 7-8-9 (metaphase I- anaphase I), MT array state 10-11 (telophase I- interkinesis), MT array state 12-13 (metaphase II- anaphase II) and MT array state 14 (telophase II) between the wild type at 21°C, HS30°C (early-late), HS34°C (early-late), LT30°C; mutants *spo11-1*, *dmc1*, *msh4* and *atm* at 21°C and HS34°C. NA: not analyzed. (Supports Figure 2 and Figure 6)

Pairwise difference	2-3-4 late leptotene- early pachytene			5-6 pachytene- diakinesis			7-8-9 metaphase I- anaphase I			10-11 telophase I- interkinesis			12-13 metaphase II- anaphase II			14 telophase II			
	Meiotic stage	Dif. in median times	95% Conf. Interval	Dif. in median times	95% Conf. Interval	Dif. in median times	95% Conf. Interval	Dif. in median times	95% Conf. Interval	Dif. in median times	95% Conf. Interval	Dif. in median times	95% Conf. Interval	Dif. in median times	95% Conf. Interval				
WT HS30°C - WT 21°C		-289	-410	-167	4	-66	74	-15	-19	-10	-6	-13	2	-17	-21	-14	-10	-38	18
WT HS30°C - WT LT30°C		-52	-145	40	-13	-73	47	7	-13	-1	2	-6	11	-8	-14	-3	-47	-82	-12
WT HS34°C - WT 21°C		-417	-519	-315	162	104	219	-13	-16	-10	7	1	13	-22	-22	-15	NA	NA	NA
WT 21°C - WT LT30°C		236	122	351	-17	-82	47	8	3	13	8	-0	15	9	3	15	-37	-66	-7
WT HS30°C early - late		NA	NA	NA	52	-11	115	NA	NA	NA	NA	NA	NA	NA	NA	NA	NA	NA	NA
WT HS34°C early - late		NA	NA	NA	129	80	179	NA	NA	NA	NA	NA	NA	NA	NA	NA	NA	NA	NA
WT HS34°C late- WT 21°C		NA	NA	NA	32	-36	100	NA	NA	NA	NA	NA	NA	NA	NA	NA	NA	NA	NA
<i>spo11-1</i> 21°C - WT 21°C		274	143	405	14	-36	64	25	20	30	10	6	15	2	-2	6	136	100	172
<i>dmc1</i> 21°C - WT 21°C		211	36	386	-17	-70	35	21	17	25	11	4	18	1	-2	4	62	46	77
<i>msh4</i> 21°C - WT 21°C		106	-18	230	-47	-93	0	21	16	25	7	1	13	3	-0	6	54	32	76
<i>atm</i> 21°C - WT 21°C		-10	-148	128	-65	-123	-7	-1	-5	3	8	1	15	-3	-7	1	26	7	45
<i>dmc1</i> 21°C- <i>spo11-1</i> 21°C		-63	-238	112	-31	-59	-3	-4	-10	2	1	-5	6	-2	-5	2	-75	-110	-39
<i>spo11-1</i> HS34°C - WT HS34°C		199	136	261	-110	-140	-80	1	-3	5	-5	-11	1	-1	-3	2	NA	NA	NA
<i>spo11-1</i> HS34°C - <i>spo11-1</i> 21°C		-492	-595	-389	38	6	70	-37	-42	-32	-9	-15	-2	-25	-29	-21	NA	NA	NA
<i>dmc1</i> HS34°C - WT HS34°C		137	97	178	-140	-170	-109	-3	-6	-1	-2	-6	2	-2	-3	-0	NA	NA	NA
<i>dmc1</i> HS34°C - <i>dmc1</i> 21°C		-491	-623	-358	40	16	63	-37	-42	-32	-6	-11	-1	-25	-27	-23	NA	NA	NA
<i>msh4</i> HS34°C - WT HS34°C		143	98	189	-124	-182	-66	-2	-5	1	-1	-19	-2	-0	-3	3	NA	NA	NA
<i>msh4</i> HS34°C - <i>msh4</i> 21°C		-379	-475	-284	84	29	139	-35	-40	-31	-11	-18	-4	-25	-29	-22	NA	NA	NA
<i>atm</i> HS34°C - WT HS34°C		275	204	345	-172	-204	-140	-3	-6	0	-4	-10	2	2	-1	4	NA	NA	NA
<i>atm</i> HS34°C - <i>atm</i> 21°C		-132	-228	-36	55	22	87	-14	-19	-10	-5	-13	2	-18	-22	-14	NA	NA	NA

Supplemental Table S1.3. Genotyping primers.

Gene T-DNA line	Primer name	Primer sequence
<i>spo11-1</i> SALK_146172	Spo11-1-3_LP Spo11-1-3_RP (+LBb1.3 for T-DNA)	AATCGGTGAGTCAGGTTTCAG CCATGGATGAAAGCGATTTAG
<i>dmc1</i> GABI_918E07	GABI_918E07-LP GABI_918E07-RP (+GABI_LB for T-DNA)	GACAGCAACGTTGAACTCCTC CTACAGGGTGTCAAGCTCTCG
<i>msh4</i> SALK_136296	MSH4_LP MSH4_RP (+LBb1.3 for T-DNA)	CGCATATGGCGCTTGTTTTAGACACTTAC GCGTTGTGGAATGGATCAATG
<i>atm</i> SALK_006953	SALK_006953-LP SALK_006953-RP (+LBb1.3 for T-DNA)	ATCCATGTGGTTCAGTCTTGC TTGGTATCCTGCAGAGGAAAG

Movie 1. Meiotic division of wild-type meiocytes at 21°C.

Progression through meiosis of meiocytes in one wild-type pollen sac at 21°C. TagRFP-TUA5 in magenta, auto-fluorescence (chloroplasts) in blue. The meiocytes, localized in the central areas of the pollen sac, reside in a pre-meiotic stage at the beginning of the movie and undergo a complete meiotic program with the first and the second meiotic divisions until the formation of tetrads. Time is expressed in min; the interval between image acquisition is 10 min, time 0 corresponds to the start of image acquisition, and not to the start of meiosis. Scale bar, 10 µm. (available in the host lab)

Movie 2. Meiotic division of wild-type meiocytes at HS30°C.

Progression through meiosis of meiocytes in one wild-type pollen sac at HS30°C. TagRFP-TUA5 in magenta, auto-fluorescence (chloroplasts) in blue. Time is expressed in min; the interval between image acquisition is 10 min, time 0 corresponds to the start of heat shock treatment. Scale bar, 10 µm. (available in the host lab)

Movie 3. Meiotic division of wild-type meiocytes at HS34°C.

Progression through meiosis of meiocytes in one wild-type pollen sac at HS34°C. TagRFP-TUA5 in magenta, auto-fluorescence (chloroplasts) in blue. Time is expressed in min; the interval between image acquisition is 10 min, time 0 corresponds to the start of heat shock treatment. Scale bar, 10 µm. (available in the host lab)

Movie 4. Meiotic division of wild-type meiocytes at LT30°C.

Progression through meiosis of meiocytes in one wild-type pollen sac at LT30°C. TagRFP-TUA5 in magenta, auto-fluorescence (chloroplasts) in blue. Time is expressed in min; the interval between image acquisition is 10 min, time 0 corresponds to the start of image acquisition. Scale bar, 10 µm. (available in the host lab)

Supplemental Movie S1. Meiotic division of *spo11-1* meiocytes at 21°C.

Progression through meiosis of meiocytes in one *spo11-1* pollen sac at 21°C. TagRFP-TUA5 in magenta, auto-fluorescence (chloroplasts) in blue. Time is expressed in min; the interval between image acquisition is 10 min, time 0 corresponds to the start of image acquisition. Scale bar, 10 µm. (available in the host lab)

Supplemental Movie S2. Meiotic division of *dmc1* meiocytes at 21°C.

Progression through meiosis of meiocytes in one *dmc1* pollen sac. TagRFP-TUA5 in magenta, auto-fluorescence (chloroplasts) in blue. Time is expressed in min; the interval between image acquisition

is 10 min, time 0 corresponds to the start of image acquisition. Scale bar, 10 μm . (available in the host lab)

Supplemental Movie S3. Meiotic division of *msh4* meiocytes at 21°C.

Progression through meiosis of meiocytes in one *msh4* pollen sac. Tubulin, TagRFP-TUA5 in magenta, auto-fluorescence (chloroplasts) in blue. Time is expressed in min; the interval between image acquisition is 10 min, time 0 corresponds to the start of image acquisition. Scale bar, 10 μm . (available in the host lab)

Supplemental Movie S4. Meiotic division of *spo11-1* meiocytes at HS34°C.

Progression through meiosis of meiocytes in one *spo11-1* pollen sac at HS34°C. TagRFP-TUA5 in magenta, auto-fluorescence (chloroplasts) in blue. Time is expressed in min; the interval between image acquisition is 10 min, time 0 corresponds to the start of heat shock treatment. Scale bar, 10 μm . (available in the host lab)

Supplemental Movie S5. Meiotic division of *dmc1* meiocytes at HS34°C.

Progression through meiosis of meiocytes in one *dmc1* pollen sac. TagRFP-TUA5 in magenta, auto-fluorescence (chloroplasts) in blue. Time is expressed in min; the interval between image acquisition is 10 min, time 0 corresponds to the start of heat shock treatment. Scale bar, 10 μm . (available in the host lab)

Supplemental Movie S6. Meiotic division of *msh4* meiocytes at HS34°C.

Progression through meiosis of meiocytes in one *msh4* pollen sac. TagRFP-TUA5 in magenta, auto-fluorescence (chloroplasts) in blue. Time is expressed in min; the interval between image acquisition is 10 min, time 0 corresponds to the start of heat shock treatment. Scale bar, 10 μm . (available in the host lab)

Supplemental Movie S7. Meiotic division of *atm* meiocytes at 21°C.

Progression through meiosis of meiocytes in one *atm* pollen sac. TagRFP-TUA5 in magenta, auto-fluorescence (chloroplasts) in blue. Time is expressed in min; the interval between image acquisition is 10 min, time 0 corresponds to the start of image acquisition. Scale bar, 10 μm . (available in the host lab)

Supplemental Movie S8. Meiotic division of *atm* meiocytes at HS34°C.

Progression through meiosis of meiocytes in one *atm* pollen sac. TagRFP-TUA5 in magenta, auto-fluorescence (chloroplasts) in blue. Time is expressed in min; the interval between image acquisition is 10 min, time 0 corresponds to the start of heat shock treatment. Scale bar, 10 μm . (available in the host lab)

**CHAPTER II. The characterization of the translational
landscape of Arabidopsis and maize meiocytes**

INTRODUCTION TO CHAPTER II

1.1. General overview of eukaryotic translation

The process of gene expression was first proposed in 1958 by Francis Crick, which he named 'the central dogma of molecular biology'. This term describes that DNA contains the genetic information that is first converted into RNA, serving as messenger to finally lead to the production of a functional protein (Crick, 1970). Gene expression consists of two main steps, transcription, which is the conversion of a DNA sequence into an RNA sequence, and translation, the synthesis of a protein sequence based on the RNA sequence (**Figure 2.1A**).

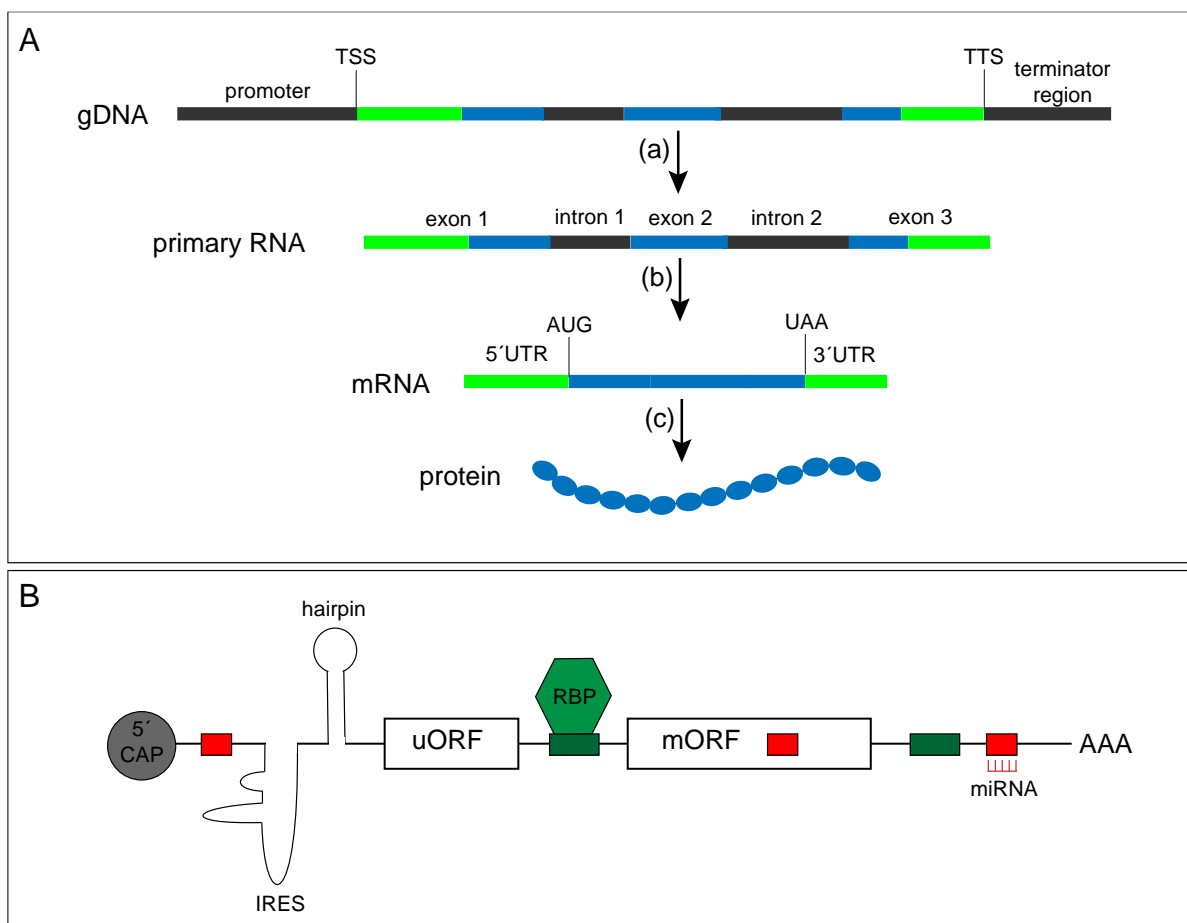


Figure 2.1. Overview of eukaryotic gene expression.

(A) Schematic representation of the central dogma of molecular biology. The structure of genomic DNA (gDNA) of a gene with its promoter region (dark grey), transcription start site (TSS), transcription termination site (TTS) and terminator region (dark grey), which are needed for transcription (a) into primary RNA. This primary RNA contains exons (green and blue) and introns (dark grey). After splicing (b) the messenger RNA (mRNA) is formed. The mRNA contains untranslated regions (5'UTR/3'UTR, green), a translation start (AUG) and stop (e.g. UAA) codon, which are needed for translation (c) into a functional protein. (B) Schematic representation of the regulatory elements of an mRNA involved in the regulation of translation of the main open reading frame (mORF). The 5'CAP

(grey) and the poly(A)-tail enhance translation. Secondary structures like internal ribosomal entry sites (IRES) stimulate cap-independent translation and hairpin structures obstruct translation. Upstream ORFs (uORF) reduce translation of the mORF. microRNAs (miRNA, red) and RNA binding proteins (RBP, green) recognize and bind small-RNA binding sites (red box) and specific protein binding sequences (dark green box), respectively.

The translation of a ribonucleotide sequence into a polypeptide chain is mediated by ribosomes and transfer RNAs (tRNAs). Ribosomes are large ribonucleoprotein complexes that can read the ribonucleotide code, *i.e.* identify and decipher the correct codons (ribonucleotide triplets), which is needed to build the corresponding amino acid sequence. tRNAs are adaptor RNA molecules that help to decode the mRNA by delivering amino acids to matching codons during translation (Schuller and Green, 2018).

Eukaryotic ribosomes (80S) comprise of two subunits that are both composed of ribosomal RNA (rRNA) and ribosomal proteins (RPs) (Carroll et al., 2008; Giavalisco et al., 2005; Hummel et al., 2012). The small subunit (40S) consists of 18S rRNA and more than 30 RPs and has a major role in decoding the messenger RNA (mRNA) sequence. The large subunit (60S) contains 25S, 5.8S and 5S rRNAs and more than 40 RPs and accomplishes the protein synthesis by loading tRNAs with their respective amino acids and catalysing peptide bond formation (Browning and Bailey-Serres, 2015).

Eukaryotic translation can be subdivided into three phases, initiation, elongation and termination, which relies on multiple RNA-protein and protein-protein interactions (**Figure 2.2**) (Browning and Bailey-Serres, 2015). In brief, translation is initiated by the binding of multi-subunit eukaryotic initiation factor complexes (eIFs), like eIF4F and eIF4G, and the poly(A)-binding proteins (PABP) to the 5'cap and poly(A)-tail, respectively. Thereafter the subsequent recruitment of a preformed 43S pre-initiation complex (43S PIC), which consist of the 40S ribosome subunit associated with multiple eIFs, GTP and the initiator tRNA^{Met}, to the cap, the 48S PIC complex scans the 5'UTR for a translation start codon (AUG). After start codon recognition, eIFs mediate the attachment of the 60S ribosome subunit, leading to the formation of the 80S ribosome and the dissociation of the eIFs (**Figure 2.2A**).

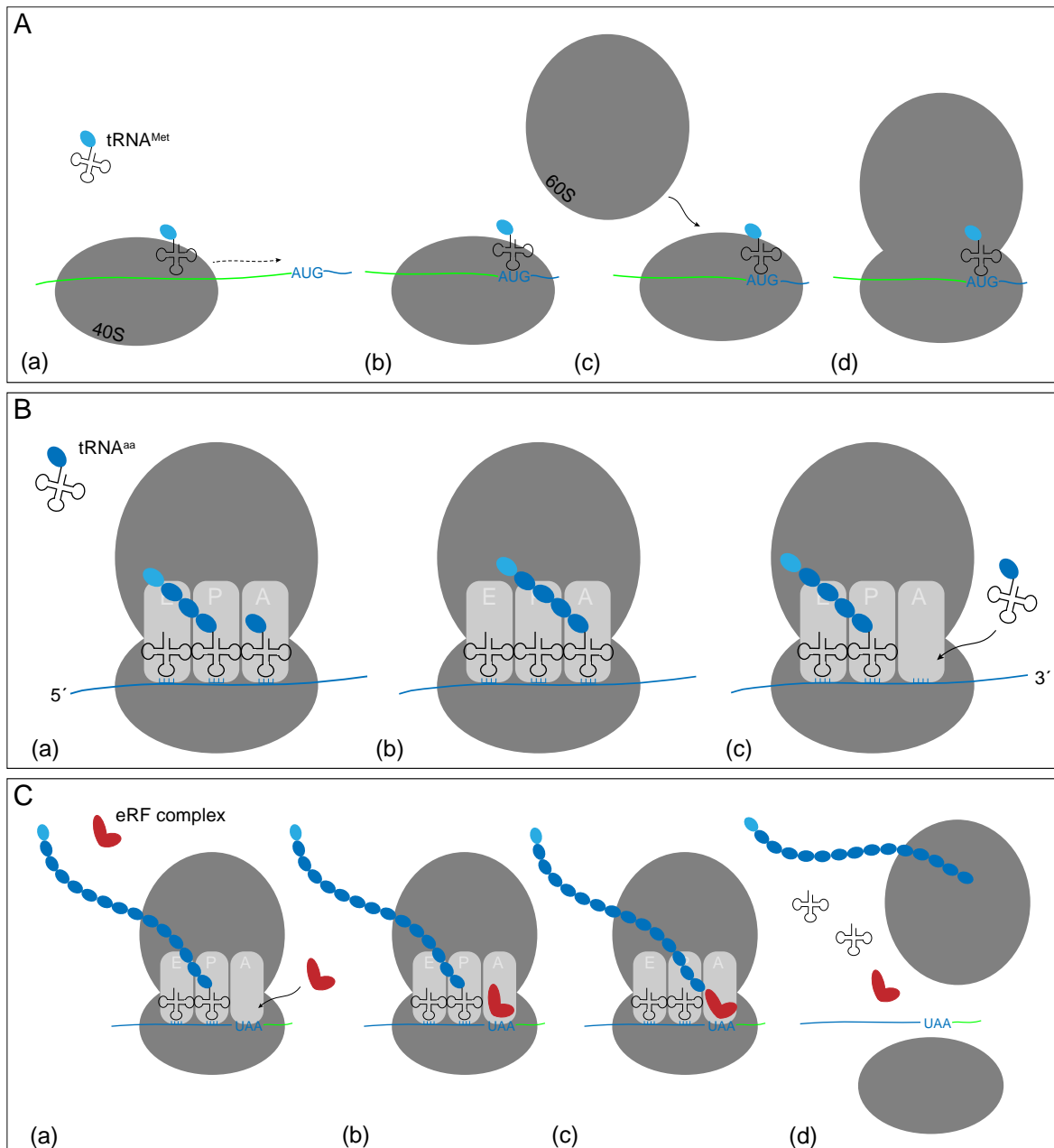


Figure 2.2. Overview of the three phases of eukaryotic translation

(A) Schematic representation of translation initiation. (a) The scanning of the 40S ribosome subunit, $tRNA^{Met}$ and associated proteins along the 5' UTR (green) of the mRNA. (b) $tRNA^{Met}$ recognizes the start codon (AUG). (c) The attachment of the 60S ribosome subunit leads to (d) the formation of the 80S ribosome at the start codon. (B) Schematic representation of translation elongation. (a) The recognition of the ribonucleotide triplet by a $tRNA^{aa}$ at the aminoacyl (A) site of the ribosome. (b) The peptide bond formation between the amino acid at the A-site and the amino acid of the tRNA at the peptidyl (P) site. (c) The translocation of the ribosome coincides with the ejection of the deacylated tRNA at the exit (E) site. This makes the A-site free and ready to be recognised by a new $tRNA^{aa}$. (C) Schematic representation of translation termination. (a) The eukaryotic release factors (eRF) complex (red) recognizes the stop codon (UAA) and (b) enters the A-site of the ribosome. (c) The eRF complex releases the peptide chain and (d) the ribosomal subunits dissociate from the mRNA.

Elongation takes place through mRNA codon recognition by an aminoacyl-tRNA at the aminoacyl (A) site of the ribosome and the peptide bond formation between the amino acid at the A-site and the amino acid of the tRNA at the peptidyl (P) site, leading to the unloading of the tRNA at the P-site. Followed by the translocation of the ribosome by one codon in the 3' direction on the mRNA, the deacylated tRNA gets ejected at the exit (E) site of the ribosome, while the tRNA bound to the nascent peptide chain is shifted from the A- to the P-site, making the A-site free for a next round of codon recognition (**Figure 2.2B**).

The elongation phase continues until the translation stop codon is recognized. Termination is mediated by a complex of eukaryotic release factors (eRFs), that enters the A-site of the ribosome instead of another aminoacyl-tRNA thus preventing the addition of more amino-acids to the formed peptide. The finished polypeptide chain gets released from the ribosome and the ribosome dissociates from the mRNA into its subunits (**Figure 2.2C**).

1.2. Translation regulation mechanisms

The mRNAs present in the cytoplasm are not always constantly translated into proteins, instead the translation of a set of mRNAs is under tight regulation. Transcripts contain several elements that influence the translation efficiency (Barrett et al., 2012; Van Der Kelen et al., 2009), e.g. the 7-methyl guanosine cap at the 5' end of the mRNA and the poly(A)-tail at the 3' end are found to function as transcriptional enhancers (**Figure 2.1B**) (Bush et al., 2009; Weill et al., 2012).

Also, the role of the untranslated region (UTR) at the 5' and 3' end of the mRNA (5'UTR and 3'UTR) in gene expression has been studied extensively (Jia et al., 2020; Liu et al., 2012). The UTRs are not only involved in the transport, subcellular localization and stability of the mRNA, which have an impact on translation, but also directly control the translation efficiency of some mRNAs (**Figure 2.1A**). In Arabidopsis, *PHYTOENE SYNTHASE (PSY)* was shown to form 2 splice variants, which only differ in their 5'UTR length. Upon different stresses, like salt stress and illumination, the transcript with the longer 5'UTR was able to switch between a high and a repressed translation state (Alvarez et al., 2016).

In addition, it was shown that distinct secondary structures influence translation, e.g. internal ribosomal entry sites (IRES) stimulate cap-independent

translation and hairpin structures obstruct translation (**Figure 2.1B**) (Yang and Wang, 2019).

Further, in *Arabidopsis* about 37% of the mRNAs contain upstream open reading frames (uORFs), which are small ORFs preceding the main ORF (mORF) that reduce the translation of the mORF (**Figure 2.1B**) (Liu et al., 2013; Wethmar et al., 2016; Zhang et al., 2020). For example, *Arabidopsis* *POLYAMINE OXIDASE* (*PAO*) transcripts are commonly regulated by uORFs. When the polyamine concentration is low, the uORF of *PAO2* gets translated, inhibiting the translation of the mORF, while high polyamine levels increase the expression of the mORF of *PAO2* (Guerrero-Gonzalez et al., 2016).

Translation can also be regulated by the binding of microRNAs (miRNA), short or long noncoding RNAs (ncRNAs) and RNA binding proteins (RBP) at recognition sites in the mRNA (**Figure 2.1B**). For example, miRNA156 and miRNA172 are involved in shoot development in the juvenile-to-adult transition by repressing or promoting the expression of transcription factors (Aleshkina et al., 2021; Prall et al., 2019; Wu et al., 2009).

1.3. Translation regulation during meiosis

A precisely coordinated and regulated gene expression is essential for developmental processes, like meiosis. The meiotic transcriptome has been studied extensively in many species, including plants such as *Arabidopsis* (Chen et al., 2010; Libeau et al., 2011; Yang et al., 2011) and maize (Dukowic-Schulze et al., 2014a). The transcriptome data provides information on gene expression patterns and also helps with the identification of several meiotic genes. However, the transcriptome does not necessarily provide information on the presence of the corresponding proteins, since transcripts are not immediately and continuously translated. Therefore, in budding yeast *Saccharomyces cerevisiae*, ribosome profiling was used for the study of the meiotic translome (Brar et al., 2012), and set the basis for the discovery of meiotic translational regulation mechanisms. Recent studies have revealed that translational regulation fine-tunes the meiotic transcriptional cascade significantly. An example of translational regulation during yeast meiosis is *NUCLEAR DIVISION CYCLE 80* (*NDC80*), coding for a kinetochore associated protein that is important for chromosome segregation at metaphase-anaphase I. It has been shown that meiotic cells express two mRNA isoforms, the canonical mRNA

and a 5'-extended *NDC80* mRNA, which contain in addition to the mORF, a regulatory uORF. The expression of the 5'-extended mRNA is activated by the meiotic initiator transcription factor (TF) INDUCER OF MEIOSIS 1 (IME1) and the uORF plays a repressive role to inhibit transcription of the canonical mRNA, thereby inhibiting NDC80 protein synthesis. At kinetochore assembly (late prophase), the mid-meiotic TF NON-DITYROSINE 80 (NDT80) activates the transcription of the canonical *NDC80* mRNA isoform, which is then translated into the NDC80 protein (Chen et al., 2017; Chia et al., 2017).

CDK-cyclin complexes are another example of translation regulation, as they are known to regulate cell cycle progression and every cell cycle stage can be characterized by a different CDK-cyclin combination, which activity is usually restricted but essential for the proper progression (Mendenhall and Hodge, 1998). In *Saccharomyces cerevisiae*, even though *CYCLIN B3* (*CLB3*) transcription is activated by the TF NDT80 early in meiosis, the CLB3 protein is not found until the onset of the second meiotic division. Translation of *CLB3* immediately after transcription led to missegregation during meiosis I, showing the importance of the delay in translation (Carlile and Amon, 2008). The timing of *CLB3* translation is controlled by REGULATOR OF IME2 4 (RIM4), an RNA-binding protein that binds the 5'UTR of *CLB3* mRNA, causing its translational repression. RIM4 is a substrate of the kinase IME2, which activity increases during the meiotic division and it has been shown that premature activation of IME2 leads to early translation of *CLB3*, suggesting that IME2 promotes translation of *CLB3* through negative regulation of RIM4 (Berchowitz et al., 2013). The same regulation of translation via RIM4 and IME2 was also shown for other transcripts, like *SPORULATION SPECIFIC 2* (*SSP2*), which is not translated before the end of MII (Jin et al., 2015). In order for RIM4 and IME2 to temporally distinguish between transcripts, additional regulators are required and indeed for late translation the RNA binding proteins POLYMERASE EPSILON SUPPRESSOR 4 (PES4) and MEX67-INTERACTING PROTEIN 6 (MIP6) were identified (Jin et al., 2017).

Also in *Drosophila*, cyclins are subjected to translational regulation during meiosis. For example, RBP4 binds the 3'UTR of *CYCB* mRNA and represses translation in early meiosis and WURSTFEST (FEST) is required for the progression and translation of *CYCB* from metaphase I onwards (Baker et al., 2015). In addition,

translation of the mitotic *CYCA* is inhibited during the meiotic prophase by the translational repressor BRUNO (BRU) acting at the 3'UTR of *CYCA*, in order to enter and maintain meiosis (Sugimura and Lilly, 2006).

Last example of a translational activation mechanism in meiosis is the cytoplasmic elongation of the poly(A) tail, mediated by the cytoplasmic polyadenylation element (CPE) present in 3'UTR of the mRNA. In *Xenopus laevis*, first CPEB1 mediates the polyadenylation of transcripts in prophase I and metaphase I and activates the translation of *CPEB4* mRNA, which replaces CPEB1 and drives the transition from metaphase I to metaphase II. In addition to the activation cascade of *CPEB4* by CPEB1, both are also differently regulated by phase-specific kinases (Igea and Mendez, 2010).

In plants, early meiotic studies in lily and tobacco made use of polysomal RNA to examine differences in translated mRNAs (Kamalay and Goldberg, 1980; Steffensen, 1966). In tobacco, they compared ribosome bound mRNA of leaf, petal, ovary and anther tissue and found a differential expression of structural genes. In addition, they demonstrated that every tissue had a different set of mRNAs which had no ribosomes bound, suggesting that post-transcriptional regulation plays an important role in gene expression (Kamalay and Goldberg, 1980). However, more research is needed to investigate if and how translational control affects meiotic gene expression and controls the progression of meiosis in plants.

As part of this research, I established a protocol for ribosome profiling of maize anthers at different meiotic stages, that can be used as a basis for translational regulation studies and will hopefully lead to the discovery of plant specific translational regulation mechanisms in the near future.

In addition to this genome wide approach, three well-known meiotic genes, *ASY3*, *TAM* and *REC8*, were selected as candidates for a gene specific approach for translational regulation. The selection of the candidates was based on a previously performed quantitative RT-PCR (qRT-PCR) time course analysis of synchronously developing flower of *apetala1 (ap1) cauliflower (cal)* double mutant plants, carrying the dexamethasone inducible flower induction construct *p35S:AP1:GLUCOCORTICOID RECEPTOR (GR)* (Wellmer et al., 2006). The qRT-PCR results of 40 meiotic genes indicated different types of transcription patterns.

ASY3 and *REC8* were selected for further analysis, since the mRNAs of *ASY3* and *REC8* appeared to be expressed shortly before the onset of meiosis and *TAM*, since its transcript levels showed no correlation with any meiotic stage (unpublished, generated by Dr. Hirofumi Nakagami). From previous protein localization studies using reporter lines, it is known that *ASY3* and *REC8* proteins are present from early leptotene onwards to late meiosis I, while *TAM* was detected from late leptotene to interkinesis (**Supplemental Figure S2.1**, unpublished, generated by Dr. Chao Yang) (Prusicki et al., 2019; Yang et al., 2019). It was further postulated that there is a time discrepancy between the occurrence of the transcript and protein, suggesting that after transcription, translation is first inhibited and only induced at later developmental stages. For this gene specific analysis of translational regulation, I aimed to investigate and visualize the temporal difference between transcription and translation using an *in vivo* system to label mRNA, called MS2-system, as well as a technique to monitor the first round of translation of the mRNA of the selected candidates, called TRICK.

2. RESULTS

2.1. Ribosome profiling of maize male reproductive organs - a genome wide approach to investigate the meiotic translome

2.1.1. Optimization of the RNA-seq and Ribo-seq procedure from maize male reproductive organs

Ribosome profiling, or Ribo-seq, is a genome wide approach to investigate the translome of any given organ at any given time, which can be compared with the corresponding transcriptome, using RNA-seq. The RNA-seq procedure starts with total RNA extraction from a desired tissue (**Figure 2.3A(a)**). To generate the required RNA library, the total RNA is randomly fragmented and fragments of 25-35 nucleotides are selected, rRNA is depleted and adapters are ligated (**Figure 2.3A(b)**). Finally, the total RNA is reverse transcribed into complementary DNA (cDNA), amplified and sequenced by Illumina.

To obtain the translome, first polysomes, *i.e.* multiple ribosomes bound to mRNA, are extracted from a desired tissue (**Figure 2.3A(c)**). The polysomes are digested into monosomes, *i.e.* single ribosomes bound to small fragments of RNA (**Figure 2.3A(d)**), from which ribosome protected fragments (RPFs) of around 25-35 nucleotides are isolated (**Figure 2.3A(e)**). To generate the RPF library, rRNA is depleted, adapters are ligated, the fragments are reverse transcribed into cDNA and amplified. Finally, the library is sent for sequencing (for more detailed protocols see Material and Methods section).

The optimization of the protocols was performed in collaboration with Dr. Adamla and Dr. Rauscher (AG Ignatova, Institute for Biochemistry and Molecular Biology, Department of Chemistry, University of Hamburg). Although the final goal was to use anthers in different meiotic stages for transcriptome and translomes analysis, maize spikelets were used for the protocol optimization (**Figure 3C**), since spikelets also contain the cells of interest, *i.e.* meiocytes, and are less labour intensive to collect, compared to the isolation of anthers.

The total RNA extraction protocol only needed minor adjustments with respect to a protocol used for Arabidopsis leaves (Lukoszek et al., 2016) and the extracted

total RNA from spikelets had, with an RNA Integrity Number (RIN) of 9.7, a very high quality (**Supplemental Figure S2.2A**).

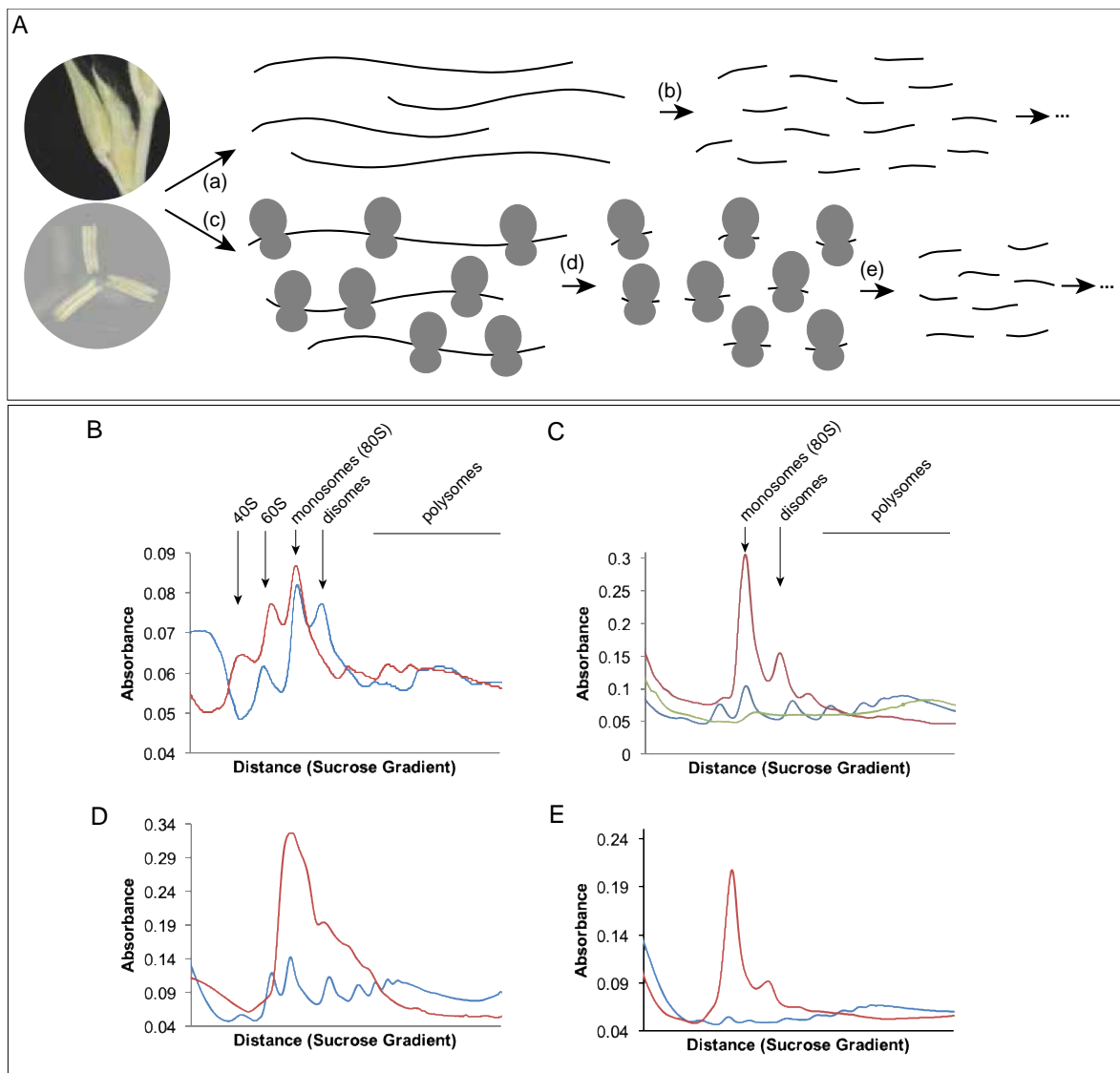


Figure 2.3. Optimization of the protocol for RNA-seq and Ribo-seq.

(A) Simplified schematic overview of the first steps of RNA-seq and Ribo-seq procedure from spikelets or isolated anthers. Upper row: RNA-seq, (a) starting with total RNA extraction and (b) random fragmentation and size selection. Lower row: Ribo-seq, (c) starting with polysome extraction, (d) RNase digestion into monosomes and (e) RPF isolation. (B-E) Graphs showing the results obtained in the course of optimising the RNase digestion of polysomes. The absorbance (measured at 260 nm) is plotted along the distance through the sucrose gradient. The complexes causing the respective absorbance peaks are indicated (40S, 60S, 80S (monosomes), disomes and polysomes), the undigested control is in blue. (B) Incomplete digestion of polysomes from spikelets (red, 1.5 U/OD/μl RNase I, 30 min, 22°C). (C) The comparison of polysome digestion from spikelets with 10 U/μl RNase I (red) and 10 U/μl RNase A (green) (45 min, 22°C). (D) The best obtained digestion of polysomes from spikelets (5 U/OD/μl RNase I, 1 h, 22°C (red)). (E) The best obtained digestion of polysomes from isolated anthers (0.2 U/μl RNase A, 45 min, 22°C (red)).

The protocol to extract the RPFs needed more optimization, especially the polysome digestion step (**Figure 2.3A(d)**) (Ingolia et al., 2009; Lukoszek et al., 2016; Mustroph et al., 2009a). In short, the extracted polysomes are incubated with a ribonuclease (RNase), in order to remove the RNA stretches that are not covered by ribosomes. This RNase treatment results in the conversion of polysomes into monosomes, from which the RPFs, also called the ribosome footprints, can be isolated. Since in many studies performing Ribo-seq the RNase used for the polysome digestion was RNase I, I also started using RNase I at first (Chotewutmontri and Barkan, 2016; Chung et al., 2015; Duncan and Mata, 2014; King and Gerber, 2016; Lei et al., 2015; McGlincy and Ingolia, 2017). However, after successfully extracting the polysomes from maize spikelets, the polysome digestion by RNase I treatment (1.5 U/OD/ μ l RNase I, 30 min, 22°C) resulted only in a slight increase in the amount of monosomes, while most of the polysome fraction remained present, as shown by sucrose gradient analysis (**Figure 2.3B**).

To improve the polysome digestion, different conditions were tested. First, the duration, ranging from 60-90 min (5 U/OD/ μ l at 22°C), temperature of the digestion ranging from 22-30°C (2 U/OD/ μ l, 40 min) and the pH of the buffers ranging from pH 7.5-8 (1.5 U/OD/ μ l, 45 min, 22°C) were tried but no significant improvement of the digestion of the polysomes was achieved (**Supplemental Figure S2.3A,B,C**). This led to the hypothesis that some maize or spikelet specific cellular components were precipitated together with the polysomes and inhibit the RNase I digestion. The nature and the underlying mechanism of those cellular components remains unknown but is interesting to investigate in future.

Further, different RNases were tested, which have a specific sequence cutting preference and efficacy. While RNase I is able to cut after all four nucleotides, RNase T only cuts after guanines and RNase A cuts after cytosine and uridine (deCardayre and Raines, 1995; Gerashchenko and Gladyshev, 2017). The polysome digestion with different RNases was performed at an extreme concentration (10 U/ μ l, 45 min, 22°C), to observe the highest RNase activity, e.g. if a sample was over digested, which means that the RNase is too efficient and even cuts the rRNA from the ribosomes, the RNase is able to digest the polysomes into monosomes at a lower concentration. At this high concentration, RNase A over digested the polysomes, even the ribosome footprints were digested, and both

RNase I and T showed a high monosome peak, with some remaining polysomes (**Figure 2.3C, Supplemental Figure S2.3D**).

Next, the concentration of the RNase I was optimized within a reasonable concentration range from 3-5 U/OD/ μ l (40 min, 22°C). The increase in the concentration of RNase I, improved the monosome peak, but no complete digestion could be obtained within a feasible concentration range of RNase I (**Supplemental Figure S2.3E**). At the end, I was able to almost completely digest the polysomes of the spikelets with 5 U/OD/ μ l of RNase I for 1 h at 22°C (**Figure 2.3D**). This monosome fraction was collected and further used to optimize and generate the RPF library from the spikelets.

However, when applying the same RNase I treatment to the polysomes extracted from isolated anthers, only a partial digestion was obtained. Thus, the optimization of the polysome digestion protocol was resumed for polysomes extracted from isolated anthers. Since a high concentration of RNase A resulted in the over digestion of the polysomes from spikelets (**Figure 2.3C**), I decided to reduce and optimize the concentration of RNase A. After testing different concentrations ranging from 0.001-10 U/ μ l RNase A (45 min, 22°C), the treatment of 0.2 U/ μ l RNase A for 45 min at 22°C resulted in a nearly complete digestion of the polysomes into monosomes (**Figure 2.3E**). This RNase A treatment was further successfully used for the polysome digestion of isolated anthers from different meiotic stages.

2.1.2. The detection of meiotic genes in the libraries generated from spikelets

The extracted total RNA and RPF from spikelets were further used to generate the total RNA and RFP libraries, respectively. The quality (*i.e.* library size) and quantity (*i.e.* concentration) of the libraries were confirmed using the Bioanalyzer 2100. While the library size (142 bp) and concentration (8.98 ng/ μ l) of the total RNA library was good, only the quantity of the RPF library was rather poor (library size of 143 bp and concentration of 1.14 ng/ μ l) but still sufficient, since a minimum molar concentration of 4 nM per library is required for sequencing (**Supplemental Figure S2.4A,B**). Both libraries were send for sequencing and analysed.

The sequencing results were analysed together with Johannes Wagner (AG Ignatova, Institute for Biochemistry and Molecular Biology, Department of Chemistry,

University of Hamburg). We were able to recover 11.6 (15.62%) and 2.2 (25.11%) million uniquely mapped reads from the total RNA and RPF libraries, respectively. This is a genome coverage of about 38.7% for the total RNA library, this represents the ratio between the total number of bases of the mapped reads and the number of bases of the genome size. The coverage of the RPF library of 7.3% was rather low, since it is recommended for Ribo-seq experiments to have a coverage of at least 14.5% (Glaub et al., 2020).

The sequencing of the libraries obtained from the spikelets was mainly performed to determine if the assay was sensitive enough to detect meiosis-specific genes. The reads per kilobase of transcript per million mapped reads (RPKM) was calculated from all detected genes in both, the total RNA and RPF libraries (listed for a selection of meiotic genes in **Table 2.1**). In the total RNA library, the mean and median of all expressed genes are 15.08 and 4.88 RPKM, respectively, and the highest transcribed known gene is an *ANTHER-SPECIFIC PROTEIN 3* (*NTHR3/YY1*, Zm00001d021226) with 3086.52 RPKM. In the RPF library, the mean and median of all detected genes are 23.58 and 5.09 RPKM, respectively, the gene with the highest ribosome occupancy is *MALE STERILE 44* (*MS44*, Zm00001d052736) with 12092.85 RPKM. Among the candidate meiotic genes, *CDKB2;1* is the highest transcribed with 21.85 RPKM and also has the highest occupancy of ribosomes, with 72.33 RPKM. Looking at potentially meiosis specific genes, a candidate homolog of *TAM* (Zm00001d010404) shows the highest values with 4.72 RPKM in the total RNA library and 1.74 RPKM in the RPF library. Other candidate homologs of meiotic genes could be barely detected or not at all, for example from the RPF library only 8 reads (raw counts) were mapped to *REC8*, which results in a RPKM of 0.

Since the RPKM of the RPFs from a transcript does not give direct information how productive the existing mRNA is translated, the translation efficiency (TE = ratio of RPF per mRNA) was calculated (**Table 2.1**). The highest TE observed in this dataset is 43.36 and the mean and median TE of all detected genes are 1.45 and 1.02, respectively. As example, a highly translated meiotic gene is *DMC1*, with a TE of 6.11.

Gene name	Gene ID	Count	RPKM	Count	RPKM	TE
		RNA	RNA	RPF	RPF	
ASY1	Zm00001d006089	177	2.50	61	2.05	0.82
DSY2 (ASY3)	Zm00001d010684	19	0	0	0	0
SPO11-1	Zm00001d013262	156	3.33	55	2.79	0.84
COM1	Zm00001d046761	19	1.35	17	2.87	2.13
RAD50	Zm00001d050612	470	1.20	66	0	0
MRE11	Zm00001d002154	30	1.04	8	0	0
NBS1	Zm00001d013976	55	2.53	13	1.42	0.56
PHS1	Zm00001d045993	62	0.77	28	0.83	1.07
RAD51	Zm00001d021898	40	2.06	29	3.55	1.72
	Zm00001d041757	53	3.31	13	1.93	0.58
DMC1	Zm00001d044629	21	1.05	54	6.39	6.11
REC8 (AFD1)	Zm00001d039133	62	0.91	9	0	0
DYAD/SWI1 (AM1)	Zm00001d013659	34	1.18	38	3.15	2.66
RBR1	Zm00001d031678	87	2.62	67	4.79	1.83
	Zm00001d052695	101	1.62	27	1.03	0.64
TAM	Zm00001d010404	116	4.72	18	1.74	0.37
SDS	Zm00001d028274	17	0.96	10	1.35	1.40
	Zm00001d048026	35	1.55	9	0.95	0.61
PRD1	Zm00001d046970	68	1.75	10	0	0
BRCA2(IV)(V)	Zm00001d024953	247	1.83	12	0	0
XRCC3	Zm00001d016839	2	0	3	1.70	0
MRE3/RCK	Zm00001d051111	61	0	14	0	0
PTD	Zm00001d009728	4	0	13	4.73	0
ZYP1a/b	Zm00001d025575	96	1.73	30	1.28	0.74
MSH2	Zm00001d022028	65	1.41	51	2.62	1.86
MSH4	Zm00001d006382	222	0.90	13	0	0
MSH5	Zm00001d010684	19	0	0	0	0
MLH1	Zm00001d011829	23	0	5	0	0
MPA1	Zm00001d031891	1241	20.45	597	23.38	1.14
MUS81	Zm00001d042130	16	0.81	13	1.56	1.93
EME1A/B	Zm00001d002082	42	1.25	20	1.42	1.13
PS1	Zm00001d004810	136	4.51	111	8.76	1.94
TETRASPORE	Zm00001d006197	0	0	0	0	0

Table 2.1. Meiotic genes detected in the total RNA and RPF libraries from spikelets.

Analysis of gene expression in spikelets by RNA-seq (RNA) and Ribo-seq (RPF). Values for a set of meiotic genes (gene name (column 1) and gene ID (column 2)) are shown as raw read counts (column 3,5), RPKM (column 4,6) and the translation efficiency (TE, ratio RPF/mRNA, column 7).

Next, the RNA and RPF reads were plotted along the gene and their distribution was analysed. *CDKB2;1* has the highest RPKM for both RNA and RPF and the distribution of the reads along the gene shows the highest coverage by ribosomes at the 5' region of the gene, which is the area where most of the reads mapped (**Figure 2.4A**). The coverage of other genes, like *TAM*, *DMC1* and *SWITCH 1 (SWI1/DYAD)*, became difficult to interpret at this stage, due to the low number of reads (**Figure 2.4B-D**).

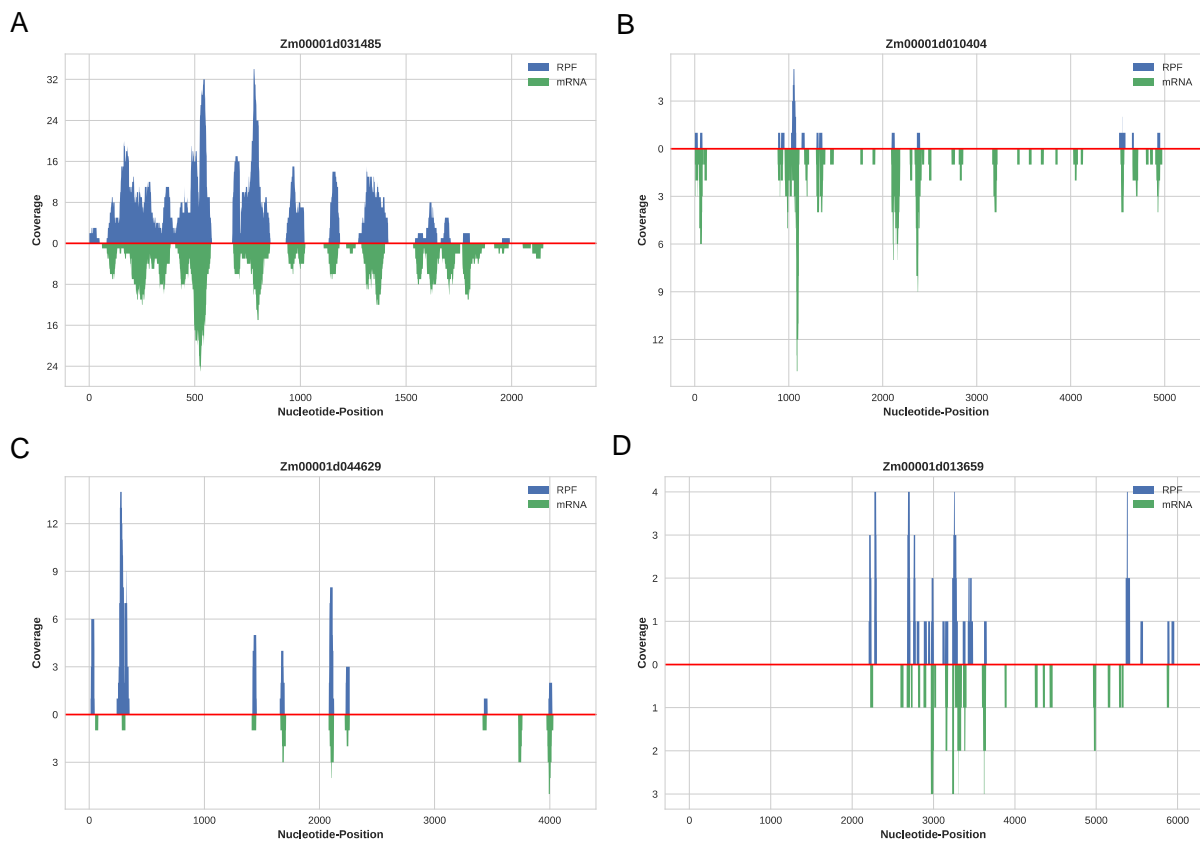


Figure 2.4. Read coverage of *CDKB2;1*, *TAM*, *DMC1* and *SWI1/DYAD*.

The RNA (green) and RPF (blue) uniquely mapped reads plotted along the gene (genomic nucleotide-position from transcriptional start to end, red line) for (A) *CDKB2;1*, (B) *TAM*, (C) *DMC1* and (D) *SWI1/DYAD*.

These results showed that it was possible to detect meiotic genes, but for most genes the RNA levels, especially in the RPF library, were around or below the detection limit. In subsequent experiments, isolated anthers were used to increase the ratio of meiocytes and surrounding tissue and more starting material, *i.e.* 30 μ g of polysomes, was used for the generation of the RPF library of the different meiotic stages.

2.1.3. Anther collection and meiotic staging

In order to study the transcriptome changes and translational regulation during the course of meiosis, RNA-seq and Ribo-seq were performed from five different meiotic phases, premeiosis (PRE), leptotene (LEP), zygotene (ZYG), pachytene (PACH) and from diakinesis to tetrad formation (MII). To identify the meiotic stage of the meiocytes from collected anthers, I made use of the fact that within a tassel branch there is a developmental gradient from top to bottom, meaning that anthers at the bottom contain meiocytes at an earlier meiotic stage than anthers at the top (**Figure 2.5A**). Following a branch, the first spikelet pair was fixated and from the second and third pairs the three big anthers were isolated and flash frozen (**Figure 3C,E**). The fourth spikelet pair was then again fixated and the anthers from the fifth and sixth pair were isolated and frozen. This pattern of harvesting was repeated for the complete branch. The fixated spikelets were used for meiotic staging by acetocarmine staining (**Figure 2.5B-M**). If for example the meiocytes in the lower fixated spikelets were in diakinesis and the meiocytes in the upper ones were in metaphase I, the isolated anthers in between were used as material for the subgroup MII. When meiotic stages found in two successive spikelet pairs covered several subgroups, the collected anthers were not used for the library preparation. This staging and collecting strategy proved to be robust and reliable to avoid cross-contamination of the meiotic subgroups.

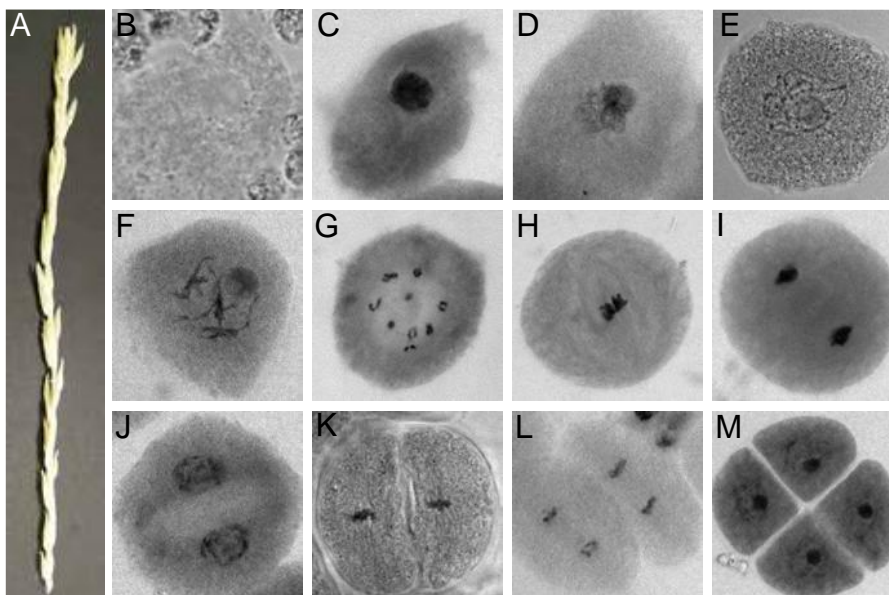


Figure 2.5. The developmental gradient of a tassel branch in *Zea mays*.

(A) Along an immature tassel branch, early meiotic stages can be found at the bottom and later stages at the top. Meiocytes staged by acetocarmine staining (B-M): (B) premeiosis, (C) leptotene, (D)

zygotene, (E) pachytene, (F) diplotene, (G) diakinesis, (H) metaphase I, (I) anaphase I, (J) interkinesis, (K) metaphase II, (L) anaphase II and (M) tetrad.

2.1.4. Quality control of the libraries generated from isolated anthers

Once enough anthers of the different meiotic stages were collected to extract 10 µg total RNA and 30 µg polysomes, the total RNA and RPF libraries were generated as described before. Before the random fragmentation of the total RNA, the quality and quantity of the extracted total RNA was confirmed using the Bioanalyzer 2100, with RNA concentrations between 159-375 ng/µl and RINs between 8-10 (**Supplemental Figure S2.2B-F**).

Further, before sequencing, also the quantity and quality of all ten libraries were confirmed using the Bioanalyzer 2100 and Qubit (**Supplemental Figure S2.4C-L**). The quantity of the RNA in the RPF libraries (4.54-15.20 ng/µl) was up to 13.3-fold higher compared to the RPF library from the spikelets (**Supplemental Figure S2.4B**). In some of the electropherograms a double peak could be detected at the predicted size of the libraries (120-140 bp), which was unanticipated and could not be explained (**Supplemental Figure S2.4C,E,G,H,K**).

The sequencing data of the ten libraries were analysed in collaboration with Dr. Dermot Harnett (AG Ohler, Institute for Medical Systems Biology, Department of Computational Regulatory Genomics, Max Delbrueck Center for Molecular Medicine Berlin). First, a quality control (QC) was performed. For the total RNA and RPF libraries from PRE, we were able to recover 13.6 (36%) and 6.7 (25%) million uniquely mapped reads, respectively. From LEP, we got 11.3 (34%) and 5.6 (28%) million uniquely aligned reads from the RNA and RPF library, respectively. Next, from ZYG we recovered 7.1 (34%) and 6.6 (31%) million uniquely aligned reads, from PACH we obtained 6.1 (37%) and 7.4 (35%) million uniquely aligned reads and from MII we got 6.6 (32%) and 10 (30%) million uniquely aligned read from the RNA and RPF library, respectively (**Figure 2.6A**). For the total RNA libraries, this is a coverage between 20.3 and 45.3% and the coverage of the RPF libraries is around 18.7-33.3%, which is clearly improved compared to the RPF library from spikelets (7.3%). Further, no reads aligned to intronic or intergenic regions of the reference genome, showing that there is no DNA contamination in any of the libraries (**Figure 2.6B**).

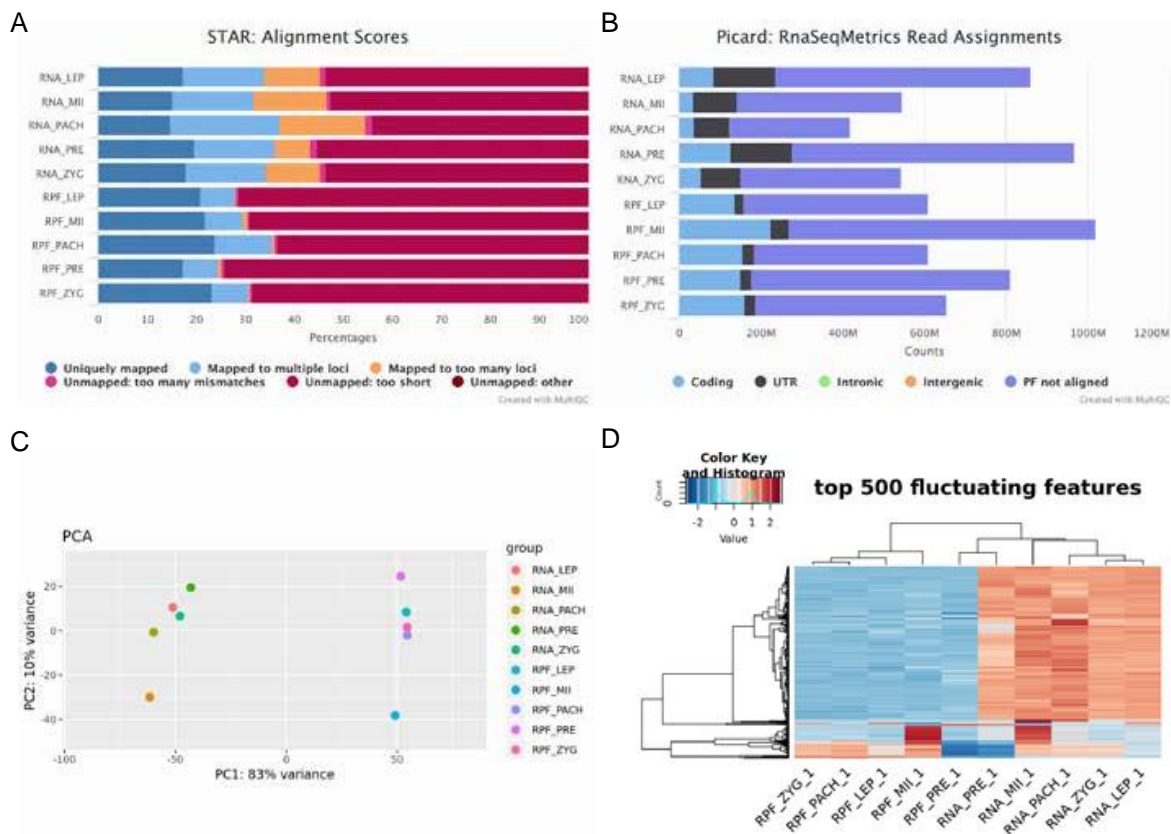


Figure 2.6. Quality control of the libraries from anthers.

(A) The alignment scores (in percentage) of the uniquely mapped reads (dark blue), reads mapped to multiple loci (light blue), reads mapped to too many loci (orange), unmapped reads due to too many mismatches (pink) and unmapped reads due to too short reads (light bordeaux) by using the STAR (an ultrafast universal RNA-seq aligner). (B) The number of reads (counts) that align to regions in the reference genome (coding sequence (blue), UTR (grey) and not aligned (purple)). (C) Principal component analysis (PCA) of the uniquely mapped reads. (D) Heatmap of the clustering of the mRNA and RPF libraries based on the similarity between the expression of the top 500 most fluctuating genes. Stages analysed: premeiosis (PRE), leptotene (LEP), zygotene (ZYG), pachytene (PACH) and diakinesis to tetrad (MII).

In addition, other quality aspects were analysed, for example the normalized gene coverage, which describes how well the mapped reads are distributed along the gene sequences. All the ten libraries have a good gene coverage, *i.e.* there is no specific region of the genes underrepresented (**Supplemental Figure S2.5A**). Further, the plot of the mapped reads per chromosome shows that all ten chromosomes are presented, with a slightly higher number of reads for chromosome one. In contrast, reads mapping to mitochondrial and plastid DNA are clearly underrepresented (**Supplemental Figure S2.5B**). The average GC content of the reads from the total RNA libraries describes, as it should, a normal distribution with a peak at around 55%, instead the distribution of the GC content of the reads from the

RPF libraries is not as expected, with a plateau of GC content between from 45 to 75%, it remains unclear why this is the case (**Supplemental Figure S2.5C**). Next, the sequence length distribution gives more information about the length of the reads, the length distribution of the total RNA and RPF libraries peak around 24 bp and 30-34 bp, respectively (**Supplemental Figure S2.5D**).

Next, we asked if the transcriptome and translomes represented by the different libraries could be differentiated. To answer this, a principal component analysis (PCA) was performed to describe and visualize the variation among the uniquely mapped reads. 93% of the variance can be explained by two principal components (**Figure 2.6C**). PC1 correlates with the nature of the library, as the total RNA and RPF libraries localise to opposite sides of the PCA-plot, showing that the variation between them is high. Interestingly PC2, which accounts for 10% of the variability, can be explained as the difference in gene expression due to the meiotic progression, since the total RNA as well as the RPF libraries are plotted vertically in the order of their meiotic stage. While for the total RNA data, LEP and ZYG are the most similar, ZYG and PACH are the most similar in the RPF analysis (**Figure 2.6C**). Although expected for meiocytes, it is surprising that anthers have a clearly different expressome at every meiotic stage. Next, the top 500 most fluctuating genes were extracted from the normalized count data and used for the clustering of the total RNA and RPF libraries by similarity in gene expression of those 500 genes, based on a distance matrix. The clustering of the expression patterns leads to analogous conclusions as the PCA, namely, that the RPF dataset of ZYG and PACH and the total mRNA dataset of LEP and ZYG are most similar, while PRE and MII show the highest variation in gene expression (**Figure 2.6D**). Thus, the sampling method is precise enough to allow a clear distinction between the meiotic subgroups on transcriptome as well as translomes level.

These results indicate that the libraries were of sufficient quality to perform further analysis and investigate the transcriptome and translome during meiosis. Here the focus is mainly on the first results of the differential expression of meiotic candidate genes during meiosis. However, the overall differential expression in this data was also observed, by performing k-means clustering of the normalized count data using cosine distances, which bases clustering on the general direction of the change and removes between gene differences in the magnitude of change.

Hierarchical clustering involves the construction of a distance matrix, and then the assembling of the genes into a tree, which cluster by similarity. This tree can be cut at any height to give an arbitrary number of clusters. Here, the tree is splitted down to a depth of 12 clusters, being 12 groups of genes with similar expression patterns (**Figure 2.7**). To assess the functional enrichment of the clusters and the overlap between the clusters, the top 10 Gene Ontology (GO) terms enriched in each cluster were calculated with AgriGO (Tian et al., 2017) (**Supplemental Figure S2.6-8**). These results give a general overview of the differential expression of the transcriptome and translatoome of maize anthers in different meiotic stages.

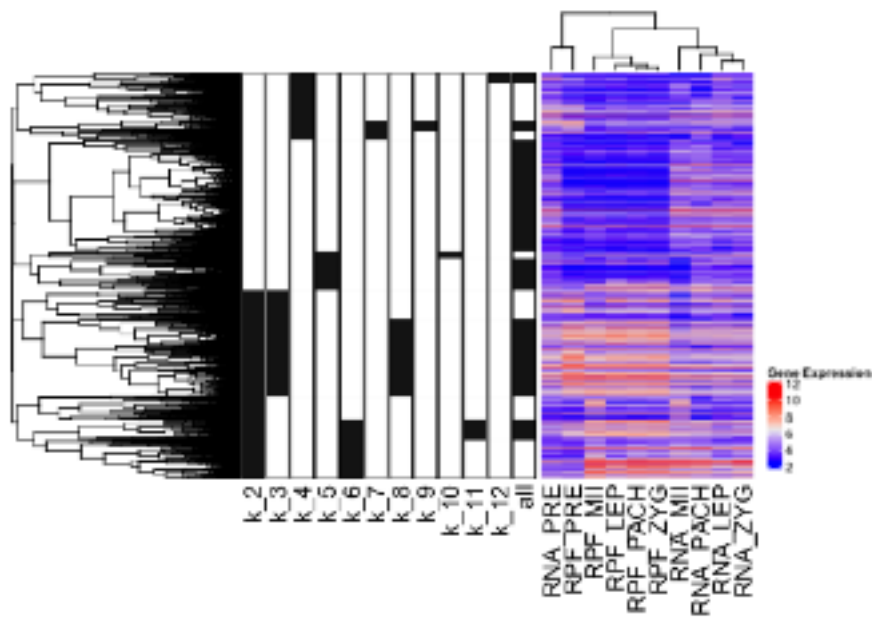


Figure 2.7. K-means clustering of genes expressed during meiosis.

The results of hierarchical clustering on the normalized count data. The tree split down to a depth of 12 clusters (k_2-12), groups of genes with similar expression patterns. On the left, the overall tree, and next to it bars showing, at each subdivision, the new cluster created. The final bar 'all' shows all the clusters (black-white coloured).

2.1.5. The expression of meiotic genes during meiosis

To analyse the meiotic transcriptome and translatoome of maize, I first assembled an extensive list of 128 meiotic genes based on previous publications. (Nelms and Walbot, 2019; Yang et al., 2011). Based on this collection, a list of 208 candidate maize orthologs was generated by Dr. Maren Heese, using the InParanoid software (<https://inparanoid.sbc.su.se/cgi-bin/index.cgi>) and a pre-calculated dataset of maize orthologs from ENSEMBL plants (<https://plants.ensembl.org>).

Among those 208 meiotic candidates, 153 genes were found to be expressed in the total RNA and RPF libraries prepared from maize anthers (**Supplemental Table S2.1**). In cases where several potential orthologs were identified, the transcriptome data helped to identify the most likely maize meiotic candidate, like Zm00001d039189 for *SMC3*, Zm00001d023283 for *CDC45*, Zm00001d006307 for *MUTL PROTEIN HOMOLOG 3 (MLH3)* and Zm00001d050061 for *RAD5B*. For all 153 genes the relative expressions graphs were analysed by plotting the library and gene length normalized counts from the five meiotic stages. 88 genes could be sorted into three main groups, namely genes of which the normalized counts of the mRNA and RPF showed the same pattern during meiosis, genes that showed a peak of RPFs at LEP and genes of which the total relative mRNA expression went down at MII while the RPF normalized counts went up. It has to be noted that since these datasets originate from only one replicate, a normalization of the data across the different meiotic stages could not be performed, therefore I further assumed that the relative transcript levels described here reflect the absolute expression levels during meiosis. The expression values and the relative expression plots from all the meiotic candidate genes will be available in the host lab.

One of the genes with a parallel pattern of mRNA and RPF normalized read counts during the meiotic division, is the candidate *CYCA1-2/TAM* ortholog Zm00001d009011. The transcription and translation of *TAM* gradually increases from PRE to ZYG, reaching the highest expression at ZYG, followed by a decrease (**Figure 2.8A**). This describes a similar expression pattern as seen for the genomic *TAM-GFP* reporter in *Arabidopsis* meiocytes (**Supplemental Figure S2.1**).

Another example for parallel behaviour of transcriptome and translome is *MEI2-LIKE 1/4 (ML1/ML4)*, a gene involved in the regulation of the meiotic nuclear division. The curves of transcription and translation stay at a low level from PRE to PACH and then show a steep increase at MII (**Figure 2.8B**). This high expression of *ML1/ML4* at MII is in accordance with its function as positive regulator of nuclear division that takes place at the end of meiosis I and meiosis II.

Next, *RAD50* and *PARTING DANCERS (PTD)* are expected to be expressed in early meiosis since they are both involved in meiotic recombination, *i.e.* *RAD50* is part of the meiotic recombination complex that processes DSBs and *PTD* is a DNA ligase

involved in the resolution of meiotic recombination intermediates. In the case of *RAD50*, the relative levels of transcription and translation are high in PRE, after which they decrease gradually until MII (**Figure 2.8C**), while the expression plot of *PTD* is consistent with a slightly later requirement as it shows an increase from PRE to LEP, reaching the highest counts at LEP and then gradually decreasing its mRNA and RPF counts till MII (**Figure 2.8D**). Taken together, these genes have a similar curve of expression for mRNA and RPF which corresponds to their known or expected protein expression pattern, thus the relative expression plots might reflect the absolute expression levels. If so, those genes most likely do not undergo any type of translational regulation.

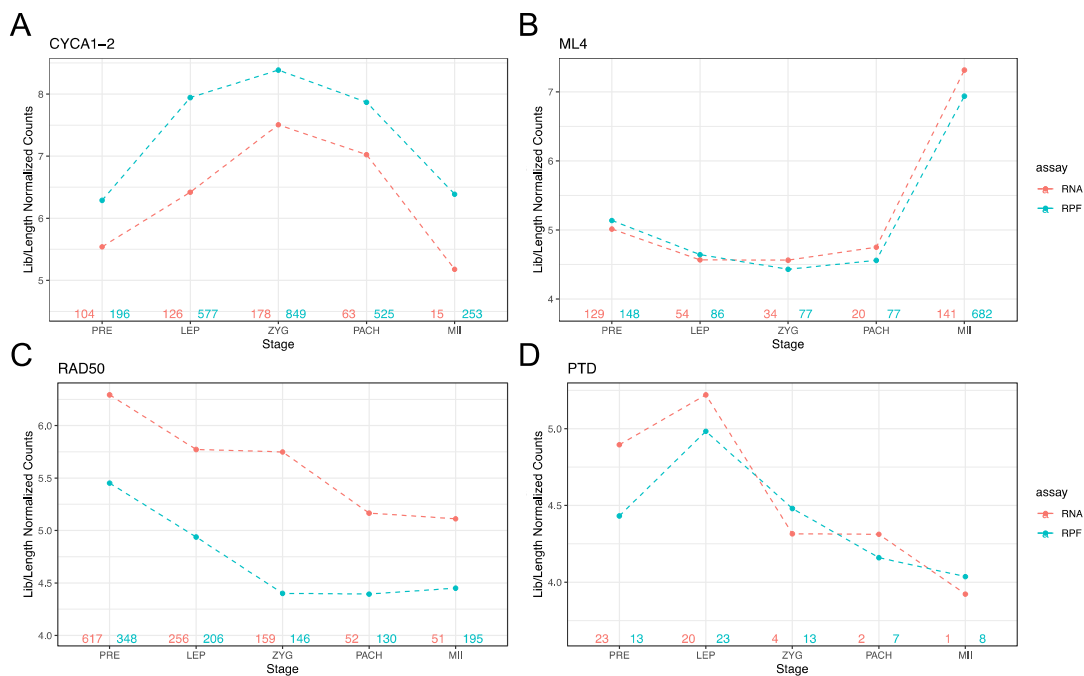


Figure 2.8. Expression plots of genes displaying the same pattern for mRNA and RFP counts during meiosis.

The RNA (red) and RPF (blue) library and length normalized counts for the different meiotic stages were plotted for (A) *CYCA1-2* (*TAM*, Zm00001d009011), (B) *ML4/ML1* (Zm00001d035763), (C) *RAD50* (Zm00001d050612) and (D) *PTD* (Zm00001d009728) in premeiosis (PRE), leptotene (LEP), zygotene (ZYG), pachytene (PACH) and from diakinesis to tetrad (MII). The number of raw reads are given at the bottom of the plots.

The second group of genes have expression profiles that show a peak of RPF counts at LEP, while the mRNA counts describe a different pattern. First example is the kinase *ATM*, playing an important role in the regulation of recombination in meiosis. The relative translation values show a steep increase from PRE to LEP and a slow decrease from LEP to MII. Its transcription describes a gradual increase from

PRE to ZYG, reaching the highest expression at ZYG and slowly decreasing thereafter (**Figure 2.9A**).

SPO22/ZIP4 is known to be involved in crossover formation and is expected to be expressed during early prophase. The RNA expression plot of *SPO22/ZIP4* shows a similar pattern as described for *ATM*, peaking at ZYG. Instead, the RPF counts show a steep increase from PRE to LEP, after which they gradually decrease (**Figure 2.9B**). Although this expression pattern fits its expected expression, for both *ATM* and *SPO22/ZIP4*, it is counterintuitive that the RNA counts peak one meiotic stage after the highest detected RPF counts. These results need to be confirmed in the future with the second biological repeat.

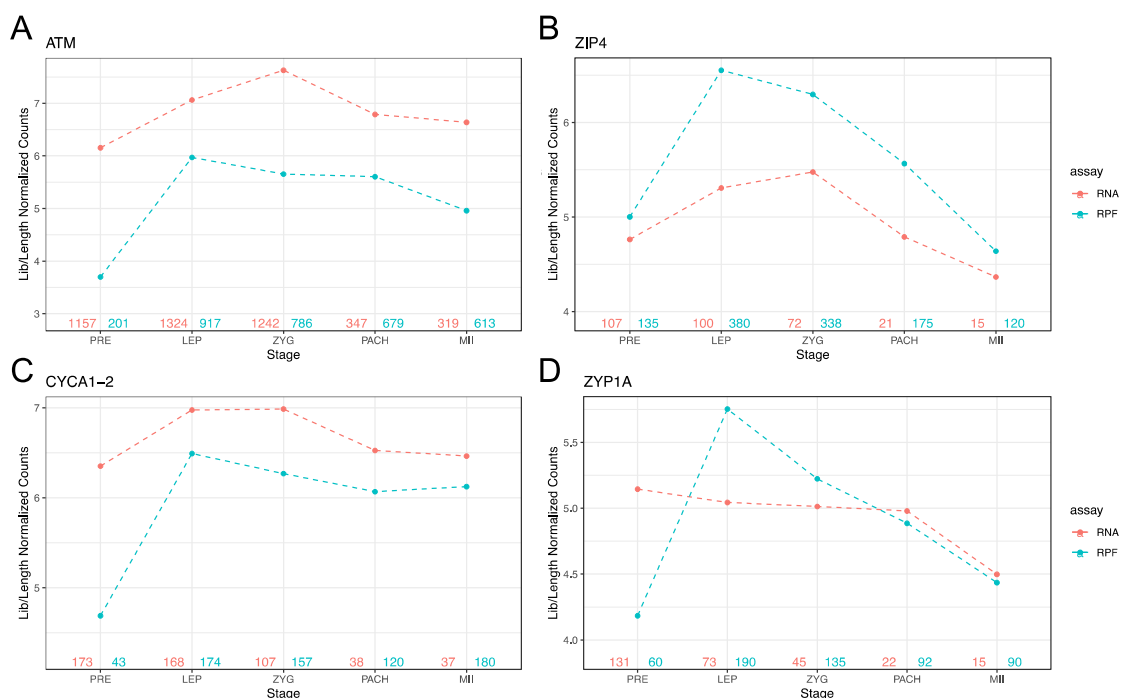


Figure 2.9. Expression plots of genes with the highest RPF at leptotene.

The RNA (red) and RPF (blue) library and length normalized counts were plotted for *ATM* (A, Zm00001d040166), *ZIP4/SPO22* (B, Zm00001d042558), *CYCA1-2/TAM* (C, Zm00001d010404) and *ZYP1A/B* (D, *ZIPPER1*, Zm00001d025575) for the different meiotic stages, premeiosis (PRE), leptotene (LEP), zygotene (ZYG), pachytene (PACH) and diakinesis to tetrad (MI). The number of raw reads are given at the bottom of the plots.

Next, the mRNA counts of another *CYCA1-2/TAM* candidate ortholog, Zm00001d010404, seem to be relatively constant during the different meiotic stages. In contrast, the RPF counts at PRE are rather low and steeply increase at LEP, remain relatively constant thereafter (**Figure 2.9C**). Compared to the other candidate ortholog, the expression curves show a clearly different expression pattern.

A last example is *ZYP1A/B*, which has an interesting expression plot, since the RNA expression is relatively constant from PRE to PACH, with a slight decrease at MII, but the relative RPF counts show a very steep increase from PRE to LEP, reaching the highest value at LEP, where after the translation values gradually decrease till MII (**Figure 2.9D**). Assuming that the relative values are proportional to the absolute levels in the meiocytes, this *ZYP1A/B* expression pattern suggests that there is translational regulation of *ZYP1A/B*. This hypothesis needs to be confirmed and further investigated in future.

In the third group of genes, the relative transcription values go down at MII, while the values for translation go up, e.g. *BUDDING UNINHIBITED BY BENZYMIDAZOL RELATED 1 (BUBR1)* and *XPG-LIKE ENDONUCLEASE 2 (GEN2)*. *BUBR1* is described to be involved in meiotic sister chromatid cohesion, needed during meiosis I, and in the SAC signalling at metaphase-anaphase I transition. Its RNA counts are first relatively stable till PACH and clearly drop at MII, while the RPF counts show first a steep decrease from PRE to LEP, followed by an increase till MII (**Figure 2.10A**). Although the RPF pattern fits the expected expression, the sudden drop of RNA expression at MII is counterintuitive and highly interesting to confirm and investigate in the future. *GEN2* plays a role in the resolution of Holliday junctions, at late prophase. The relative RNA expression peaks at PACH and steeply decreases at MII, while the RPF counts gradually increase from PRE to PACH, followed by a steep increase at MII (**Figure 2.10B**). This result suggests a delay in translation which should be investigated more closely in future.

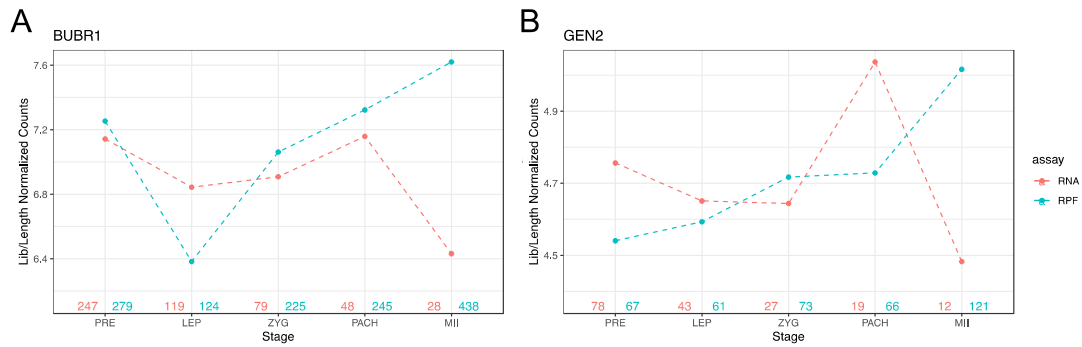


Figure 2.10. Expression plots of genes displaying a decrease of RNA levels and an increase of RPFs at MII.

The RNA (red) and RPF (blue) library and length normalized counts were plotted for *BUBR1* (A, Zm00001d015863) and *GEN2* (B, Zm00001d034968) for the different meiotic stages, premeiosis (PRE), leptotene (LEP), zygotene (ZYG), pachytene (PACH) and diakinesis to tetrad (MII). The number of raw reads are given at the bottom of the plots.

In addition to the three main expression patterns described above, I would like to point out four more genes with interesting curves. First, for one of the candidate orthologs of *PHYTOCHROME C (PHYC)*, Zm00001d013262, its mRNA expression seems to be relatively constant with a slight decrease from LEP onwards, while the RPF counts show a clear increase from ZYG to MII (**Figure 2.11A**). Next, in the case of *MLH3*, the RNA expression pattern shows an increase from PRE to LEP, followed by a decrease, while the translation pattern has an increase from PRE to ZYG and then slightly decreases again (**Figure 2.11B**). So, the mRNA counts peak one stage prior to highest detected RPF counts, indicating translational control. Also for two of the candidate orthologs of *MS5*, *i.e.* Zm00001d027809 and Zm00001d038642, the mRNA counts increase one meiotic stage prior to the increase of the RPF counts (**Figure 2.11C,D**). If the obtained results can be confirmed by a second replicate, those genes are promising candidates to further investigate translational regulation.

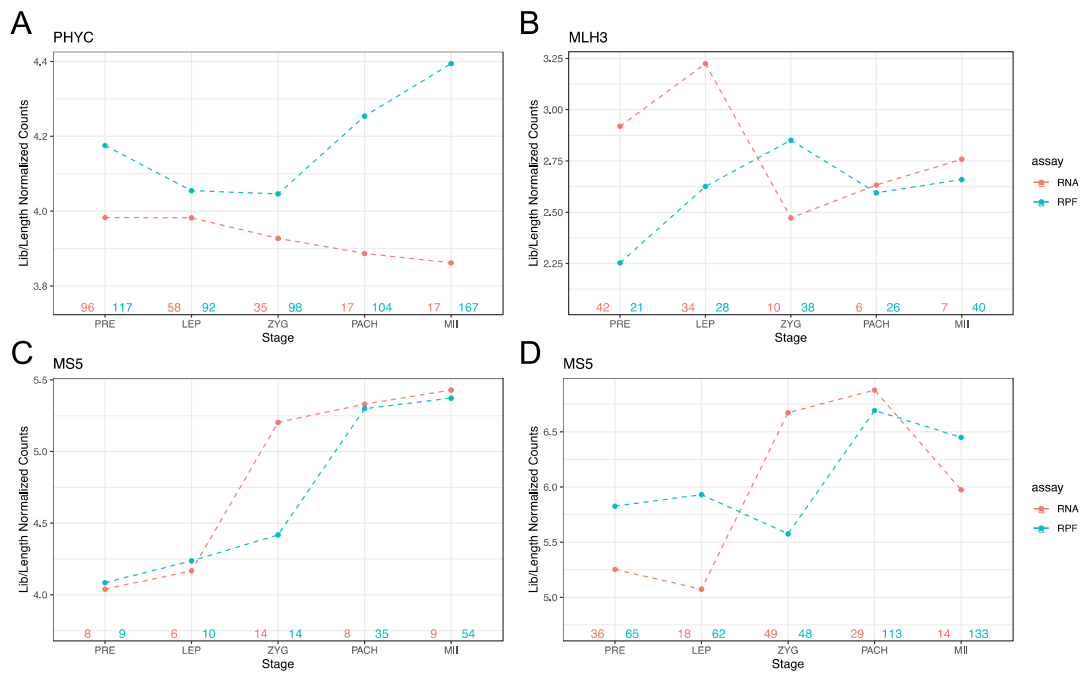


Figure 2.11. Expression plots of additional genes with potential for translational regulation.

The RNA (red) and RPF (blue) library and length normalized counts were plotted for *PHYC* (A, Zm00001d013262), *MLH3* (B, Zm00001d006307), *MS5* (C, Zm00001d027809) and *MS5* (D, Zm00001d038642) for the different meiotic stages, premeiosis (PRE), leptotene (LEP), zygotene (ZYG), pachytene (PACH) and diakinesis to tetrad (MI I). The number of raw reads are given at the bottom of the plots.

Overall, the differential expression analysis of the transcriptome and translome during meiosis led to highly interesting observations and should be studied in more detail in the future. The above presented expression plots can only be considered as preliminary data, since at least one additional replicate is needed to allow for a robust expression analysis. The libraries for one additional biological repeat were generated and the quality of the libraries was confirmed to be sufficient for sequencing (**Supplemental Figure S2.9**). Unfortunately, due to technical changes at the Illumina Sequencing Platform, *i.e.* the introduction of new flow cells causing adaptor incompatibility with my libraries, it was not possible to sequence the second repeat with the current system. Ongoing contact with an institute that still has the Illumina HiSeq 2500 sequencing system with compatible flow cells for my libraries will likely allow for the sequencing of the second repeat in the near future and the analysis of the sequencing data will be resumed.

2.2. The gene specific approach- A TRICKy system in Arabidopsis

2.2.1. The principle of the MS2-system and TRICK

The MS2-system is an experimental setup to monitor and compare the mRNA level and protein level from a gene of interest on a cellular level. This technique makes use of components of the MS2-bacteriophage, that forms a viral capsid through RNA-protein interaction and protein multimerization using its RNA and coat proteins. The MS2-system was first described in yeast (Bertrand et al., 1998). A transcript of interest fused to multiple copies of the MS2 RNA hairpin structure is co-expressed with a modified MS2-coat protein (MCP) with a fluorescent tag. The MS2-loops do not naturally occur in eukaryotes and the highly specific and sensitive binding of multiple MCPs to the MS2 hairpin structures leads to the possibility to image mRNA *in vivo*. This technique is widely used in different biological systems. Here the MS2-system is used in combination with a classical GFP reporter, meaning the fusion of a green fluorescent tag to the genomic sequence of a gene of interest and the MS2-hairpin loops inserted in the 3'UTR of the gene, called the mRNA reporter (**Figure 2.12A**). It is very important that the mRNA reporter is functional and rescues in the mutant background. In addition, the protein localization should be identical to the localization of the classical genomic reporter of that gene. It was anticipated that simultaneous visualization of the mRNA and protein of interest would be possible, allowing a comparison throughout the meiotic division.

The modified MCP, also called the RNA biosensor, is designed to localize to the nucleus of the cell, due to its nuclear localization signal (NLS). Further, RFP is used as tag to visualize for the biosensor (**Figure 2.12B,C,C'**). After transcription of the mRNA reporter, the biosensor is expected to bind to the MS2 RNA hairpin loops (**Figure 2.12D,D'**). Next, according to findings in yeast, the mRNA reporter together with its bound biosensor is exported from the nucleus into the cytoplasm, where translation takes place (**Figure 2.12E**). The cytoplasmic portion of mRNA reporter can be visualized due to the co-exported RNA biosensor, resulting in a red fluorescent signal in the cytoplasm (**Figure 2.12E'**). Once gene of interest gets translated, green fluorescence appears labelling the protein of interest (**Figure 2.12F,F'**). In addition to the comparison of the cytoplasmic mRNA level and general protein level at any given developmental stage, this system can also visualize if

translation happens immediately or is delayed after the mRNA is exported into the cytoplasm. A time discrepancy in the appearance of the cytoplasmic mRNA (red fluorescent signal) and the protein (green fluorescent signal) would indicate translational regulation.

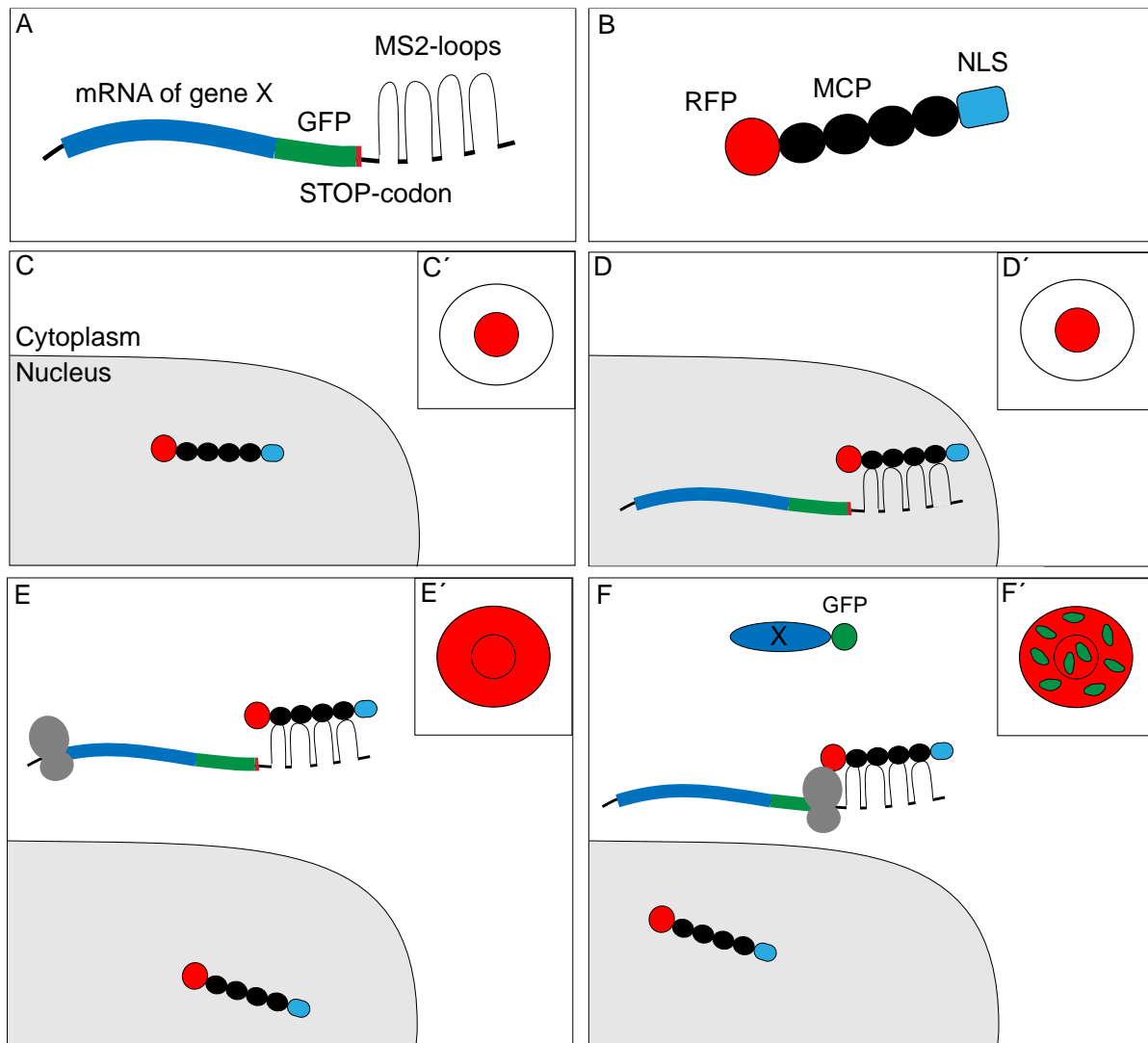


Figure 2.12. Scheme of the principle of the MS2-system.

A schematic representation of the mRNA reporter (A; mRNA of the gene of interest X in blue; GFP in green; stop codon in dark red) and the RNA biosensor (B; RFP in red; MCP in black; NLS in light blue). The anticipated events of the MS2-system on cellular level: (C) before transcription, (D) after transcription, (E) before translation and (F) after translation of the mRNA reporter. The corresponding fluorescent pattern is given in the upper right corner (C', D', E', F'; RFP in red; GFP in green).

To investigate more precisely the spatiotemporal translational regulation of a gene of interest, another system called Translating RNA Imaging by Coat Protein Knock-off (TRICK) was used to visualize the first round of translation. This system was first described in *Drosophila* oocytes (Halstead et al., 2015). In addition to the MS2-system, TRICK also makes use of a PP7-system, which is based on the same principle as the MS2-system. More specifically, the PP7 bacteriophage coat proteins (PCP) bind to its cognate RNA structures, the PP7-RNA hairpin loops, with very high affinity. The PP7-system was first used in yeast, to study transcription initiation and elongation (Larson et al., 2011). For the TRICK system, the two biosensors are used, MS2-biosensor and PP7-biosensor, in combination with a more elaborate mRNA reporter, which consist of the fusion of the gene of interest with the PP7-hairpin loops within the coding DNA sequence (CDS) and the MS2-hairpin loops after the CDS, within the 3'UTR (**Figure 2.13A,B**).

The TRICK system is designed to work as follows: the biosensors localize to the nucleus, due to their NLS, and after transcription of the mRNA reporter, both biosensors bind their respective hairpin loops (**Figure 2.13C**). The co-expression of the biosensors can be anticipated as a yellow nuclear signal, coming from a merge of RFP of the MS2-biosensor and GFP of the PP7-biosensor (**Figure 2.13C'**). The export of the mRNA reporter and its bound biosensors out of the nucleus can be visualized by the appearance of a yellow signal in the cytoplasm (**Figure 2.13D,D'**). During the first round of translation, the ribosome knocks off the PP7-biosensor, since PCP is bound to the mRNA hairpin loops before the translation stop codon, and the PP7-biosensor relocates to the nucleus (**Figure 2.13E,E'**). Thus, after the first round of translation only the MS2-biosensor remains bound to the mRNA reporter, resulting in only red fluorescent signal in the cytoplasm (**Figure 2.13F, F'**).

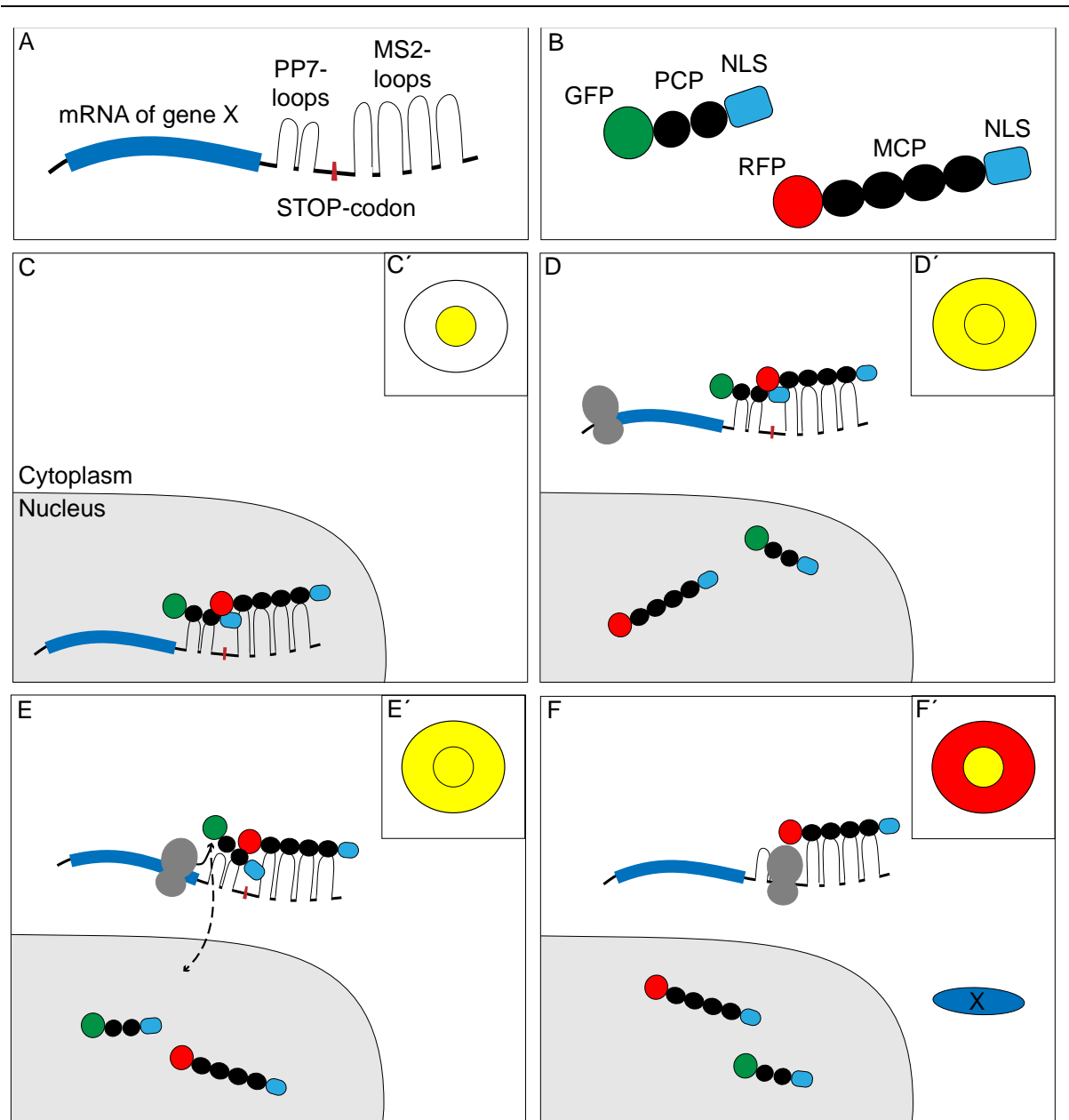


Figure 2.13. Scheme of the principle of TRICK.

A schematic representation of the mRNA reporter (A; mRNA of the gene of interest X in blue; stop codon in dark red) and the two RNA biosensors (B; GFP in green; RFP in red; PCP and MCP in black; NLS in light blue). The anticipated events of the TRICK system on cellular level: (C) after transcription, (D) before translation, (E) during the first round of translation and (F) after the first round of translation. The corresponding fluorescent pattern is given in the upper right corner (C', D', E', F'; RFP in red; colocalization of RFP and GFP in yellow).

2.2.2. The mRNA reporters of the MS2-system

For this gene-specific approach to investigate translational regulation, three meiotic genes *ASY3*, *TAM* and *REC8* were selected. The MS2-loops were first inserted directly after the stop codon of a previously generated and functional genomic reporter of *ASY3* (Yang et al., 2019). The resulting *ASY3:GFP:MS2:UTR* construct was transformed into the *asy3* mutant and its expression was checked in male meiocytes and compared to the previously described *ASY3* localization (Yang et al., 2019). Briefly, *ASY3:GFP* is localized in the nucleus from early leptotene onwards, gradually appearing on the condensing chromosomes, labelling the chromosomes very clearly from zygotene to pachytene, after which the *ASY3* signal strongly declines and become undetectable.

However, the *ASY3:GFP:MS2:UTR* reporter did not display any fluorescent signal, suggesting that the insertion of the MS2-loops directly after the stop codon led to problems to express *ASY3* (**Figure 2.14A**). For this reason, a series of MS2-loops insertion constructs were generated at different positions within the 3'UTR of the mRNA. According to the TAIR database (www.arabidopsis.org), *ASY3* has a predicted 3'UTR of 376 bp, thus I choose to generate and test the following constructs: *ASY3:GFP:100bpUTR:MS2*, *ASY3:GFP:200bpUTR:MS2*, *ASY3:GFP:300bpUTR:MS2* and *ASY3:GFP:UTR:MS2*. In order to assess the functionality of the reporters, the constructs were transformed into the *asy3* mutant. A weak but nuclear signal from the *ASY3:GFP:100bpUTR:MS2* reporter could be detected (**Figure 2.14A**), instead the insertion of the MS2-loops further downstream of the stop codon resulted in a stronger signal, qualitatively similar to the original *ASY3* reporter (**Figure 2.14A**). Both *ASY3:GFP:200bpUTR:MS2*, *ASY3:GFP:300bpUTR:MS2* and *ASY3:GFP:UTR:MS2* showed clear *ASY3* nuclear localization as described before (**Figure 2.14A**). Taken together, four out of the five MS2-insertion constructs led to a qualitatively correct *ASY3* localization, although the signal of the *ASY3:GFP:100bpUTR:MS2* construct was clearly weaker, showing that the insertion site of MS2-loops has an influence on expression strength.

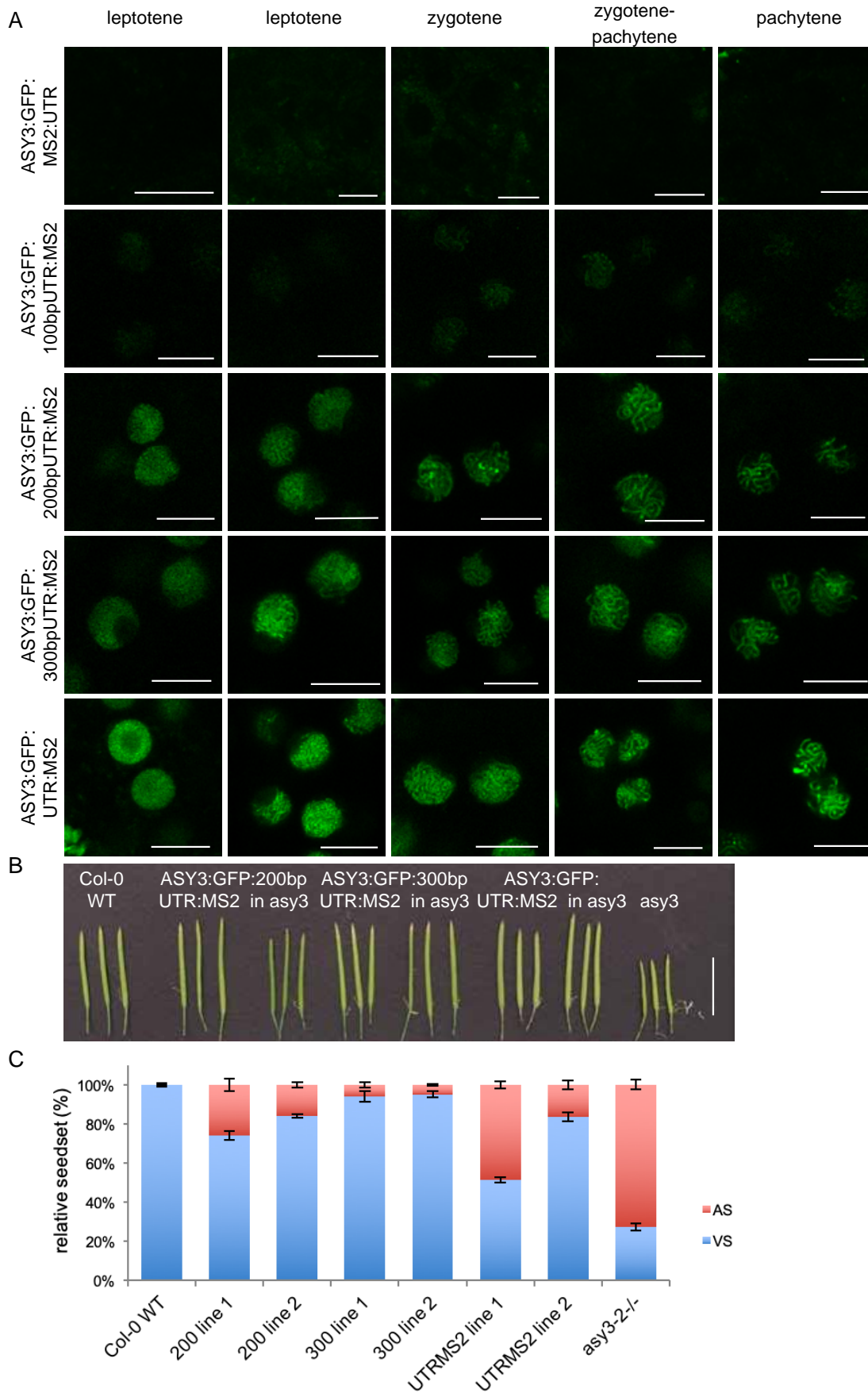


Figure 2.14. The ASY3 mRNA reporters.

(A) The different ASY3 mRNA reporters *ASY3:GFP:MS2:UTR* (row 1), *ASY3:GFP:100bpUTR:MS2* (row 2), *ASY3:GFP:200bpUTR:MS2* (row 3), *ASY3:GFP:300bpUTR:MS2* (row 4) and *ASY3:GFP:UTR:MS2* (row 5) in *Arabidopsis* male meiocytes from leptotene (column 1-2), zygotene (column 3) to pachytene (column 4-5) (*ASY3:GFP* in green; scale bar, 10 μ m). (B) Siliques and (C) relative seed set of the Col-0 wild type, *ASY3:GFP:200bpUTR:MS2* in *asy3* (200 line 1,2), *ASY3:GFP:300bpUTR:MS2* in *asy3* (300 line 1,2), *ASY3:GFP:UTR:MS2* in *asy3* (UTRMS2 line 1,2) and *asy3*. AS: aborted seeds; VS: viable seeds; Scale bar, 1 cm. Error bars represent standard deviations.

Next, I investigated if the three constructs with the highest expression can rescue the *asy3* mutant phenotype, by analysing the seed set of two independent lines per construct. While the *asy3* mutant control showed only 27% viable seeds, which was consistent with previous study (Ferdous et al., 2012), the wildtype control had 100% viable seeds. The seed viability of the MS2-construct containing plants ranged between 51 and 95% (**Figure 2.14B,C**). The two *ASY3:GFP:300bpUTR:MS2* lines showed the highest seed viability with 94% and 95% of viable seeds (**Figure 2.14B,C**). Taken together, the different MS2-insertion constructs rescue the mutant phenotype only partially.

Further, in order to test for a functional mRNA reporter, the presence of the MS2-loops into the mRNA needed to be confirmed. To this end, an RT-PCR was performed to detect the presence of the loops in the mRNA reporter. For all the tested constructs, except the *ASY3:GFP:UTR:MS2*, the MS2-loops could be detected (**Supplemental Figure S2.10A,B**).

Based on these results, *ASY3:GFP:200bpUTR:MS2* and *ASY3:GFP:300bpUTR:MS2* were selected as the best candidates to be crossed with the biosensors.

For the generation and selection of suitable *TAM* mRNA reporters, the same procedure as for the *ASY3* mRNA reporters was performed. A series of MS2-loops insertions at different positions within the 3'UTR of the previously generated genomic *TAM* reporter were constructed (unpublished, generated by Dr. Chao Yang). *TAM* had a predicted 3'UTR length of 250 bp and I choose five different insertion positions for the MS2-loops, resulting in the generation of *TAM:GFP:MS2:UTR*, *TAM:GFP:20bpUTR:MS2*, *TAM:GFP:50bpUTR:MS2*, *TAM:GFP:100bpUTR:MS2* and *TAM:GFP:200bpUTR:MS2* reporter constructs, which were all transformed in the heterozygous *tam* mutant.

The expression of these reporters was analysed and compared with the previously described TAM localization (unpublished, generated by Dr. Chao Yang). Briefly, TAM localizes in the cytoplasm from early leptotene onwards. The protein amount gradually increases, reaching the highest expression level at early diplotene, after which it decreases until the end of meiosis I and the residual protein relocates to the organellar band at interkinesis (**Supplemental Figure S2.1**).

The expression of the TAM:GFP:MS2:UTR and TAM:GFP:20bpUTR:MS2 was undetectable, while the reporter TAM:GFP:50bpUTR:MS2 showed a very weak but cytoplasmic localization as described above (**Figure 2.15A**). The more downstream from the stop codon the MS2-loops were inserted, the higher the expression of TAM:GFP, with a clearly visible expression in the TAM:GFP:100bpUTR:MS2 and TAM:GFP:200bpUTR:MS2 expressing plants (**Figure 2.15A**).

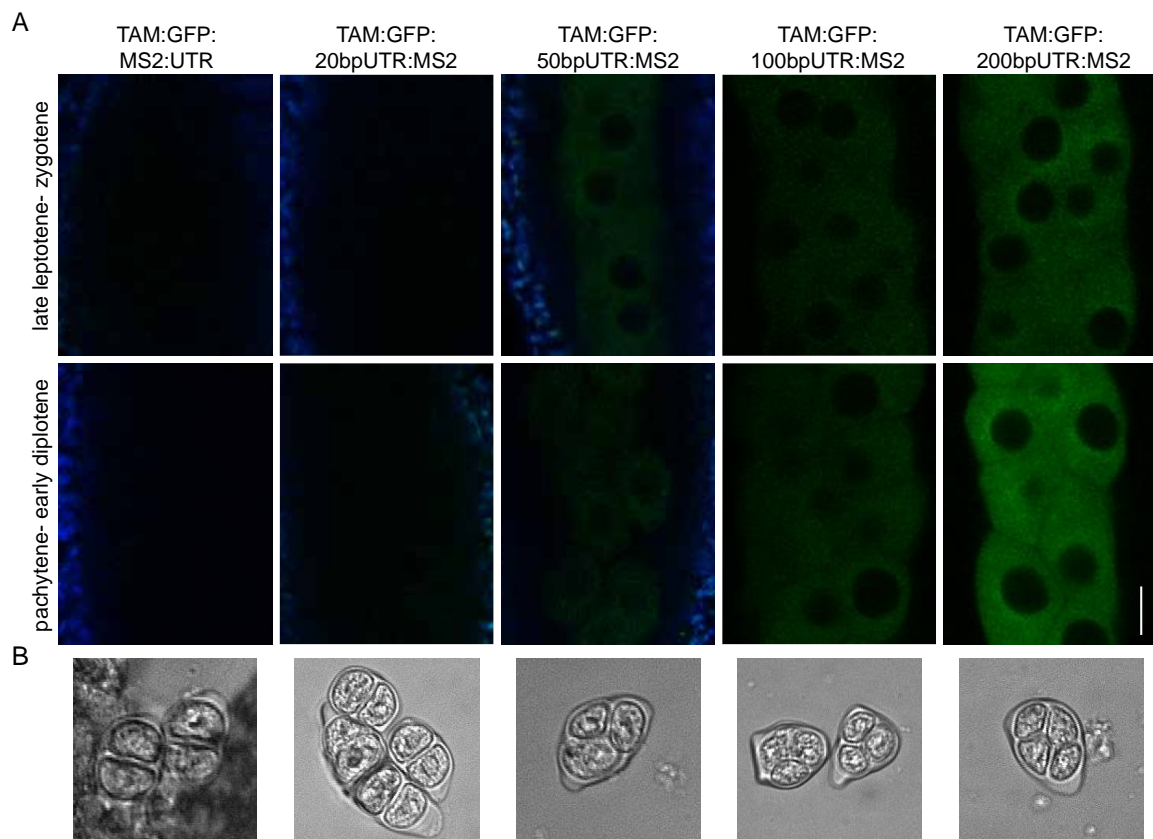


Figure 2.15. The TAM mRNA reporters.

(A) The different TAM mRNA reporters TAM:GFP:MS2:UTR (column 1), TAM:GFP:20bpUTR:MS2 (column 2), TAM:GFP:50bpUTR:MS2 (column 3), TAM:GFP:100bpUTR:MS2 (column 4) and TAM:GFP:200bpUTR:MS2 (column 5) in Arabidopsis male meiocytes from late leptotene-zygotene (row 1) to pachytene-early diplotene (row 2) (TAM:GFP in green; autofluorescence in blue; scale bar, 10 μ m). (B) Dyad or tetrad formation in TAM:GFP:MS2:UTR in *tam* (column 1),

TAM:GFP:20bpUTR:MS2 in *tam* (column 2), *TAM:GFP:50bpUTR:MS2* in *tam* (column 3), *TAM:GFP:100bpUTR:MS2* in *tam* (column 4) and *TAM:GFP:200bpUTR:MS2* in *tam* (column 5).

Homozygous *tam* mutants undergo only the first meiotic division and display a premature cell wall deposition during interkinesis. This leads to formation of dyads, instead of tetrads, resulting in an increased pollen size (Jha et al., 2014). The functionality of the MS2-constructs was analysed in the T2-generation, by the presence of dyads or tetrads in *tam* homozygous mutant background plants. The plants expressing *TAM:GFP:MS2:UTR* and *TAM:GFP:20bpUTR:MS2* formed dyads, *i.e.* the constructs were unable to rescue the *tam* mutant phenotype. Instead plants carrying the other constructs *TAM:GFP:50bpUTR:MS2*, *TAM:GFP:100bpUTR:MS2* and *TAM:GFP:200bpUTR:MS2* did not form dyads, but normal tetrads, which confirmed the functionality of these constructs (**Figure 2.15B**). Last but not least, the presence of the MS2-loops in the *TAM* mRNA reporters was confirmed using RT-PCR (**Supplemental Figure S2.10C**).

The *TAM:GFP:200bpUTR:MS2* construct was selected as the best candidate of the *TAM* mRNA reporter to be crossed with the biosensors. Due to the fact that the mRNA reporters *TAM:GFP:100bpUTR:MS2* and *TAM:GFP:200bpUTR:MS2* were generated at a later time point in the project, the *TAM:GFP:50bpUTR:MS2* reporter was crossed with the biosensors and analysed.

From the expression and functionality analysis of both *ASY3* and *TAM* mRNA reporters, it is clear that the position of the MS2-loops into the mRNA affects its translation or mRNA stability. The optimal distance between the CDS and the MS2-loops in order to achieve a functional mRNA reporter seemed to be around 200 bp in both cases.

Last, the *REC8* mRNA reporters were generated. Similar to the *ASY3* and *TAM* mRNA reporters, a series of MS2-loops insertion constructs were generated also for *REC8*. The predicted 3'UTR length of *REC8* is 125 bp and five different insertion positions were selected: directly after stop codon (*REC8:GFP:MS2:UTR*), 20 bp (*REC8:GFP:20bpUTR:MS2*), 40 bp (*REC8:GFP:40bpUTR:MS2*), 70 bp (*REC8:GFP:70bpUTR:MS2*) downstream of the stop codon within the 3'UTR and directly at the end of the 3'UTR (*REC8:GFP:UTR:MS2*). All constructs were made by

Manuel Torralba (Erasmus Bachelor student) under my supervision and transformed into the heterozygous *rec8* mutant.

In the T1-generation the expression of the reporters was analysed and compared with the previously described REC8 localization (Prusicki et al., 2019). Briefly, REC8 is expressed in the nucleus of the meiocytes, showing a diffuse, slowly increasing nuclear signal starting shortly before leptotene which then gradually becomes more distinct as it localizes to the condensing chromosomes. At pachytene, REC8 labels the chromosomes as thick thread like structures. Subsequently REC8 gets removed from the chromosomes, changing its distinct chromosomal localization into a diffuse signal until complete disappearance at anaphase I onset.

Surprisingly, a weak nuclear signal in plants carrying the *REC8:GFP:MS2:UTR* reporter could be detected. *REC8:GFP:20bpUTR:MS2* and *REC8:GFP:70bpUTR:MS2* plants showed very weak REC8 expression and in the *REC8:GFP:40bpUTR:MS2* plants no expression could be detected. The *REC8:GFP:UTR:MS2* reporter showed, although weaker, REC8 localization as described above for the original reporter (**Figure 2.16**).

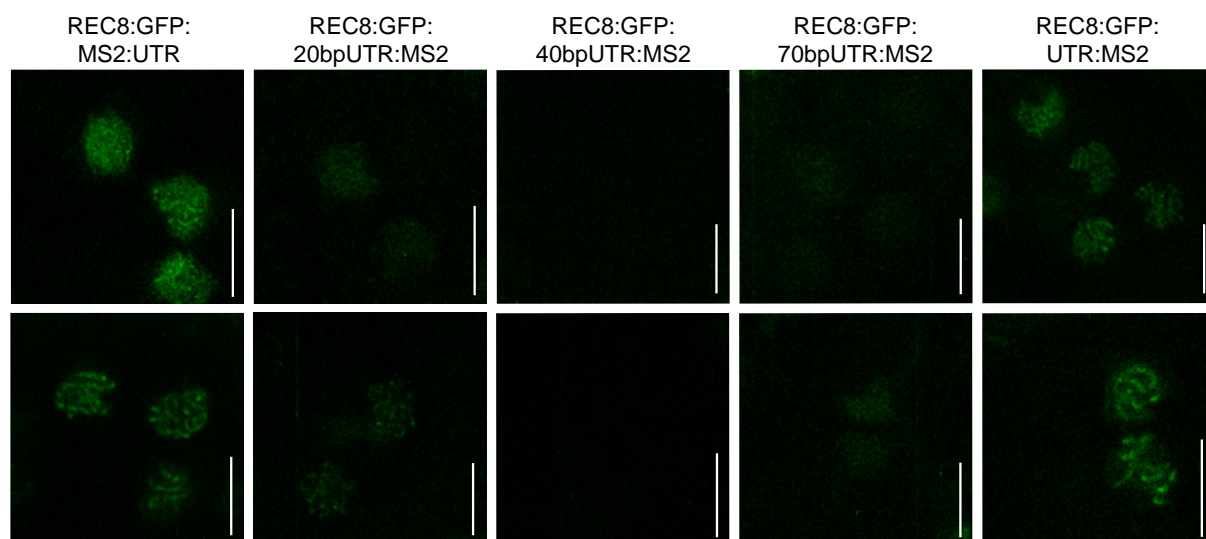


Figure 2.16. The REC8 mRNA reporters.

The REC8 mRNA reporters *REC8:GFP:MS2:UTR* (column 1), *REC8:GFP:20bpUTR:MS2* (column 2), *REC8:GFP:40bpUTR:MS2* (column 3), *REC8:GFP:70bpUTR:MS2* (column 4) and *REC8:GFP:UTR:MS2* (column 5) in Arabidopsis male meiocytes in prophase I (REC8:GFP in green; scale bar, 10 μ m).

The functionality of these reporters was analysed in the T2-generation, by investigating their capacity to rescue the sterility phenotype of the homozygous *rec8* mutant. Unfortunately, all constructs failed to rescue the mutant phenotype, showing severe sterility defects (data not shown). Although two out of the five *REC8* mRNA reporters showed weak *REC8* expression, none of them could rescue the *rec8* mutant phenotype, which made these mRNA reporters unreliable for further analysis. Most probably, the expression level of the *REC8* mRNA reporter was not high enough, *i.e.* not enough protein, to rescue to *rec8* mutant phenotype.

2.2.3. The RNA biosensors

The RNA biosensors are designed to track the mRNA of your gene of interest. The biosensor consists of either MCP or PCP, which binds specifically to the MS2- and PP7-loops, respectively, fused with RFP and an NLS (**Figure 2.12B, 2.13B**). Two promoters that are expressed in meiocytes and throughout the complete meiotic division were selected to drive their expression: pCDKA;1 and pUBIQUITIN 10 (pUBQ10). Both biosensor constructs were made and transformed into wild-type plants and were expected to show a nuclear signal, due to their NLS (**Figure 2.12C,C'**).

First, the MCP biosensor was analysed. The expression level of both pCDKA;1:NLS:MCP:RFP and pUBQ10:NLS:MCP:RFP was relatively weak in the meiocytes, compared to the surrounding somatic cells (**Figure 2.17A,B**). In addition, the biosensors showed mainly a nucleolar localization in the meiocytes, while in the somatic tissue also the nucleoplasm displayed a clear signal. However also here the nucleolar signal was much stronger. When both MCP and PCP biosensors were co-expressed the localization of the MCP biosensor in meiocytes was again nucleolar, as seen for the MCP reporter alone, while the PCP biosensor showed some nucleoplasmic but also mainly nucleolar localization (**Figure 2.17C**).

To test if the nucleolar localization is specific for meiocytes and surrounding tissue, the expression of the MCP biosensor was analysed in root cells. The cell wall of the root cells was stained with propidium iodide (PI), which unfortunately has an overlapping emission peak (max of 636 nm) with the emission peak of RFP (max of 558 nm). Nonetheless, both signals have very distinct localization and are distinguishable. In this analysis, the nucleolar localization of the MCP reporter could be confirmed also for root cells (**Figure 2.17D**). The nucleolar localization of the

biosensors raised the question if the MCP and PCP would be able to bind to the MS2- and PP7-loops, respectively, since the mRNA is expected to accumulate in the nucleoplasm.

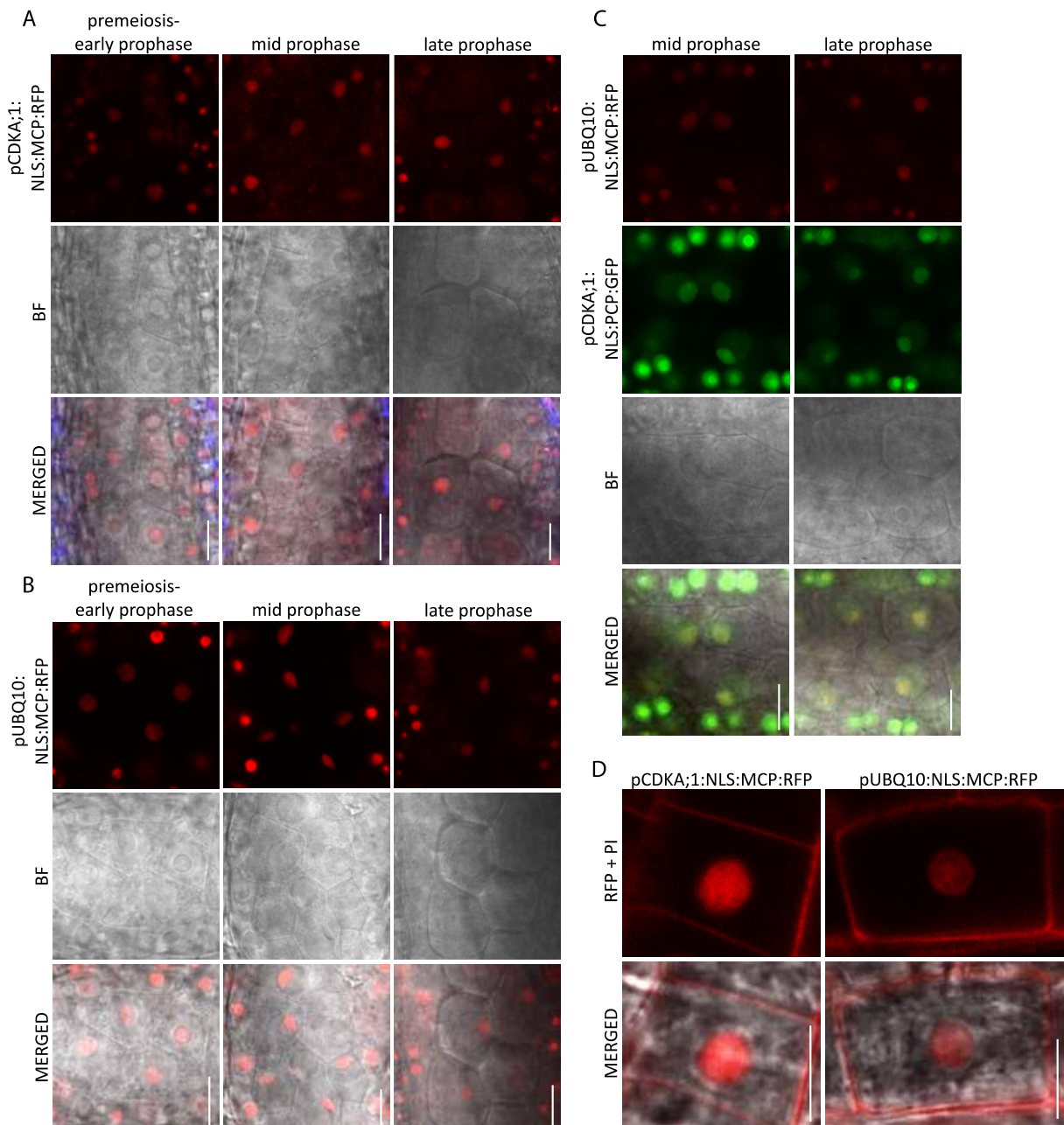


Figure 2.17. The RNA biosensors.

The RNA biosensors (A) *pCDKA;1:NLS:MCP:RFP* and (B) *pUBQ10:NLS:MCP:RFP* in Arabidopsis male meiocytes from premeiosis-early prophase (column 1), mid prophase (column 2) to late prophase (column 3) (MCP:RFP in red; autofluorescence in blue; bright field (BF); scale bar, 10 μm). (C) The MCP and PCP biosensors co-expressed, *pUBQ10:NLS:MCP:RFP* and *pCDKA;1:NLS:PCP:GFP*, in Arabidopsis male meiocytes from mid prophase (column 1) to late prophase (column 2) (MCP:RFP in red; PCP:GFP in green; bright field (BF); scale bar, 10 μm). (D) The RNA biosensors *pCDKA;1:NLS:MCP:RFP* (column 1) and *pUBQ10:NLS:MCP:RFP* (column 2) in Arabidopsis root cells (MCP:RFP and PI in red; scale bar, 10 μm).

2.2.4. The MS2-system in Arabidopsis male meiocytes

To answer the question if the biosensors would be able to bind to the bacteriophage loops, the different MCP biosensors were crossed with the selected mRNA reporters of *ASY3* and *TAM* and plants co-expressing the biosensor and mRNA reporter were analysed in the T1-generation.

Both crosses of the *ASY3* mRNA reporters with the biosensors, *ASY3:GFP:200bpUTR:MS2* x *pCDKA;1:NLS:MCP:RFP* and *ASY3:GFP:300bpUTR:MS2* x *pUBQ10:NLS:MCP:RFP*, displayed a very weak nucleolar localization of the biosensor and nuclear localization of the mRNA reporter (**Figure 2.18A**). Due to very weak signal, no clear cytoplasmic dots from the biosensor could be detected. To improve the signal-to-noise ratio, a more sensitive detection mode called the photon-counting mode, which is used for single molecule experiments, was utilized. By applying the photon-counting mode up to one dot-like structure per cell could be detected, localizing in the nucleus and/or in the cytoplasm near the nucleus (**Figure 2.18A**). To investigate if the observed dots are coming from the binding of the biosensor to the *ASY3* mRNA reporter, the photon-counting mode was also applied to the biosensor alone. However, similar dot-like structures were detected in the nuclei of the meiocytes of the *pUBQ10:NLS:MCP:RFP* plants, showing that these dots occur independently of the presence of the mRNA reporter (**Figure 2.18A**).

Next, the cross of *TAM:GFP:50bpUTR:MS2* x *pCDKA;1:NLS:MCP:RFP* was analysed and dot-like structures could be observed in the nucleus and/or in cytoplasm near the nucleus (**Figure 2.18B**). Compared to the results from plants expressing the biosensor alone and plants co-expressing the *ASY3* mRNA and the biosensor, the number of dots were increased for the *TAM* mRNA reporter with the biosensor (up to 3 dots per cell). Yet, it remains unclear whether these dots are the result of the biosensors binding to the *TAM* mRNA reporter or rather technical artefacts.

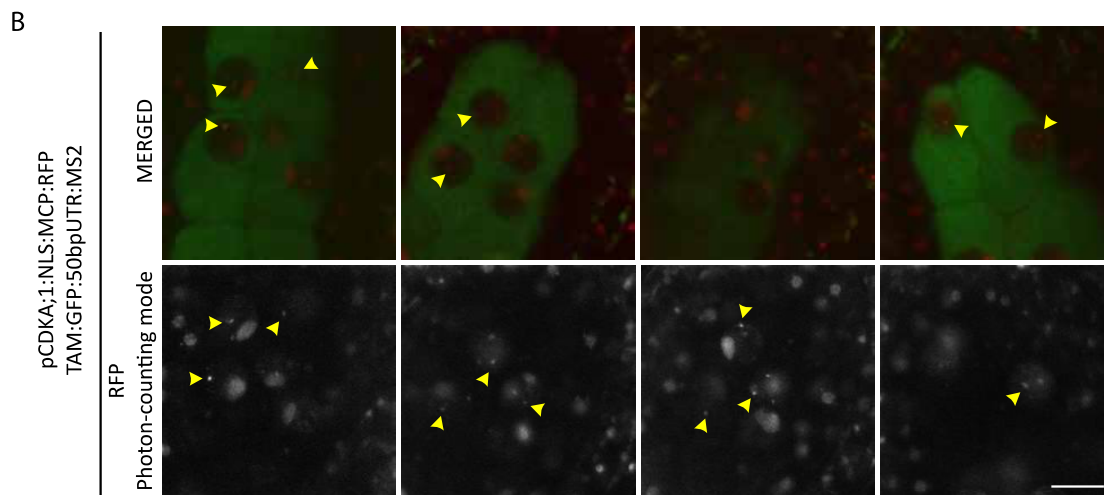
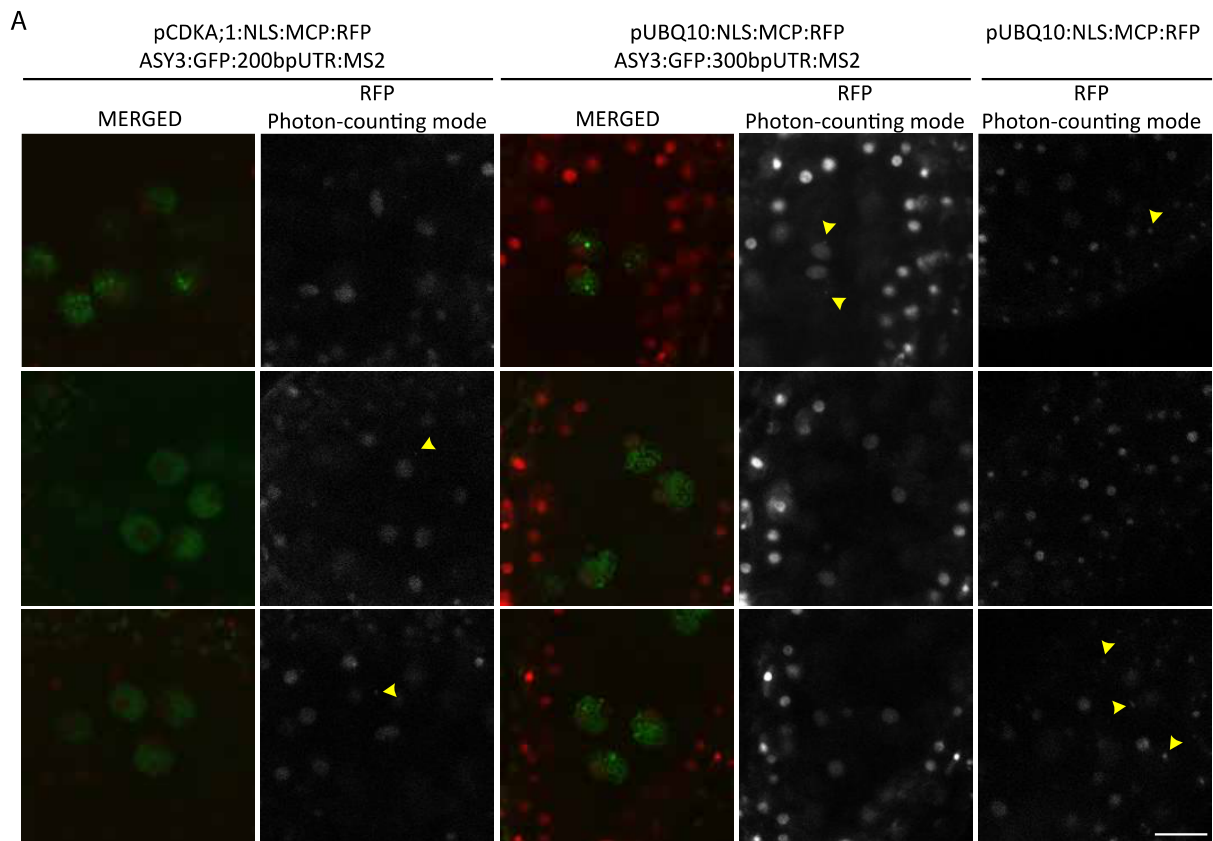


Figure 2.18. The MS2-system in Arabidopsis male meiocytes.

Attempts to visualize the ASY3 and TAM mRNA reporters by the use of the MCP biosensors. (A) *pCDKA;1:NLS:MCP:RFP* x *ASY3:GFP:200bpUTR:MS2*, *pUBQ10:NLS:MCP:RFP* x *ASY3:GFP:300bpUTR:MS2* and MCP biosensor *pUBQ10:NLS:MCP:RFP*. (B) *pCDKA;1:NLS:MCP:RFP* x *TAM:GFP:50bpUTR:MS2*. MERGED: MCP:RFP in red and ASY3/TAM:GFP in green; RFP Photon-counting mode in white; yellow arrow heads highlight RFP-dot like structures; scale bar, 10 μ m.

3. DISCUSSION

Multiple meiotic aspects have been intensively studied since long time in many organisms, from chromosome organization, including meiotic recombination, to the effect of environmental conditions, like heat stress, e.g. (Bishop et al., 1992; Dowrick, 1957; Pao and Li, 1948). Nonetheless, the impact of translational control influencing the amount of meiotic proteins needed for those dynamic processes during the meiotic division remains largely unknown, especially in plants. In this thesis, I attempted to get more insights into plant translational regulation, via a genome wide approach using maize anthers, *i.e.* ribosome profiling, and a gene specific approach to follow translation by microscopic analysis in *Arabidopsis*, *i.e.* TRICK.

3.1. The identification of maize meiotic orthologs in inbred line A188

For the genome wide study in maize, spikelets and anthers from the inbred line A188 were used, while as template for the mapping of the obtained reads the B73 reference genome (RefGen_V3 and RefGen_V4) was used, since the genome sequence of A188 was still unknown. Recently, the genome assembly of A188, obtained by high-resolution sequencing, was published and the comparison of the A188 and B73 genomes revealed multiple duplication events and more than 13,000 genes have large structural variations (Ge et al., 2021; Lin et al., 2021). Duplication events can lead to imprecise mapping results because either two expression profiles get mixed or one expression profile is diluted over the duplicated genes. In addition, mapping to another reference genome leads to information loss due to unmappable reads as a result of limited sequence homology. In the future, it would be preferred to revise the mapping analysis with the recently published genome assembly of A188, in order to get more precise mapping results.

Further, not for all the meiotic genes, known from *Arabidopsis*, maize orthologs could be identified unequivocally on sequence level, therefore an extensive list including all possible candidate meiotic genes based on the B73 genome annotation was assembled for this study. Previous studies in maize showed that the maize genome often has two homologs of genes from ancestor *Andropogoneae*, due to an allopolyploidization event that occurred between two ancestors of maize (Schnable et al., 2011). For example, two meiotic recombination genes, *RAD51* and

MRE11, have two homologs in maize, *RAD51A1* and *RAD51A2* and *MRE11A* and *MRE11B*, respectively, which might originate from this duplication event (Franklin et al., 1999). Based on my sequencing data of maize anthers, I was able to identify the most likely maize ortholog of *SMC3*, *MLH3*, *RAD5B* and *CDC45* among the possible candidates, since only Zm00001d039189, Zm00001d006307, Zm00001d050061 and Zm00001d023283 were found to be expressed in maize anthers. On the other hand, for other meiotic genes, multiple possible candidates remain, e.g. the *TAM* ortholog remains unclear, since expression was detected from Zm00001d010404, Zm00001d009011 and Zm00001d040381. When comparing the expression pattern over the time course of meiosis with its known protein expression in Arabidopsis, the best *TAM* candidate is Zm00001d009011. This needs to be further confirmed since presence of mRNA does not necessarily reflect protein presence.

3.2. Towards a high-resolution atlas of meiotic translation in maize

Although the results of my ribosome profiling experiments of maize anthers described in this thesis are preliminary due to the absence of biological and technical replicates, the first analysis showed that this approach can potentially lead to the discovery of plant specific translational regulatory mechanisms. I assumed that the relative expression values reflect the absolute expression. Nevertheless, several results of the analyses support this assumption, first hierarchical clustering and PCA showed that the sequencing data from different meiotic stage are clearly different. Further, there were enough reads to analyse meiotic genes and in addition diverse expression patterns during meiosis could be observed, of which the expression profiles of several genes could be confirmed by its well-known function/protein expression.

Interestingly, the expression pattern of several genes already suggests that those genes possibly undergo translational regulation, e.g. *ZYP1* mRNA level is relatively constant during meiosis I, while the translation showed a peak at leptotene. If the obtained results can be confirmed by replicates, the translational regulation of those transcripts should be further investigated. At first, the anticipated temporal discrepancy between mRNA and protein accumulation should be verified. The transcript levels during meiosis should be confirmed by another method such as real-time quantitative RT-PCR or RNA in situ hybridisation of anthers that contain meiocytes in the different meiotic stages. In addition, protein expression in maize

anthers should be monitored by western blot analysis using antibodies against the protein of interest, if available, or by the analysis of quantitative immunofluorescence localization or fluorescently labelled reporter constructs. At the moment, the best candidate to confirm the temporal discrepancy between transcript and protein appearance is *ZYP1*, since a genomic reporter has been generated and available in the working group. Although in yeast no translational control was reported for the ortholog of *ZYP1*, both transcription and translation coincide precisely with the SC formation (Brar et al., 2012), my dataset provides a more detailed resolution of prophase I compared to analysis in yeast, due to the precise sampling of prophase I stages. The obtained dataset could potentially contribute to more insights into prophase specific regulation but further investigation is needed to confirm my preliminary results for *ZYP1* and other genes.

In budding yeast, high throughput sequencing using ribosome profiling allowed the monitoring of meiotic translation and mRNA abundance, resulting in a high-resolution meiotic atlas and demonstrates that translational control regulates the magnitude and timing of protein expression during meiosis. For example, the mRNA of both *SPORULATION SPECIFIC 1 (SPS1)* and *SPS2* is present from late prophase onwards, but only translation of *SPS1* is strongly repressed until meiosis II (Brar et al., 2012). Similar translation regulation mechanisms were also found for multiple other genes, also in other species, *i.e.* mice and *Drosophila* (Baker et al., 2015; Berchowicz et al., 2013; Carlile and Amon, 2008; Jin et al., 2015; Luong et al., 2020; Takei et al., 2021). The regulation of mRNA levels and the translation efficiency reflect the control of protein production, so measuring both translation rates and mRNA levels from my datasets will allow the evaluation of their contributions.

Besides the translational control of canonical ORFs, around 8% of the genes expressed during yeast meiosis are regulated via a non-canonical regulation that involves a temporally regulated switch between a translatable transcript and a 5'-extended isoform that is not efficiently translated into protein and contains an uORF (Cheng et al., 2018). The poor translation of the mORF is dependent on the translation of uORF. This type of regulation was described for *NDC80*, which encoding protein is required for kinetochore function. The long translationally silent transcript is present early in meiosis and the short translatable version is only

induced later by TF NDT80 (Cheng et al., 2018). This non-canonical gene regulation and its importance was also reported for several other genes, for example two DNA replication genes *CELL DIVISION CYCLE 6 (CDC6)* and *SYNTHETICALLY LETHAL WITH DPB11-1 2 (SLD2)*. The repression of *CDC6* and *SLD2* mORFs by the uORFs leads to the inhibition of DNA replication between meiosis I and meiosis II (Phizicky and Bell, 2018).

Also in Arabidopsis, similar regulation mechanism has been reported. It was shown that *JASON (JAS)*, of which its protein is involved in the spindle position during meiosis (Brownfield et al., 2015), has two isoforms, a short and long version, and the ratio of those two versions is developmentally controlled and ensures the expression of the short version of *JAS* during meiosis, which promotes chromosome segregation (Cabout et al., 2017). It is likely that more genes in Arabidopsis, but also in maize, undergo non-canonical translational regulation. Those isoforms can be identified by the mapping of the ribosome footprints outside the annotated ORFs. The alternative isoform might be the cause of anti-correlation of the mRNA levels and the protein which can be detected from the expression profiles.

Although, translational control in eukaryotes seems to occur mainly at the level of translation initiation, a recent study focused on the potential regulatory role of translation elongation. By using computational approaches that were applied to ribosome profiling data, they revealed the translation elongation dynamics. Unique elongation changes during meiosis II were observed, including a global inhibition of translation elongation at the onset of anaphase II which coincides with a sharp shift toward increased elongation for genes required at this meiotic phase (Sabi and Tuller, 2019). It would be interesting to apply this approach to the maize anther ribosome profiling data. In addition, the investigation of translation elongation dynamics under stress conditions might reveal new insights into stress adaptation mechanisms.

3.3. Tapetum-dependent male meiosis

Although recently, a technique to isolate meiocytes from anthers was published and applied for example to analyse the meiotic transcriptome (Dukowic-Schulze et al., 2014b), I used the complete anther for the generation of the libraries. For ribosome profiling a short collection time of the material is crucial to avoid a stress response

contamination of the libraries. Even though the anther collection used here was already labour intensive, it is faster compared to the isolation of meiocytes for the current Ribo-seq protocols. An alternative approach could be ribosome profiling from single isolated meiocytes. However, this method is still in development and not yet optimized to give satisfactory results.

Using anthers in my experiments led to the discovery that the general state of transcription and translation of the complete anther is differently between the distinct meiotic stages. First, this confirmed the reliability of the sampling method used. Second, the differential expressomes are most likely not only due to transcriptional differences between meiocytes, but also reflect the simultaneous development of the tapetal cells which at that time undergo one round of mitosis without cytokinesis resulting in the formation of binucleate tapetal cells (Weiss and Maluszynska, 2001). It is further known that tapetal cells play an important role in the development of the meiocytes (Lei and Liu, 2019). Defective tapetum development is often associated with disrupted development of meiocytes and leads to reduced or impaired fertility (Cao et al., 2015; Chen et al., 2018; Ji et al., 2013; Yi et al., 2016). The development of tapetum and pollen mother cells (PMCs) is coordinated and in addition these cell layers partially share regulatory factors (Pacini et al., 1985; Scott et al., 2004; Yang et al., 1999). In addition, tapetum-specific programmed cell death (PCD) and disintegration are essential for proper microspore development and pollen maturation, e.g. in rice *ms1*, *tapetum degeneration retardation (tdr)* and *persistent tapetal cell 1 (ptc1)* mutants show male sterility due to premature or delayed degradation of the tapetum (Ku et al., 2003; Li et al., 2006; Vizcay-Barrena and Wilson, 2006). These studies clearly show that the meiotic division is regulated by the surrounding tapetum. On the other hand, from live cell imaging of Arabidopsis anthers, it is known that the tapetal division only poorly correlates with any of the meiotic stages between zygotene and diplotene, which led to the conclusion that there is no tight correlation between the development of meiocytes and tapetum (Prusicki et al., 2019). Although, this conclusion cannot be confirmed by the previous studies, it seems that overall the meiotic division is coordinated by the tapetum but their development is not strictly correlated.

This further leads to the questions how exactly the tapetum regulates the meiotic development and on which level. In rice, the *eternal tapetum 1 (eat1)* mutant

shows defects in tapetum PCD, irregular chromatin condensation at diakinesis and metaphase I, as well as abnormal anaphase I maturation. Although EAT1 is exclusively expressed in tapetal cells, EAT1 promotes non-cell-autonomously the meiotic transcription of 24-PHASRNAs, longer precursor RNAs of the 24-nt phasiRNAs (phased secondary small interfering RNA) (Ono et al., 2018). Surprisingly, it is likely the 24-nt phasiRNAs that transfers from tapetum to the PMCs. Also in maize anthers, phasiRNAs are expressed and their production is temporally regulated (Dukowic-Schulze et al., 2016; Zhai et al., 2015). In Arabidopsis anthers, it was recently shown that 24-nt small interfering RNAs (siRNAs) produced in tapetum moved to meiocytes and induce methylation of target genes (Long et al., 2021). Both, the role of the tapetal cells and the siRNAs as mobile signal for the development of meiocytes are highly interesting and the regulatory mechanisms of the different siRNAs, like DNA methylation or mRNA degradation of target genes in meiocytes, are still largely unknown. The comparison of total RNA and small RNA libraries of whole anthers (or isolated tapetum) and isolated meiocytes per meiotic stage will be beneficial to study the precise coordination and mutual influence of development between tapetum and meiocytes on a whole genome level.

3.4. MS2-system and TRICK, tricky systems to follow translation in Arabidopsis

In a second approach to study translational control, I aimed to establish a gene specific approach using the MS2-system and TRICK, used in different biological systems to visualize transcript localization and translation in single cells. However, the experimental setup in Arabidopsis meiocytes was more difficult than expected and unfortunately, I did not succeed in imaging the translation of meiotic candidate genes *ASY3*, *TAM* and *REC8*. Both, the mRNA reporters and the RNA biosensors did not function as expected.

First, the introduction of the hairpin loops into the 3'UTR of the gene affected the functionality of the mRNA reporter for most of the constructs. The optimal insertion site of the MS2-loops was around 200 bp after the stop codon for two of the three genes. This led, in case of *ASY3* and *TAM*, to a functional mRNA reporter. Despite, it remains unclear how the loop structures affected the functionality of the reporters using the other insertion positions. The 3'UTR is known to be involved in the subcellular localization and translational repression, since the 3'UTR often

contains subcellular localisation sequences/motifs and repressor binding sites (Besse and Ephrussi, 2008; Mili and Macara, 2009). It is likely that the MS2-loops alter the translation itself, yet they might also affect the stability of the mRNA. It has been reported in yeast that the incorporation of MS2-loops into mRNAs can lead to the accumulation of RNA fragments. It was further suggested that the hairpin structures have the potency to impair with mRNA decay (Garcia and Parker, 2015, 2016; Haimovich et al., 2016). There is also evidence that the MS2- and PP7-loops affect the mRNA nuclear and/or cytoplasmic processing and cause enrichment of stem-loop fragments in processing bodies (PBs) (Heinrich et al., 2017). The use of less stem-loops in the construct design could reduce RNA fragmentation, but on the other hand this reduction might preclude live cell imaging, as there is a threshold for the signal-to-noise ratio of transcript over background signal.

In addition to the challenges of introducing hairpin repeats within the target RNA, the RNA biosensor also did not localize as expected. The biosensors driven by the *CDKA;1* and *UBQ10* promoters predominantly localize to the nucleolus, instead of localizing to the nucleoplasm. The nucleolus' primary function is the generation of ribosome-subunits, however proteome analysis revealed that only approximately 30% of the nucleolar proteins have a function in ribosomal-subunit biogenesis (Pendle et al., 2005). Additional proteins occurring in the nucleolus include pre-mRNA processing factors and proteins involved in cell-cycle control as well as DNA replication and repair and stress response (Boisvert et al., 2007). An example for the role of the nucleolus in regulating stress responses in mammals is through the stabilization of tumor-suppressor p53 in the nucleolus as a sensor for cellular stress signals (Wsierska-Gadek and Horky, 2003). A reason for the nucleolar accumulation of the biosensors could be that MCP, as it is not naturally occurring in plants, causes a cellular stress signal by which the biosensor gets sequestered in the nucleoli. There they might become a target for ubiquitination in the nucleolus, leading to nuclear export and degradation by the 26S proteasome, as shown for p53 in mammals (Wsierska-Gadek and Horky, 2003). If the dot-like structures observed around the nucleus of meiocytes expressing the RNA biosensor and co-expressing the *ASY3* and/or *TAM* mRNA reporter and RNA biosensor are related to protein degradation of the biosensor, this could be tested by inhibiting the proteolytic activity

of the 26S proteasome, by applying the proteasome inhibitor drug MG132 (Han et al., 2009).

A two-component vector system, consisting of a biosensor and corresponding stem-loops for any target RNA, based on GATEWAY™ technology was developed for high-throughput studies in plants (Schonberger et al., 2012). In this study, the expression of the biosensors and tagged target mRNAs was confirmed via transient expression in *N. benthamiana* leaves. MCP in absence of a target mRNA showed, in addition to the expected nuclear signal, also a very bright signal in the nucleolus. This is a similar localization pattern to what I observed in *Arabidopsis* meiocytes and root cells. Since the two-component system worked in tobacco (Schonberger et al., 2012), I assumed that this aspect of the experimental setup would not cause any problem. However, when my experiments with *Arabidopsis* were not successful, I contacted the authors of this system for technical advice. Surprisingly, although the two-component system initially looked very promising, the authors did not manage to apply this system successfully in *Arabidopsis* (unpublished, Dr. Ulrich Hammes). Additional problems were observed in their experiments, including suppression or even complete silencing of the reporter constructs. Even after several optimization attempts, their system still did not succeed in *Arabidopsis*.

As an alternative to the MS2-loops, a smaller type of loop structures could be used, e.g. the λ N₂₂-loops, which might not cause mRNA decay (Ozawa et al., 2007). Also, the U1A stem-loops were reported to not show fragmentation of 3-PHOSPHOGLYCERATE KINASE 1 (*PGK1*) transcript, compared to the MS2-loops (Garcia and Parker, 2015). Another alternative labelling system for *in vivo* RNA imaging, based on the RNA-binding domain of a translational repressor *PUMILIO 1* (*PUM*) in humans, is called Pumilio-bimolecular fluorescence complementation (BiFC). The main advantage of this method is that the target transcript does not need to be tagged with foreign sequences, since this system makes use of two RNA-binding domains of PUM that are engineered to recognize specific sequences of the target mRNA (Cheong and Hall, 2006; Ozawa et al., 2007). A great knowledge about the target mRNA is needed for the design of the specific PUM-variants, e.g. the secondary structure of the mRNA, since the two PUMs need to bind in close proximity of one another. Pumilo-BiFC has been successfully used *in planta*, to

visualize the localisation of virus RNA to invaginations of the chloroplast envelope (Wei et al., 2010). This system in combination with the genomic reporter would allow the investigation of the temporal differences between transcript appearance and translation.

Nonetheless, the MS2-system was successfully used in plant research to study the localization of mRNAs and miRNAs. For example, in Arabidopsis the mRNAs of *SKU5 SIMILAR 14 (SKS14)* and *AT59* (orthologue of the tomato *LATE ANTHEL TOMATO 59 (LAT59)*) were shown to be recruited to cytoplasmic granules in mature pollen (Scarpin et al., 2017). In rice endosperm cells, the MS2-system was used to study the transport of *prolamine* mRNA to PBs (Hamada et al., 2003). These studies have in common that the target RNA is recruited to distinct subcellular structures, like granules and PBs, leading to a high and local concentration of the RNA. However, it should be noted that this possibly could be an artefact of the use of the stem-loops. In yeast, the mRNA of *PGK1* was first shown to localize to PBs using 16xU1A stem-loops, yet a later study, who visualised unlabelled *PGK1* transcript (not tagged with stem-loops) using single molecule fluorescence in situ hybridisation (smFISH), could not confirm the enrichment of *PGK1* in PBs (Heinrich et al., 2017). Still, these studies indicate that the problems of the MS2-system are target mRNA concentrations below the detection limit and artefacts in mRNA localisation, rather than the functionality of the reporter constructs. It is likely that the detection of *ASY3* and *TAM* mRNA is more challenging, as there is presumably no local enrichment of these mRNAs in the cytoplasm of the meiocytes. Although the MS2-system seems not suitable to image the dynamics of my target transcripts during unperturbed meiosis, this system could be used in the future to investigate for example the localization of mRNAs under heat stress to see if they are possibly incorporated into stress granules. It was shown that *CDKA;1-mVenus* protein localizes to SGs in roots and meiocytes upon exposure to high temperatures (Kosmacz et al., 2019) (see Chapter 1). It would be interesting to investigate if the mRNA of *CDKA;1* and possibly other mRNAs are recruited to SGs upon heat stress using the MS2-system.

4. MATERIAL AND METHODS

4.1. Plant materials and growth conditions

The *Zea mays* plants used in this study were from the inbred line A188 and all *Arabidopsis* (*Arabidopsis thaliana*) plants used in this study were in the Columbia (Col-0) accession. Seeds for T-DNA insertion mutants for *ASY3* (SAIL_423_H01), *TAM* (SAIL_505_C06) and *REC8* (SAIL_807_B08) were obtained from the SAIL T-DNA mutation collection via NASC (<http://arabidopsis.info/>).

The *Zea mays* seeds were directly germinated on soil and grown in the greenhouse (16 h light around 24°C/ 8 h dark around 22°C).

Arabidopsis seeds were surface sterilized with chlorine gas and germinated on 1% (w/v) agar containing half-strength Murashige and Skoog (MS) salts and 1% (w/v) sucrose, pH 5.8. When required, antibiotics were added for seed selection. All plants were grown under long-day conditions (16 h light at 21°C (+/- 0.5°C)/ 8 h dark at 18°C (+/- 0.5°C), with 60% humidity).

4.2. Maize meiocyte staging

For the determination of the meiotic stage of maize anthers the acetocarmine staining method was used (Sheehan and Pawlowski, 2012). Spikelets were fixated in 3:1 ethanol:acetic acid for a minimum of 24 h at 4°C, following washing steps with 70% ethanol and stored at 4°C. Spikelets were dissected and the anther were isolated and transferred to a drop of acetocarmine solution (2% acetocarmine and 45% acetic acid) on a microscope slide. Anthers were squashed in the acetocarmine and covered by a cover slip. After heating for 10 min at 60°C, the meiotic stage was determined and imaged under a Zeiss Axioskop light microscope.

4.3. Total RNA and polysome isolation

Anthers were isolated and flash frozen using liquid nitrogen and stored at -80°C. After stage determination, 100-150 anthers were pooled per meiotic stage, and grinded into fine powder.

Total RNA and polysomes were isolated according to (Lukoszek et al., 2016; Mustroph et al., 2009b) with some modifications. Total RNA was extracted using TRIzol reagent (Invitrogen), chloroform-IAA (0.1 Vol, 24:1) was added, incubated (3 min, RT) and centrifuged (15 min, 4°C, 14.000 xg). Supernatant was isolated and RNA was precipitated by adding isopropanol (1 Vol, 100%) for 3 h at -20°C. After centrifugation (40 min, 4°C, 21.000 xg), the pellet was dissolved in ice-cold ethanol (80%, RNase free), centrifuged (20 min, 4°C, 21.000 xg) and dissolved in DEPC-water). DNase treatment was performed (Fermentas), RNA was purified using clean & concentrator-5 spin columns (ZYMO Research, CAT R1016), RNA integrity was checked using Agilent Bioanalyzer 2100 (RNA 6000 Nano Kit, Agilent, CAT 5067-1511) and spiked with ERCC RNA Spike-In Mix (Ambion, CAT 4456740). rRNA was depleted using RiboMinus Plant Kit (Invitrogen, CAT A10838) and the total RNA was randomly fragmented by alkaline lysis in

alkaline fragmentation solution (2 mM EDTA, 12 mM Na₂CO₃, 87 mM NaHCO₃) for 40 min at 95°C. The randomly fragmented RNA was recovered by precipitation.

For the isolation of polysomes, the grinded anthers were mixed in polysome extraction buffer (0.2 M Tris pH 7.5, 0.2 M KCl, 0.025 M EGTA, 0.035 M MgCl₂, 1% Brij-35, 1% Triton X-100, 1% Igepal CA 630, 1% Tween 20, 1% DOC, 1% PTE, 5 mM DTT, 1 mM AEBSF, 100 µg/ml cyclohexamid, 100 µg/ml chloramphenicol) and incubated on ice for 10 min. The supernatant, after 2 rounds of centrifugation (20 min, 4°C, 16.000 xg), was loaded onto a sucrose cushion solution (0.4 M Tris pH 7.5, 0.2 M KCl, 0.005 M EGTA, 0.035 M MgCl₂, 1.75 M sucrose, 5 mM DTT, 100 µg/ml cyclohexamid, 100 µg/ml chloramphenicol) and ultracentrifuged (2.5 h, 4°C, 170.000 xg, Optima MAX-XP with TLA-55 fixed-angle rotor, Beckman Counter). The ribosome containing pellet was gently resuspended in ice-cold resuspension buffer (0.2 M Tris pH 7.5, 0.2 M KCl, 0.025 M EGTA, 0.0035 M MgCl₂, 5 mM DTT, 100 µg/ml cyclohexamid, 100 µg/ml chloramphenicol).

4.4. Digestion and isolation of RPFs

Purified polysomes (15 µg) were digested with RNase A (0.5 U) at 22°C for 45 min and directly loaded onto 15-60% sucrose gradient and ultracentrifuged (1 h, 4°C, 237.000 xg, Optima XPM with SW 55 Ti swinging-bucket rotor, Beckman Counter). The monosome fraction was extracted using the hot acid phenol method: SDS (0.1 Vol, 10%) was added and incubated at 65°C, where after preheated acid phenol-chloroform (1 Vol, 5:1, pH 4.5, Ambion) was added and incubated for 10 min at 65°C. After 10 min on ice and centrifugation (5 min RT, full speed), the aqueous phase was separated, acid phenol-chloroform (1 Vol) was added, vortexed (5 min, RT) and centrifuged (5 min, RT, full speed). The aqueous phase was separated, chloroform-IAA (1 Vol, 24:1) was added, vortexed (1 min, RT) and centrifuged (5 min, RT, full speed). The aqueous phase was separated, glycogen (2 µl) and NaOAc (0.1 Vol, 3 M, pH 5.5) added and the RPFs were concentrated by isopropanol and ethanol precipitation and dissolved in DEPC-water. rRNA was depleted using RiboMinus Plant Kit.

4.5. Preparation of RPF and total mRNA libraries

The sequencing libraries were prepared according to (Ingolia et al., 2009). Purified RPFs and fragmented RNA were dephosphorylated (T4 PNK, New England Biolabs), loaded onto a 15% TAE-polyacrylamide gel (Acrylamid 40, acrylamide/polyacrylamide 19:1; 8M urea) and run for at least 1h at 9mA. After staining with SybrGold for 10 min in the dark, fragments of the size 25-35 nucleotides were cut out of the gel and isolated by centrifugation (5 min, RT, 17.000 xg) to crush the gel, eluted by incubating with stop/precipitation solution (3 M NaAcO, pH 5.5, glycogen and RiboLock (Thermo Fischer Scientific)) for 4 h at 4 °C and purified by precipitation with isopropanol. To those fragments 3' and 5' adaptors were ligated (T4 RNA ligase, New England Biolabs) (**Table 2.2**) and reverse transcript into cDNA by using Rever Aid H Minus Reverse Transcriptase (Fermentas) (**Table 2.2**). RNA was degraded by adding NaOH (1 M) and

incubated for 10 min at 90°C and neutralized (1 M HEPES-NaOH, pH 7.0). The libraries were amplified and barcoded, after an optimization round, with Pfu DNA polymerase (Fermentas)(**Table 2.2, Table 2.3**) and purified by loading on a 10% TAE-polyacrylamide gel (Acrylamid 40, acrylamide/polyacrylamide 19:1), run for at least 1.5 h at 12 mA, fragments of 140 bp cut out of the gel isolated by centrifugation (5 min, RT, 17.000 xg) to crush the gel in DNA elution buffer (10 mM Tris-HCl, H 8.0, 300 mM NaCl and 1 mM EDTA), eluted by incubating with stop/precipitation solution (0.1 vol, 3 M NaACo, pH 5.5, glycogen) and purified by precipitation with isopropanol and resuspended in MilliQ-water. The library size and concentration was determined by using the Bioanalyzer 2100 (DNA 1000 Kit, Aligent, CAT 5067-1504) and Qubit (dsDNA HS kit, Life Technologies, CAT Q32851). The libraries were subjected to deep sequencing on the Illumina Hiseq 2500 platform.

Table 2.2. Primers library generation and amplification.

Primer name	Primer sequence
Primers originate from Illumina TrueSeq small RNA sample Prep Kits	
Primers for library generation (adapter ligation and RT)	
3' Adapter RNA (RA3) part #15013207	5' rApp/TGGAATTCTCGGGTGCCAAGG/3ddC/
5' Adapter (RA5) part #15013205	GUUCAGAGUUCUACAGUCCGACGAUC
RNA RT primer (RTP) part #15013981	CCTTGGCACCCGAGAATTCCA
Primers for library amplification and barcoding (index)	
PCR Primer (RP1), forward part # 15013198	AATGATACGGCGACCACCGACAGGTTTCAGAGTTC TACAGTCCGA
PCR Primer (RPI1), reverse Index 1	CAAGCAGAAGACGGGCATACGAGAT CGTGAT GTGA CTGGAGTTCCTTGGCACCCGAGAATTCCA
PCR Primer (RPI3), reverse Index 3	CAAGCAGAAGACGGGCATACGAGAT GCCTAAG TGA CTGGAGTTCCTTGGCACCCGAGAATTCCA
PCR Primer (RPI4), reverse Index 4	CAAGCAGAAGACGGGCATACGAGAT TGGTCA GTGA CTGGAGTTCCTTGGCACCCGAGAATTCCA
PCR Primer (RPI5), reverse Index 5	CAAGCAGAAGACGGGCATACGAGAT CACTGT GTGA CTGGAGTTCCTTGGCACCCGAGAATTCCA
PCR Primer (RPI6), reverse Index 6	CAAGCAGAAGACGGGCATACGAGAT ATTGGC GTGA CTGGAGTTCCTTGGCACCCGAGA ATTCCA

Table 2.3. PCR-program for library amplification using Pfu DNA polymerase.

Step	Time	Temperature (°C)
1. initial denaturation	2 min	95
2. denaturation	30 sec	95
3. primer annealing	30 sec	60
4. elongation	15 sec	72
repeat steps 2-3-4	10-25 cycles	
5. final elongation	10 min	72

4.6.RNA-seq and Ribo-seq data processing

The libraries from the spikelets were analysed in collaboration with Johannes Wagner Wagner (AG Ignatova, Institute for Biochemistry and Molecular Biology, Department of Chemistry, University of Hamburg). First, quality trimming was performed using fastq quality trimmer (FASTXToolkit 0.0.13), reads shorter than 16 nt and base call quality lower than 20 were removed and adapter sequences were removed using Cutadapt 1.2.1. After pre-processing, the reads that mapped to a rRNA reference were removed. The reads that did not map to rRNA were subsequently mapped to the reference genome Zm-B73-REFERENCE-GRAMENE-3.0. The artificial Spike In sequences were also added to the reference genome. The mapping steps were performed using Bowtie 0.12.9 allowing maximum 2 mismatches per read and discarding every read mapping to several positions in the genome. To extract feature specific information, the mapped reads were counted strand specifically using HTSeq-count version 0.5.3p9. For each gene, the union of annotated transcripts was created. Within the single transcripts CDSs were used to create a union CDS. Regions within the union transcript, which did not belong to the union CDS were assigned as UTRs. The positions of UTRs and start and stop positions were extracted from the reference genome. The counts were further normalized to gene length and total number of feature mapped reads (sequencing depth), to reads per kilobase per million mapped reads (RPKM).

The anther libraries were analysed in collaboration with Dr. Dermot Harnett (AG Ohler, Institute for Medical Systems Biology, Department of Computational Regulatory Genomics, Max Delbrueck Center for Molecular Medicine Berlin). Raw sequence data was converted to FASTQ format using bcl2fastq. Adapters (sequence TGGAAATTCTCGGGTGCCAAGG) were removed from RNA- and Ribo-seq reads with cutadapt, as well as sequences with a quality score less than 20 or a remaining sequence length less than 12, and after removing duplicate read sequences, 4bp UMIs were trimmed from either end of each sequence using a custom perl script. RNA- and Ribo-seq reads were then aligned to an index of common contaminants (including tRNA, rRNA, and snoRNA sequences) using bowtie2. The resulting processed read files were then aligned to coding sequences (the pc_transcripts fasta file), and separately, to the reference genome, from Zm-B73-REFERENCE-GRAMENE-4.0 (*Zea mays*) using STAR, with the following settings: STAR --outSAMmode NoQS --outSAMattributes NH NM --seedSearchLmax 10 --outFilterMultimapScoreRange 0 --outFilterMultimapNmax 255 --outFilterMismatchNmax 1 --outFilterIntronMotifs RemoveNoncanonical. Multiqc was used to check the quality of read data and alignments, and produce plots of reads recovered. Picard was used to create plots of read coverage by region. Reads overlapping genes were quantified using Feature Counts, PCA plots, heat maps, and plots of individual gene expression were created using a set of R scripts.

4.7. Genotyping

Genomic DNA was extracted from leaves of 2-3-week-old Arabidopsis plants. The leaves were grinded in 2 ml Eppendorf tubes with 2 metal beads in 400 µl magic buffer (50 mM Tris HCl (pH 7.5), 300 mM NaCl and 300 mM sucrose) in a Retsch mill for 2 min at 25 rpm. Tubes were centrifuged for 10 min at 14000 rpm. Supernatant (extracted genomic DNA) was diluted (1:10) and stored at -20°C. Genotyping PCR was performed using DreamTaq DNA polymerase in a PCR reaction mix (DreamTaq Green PCR Master Mix (2X)(Thermo Fischer Scientific (CAT K1081)), forward primer (100 mM), reverse primer (100 mM) and 1 µl extracted genomic DNA) in a Thermocycler with adjusted PCR program (**Table 2.4**). For the genotyping primers used see **Table 2.5**. PCR products were loaded on an agarose gel (1% agar, 1x TEA-buffer (40 mM Tris-Actetate and 2 mM EDTA), 100 ng/ml ethidium bromide) and gel electrophoresis was performed for 30-40 min at 100-120 V.

Table 2.4. PCR-program using Taq and PrimeSTAR MAX DNA polymerase.

Step	Time (Taq/PrimeSTAR Max)	Temperature (°C) (Taq/PrimeSTAR Max)
1. initial denaturation	5 min/2 min	95/98
2. denaturation	30 sec/10 sec	95/98
3. primer annealing	30 sec/5 sec	55/55
4. elongation	1 min/kb/20 sec/kb	72/72
repeat steps 2-3-4	25-30 cycles	
5. final elongation	10 min/2 min	72/72
6. hold	∞	16

Table 2.5. Genotyping primers.

Gene T-DNA line	Primer name	Primer sequence
ASY3 SAIL_423_H01	ASY3-2-R1 (+LB3 for T-DNA)	GCAAGAGCAATACTCCAC
TAM SAIL_505_C06	TAM_L (+LB3 for T-DNA) TAM_U	CAGAAATCCTCCACTTGCG GACTTGATGGATCCACAGC
REC8 SAIL_807_B08	SAIL_807_B08-RP (+LB3 for T-DNA) SAIL_807_B08-LP	GGGGGAAAAGAGAAAGGTTT CTCATATTCACGGTGCTCCC
SAIL	LB3	TAGCATCTGAATTTTATAACC AATCTCGATACAC

4.8. Plasmids and plant transformation

The *TAM:GFP-ASY3:RFP* double reporter line was generated by Dr. Chao Yang, unpublished. The biosensors, *pCDKA;1:NLS:MCP:RFP*, *pUBQ10:NLS:MCP:RFP* and *pUBQ10:NLS:MCP:RFP-pCDKA;1:NLS:PCP:GFP*, were generated by Dr. Wojciech Urban.

For the mRNA reporters, the MS2-loop, provided by (Halstead et al., 2015), were inserted into the cloning plasmids of the genomic reporters using SliCE (Prusicki et al., 2019; Yang et al.,

2019; Zhang et al., 2014). The insert and backbone were amplified by PrimeSTAR Max DNA polymerase in a PCR reaction mix (PrimeSTAR Max Premix (TAKARA BIO INC (CAT R045A)), forward primer (100 mM), reverse primer (100 mM) and 5-10 ng template) in a Thermocycler with adjusted PCR program (**Table 2.4**). For the SLiCE primers used see **Table 2.6**. The PCR product was mixed with DNA Gel Loading Dye (6X) (Thermo Fisher Scientific (CAT R0611)), agarose gel electrophoresis was performed and PCR product was extracted from the gel (NucleoSpin Gel and PCR Clean-up kit- MACEREY-NAGEL (CAT 740609.250).

Table 2.6. SLiCE primers.

Primer name	Primer sequence
ASY3:GFP:MS2:UTR	
J50-SL-ASY3GFPMS2.-F	<u>ATATCGAAGCAACCCAGCTTTCTTGTACAAAGTT</u>
J51-SL-ASY3GFPMS2.-R	<u>AGACTCAGTGtggttgtccaaactcatcGGATCT</u>
J52-SL-MS23UTR-F	<u>agtttggacaaaccaCACTGAGTCTCACAGAATCAATCA</u>
J53-SL-MS23UTR-R	<u>CAAGAAAGCTGGGTTGCTTCGATATATATCAAGATATCA</u>
ASY3:GFP:UTR:MS2	
J54-SL-3UTRMS2-F	<u>GGTGGACCCGGGTGACACTGAGTCTCACAGAATCAATCA</u>
J55-SL-3UTRMS2-R	<u>GATCCttatcactcgGCTTCGATATATATCAAGATATCA</u>
J56-SL-ASY3GFP.MS2-F	<u>AGACTCAGTGTCACCCGGGTCCACCTCCCTTGTA</u>
J57-SL-ASY3GFP.MS2-R	<u>ATATCGAAGCcgagtgataaGGATCTcGGATCCT</u>
ASY3:GFP:100bpUTR:MS2	
J58-SL-ASY3GFP100-F	<u>ggacaaaccaCAAGCAAACCAGCCTTTGGTTTA</u>
J59-SL-ASY3GFP100-R	<u>ttatcactcgAGAGGTTTTTCTTTCCTGGTTAAC</u>
J60-SL-100.MS2-F	<u>AAAAACCTCTCGAGTGATAAGGATCTCGGATCC</u>
J61-SL-100.MS2-R	<u>GTTTTGCTTGTGGTTTGTCCAAACTCATCGGATCT</u>
ASY3:GFP:200bpUTR:MS2	
J62-SL-ASY3GFP200-F	<u>ggacaaaccaTATAGAATAGTTTATTGTTCACTG</u>
J63-SL-ASY3GFP200-R	<u>ttatcactcgCGAATACGAATCAATGACAATGAG</u>
J64-SL-200.MS2-F	<u>TTCGTATTCGCGAGTGATAAGGATCTCGGATCC</u>
J65-SL-200.MS2-R	<u>CTATTCTATATGGTTTGTCCAAACTCATCGGATCT</u>
ASY3:GFP:300bpUTR:MS2	
J66-SL-ASY3GFP300-F	<u>ggacaaaccaGCCAGCAACTGCAGATATTTTTTA</u>
J67-SL-ASY3GFP300-R	<u>ttatcactcgAAAAATAAATTA AAAAAGAAACCTT</u>
J68-SL-300.MS2-F	<u>ATTTATTTTTCGAGTGATAAGGATCTCGGATCC</u>
J69-SL-300.MS2-R	<u>AGTTGCTGGCTGGTTTGTCCAAACTCATCGGATCT</u>
TAM:GFP:MS:UTR	
J70-SL-TAMGFP-F	<u>ggacaaaccatagtgtttctggatacgtttttt</u>
J71-SL-TAMGFP-R	<u>ttatcactcgTCACCCGGGTCCACCTCCcttgta</u>
J72-SL-tamMS2-F	<u>ACCCGGGTGACGAGTGATAAGGATCTCGGATCC</u>
J73-SL-tamMS2-R	<u>agaaacactaTGTTTTGTCCAAACTCATCGGATCT</u>
TAM:GFP:20bpUTR:MS2	
J94-SL-TAMGFP20-F	<u>ggacaaaccatttttaccctcgtgtattgtacat</u>
J95-SL-TAMGF20P-R	<u>ttatcactcgaacgtatccagaacactaTCAC</u>
J96-SL-tam20MS2-F	<u>ggatacgtttCGAGTGATAAGGATCTCGGATCC</u>
J97-SL-tam20MS2-R	<u>agggtaaaaaTGTTTTGTCCAAACTCATCGGATCT</u>
TAM:GFP:50bpUTR:MS2	
J98-SL-TAMGFP50-F	<u>ggacaaaccagataaaaaattcatcagtcgggtca</u>

J99-SL-TAMGFP50-R	<u>ttatcactcgaacaatatgtacaatacacgaggg</u>
J100-SL-tam50MS2-F	<u>acatattggtCGAGTGATAAGGATCTCGGATCC</u>
J101-SL-tam50MS2-R	<u>aattttatcTGGTTTGTCCAAACTCATCGGATCT</u>
TAM:GFP:100bpUTR:MS2	
J124-SLTAMGFP100-F	<u>ggacaaaccaatgatgtgtagatgaaatac</u>
J125-SLTAMGFP100-R	<u>ttatcactcgctctatcggactgagtacat</u>
J126-SLMS2tam100-F	<u>tccgatagagCGAGTGATAAGGATCTCGGATCC</u>
J127-SLMS2tam100-R	<u>tacacatcatTGGTTTGTCCAAACTCATCGGATCT</u>
TAM:GFP:200bpUTR:MS2	
J120-SLTAMGFP200-F	<u>ggacaaaccaggttgaagtgcagaccaacc</u>
J121-SLTAMGFP200-R	<u>ttatcactcgaccacaacgacatccatagc</u>
J122-SLtam200MS2-F	<u>tcgttggtCGAGTGATAAGGATCTCGGATCC</u>
J123-SLtam200MS2-R	<u>cactcaaccTGGTTTGTCCAAACTCATCGGATCT</u>
REC8:GFP:MS2:UTR	
J74-SL-REC8GFP-F	<u>ggacaaaccaGGTTTGATTTCTAAATTATAAAAG</u>
J75-SL-REC8GFP-R	<u>ttatcactcgTTACCCGGGTCCACCTCCCTTGTA</u>
J76SL-rec8MS2-F	<u>ACCCGGGTAACGAGTGATAAGGATCTCGGATCC</u>
J77-SL-rec8MS2-R	<u>AAATCAAACCTGGTTTGTCCAAACTCATCGGATCT</u>
REC8:GFP:20bpUTR:MS2	
J78-SL-REC8GFP20-F	<u>ggacaaaccaAAAGATTCTGGTGAACCGATTATC</u>
J79-SL-REC8GFP20-R	<u>ttatcactcgTATAATTTAGAAATCAAACCTTAC</u>
J80-SL-rec820MS2-F	<u>CTAAATTATACGAGTGATAAGGATCTCGGATCC</u>
J81-SL-rec820MS2-R	<u>CAGAATCTTTTGGTTTGTCCAAACTCATCGGATCT</u>
REC8:GFP:40bpUTR:MS2	
J82-SL-REC8GFP40-F	<u>ggacaaaccaATCCATAGTTGTTTTGCTTTTCAT</u>
J83-SL-REC8GFP40-R	<u>ttatcactcgAATCGTTCCACCAGAATCTTTTAT</u>
J84-SL-rec840MS2-F	<u>TGAACCGATTTCGAGTGATAAGGATCTCGGATCC</u>
J85-SL-rec840MS2-R	<u>AACTATGGATTGGTTTGTCCAAACTCATCGGATCT</u>
REC8:GFP:70bpUTR:MS2	
J86-SL-REC8GFP70-F	<u>ggacaaaccaAGCAGAGAGAGTTTCGTAGACTTTT</u>
J87-SL-REC8GFP70-R	<u>ttatcactcgAGAATATGAAAAGCAAAACAATA</u>
J88-SL-rec870MS2-F	<u>TTCATATTCTCGAGTGATAAGGATCTCGGATCC</u>
J89-SL-rec870MS2-R	<u>TCTCTCTGCTTGGTTTGTCCAAACTCATCGGATCT</u>
REC8:GFP:UTR:MS2	
J90-SL-REC8GFP90-F	<u>ggacaaaccaTTTTTTAAGTTATAAAGAGCAAGC</u>
J91-SL-REC8GFP90-R	<u>ttatcactcgGTCTACGAACTCTCTCTGCTAGAA</u>
J92-SL-rec890MS2-F	<u>GTTTCGTAGACCGAGTGATAAGGATCTCGGATCC</u>
J93-SL-rec890MS2-R	<u>ACTTAAAAAATGGTTTGTCCAAACTCATCGGATCT</u>

The SLiCE reaction (50- 200 ng of linearized vector:insert 1:1-1:10 ratio, 10x SLiCE buffer (0.5 mM Tris-HCl (pH 7.5), 0.1 mM MgCl₂, 0.01 mM ATP, 0.01 mM DTT) and SLiCE extract) was incubated for 1 h at 37°C. The SLiCE reaction was used for transformation into chemical competent TOP10 *E.coli* cells (Thermo Fisher Scientific (CAT C404010)), 45 sec at 42°C, 5 min on ice, recovered with LB-medium (1% Tryptone, 0.5% yeast extract and 0.5% NaCl) for 1 h at 37°C at 350 rpm, spread on LB-plate (1% Tryptone, 0.5% yeast extract, 0.5%

NaCl and 0.8% agar) with selective antibiotics (50 µg/ml Kanamycin (Kan)) and left to grow overnight at 37°C.

Colony PCR was performed using DreamTaq DNA polymerase in a PCR reaction mix (DreamTaq Green PCR Master Mix (2X), forward primer (100 mM), reverse primer (100 mM)) in a Thermocycler with adjusted PCR program (**Table 2.4**). For the colony primers used see **Table 2.7**. Positive colonies were grown in LB liquid culture with antibiotics overnight at 37°C shaking at 200 rpm and plasmid extracted (Presto Mini Plasmid Kit- Geneaid (CAT PDH300)). The extracted plasmids were tested with a restriction digest and sequenced (Eurofins Genomics, **Table 2.8**) and followed by LR recombination reaction (150 ng donor plasmid, 150 ng pGWB501, TE-buffer (10 mM Tris-HCl (pH 7.5) and 1 mM EDTA), LR Clonase (Gateway LR Clonase II Enzyme mix- Thermo Fisher Scientific (CAT 11791020)) overnight at 16°C. The LR reaction was used for transformation into chemical competent TOP10 *E.coli* cells. Next grown on LB-plates with selective antibiotics (100 µg/ml Spectinomycin (Spec)), colony PCR was performed, positive colonies were cultivated in liquid cultures, plasmid was extracted and tested with restriction digest.

Table 2.7. Colony PCR primers.

Primer name	Primer sequence	Construct
GFP-300F	GAAGGGCATCGACTTCAAGG	
Colony PCR primers for ASY3 constructs (with GFP-300F)		
J55	GATCCttatcactcgGCTTCGATATATATCAAGATATCA	UTRMS2
J65	CTATTCTATATGGTTTGTCCAAACTCATCGGATCT	200MS2
J61	GTTTTGCTTGTGGTTTGTCCAAACTCATCGGATCT	100MS2
J69	AGTTGCTGGCTGGTTTGTCCAAACTCATCGGATCT	300MS2
J53	CAAGAAAGCTGGGTTGCTTCGATATATATCAAGATATCA	MS2UTR
seqGFPMS2.11	GCTCCAGTATTCCAGGGTTCATCAG	MS2UTR
Colony PCR primers for TAM constructs (with GFP-300F)		
J73	AGAAACACTATGGTTTGTCCAAACTCATCGGATCT	MS2UTR
J97	AGGGTAAAAATGGTTTGTCCAAACTCATCGGATCT	20MS2
J101	AATTTTTATCTGGTTTGTCCAAACTCATCGGATCT	50MS2
J123	CACTTCAACCTGGTTTGTCCAAACTCATCGGATCT	200MS2
J127	TACACATCATTGGTTTGTCCAAACTCATCGGATCT	100MS2
Colony PCR primers for REC8 constructs (with GFP-300F)		
77	AAATCAAACCTGGTTTGTCCAAACTCATCGGATCT	MS2UTR
81	CAGAATCTTTTGGTTTGTCCAAACTCATCGGATCT	20MS2
85	AACTATGGATTGGTTTGTCCAAACTCATCGGATCT	40MS2
89	TCTCTGCTTGGTTTGTCCAAACTCATCGGATCT	70MS2
93	ACTTAAAAAATGGTTTGTCCAAACTCATCGGATCT	90MS2

Table 2.8. Sequencing primers.

Primer name	Primer sequence
seq-ASY3-GFP-MS2.1	CTTCCGACTGAGCCTTTCGTTTTAT
seq-ASY3-GFP-MS2.2	TCATCGGAAATTAGGGACTCTTGAG
seq-ASY3-GFP-MS2.3	ATGCTACCAGAAGGCCAGTAACCAG
seq-ASY3-GFP-MS2.4	ATAAACATGAACGGCCGAGTAATAT
seq-ASY3-GFP-MS2.5	TCAGTATGCTTCTTAATTCTTATCC
seq-ASY3-GFP-MS2.6	AACTTTGAGAGAAAACCTGAAATCTG
seq-ASY3-GFP-MS2.7	TCGGCTCTAACATAGACATGAAACT
seq-ASY3-GFP-MS2.8	AAACTCACTTGATAACTTTTTATCT
seq-ASY3-GFP-MS2.9	TGCCCTGGCCCACCCTCGTGACCAC
seq-ASY3-GFP-MS2.10	GAGTTCGTGACCGCCGCCGGGATCA
seq-ASY3-GFP-MS2.11	GCTCCAGTATTCCAGGGTTCATCAG
seq-ASY3-GFP-MS2.12	GCCTCCAGGTCTGAATCTTCAAACGA
S2-TAM-400-F	ACGGTGTTTCGTGGTGGCTTGAGC
S3-TAM-1100-F	GCTCTAAAACAGAGTTAGAGCAC
S4-TAM-1800-F	ATATATCAGAATCACAACCTTTTG
S5-TAM-2500-F	GAACCTTAGCCAAGACTCGAACCT
S6-TAM-3200-F	TCTGAATTGTCAAAGTTGAAATT
S7-TAM-3900-F	CTACTTGAAGTTCGAATTAACAA
S8-TAM-4500-F	GATGTGGTTGCAATCAGAAAGAA
S9-TAM-5200-F	CACAACATCGAGGACGGCAGCGT
S10-TAM-5100-F	GATCTCTCGACAGATCCTACCTG
S11-TAM-5500-F	ATCTCTCGAGTGATAAGGATCCT
K1_REC8P_SEQ	CTTCACCCCAGCCAAGACATT
K2_REC8P_SEQ	CTTCAACATTCGAAGACCCGT
K3_REC8P_SEQ	CCGGAATTATCAAATCCGCAG
K4_REC8P_SEQ	CGGTAGGGGCCGCCTGAGCTC
K5_REC8_SEQ	TAGAAAGGAAATGTTGAGACT
K6_REC8_SEQ	TGATTTTGCAACCTCTGTTTC
K7_REC8_SEQ	GTTCTTCAATGTTTTGTTTAT
K8_REC8_SEQ	GGCGTGTTGGATTTTTTTGTT
K9_REC8_SEQ	ATGGGCTGTGGAAATGGACAA
K10_REC8_SEQ	TCATCCACCTTTCAGCAAAAA
K11_REC8_SEQ	ATCGTAGGGACGGATTTGCTG
K12_REC8_SEQ	CCTCATCATCTGGTCTCTCTC
K13_REC8_SEQ	ATATTTAGCGTAAGTTATTTG
K14_REC8_SEQ	AGTGTGCAATCAATCAGACGA
K15_MS2_SEQ	GGACGAGCTGTACAAGGGAGG
K16_UTR_Rev_SEQ	GTAAGAACGCTTGCTCTTT
seq_MS2only-F	CGAGTGATAAGGATCTCGGATCC
seq_MS2loops-F	CTCTCGAGTGATAAGGATCC
seq_MS2-R	TGGTTTGTCCAACTCATCG

The expression plasmid (1 µg) was first transformed into chemical competent GV3101 MP90 *Agrobacterium tumefaciens* cells (DNA Cloning Service), 5 min 37°C, recovered with LB-medium for 2 h at 28°C at 350 rpm, spread on LB-plate with selective antibiotics (100 µg/ml Spec and 30 µg/ml Gentamycin(Gent)) and left to grow for 2 days at 28°C. Colony PCR was performed and positive colonies were used for plant transformation. Colonies were cultivated in LB cultures with selective antibiotics at 28°C, cells were pelleted by centrifugation for 10 min at 18°C at 5000 rpm, dissolved in transformation solution (5% sucrose, 0.05% Silwet-77). The constructs were transformed into Arabidopsis plants (wild type and T-DNA insertion mutants) by floral dipping (Clough and Bent, 1998), plants were left to set seed and T1-seeds collected.

4.9.RT-PCR

For the confirmation of the MS2-loops in the mRNA of the gene of interest, 3 inflorescences per plant were collected in a 1.5 ml Eppendorf tube with 2 metal beads, flash frozen using liquid nitrogen and grinded to fine powder in a Retsch mill for 2 times 1 min at 20 rpm. RNA was extracted using TRIZOL and chloroform (5:1 ratio TRIZOL:chloroform). After centrifugation (10 min, 4°C, full speed), to the upper phase isopropanol (1:1) was added, inverted and incubated on ice for 5 min, continued by centrifugation (10 min, 4°C, full speed). The pellet was repeatedly washed with ice-cold EtOH (75%) and finally resuspended in nuclease free H₂O. 1 µg of total RNA was used for cDNA synthesis (RevertAid First Strand cDNA Synthesis Kit – Thermo Scientific (CAT K1622)) and the cDNA was further used for PCR. Primers spanned from GFP over the MS2-loops and as control primers spanning over the gene and GFP fusion (**Table 2.9**).

Table 2.9. RT-PCR primers.

Primer name	Primer sequence	Expected fragment size
GFP-MS2-loops spanning primers for ASY3 constructs		
GFP-300F	GAAGGGCATCGACTTCAAGG	
J61	GTTTTGCTTGTGGTTTGTCCA AACTCATCGGATCT	With GFP-300F ~1700-2000 bp (used for MS2UTR- 200/300MS2)
J56a	AGACTCAGTGTCAACCCGGGTC CACCTCCCTTGTA	With J61 ~1700 bp (used for UTRMS2)
ASY3-GFP spanning primers		
GFP-300R	TTGAAGTCGATGCCCTTCAG	
J39	CATCACACCAAAAACCTCATTG	With GFP-300R ~600 bp
TAM-GFP spanning primers		
S8	GATGTGGTTGCAATCAGAAAGAA	With GFP-300R ~600 bp
GFP-MS2-loops spanning primers for TAM constructs		
J73	AGAAACACTATGGTTTGTCCAAA CTCATCGGATCT	With GFP-300F ~1700-1750bp

4.10. Confocal microscopy

For protein localization experiments, healthy flower buds were dissected and the reproductive organs were isolated and transferred in a drop of water on a microscope slide and covered by a cover slip. Anthers were imaged using a Leica TCS SP8 inverted confocal microscope or a Zeiss LSM780 upright confocal microscope. GFP and RPF were excited at $\lambda = 488$ nm and 561 nm, respectively, and detected between 498-560 nm and 520-650 nm, respectively. Auto-fluorescence was detected between 680-750 nm.

4.11. Propidium iodide (PI) staining

The root tips of 10 days old seedlings were incubated for 5 min in 10 μ M PI on a microscope slide covered by a cover slip. The root tips were then imaged using a Leica TCS SP8 inverted confocal microscope.

4.12. Phenotypic analysis

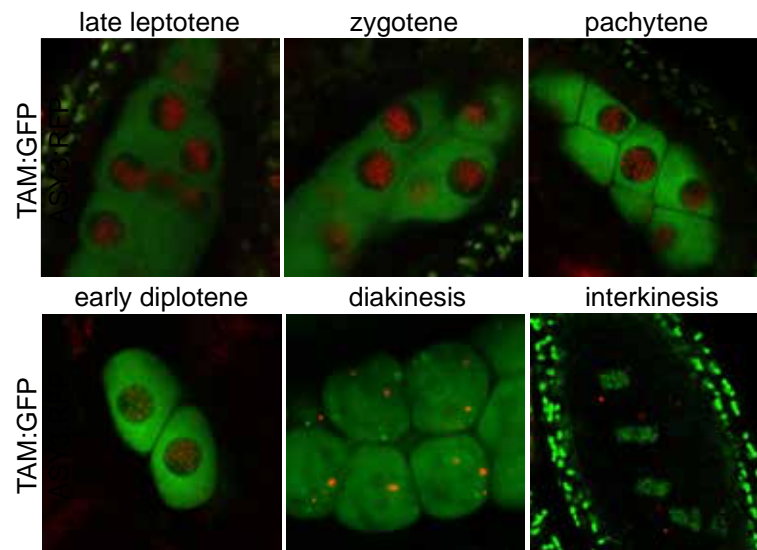
The seed viability was determined from green mature/elongated siliques. Per plant, 10 siliques were cut and placed on double sided tape and opened by cutting along the septum. Both the viable green seeds and aborted shrunken white seeds were counted and the relative seed set was calculated and evaluated.

For the confirmation of the dyad/tetrad formation, healthy flower buds were dissected and the anthers were isolated and transferred in a drop of water on a microscope slide and covered by a cover slip. Anthers in dyad/tetrad stages were imaged under a Zeiss Axioskop light microscope.

4.13. Accession numbers

Accession numbers based on TAIR (<https://www.arabidopsis.org>) for all genes examined in this study are ASY3 (at2g46980), TAM (at1g77390) and REC8 (at5g05490).

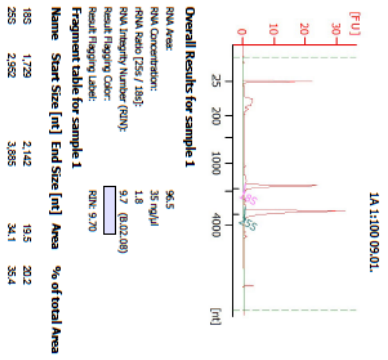
5. SUPPLEMENTAL DATA CHAPTER II



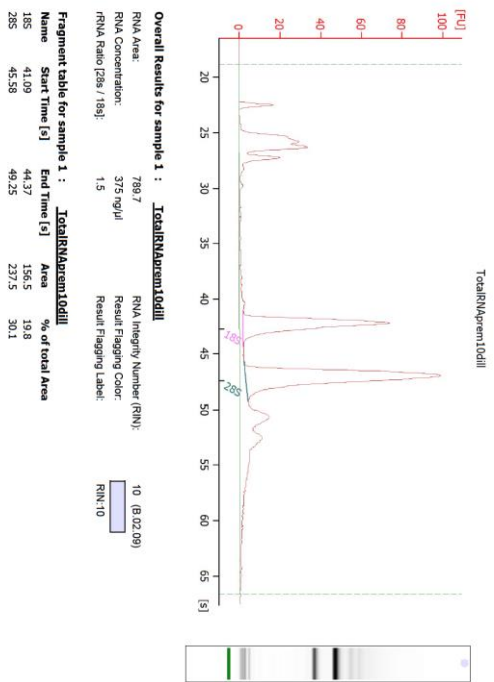
Supplemental Figure S2.1. The TAM reporter.

The genomic TAM reporter, *TAM:GFP*, together with the *ASY3:RFP* for staging, in *Arabidopsis* male meiocytes from late leptotene, zygotene, pachytene, early diplotene, diakinesis to interkinesis, generated by Dr. Chao Yang. TAM:GFP in green; ASY3:RFP in red.

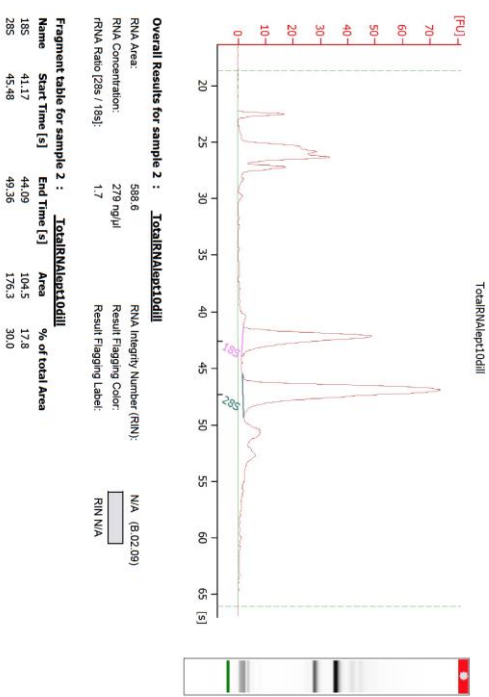
A



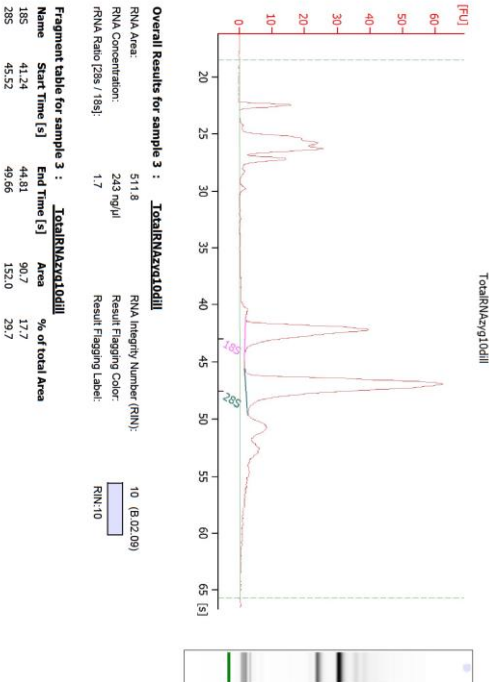
B

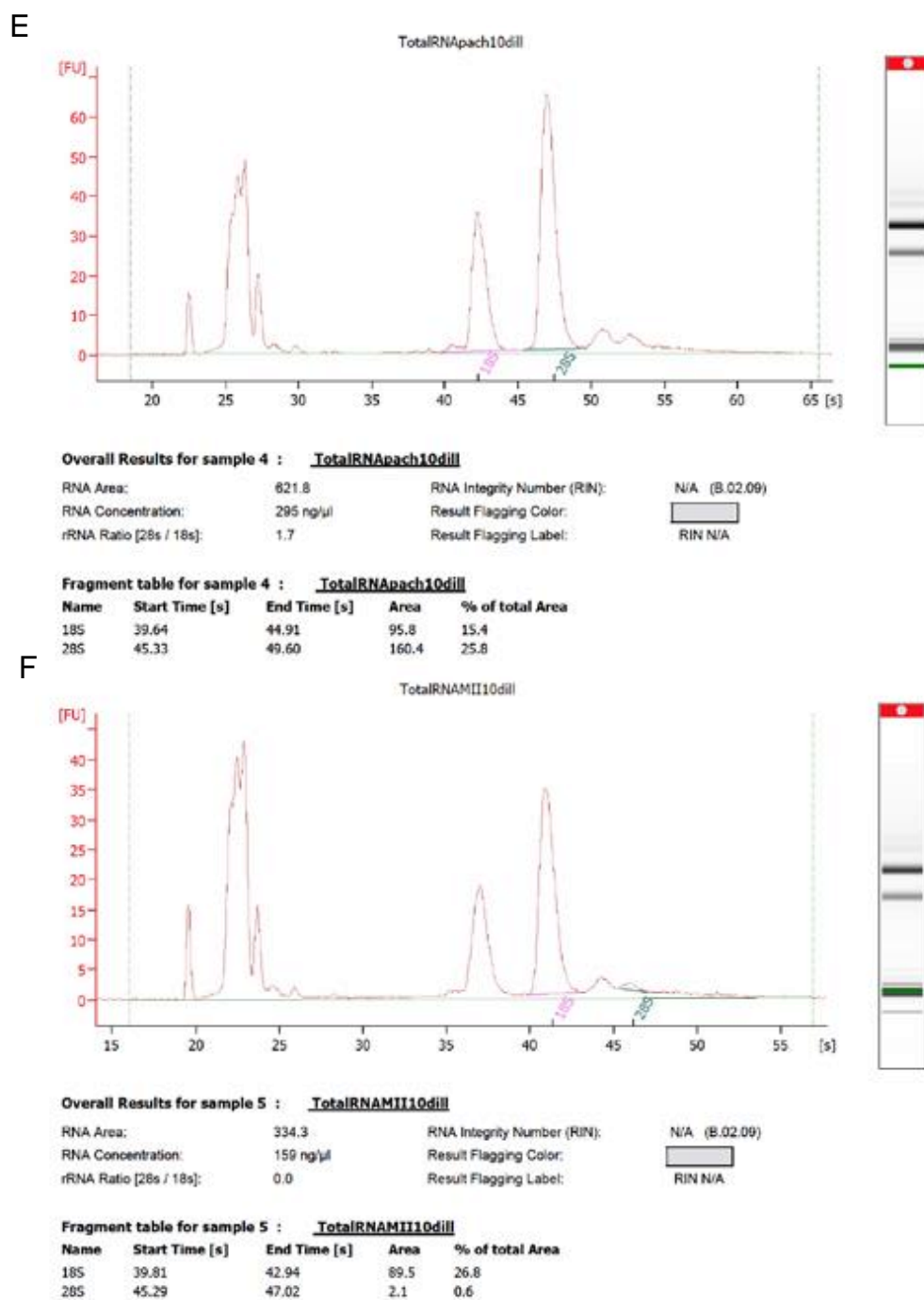


C



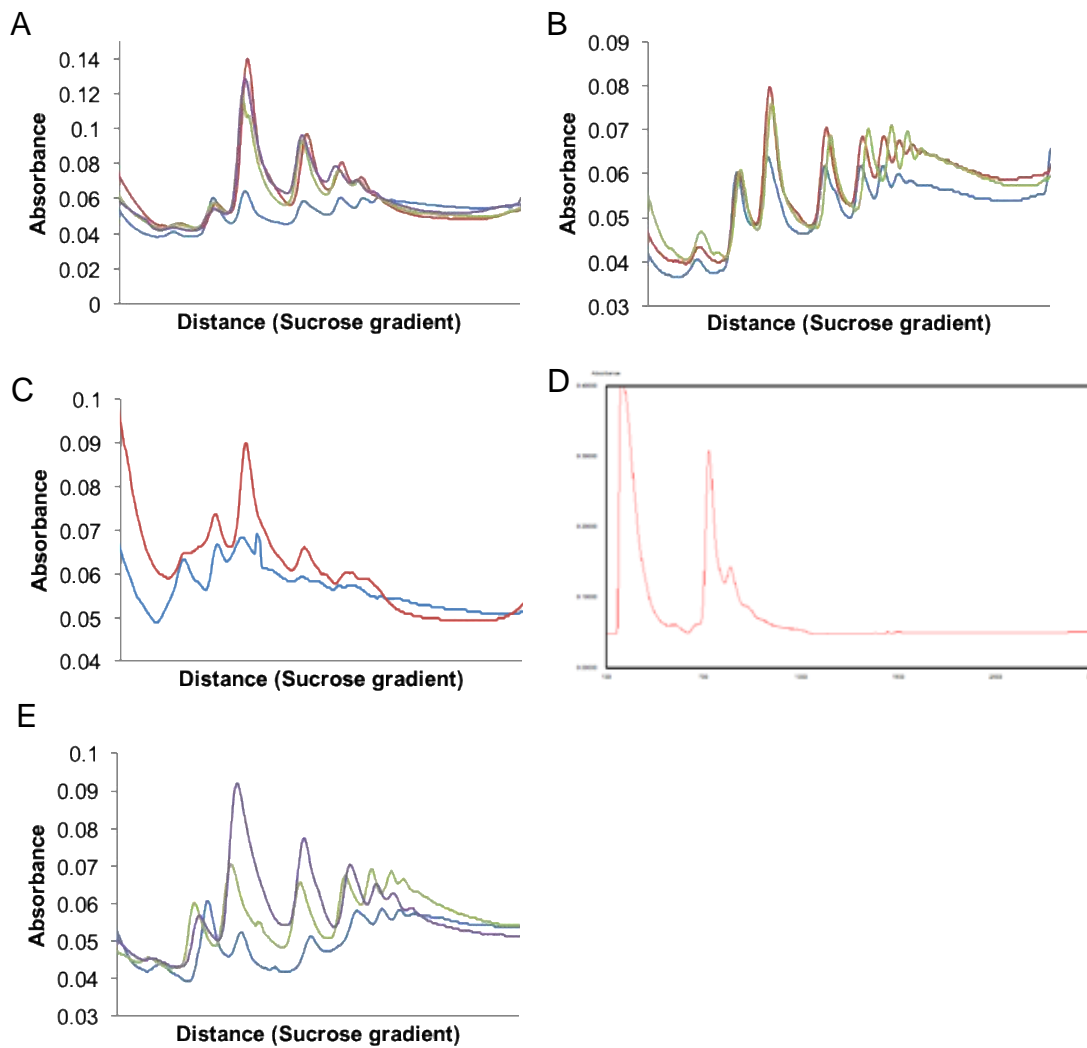
D





Supplemental Figure S2.2. Quality of the extracted total RNA.

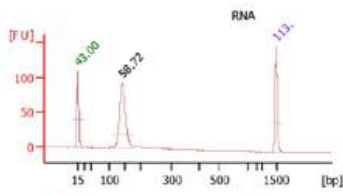
The quality of the extracted total RNA was analysed using the BioAnalyzer 2100. The results from total RNA extracted from (A) spikelets and from anthers in (B) premeiosis, (C) leptotene, (D) zygotene, (E) pachytene and (F) meiosis II.



Supplemental Figure S2.3. Optimization of polysome digestion into monosomes.

The absorbance at 260 nm was measured along the distance in the sucrose gradient. Different optimization attempts are shown in different colours, blue always indicates the undigested control. (A) Optimization of the durations of digestion with RNase I for 60 min (red), 75 min (green) and 90 min (purple) (5 U/OD/μl at 22°C). (B) Optimization of the temperature of the digestion with RNase I at 26°C (red) and 30°C (green) (2 U/OD/μl, 40 min). (C) Polysome digestion with pH 7.5 of the extraction buffers (1.5 U/OD/μl, 45 min, 22°C; red). (D) Polysome digestion using RNase T (10 U/μl, 45 min, 22°C). (E) Optimization of the concentrations of RNase I of 3 U/OD/μl (green) and 5 U/OD/μl (purple) (40 min, 22°C).

A



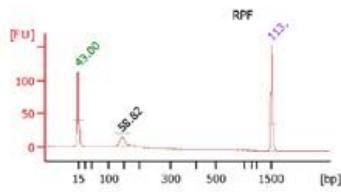
Overall Results for sample 1 : RNA

Number of peaks found: 1

Peak table for sample 1 : RNA

Peak	Size [bp]	Conc. [ng/μl]	Molarity [nmol/l]	Observations
1	15	4.20	424.2	Lower Marker
2	142	8.98	96.0	
3	1,500	2.10	2.1	Upper Marker

B



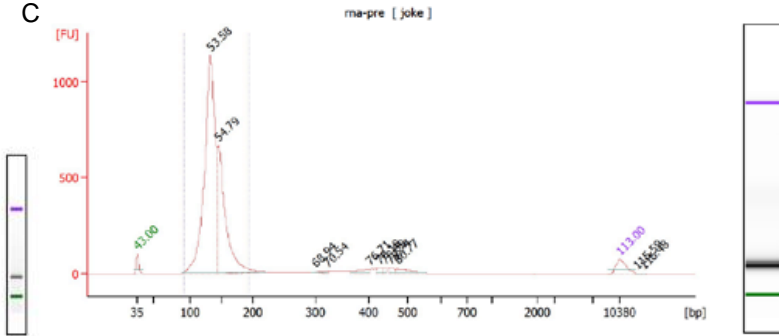
Overall Results for sample 2 : RPF

Number of peaks found: 1

Peak table for sample 2 : RPF

Peak	Size [bp]	Conc. [ng/μl]	Molarity [nmol/l]	Observations
1	15	4.20	424.2	Lower Marker
2	143	1.14	12.1	
3	1,500	2.10	2.1	Upper Marker

C



Overall Results for sample 1 : rna-pre

Number of peaks found: 11

Corr. Area 1: 5,865.6

Noise: 0.5

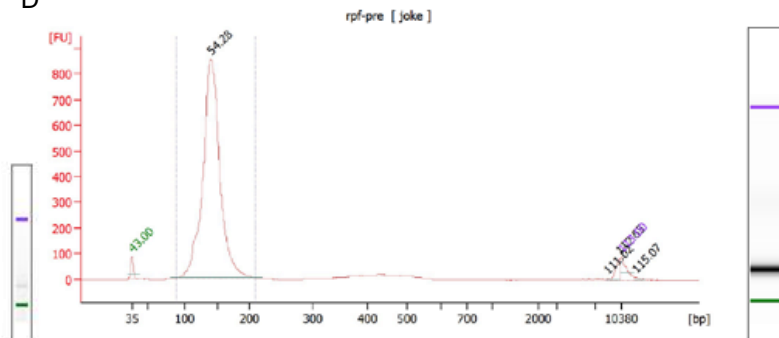
Peak table for sample 1 : rna-pre

Peak	Size [bp]	Conc. [pg/μl]	Molarity [pmol/l]	Observations
1	35	125.00	5,411.3	Lower Marker
2	132	4,533.79	52,067.5	
3	145	2,022.99	21,132.3	
4	301	4.69	23.6	
5	322	15.52	73.1	
6	401	46.09	174.0	
7	427	23.73	84.1	
8	440	15.43	53.1	
9	455	21.50	71.6	
10	473	59.51	190.6	
11	10,380	75.00	10.9	Upper Marker
12	12,683	0.00	0.0	
13	13,477	0.00	0.0	

Region table for sample 1 : rna-pre

From [bp]	To [bp]	Corr. Area	% of Total	Average Size [bp]	Size distribution in CV [%]	Conc. [pg/μl]	Molarity [pmol/l]	Color
91	193	5,865.6	89	137	11.2	6,544.79	72,653.5	■

D



Overall Results for sample 2 : rpf-pre

Number of peaks found: 4

Corr. Area 1: 4,914.5

Noise: 0.6

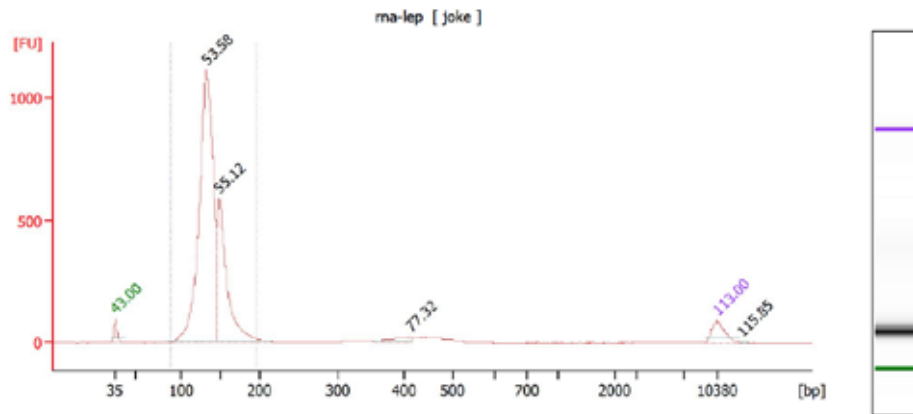
Peak table for sample 2 : rpf-pre

Peak	Size [bp]	Conc. [pg/μl]	Molarity [pmol/l]	Observations
1	35	125.00	5,411.3	Lower Marker
2	140	8,228.47	89,311.7	
3	8,616	2.38	0.4	
4	10,066	46.67	7.0	
5	10,380	75.00	10.9	Upper Marker
6	12,223	0.00	0.0	

Region table for sample 2 : rpf-pre

From [bp]	To [bp]	Corr. Area	% of Total	Average Size [bp]	Size distribution in CV [%]	Conc. [pg/μl]	Molarity [pmol/l]	Color
87	209	4,914.5	90	141	11.5	8,318.60	90,143.8	■

E



Overall Results for sample 3 : ma-lep

Number of peaks found: 4 Corr. Area 1: 5,631.1
 Noise: 0.5

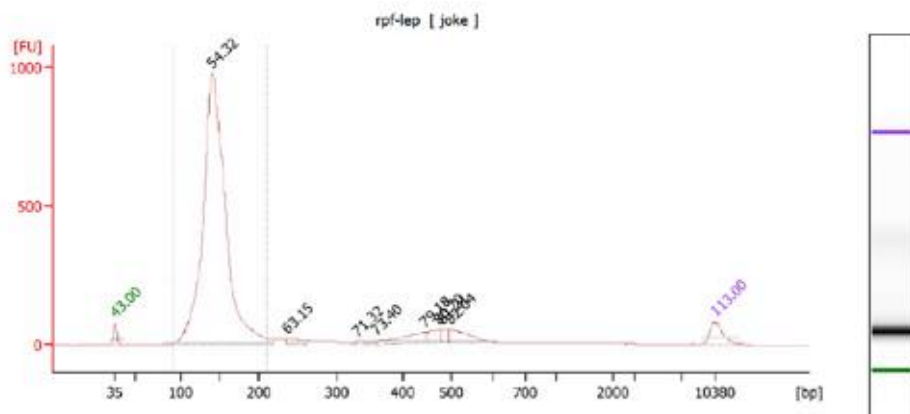
Peak table for sample 3 : ma-lep

Peak	Size [bp]	Conc. [pg/μl]	Molarity [pmol/l]	Observations
1	35	125.00	5,411.3	Lower Marker
2	132	4,245.31	48,750.4	
3	149	1,517.75	15,468.0	
4	412	63.79	234.5	
5	10,380	75.00	10.9	Upper Marker
6	12,914	0.00	0.0	

Region table for sample 3 : ma-lep

From [bp]	To [bp]	Corr. Area	% of Total	Average Size [bp]	Size distribution in CV [%]	Conc. [pg/μl]	Molarity [pmol/l]	Color
88	197	5,631.1	93	138	11.1	5,754.23	63,988.6	■

F



Overall Results for sample 4 : rpf-lep

Number of peaks found: 8 Corr. Area 1: 5,703.8
 Noise: 0.4

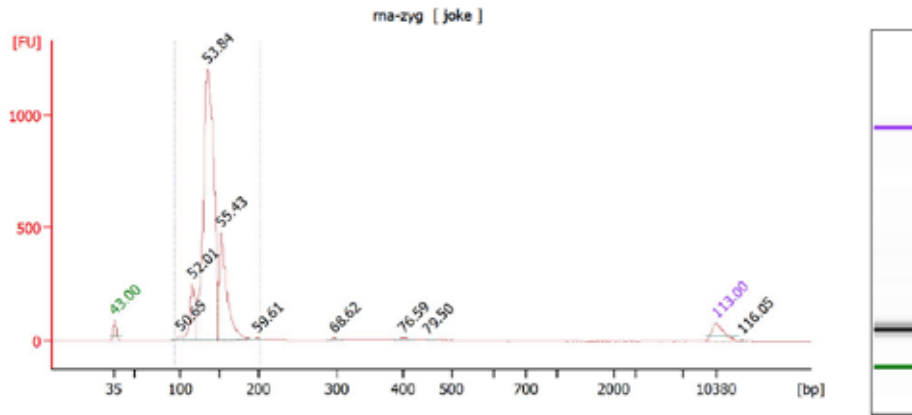
Peak table for sample 4 : rpf-lep

Peak	Size [bp]	Conc. [pg/μl]	Molarity [pmol/l]	Observations
1	35	125.00	5,411.3	Lower Marker
2	140	6,224.28	67,371.9	
3	237	60.66	387.3	
4	332	5.71	26.1	
5	359	16.41	69.3	
6	445	135.16	460.1	
7	472	70.89	227.6	
8	481	49.71	156.6	
9	496	138.91	424.6	
10	10,380	75.00	10.9	Upper Marker

Region table for sample 4 : rpf-lep

From [bp]	To [bp]	Corr. Area	% of Total	Average Size [bp]	Size distribution in CV [%]	Conc. [pg/μl]	Molarity [pmol/l]	Color
92	211	5,703.8	83	145	12.2	6,152.10	65,197.3	■

G



Overall Results for sample 5 : ma-zyg

Number of peaks found: 9 Corr. Area 1: 4,666.2
 Noise: 0.4

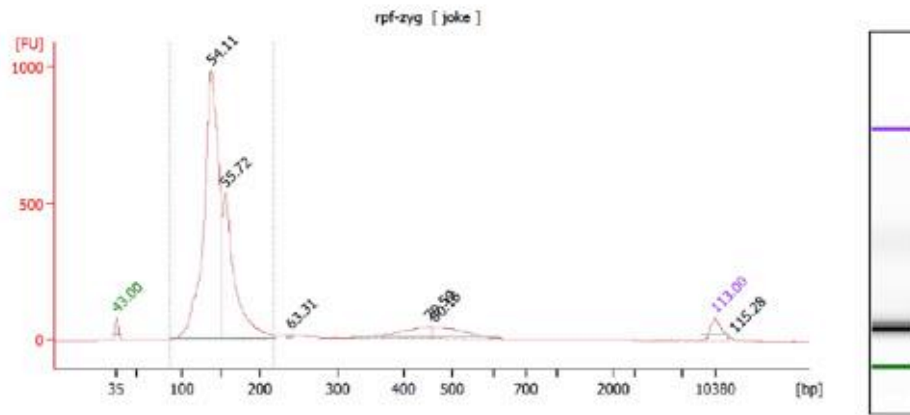
Peak table for sample 5 : ma-zyg

Peak	Size [bp]	Conc. [pg/μl]	Molarity [pmol/l]	Observations
1	35	125.00	5,411.3	Lower Marker
2	100	31.47	476.8	
3	115	469.89	6,200.3	
4	135	3,839.70	43,179.8	
5	152	1,062.33	10,580.6	
6	198	7.85	59.9	
7	297	9.67	49.3	
8	400	18.50	70.2	
9	451	6.01	20.2	
10	10,380	75.00	10.9	Upper Marker
11	13,092	0.00	0.0	

Region table for sample 5 : ma-zyg

From [bp]	To [bp]	Corr. Area	% of Total	Average Size [bp]	Size distribution in CV [%]	Conc. [pg/μl]	Molarity [pmol/l]	Color
94	202	4,666.2	93	139	9.9	5,442.52	59,771.8	■

H



Overall Results for sample 6 : rpf-zyg

Number of peaks found: 6 Corr. Area 1: 5,498.1
 Noise: 0.4

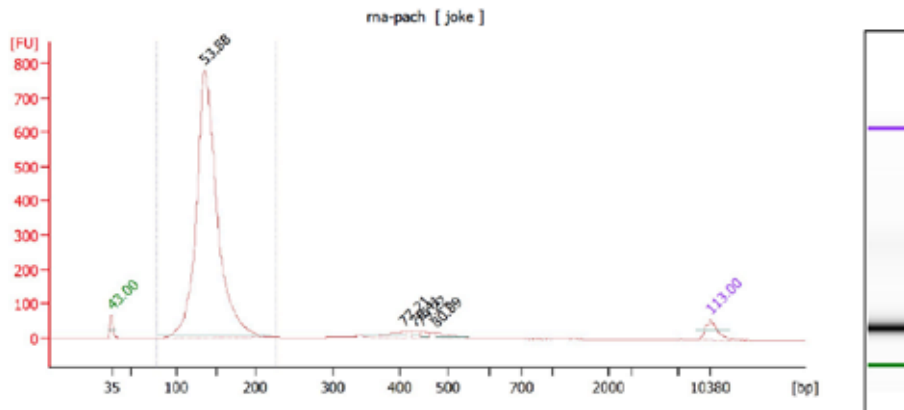
Peak table for sample 6 : rpf-zyg

Peak	Size [bp]	Conc. [pg/μl]	Molarity [pmol/l]	Observations
1	35	125.00	5,411.3	Lower Marker
2	138	5,013.04	55,183.7	
3	155	2,069.89	20,194.9	
4	239	18.22	115.4	
5	452	225.70	756.0	
6	462	216.74	710.2	
7	10,380	75.00	10.9	Upper Marker
8	12,406	0.00	0.0	

Region table for sample 6 : rpf-zyg

From [bp]	To [bp]	Corr. Area	% of Total	Average Size [bp]	Size distribution in CV [%]	Conc. [pg/μl]	Molarity [pmol/l]	Color
88	217	5,498.1	82	145	13.1	7,196.67	76,321.5	■

I



Overall Results for sample 7 : rna-pach

Number of peaks found: 5 Corr. Area 1: 4,248.4
 Noise: 0.3

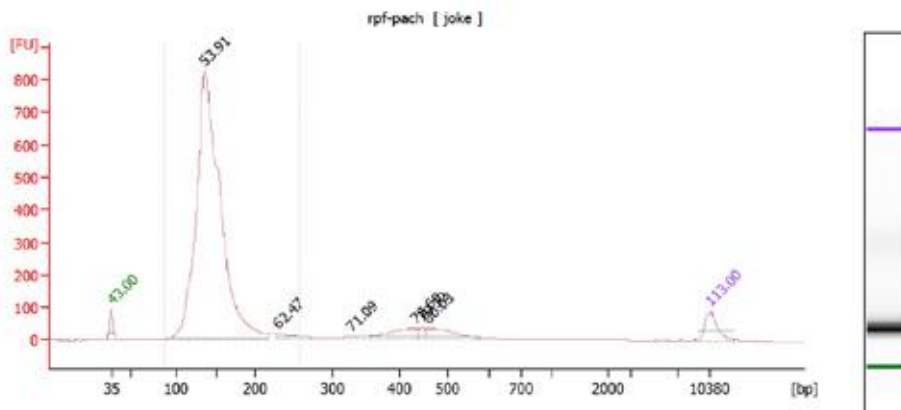
Peak table for sample 7 : rna-pach

Peak	Size [bp]	Conc. [pg/μl]	Molarity [pmol/l]	Observations
1	35	125.00	5,411.3	Lower Marker
2	135	7,237.25	81,115.1	
3	410	84.53	312.1	
4	431	23.60	82.9	
5	446	26.86	91.3	
6	475	49.04	156.3	
7	10,380	75.00	10.9	Upper Marker

Region table for sample 7 : rna-pach

From [bp]	To [bp]	Corr. Area	% of Total	Average Size [bp]	Size distribution in CV [%]	Conc. [pg/μl]	Molarity [pmol/l]	Color
77	226	4,246.4	91	141	12.5	7,240.95	79,042.5	Blue

J



Overall Results for sample 8 : rpf-pach

Number of peaks found: 6 Corr. Area 1: 5,193.7
 Noise: 0.3

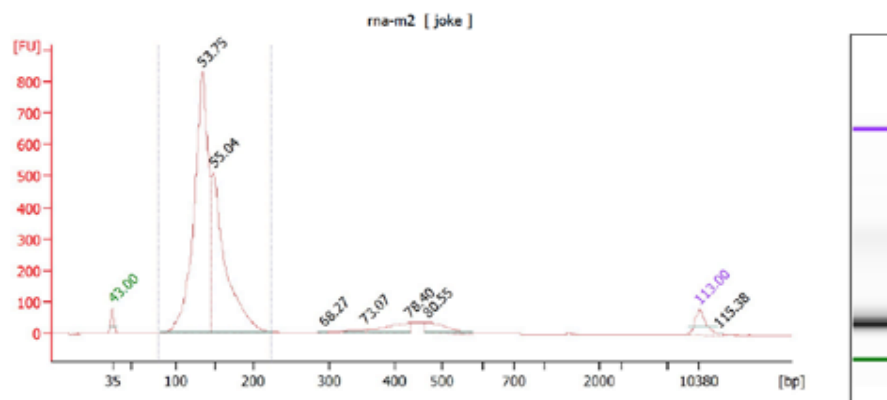
Peak table for sample 8 : rpf-pach

Peak	Size [bp]	Conc. [pg/μl]	Molarity [pmol/l]	Observations
1	35	125.00	5,411.3	Lower Marker
2	136	5,655.28	63,233.0	
3	230	60.45	398.4	
4	329	4.52	20.9	
5	435	133.77	466.1	
6	447	27.38	92.7	
7	460	121.26	399.2	
8	10,380	75.00	10.9	Upper Marker

Region table for sample 8 : rpf-pach

From [bp]	To [bp]	Corr. Area	% of Total	Average Size [bp]	Size distribution in CV [%]	Conc. [pg/μl]	Molarity [pmol/l]	Color
87	257	5,193.7	87	146	16.1	5,725.61	60,925.9	Blue

K



Overall Results for sample 9 : rna-m2

Number of peaks found: 7 Corr. Area 1: 4,985.7
 Noise: 0.4

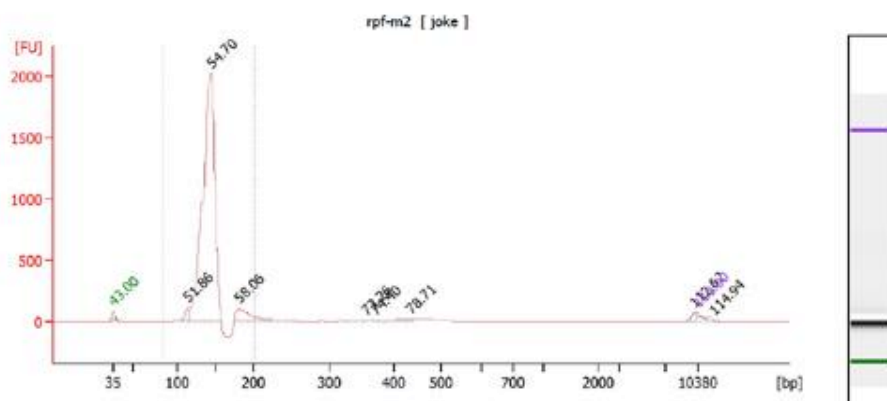
Peak table for sample 9 : rna-m2

Peak	Size [bp]	Conc. [pg/μl]	Molarity [pmol/l]	Observations
1	35	125.00	5,411.3	Lower Marker
2	134	4,281.78	48,477.0	
3	148	2,501.53	25,643.1	
4	294	6.43	33.2	
5	354	32.29	138.1	
6	431	139.91	491.4	
7	469	131.86	425.8	
8	10,380	75.00	10.9	Upper Marker
9	12,496	0.00	0.0	

Region table for sample 9 : rna-m2

From [bp]	To [bp]	Corr. Area	% of Total	Average Size [bp]	Size distribution in CV [%]	Conc. [pg/μl]	Molarity [pmol/l]	Color
80	224	4,985.7	88	143	14.5	6,802.09	73,696.0	■

L



Overall Results for sample 10 : rpf-m2

Number of peaks found: 8 Corr. Area 1: 6,813.0
 Noise: 0.4

Peak table for sample 10 : rpf-m2

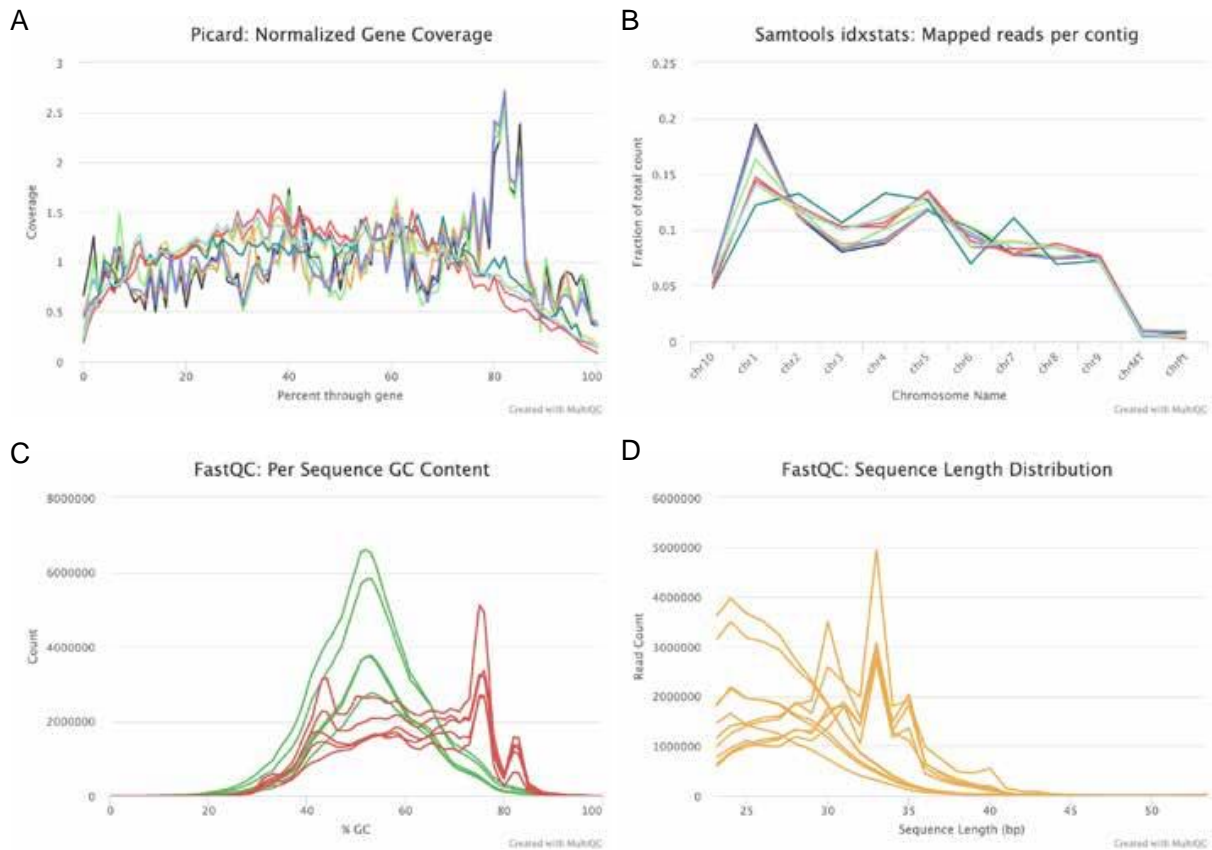
Peak	Size [bp]	Conc. [pg/μl]	Molarity [pmol/l]	Observations
1	35	125.00	5,411.3	Lower Marker
2	113	320.38	4,288.9	
3	144	15,672.48	164,796.8	
4	181	921.25	7,700.0	
5	357	31.93	135.6	
6	371	10.58	43.2	
7	437	124.39	431.5	
8	10,043	49.61	7.5	
9	10,380	75.00	10.9	Upper Marker
10	12,107	0.00	0.0	

Region table for sample 10 : rpf-m2

From [bp]	To [bp]	Corr. Area	% of Total	Average Size [bp]	Size distribution in CV [%]	Conc. [pg/μl]	Molarity [pmol/l]	Color
84	203	6,813.0	93	141	9.5	16,943.48	182,440.1	■

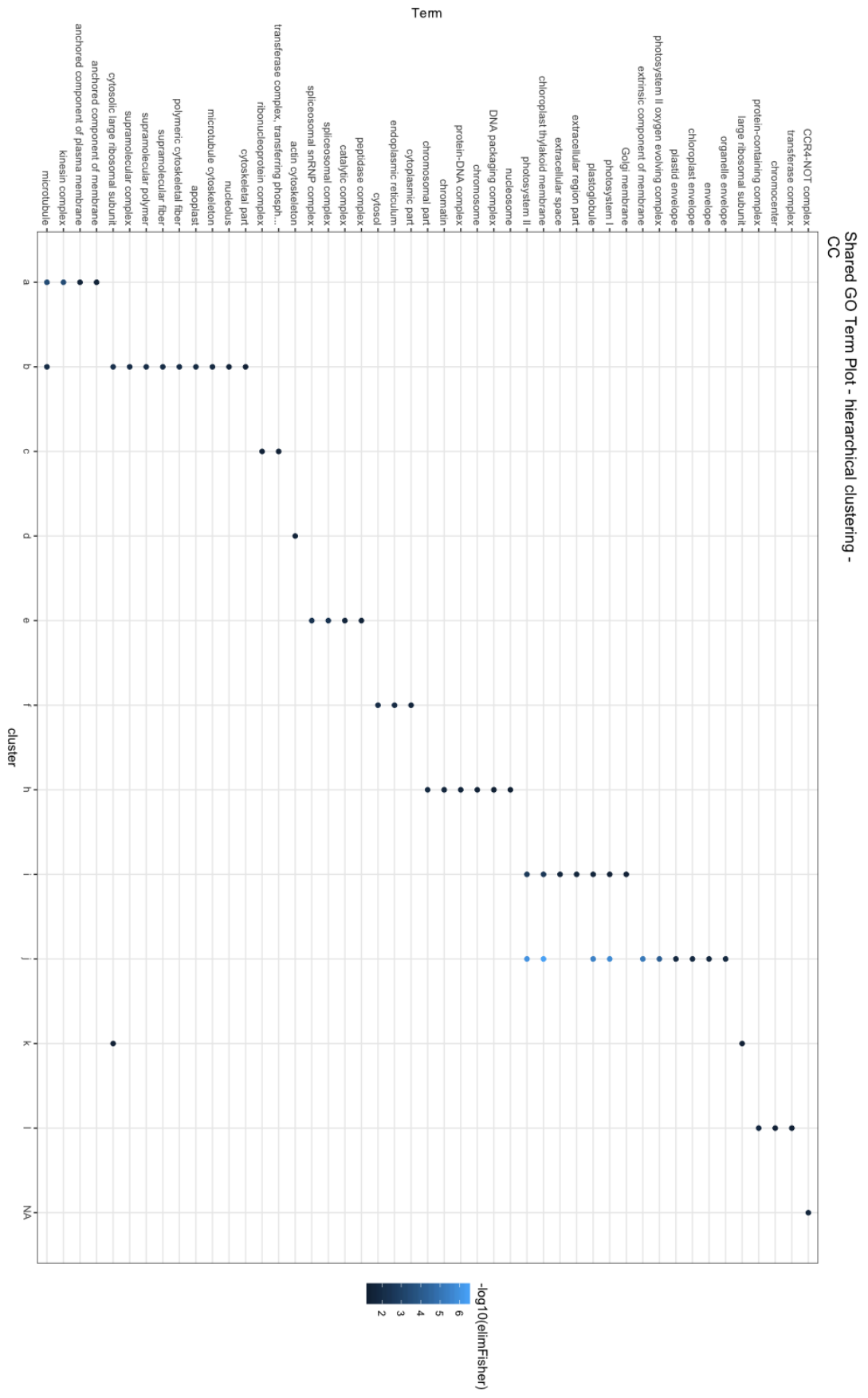
Supplemental Figure S2.4. Quality of the RNA and RPF libraries of the spikelet test run and first anther replicate.

The quality of the prepared libraries was analysed using the BioAnalyzer 2100. The results for the (A) RNA library and (B) RPF library from spikelets and the first replicate of the RNA and RPF libraries from anthers in (C,D) premeiosis, (E,F) leptotene, (G,H) zygotene, (I,J) pachytene and (K,L) meiosis II.



Supplemental Figure S2.5. The quality control of the mRNA and RPF libraries from anthers.

(A) Normalized gene coverage plotted along genes (in percentage) of the mRNA and RPF libraries during meiosis. (B) The mapped reads per chromosome of the mRNA and RPF libraries during meiosis. Colour coding: RNA_PRE (orange), RNA_LEP (blue), RNA_ZYG (purple), RNA_PACH (green), RNA_MII (black), RPF_PRE (red), RPF_LEP (dark pink), RPF_ZYG, (light blue), RPF_PACH (cyan) and RPF_MII (yellow). (C) The GC content per sequence for the RNA libraries (green) and RPF libraries (red). (D) Sequence length distribution of the mRNA and RPF libraries during meiosis.



Supplemental Figure S2.7. GO analysis of the clusters for GO category Cellular Component (CC).

Supplemental Table S2.1. Meiotic genes detected in the RNA and RPF libraries of anthers during meiosis.

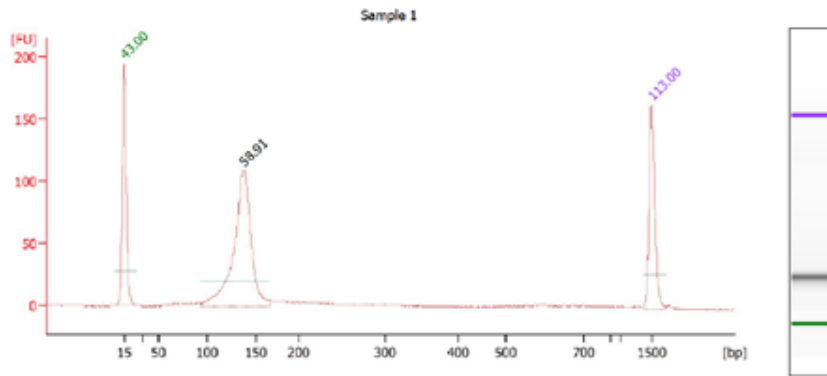
Gene name	Gene ID (<i>A.thaliana</i>)	Gene ID (<i>Z.mays</i>)	Description
<i>AGO9</i>	AT5G21150	Zm00001d008249 Zm00001d039214 Zm00001d040429	Protein argonaute 9
<i>AHP2</i>	AT3G29350	Zm00001d005344 Zm00001d031961 Zm00001d049952	AHP2
<i>ARP6</i>	AT3G33520	Zm00001d024059	SUF3
<i>ASY1</i>	AT1G67370	Zm00001d006089	Meiosis-specific protein ASY1
<i>ASY3</i>	AT2G46980	Zm00001d015469	Meiosis-specific protein ASY3
<i>ATM</i>	AT3G48190	Zm00001d040166	Serine/Threonine-kinase ATM-like protein
<i>ATPRD3</i>	AT1G01690	Zm00001d027300	Putative recombination initiation defects 3
<i>ATRAD3</i>	AT5G40820	Zm00001d014813	Ataxia telangiectasia-mutated and RAD3-related
<i>ATRAD51B</i>	AT2G28560	Zm00001d010986	DNA repair (Rad51) family protein
<i>ATRAD51C</i>	AT2G45280	Zm00001d044278	RAS associated with diabetes protein 51C
<i>ATRM1</i>	AT5G63540	Zm00001d003937	Domain of unknown function (DUF1767)
<i>ATSMC2/2-1</i>	AT3G47460/AT5G62410	Zm00001d042468	Structural maintenance of chromosomes protein / 2-1
<i>ATSRP2</i>	AT2G14540	Zm00001d013737	Serpin-Z2
<i>BUB3.1</i>	AT3G19590	Zm00001d034081 Zm00001d045389	BUB3.1
<i>BUBR1</i>	AT2G33560	Zm00001d015863	BUBR1
<i>CDC45</i>	AT3G25100	Zm00001d023283	Cell division cycle 45-like protein
<i>CDKA-1</i>	AT3G48750	Zm00001d053930	Cyclin-dependent kinase A-1
<i>CDKB1-2/1-1</i>	AT2G38620/AT3G54180	Zm00001d044672	Cyclin-dependent kinase B1-2 / B1-1
<i>CDKB2-2/2-1/1-2/1-1</i>	AT1G20930/AT1G76540/ AT2G38620/AT3G54180	Zm00001d046912 Zm00001d031485	Cyclin-dependent kinase B2-2/CDKB2/B1-2/ B1-1
<i>CDKG1</i>	AT5G63370	Zm00001d003222 Zm00001d017128 Zm00001d025739	Cyclin-dependent kinase G1
<i>CYCA1-2</i>	AT1G77390	Zm00001d010404 Zm00001d009011 Zm00001d040381	TAM
<i>CYCB3;1</i>	AT1G16330	Zm00001d002662 Zm00001d026129 Zm00001d036360	CYCB3
<i>DMC1</i>	AT3G22880	Zm00001d044629	Meiotic recombination protein DMC1 homolog
<i>DYAD</i>	AT5G23610/AT5G51330	Zm00001d013659	SWITCH1
<i>EMB2773</i>	AT5G15540	Zm00001d018657 Zm00001d007943	Sister chromatid cohesion protein SCC2
<i>EME1A/B</i>	AT2G21800/AT2G22140	Zm00001d002082	essential meiotic endonuclease 1A/Crossover junction endonuclease 1B

<i>ESP</i>	AT4G22970	Zm00001d052143	homolog of separase
<i>FANCM</i>	AT1G35530/AT1G36020	Zm00001d046331	DEAD/DEAH box RNA helicase family protein
<i>FIGL1</i>	AT3G27120	Zm00001d041083	ATPase family AAA domain-containing protein
<i>GEN1</i>	AT1G01880	Zm00001d021204 Zm00001d006168	Flap endonuclease GEN-like 1
<i>GEN2</i>	AT3G48900	Zm00001d034968	Flap endonuclease GEN-like 2
<i>GR1</i>	AT3G52115	Zm00001d046761	Protein gamma response 1
<i>HOP2</i>	AT1G13330	Zm00001d013447	Homologous-pairing protein 2 homolog
<i>JASON</i>	AT1G06660	Zm00001d036637 Zm00001d053808	Protein JASON
<i>KIN14C</i>	AT4G21270	Zm00001d002186	Kinesin-like protein
<i>KIN7B, TES</i>	AT3G43210	Zm00001d002817 Zm00001d021269 Zm00001d045554 Zm00001d051308	Kinesin-like protein
<i>MAD2</i>	AT3G25980	Zm00001d025721 Zm00001d003249	Mitotic spindle checkpoint protein
<i>MCM8</i>	AT3G09660	Zm00001d010567	Probable DNA helicase
<i>MEE43/BRCA2B</i>	AT4G00020/AT5G01630	Zm00001d024953	BREAST CANCER 2 like 2A / SUSCEPTIBILITY 2 homolog B
<i>MEI1</i>	AT1G77320	Zm00001d004709	transcription coactivators
<i>MHF1</i>	AT5G50930	Zm00001d003888	Protein MHF1 homolog
<i>MHF2</i>	AT1G78790	Zm00001d003274	Protein MHF2 homolog
<i>ML4/ML1</i>	AT5G07290/AT5G61960	Zm00001d035763	Protein MEI2-like 4/1
<i>ML5/ML2</i>	AT1G29400/AT2G42890	Zm00001d035869 Zm00001d045611	Protein MEI2-like 5/ML2
<i>MLH1</i>	AT4G09140	Zm00001d011829	DNA mismatch repair protein
<i>MLH3</i>	AT4G35520	Zm00001d006307	MUTL protein homolog 3
<i>MMD1</i>	AT1G66170	Zm00001d012233 Zm00001d013416 Zm00001d020680 Zm00001d048969	PHD finger protein MALE MEIOCYTE DEATH 1
<i>MND1</i>	AT4G29170	Zm00001d005140	Meiotic nuclear division protein 1 homolog
<i>MPS1</i>	AT5G57880	Zm00001d050498	Protein MULTIPOLAR SPINDLE 1
<i>MRE11</i>	AT5G54260	Zm00001d002154	DNA repair and meiosis protein
<i>MS5</i>	AT4G20900	Zm00001d006237 Zm00001d022627 Zm00001d027809 Zm00001d038642 Zm00001d048444	Tetratricopeptide repeat (TPR)-like superfamily protein
<i>MSH2</i>	AT3G18524	Zm00001d022028 Zm00001d029152	DNA mismatch repair protein
<i>MSH4</i>	AT4G17380	Zm00001d006382	DNA mismatch repair protein
<i>MUS81</i>	AT4G30870	Zm00001d042130 Zm00001d042128	Crossover junction endonuclease
<i>NBS1</i>	AT3G02680	Zm00001d013976	Nijmegen breakage syndrome 1

			protein
<i>PHS1</i>	AT1G10710	Zm00001d045993	Protein POOR HOMOLOGOUS SYNAPSIS 1
<i>PHYC</i>	AT5G35840	Zm00001d013262 Zm00001d034038	Phytochrome C
<i>PMS1</i>	AT4G02460	Zm00001d050929	DNA mismatch repair protein
<i>PRD1</i>	AT4G14180	Zm00001d046970	Protein PRD1
<i>PS1</i>	AT1G34355	Zm00001d004810	FHA domain-containing protein
<i>PTD</i>	AT1G12790	Zm00001d009728	Protein PARTING DANCERS
<i>RAD5</i>	AT5G22750	Zm00001d050643 Zm00001d050642	DNA repair protein
<i>RAD50</i>	AT2G31970	Zm00001d050612	DNA repair protein
<i>RAD51</i>	AT5G20850	Zm00001d021898 Zm00001d041757	DNA repair protein RAD51 homolog 1
<i>RAD51D</i>	AT1G07745	Zm00001d022332	DNA repair protein RAD51 homolog 4
<i>RAD5B</i>	AT5G43530	Zm00001d050061	DNA repair protein
<i>RBR1</i>	AT3G12280	Zm00001d052666 Zm00001d031678 Zm00001d007407 Zm00001d052695	RBR1
<i>RCK</i>	AT3G27730	Zm00001d051111	DNA helicase ROCK-N-ROLLERS
<i>RECQL2</i>	AT1G31360	Zm00001d030366	RECQ helicase L2
<i>RECQL3</i>	AT4G35740	Zm00001d018287	ATP-dependent DNA helicase Q-like 3
<i>RECQL4A</i>	AT1G10930	Zm00001d015212	ATP-dependent DNA helicase Q-like 4A
<i>RFC1</i>	AT5G22010	Zm00001d007500	Replication factor C subunit 1
<i>RPA1A</i>	AT2G06510	Zm00001d052113	Replication protein A 70 kDa DNA-binding subunit A
<i>RPA1B/RPA1D</i>	AT5G08020/AT5G61000	Zm00001d037561 Zm00001d028210 Zm00001d048086	Replication protein A 70 kDa DNA-binding subunit B/ A subunit
<i>RPA1C</i>	AT5G45400	Zm00001d035666	Replication protein A 70 kDa DNA-binding subunit C
<i>RPA2A/RPA2B</i>	AT2G24490/AT3G02920	Zm00001d018531 Zm00001d036531 Zm00001d017324	RPA32A/Replication protein A 32 kDa subunit B
<i>RPA3A/RPA3B</i>	AT3G52630/AT4G18590	Zm00001d040276	Replication protein A 14 kDa subunit A/B
<i>SCC3</i>	AT2G47980	Zm00001d007679 Zm00001d007677	SCC3
<i>SDS</i>	AT1G14750	Zm00001d028274 Zm00001d048026	Cyclin family protein
<i>SGO1</i>	AT3G10440	Zm00001d032805	SHUGOSHIN 1
<i>SGO2</i>	AT5G04320	Zm00001d019148	SHUGOSHIN 2
<i>SHOC1</i>	AT5G52290	Zm00001d017387	Protein SHORTAGE IN CHIASMATA 1
<i>SKP1A/SKP1B</i>	AT1G75950/AT5G42190	Zm00001d006914 Zm00001d022618 Zm00001d027231	SKP1-like protein 1A/1B

		Zm00001d049230	
<i>SMC1</i>	AT3G54670	Zm00001d031847	Structural maintenance of chromosomes protein 1
<i>SMC3</i>	AT2G27170	Zm00001d039189	Structural maintenance of chromosomes protein 3
<i>SMC5</i>	AT5G15920	Zm00001d014500	Structural maintenance of chromosomes protein 5
<i>SMC6A/SMC6B</i>	AT5G07660/AT5G61460	Zm00001d020001	Structural maintenance of chromosomes protein 6A/B
<i>SMG7</i>	AT5G19400	Zm00001d005502 Zm00001d019920	Protein SMG7
<i>SPO11-2</i>	AT1G63990	Zm00001d049550	Meiotic recombination protein
<i>SRS2</i>	AT4G25120	Zm00001d006443	ATP-dependent DNA helicase SRS2-like protein
<i>SYN1</i>	AT5G05490	Zm00001d039133 Zm00001d039132	Sister chromatid cohesion 1 protein 1
<i>SYN3</i>	AT3G59550	Zm00001d024094	Sister chromatid cohesion 1 protein 3
<i>TOP3A</i>	AT5G63920	Zm00001d027801	DNA topoisomerase 3-alpha
<i>TPD1/TDL1</i>	AT4G24972/AT1G32583	Zm00001d023681	TPD1/ protein homolog 1
<i>VIP3</i>	AT4G29830	Zm00001d048691	WD repeat-containing protein
<i>XRCC2</i>	AT5G64520	Zm00001d042691	homolog of X-ray repair cross complementing 2
<i>XRI1</i>	AT5G48720	Zm00001d004036 Zm00001d025182 Zm00001d042357	XRI1
<i>ZIP4</i>	AT1G10970	Zm00001d036965	Zinc transporter 4, chloroplastic
<i>ZIP4/SPO22</i>	AT5G48390	Zm00001d042558	TPR repeat-containing protein
<i>ZYP1B/ZYP1B</i>	AT1G22260/AT1G22275	Zm00001d025575	Synaptonemal complex protein 2
	AT1G63770	Zm00001d031891	Peptidase M1 family protein
	AT1G36020	Zm00001d053059	DEAD/DEAH-box RNA helicase family protein
<i>PSS1</i>	AT3G63480	Zm00001d035091	ATP binding microtubule motor family protein
<i>CRC1/PCH2</i>	AT4G24710	Zm00001d025687	P-loop containing nucleoside triphosphate hydrolases superfamily protein

A



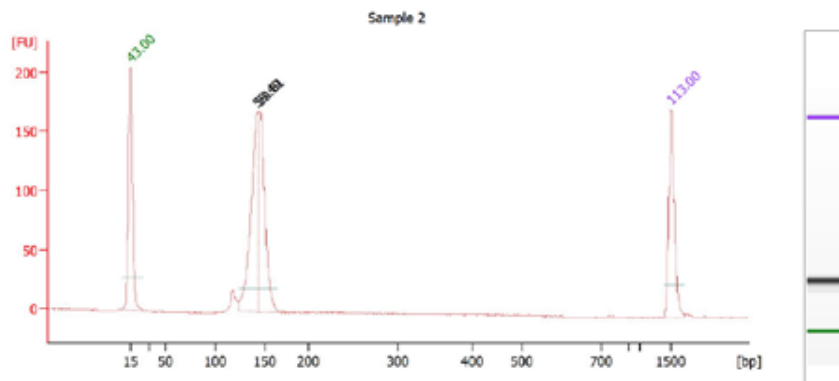
Overall Results for sample 1 : Sample 1

Number of peaks found: 1

Peak table for sample 1 : Sample 1

Peak	Size [bp]	Conc. [ng/μl]	Molarity [nmol/l]	Observations
1	15	4,20	424,2	Lower Marker
2	138	9,46	104,1	
3	1.500	2,10	2,1	Upper Marker

B



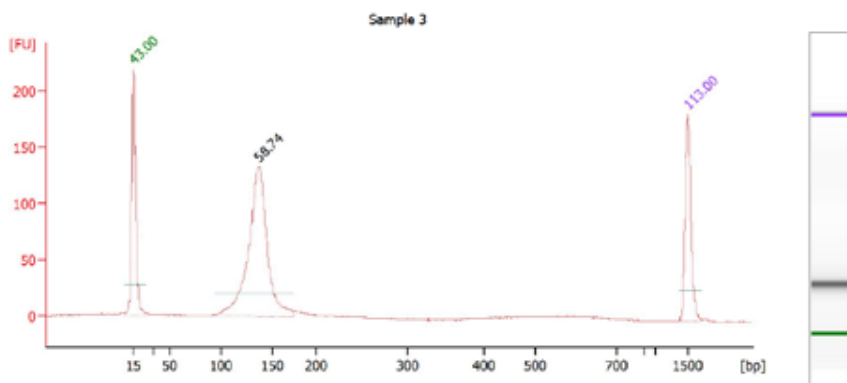
Overall Results for sample 2 : Sample 2

Number of peaks found: 2

Peak table for sample 2 : Sample 2

Peak	Size [bp]	Conc. [ng/μl]	Molarity [nmol/l]	Observations
1	15	4,20	424,2	Lower Marker
2	142	6,11	65,1	
3	145	5,02	52,5	
4	1.500	2,10	2,1	Upper Marker

C



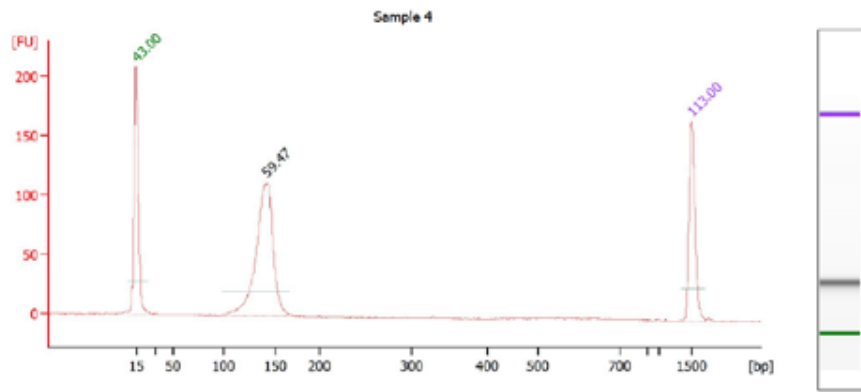
Overall Results for sample 3 : Sample 3

Number of peaks found: 1

Peak table for sample 3 : Sample 3

Peak	Size [bp]	Conc. [ng/μl]	Molarity [nmol/l]	Observations
1	15	4,20	424,2	Lower Marker
2	136	10,81	120,0	
3	1.500	2,10	2,1	Upper Marker

D



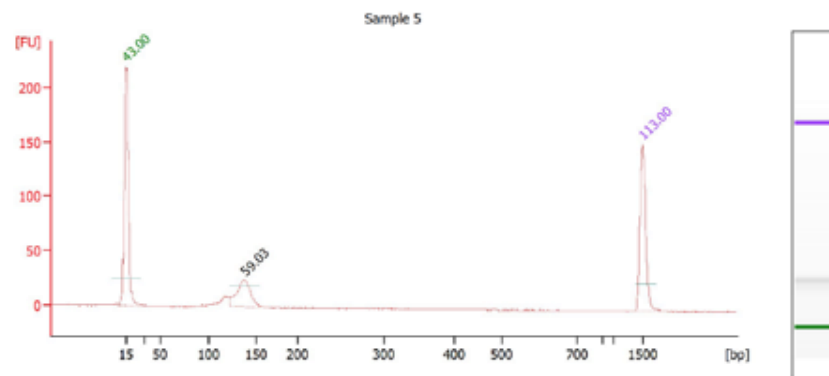
Overall Results for sample 4 : Sample 4

Number of peaks found: 1

Peak table for sample 4 : Sample 4

Peak	Size [bp]	Conc. [ng/μl]	Molarity [nmol/l]	Observations
1	15	4,20	424,2	Lower Marker
2	142	8,75	93,4	
3	1.500	2,10	2,1	Upper Marker

E



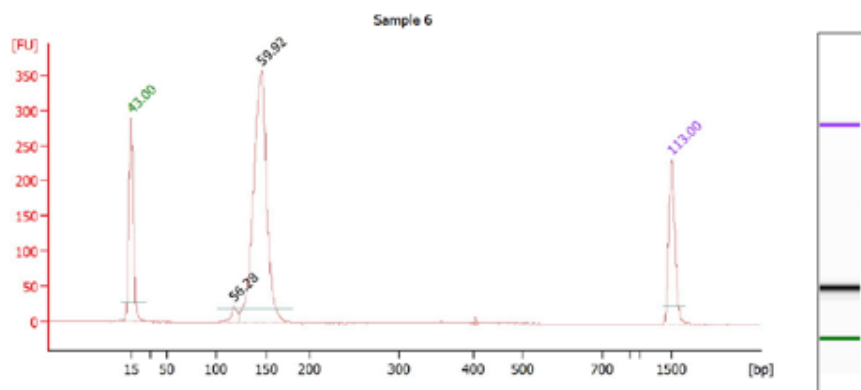
Overall Results for sample 5 : Sample 5

Number of peaks found: 1

Peak table for sample 5 : Sample 5

Peak	Size [bp]	Conc. [ng/μl]	Molarity [nmol/l]	Observations
1	15	4,20	424,2	Lower Marker
2	138	1,80	19,8	
3	1.500	2,10	2,1	Upper Marker

F



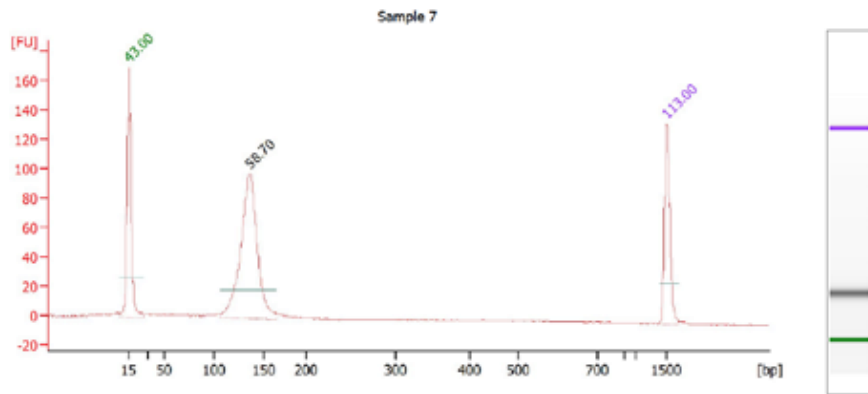
Overall Results for sample 6 : Sample 6

Number of peaks found: 2

Peak table for sample 6 : Sample 6

Peak	Size [bp]	Conc. [ng/μl]	Molarity [nmol/l]	Observations
1	15	4,20	424,2	Lower Marker
2	117	0,44	5,7	
3	146	15,02	156,3	
4	1.500	2,10	2,1	Upper Marker

G



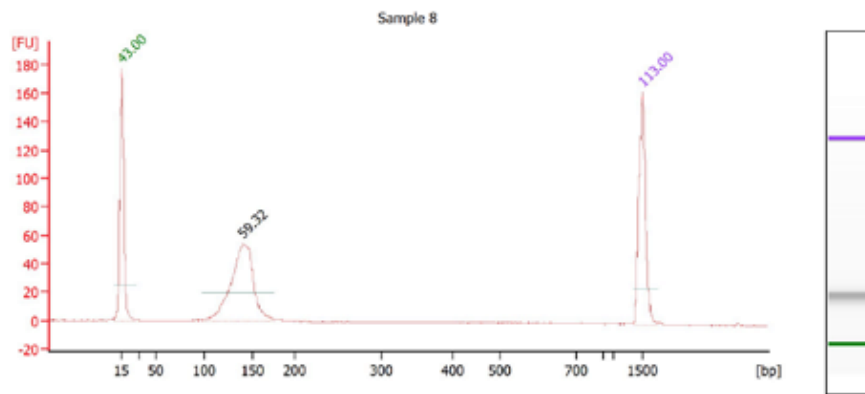
Overall Results for sample 7 : Sample 7

Number of peaks found: 1

Peak table for sample 7 : Sample 7

Peak	Size [bp]	Conc. [ng/ μ l]	Molarity [nmol/l]	Observations
1	15	4,20	424,2	Lower Marker
2	136	10,13	112,7	
3	1.500	2,10	2,1	Upper Marker

H



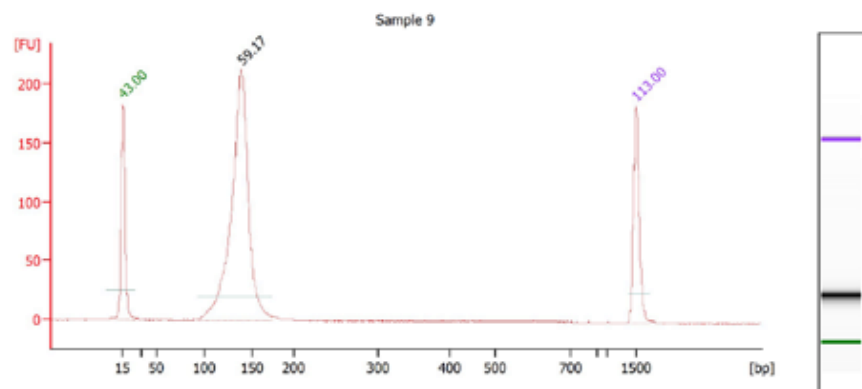
Overall Results for sample 8 : Sample 8

Number of peaks found: 1

Peak table for sample 8 : Sample 8

Peak	Size [bp]	Conc. [ng/ μ l]	Molarity [nmol/l]	Observations
1	15	4,20	424,2	Lower Marker
2	140	5,25	56,9	
3	1.500	2,10	2,1	Upper Marker

I



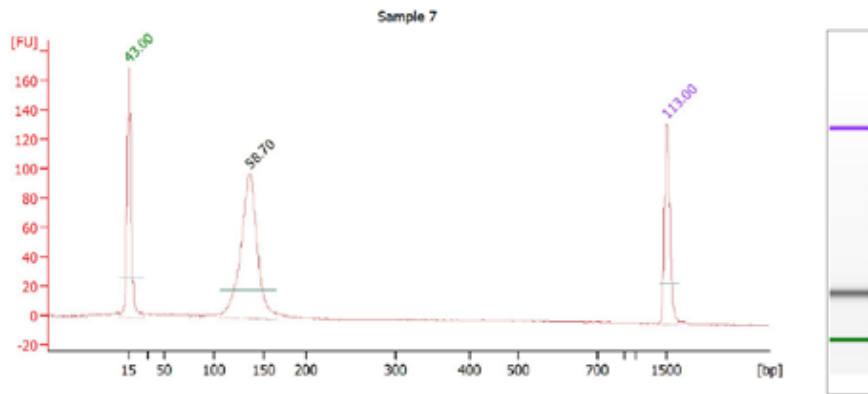
Overall Results for sample 9 : Sample 9

Number of peaks found: 1

Peak table for sample 9 : Sample 9

Peak	Size [bp]	Conc. [ng/ μ l]	Molarity [nmol/l]	Observations
1	15	4,20	424,2	Lower Marker
2	139	16,42	179,2	
3	1.500	2,10	2,1	Upper Marker

G



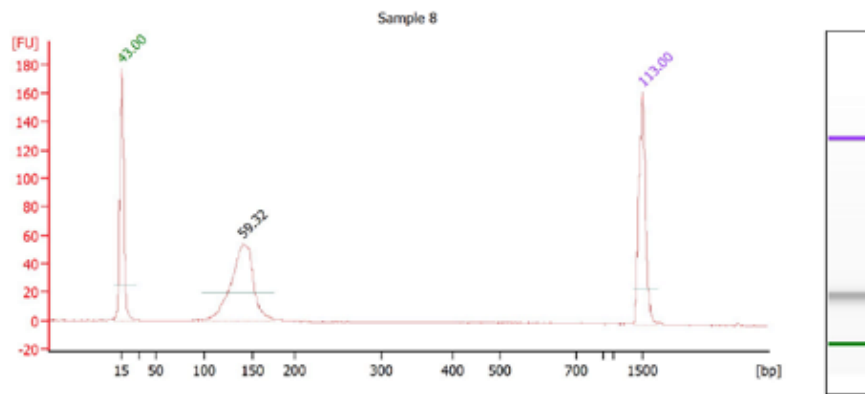
Overall Results for sample 7 : Sample 7

Number of peaks found: 1

Peak table for sample 7 : Sample 7

Peak	Size [bp]	Conc. [ng/ μ l]	Molarity [nmol/l]	Observations
1	15	4,20	424,2	Lower Marker
2	136	10,13	112,7	
3	1.500	2,10	2,1	Upper Marker

H



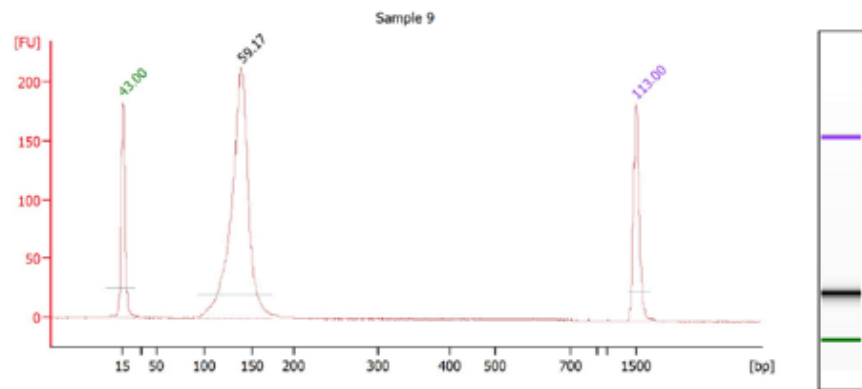
Overall Results for sample 8 : Sample 8

Number of peaks found: 1

Peak table for sample 8 : Sample 8

Peak	Size [bp]	Conc. [ng/ μ l]	Molarity [nmol/l]	Observations
1	15	4,20	424,2	Lower Marker
2	140	5,25	56,9	
3	1.500	2,10	2,1	Upper Marker

I



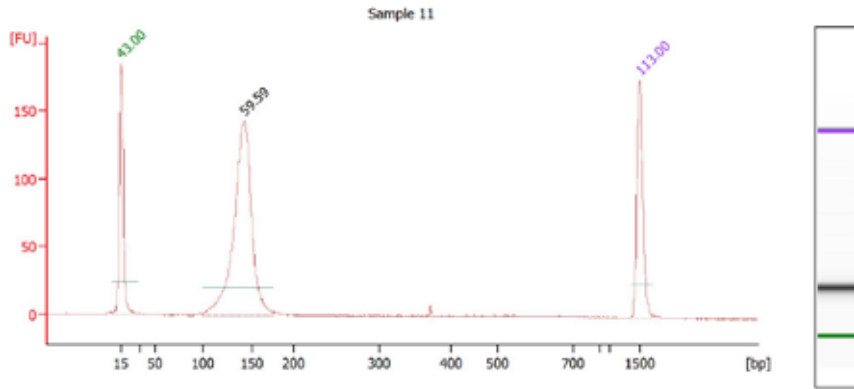
Overall Results for sample 9 : Sample 9

Number of peaks found: 1

Peak table for sample 9 : Sample 9

Peak	Size [bp]	Conc. [ng/ μ l]	Molarity [nmol/l]	Observations
1	15	4,20	424,2	Lower Marker
2	139	16,42	179,2	
3	1.500	2,10	2,1	Upper Marker

J



Overall Results for sample 11 : Sample 11

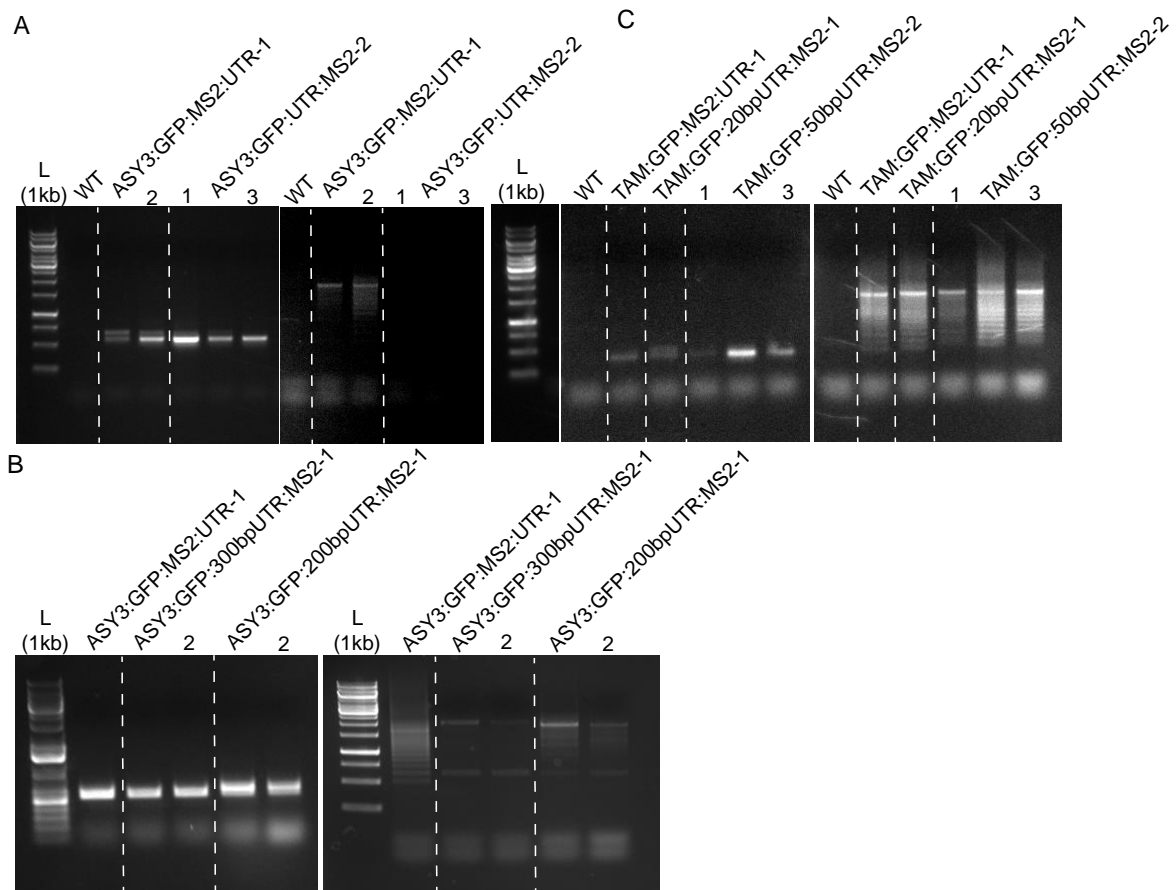
Number of peaks found: 1

Peak table for sample 11 : Sample 11

Peak	Size [bp]	Conc. [ng/ μ l]	Molarity [nmol/l]	Observations
1	15	4,20	424,2	Lower Marker
2	142	11,45	122,0	
3	1.500	2,10	2,1	Upper Marker

Supplemental Figure S2.9. Quality of the RNA and RPF libraries of the second anther replicate.

The quality of the prepared libraries was analysed using the BioAnalyzer 2100. The results for the RNA libraries and RPF libraries of the second replicate from anthers in (A,B) premeiosis, (C,D) leptotene, (E,F) zygotene, (G,H) pachytene and (I,J) meiosis II.



Supplemental Figure S2.10. Confirmation of MS2-loops in the ASY3 and TAM mRNA reporters.

Agarose gels stained with ethidium bromide after electrophoresis showing the amplification of a part of the gene-GFP fusion (left) and the MS2-loops in the mRNA (right). (A) The results of *ASY3:GFP:MS2:UTR* and *ASY3:GFP:UTR:MS2* plants. (B) The results of *ASY3:GFP:MS2:UTR*, *ASY3:GFP:300bpUTR:MS2* and *ASY3:GFP:200bpUTR:MS2* plants. (C) The results of *TAM:GFP:MS2:UTR*, *TAM:GFP:20bpUTR:MS2* and *TAM:GFP:50bpUTR:MS2*. Size ladder (L) 1kb DNA ladder Thermo Fisher Scientific.

REFERENCES

- Aleshkina, D., Iyyappan, R., Lin, C.J., Masek, T., Pospisek, M., and Susor, A. (2021). ncRNA BC1 influences translation in the oocyte. *RNA Biol*, 1-12.
- Alvarez, D., Voss, B., Maass, D., Wust, F., Schaub, P., Beyer, P., and Welsch, R. (2016). Carotenogenesis Is Regulated by 5'UTR-Mediated Translation of Phytoene Synthase Splice Variants. *Plant Physiol* 172, 2314-2326.
- Anderson, P., and Kedersha, N. (2002). Visibly stressed: the role of eIF2, TIA-1, and stress granules in protein translation. *Cell Stress Chaperones* 7, 213-221.
- Anderson, P., and Kedersha, N. (2008). Stress granules: the Tao of RNA triage. *Trends Biochem Sci* 33, 141-150.
- Anderson, T.R., Hawkins, E., and Jones, P.D. (2016). CO₂, the greenhouse effect and global warming: from the pioneering work of Arrhenius and Callendar to today's Earth System Models. *Endeavour* 40, 178-187.
- Arabidopsis Genome, I. (2000). Analysis of the genome sequence of the flowering plant *Arabidopsis thaliana*. *Nature* 408, 796-815.
- Armstrong, S.J., Caryl, A.P., Jones, G.H., and Franklin, F.C. (2002). Asy1, a protein required for meiotic chromosome synapsis, localizes to axis-associated chromatin in *Arabidopsis* and *Brassica*. *J Cell Sci* 115, 3645-3655.
- Armstrong, S.J., Franklin, F.C.H., and Jones, G.H. (2003). A meiotic time-course for *Arabidopsis thaliana*. *Sexual Plant Reproduction* 16, 141-149.
- Azumi, Y., Liu, D., Zhao, D., Li, W., Wang, G., Hu, Y., and Ma, H. (2002). Homolog interaction during meiotic prophase I in *Arabidopsis* requires the SOLO DANCERS gene encoding a novel cyclin-like protein. *EMBO J* 21, 3081-3095.
- Baker, C.C., Gim, B.S., and Fuller, M.T. (2015). Cell type-specific translational repression of Cyclin B during meiosis in males. *Development* 142, 3394-3402.
- Bannigan, A., Scheible, W.R., Lukowitz, W., Fagerstrom, C., Wadsworth, P., Somerville, C., and Baskin, T.I. (2007). A conserved role for kinesin-5 in plant mitosis. *J Cell Sci* 120, 2819-2827.
- Barchi, M., Mahadevaiah, S., Di Giacomo, M., Baudat, F., de Rooij, D.G., Burgoyne, P.S., Jasin, M., and Keeney, S. (2005). Surveillance of different recombination defects in mouse spermatocytes yields distinct responses despite elimination at an identical developmental stage. *Mol Cell Biol* 25, 7203-7215.
- Barrett, L.W., Fletcher, S., and Wilton, S.D. (2012). Regulation of eukaryotic gene expression by the untranslated gene regions and other non-coding elements. *Cell Mol Life Sci* 69, 3613-3634.
- Bennett, M.D., Smith, J.B., and Kemble, R. (1972). THE EFFECT OF TEMPERATURE ON MEIOSIS AND POLLEN DEVELOPMENT IN WHEAT AND RYE. *Canadian Journal of Genetics and Cytology* 14, 615-624.
- Berchowitz, L.E., Francis, K.E., Bey, A.L., and Copenhaver, G.P. (2007). The role of AtMUS81 in interference-insensitive crossovers in *A. thaliana*. *PLoS Genet* 3, e132.
- Berchowitz, L.E., Gajadhar, A.S., van Werven, F.J., De Rosa, A.A., Samoylova, M.L., Brar, G.A., Xu, Y., Xiao, C., Futcher, B., Weissman, J.S., *et al.* (2013). A developmentally regulated translational control pathway establishes the meiotic chromosome segregation pattern. *Genes Dev* 27, 2147-2163.
- Bertrand, E., Chartrand, P., Schaefer, M., Shenoy, S.M., Singer, R.H., and Long, R.M. (1998). Localization of ASH1 mRNA particles in living yeast. *Mol Cell* 2, 437-445.
- Besse, F., and Ephrussi, A. (2008). Translational control of localized mRNAs: restricting protein synthesis in space and time. *Nat Rev Mol Cell Biol* 9, 971-980.

-
- Bilgir, C., Dombeki, C.R., Chen, P.F., Villeneuve, A.M., and Nabeshima, K. (2013). Assembly of the Synaptonemal Complex Is a Highly Temperature-Sensitive Process That Is Supported by PGL-1 During *Caenorhabditis elegans* Meiosis. *G3 (Bethesda)* 3, 585-595.
- Bishop, D.K., Park, D., Xu, L., and Kleckner, N. (1992). DMC1: a meiosis-specific yeast homolog of *E. coli* recA required for recombination, synaptonemal complex formation, and cell cycle progression. *Cell* 69, 439-456.
- Boisvert, F.M., van Koningsbruggen, S., Navascues, J., and Lamond, A.I. (2007). The multifunctional nucleolus. *Nat Rev Mol Cell Biol* 8, 574-585.
- Bolanos-Villegas, P., De, K., Pradillo, M., Liu, D., and Makaroff, C.A. (2017). In Favor of Establishment: Regulation of Chromatid Cohesion in Plants. *Front Plant Sci* 8, 846.
- Bombliès, K., Higgins, J.D., and Yant, L. (2015). Meiosis evolves: adaptation to external and internal environments. *New Phytol* 208, 306-323.
- Bommert, P., Satoh-Nagasawa, N., Jackson, D., and Hirano, H.Y. (2005). Genetics and evolution of inflorescence and flower development in grasses. *Plant Cell Physiol* 46, 69-78.
- Borner, G.V., Kleckner, N., and Hunter, N. (2004). Crossover/noncrossover differentiation, synaptonemal complex formation, and regulatory surveillance at the leptotene/zygotene transition of meiosis. *Cell* 117, 29-45.
- Brar, G.A., Yassour, M., Friedman, N., Regev, A., Ingolia, N.T., and Weissman, J.S. (2012). High-resolution view of the yeast meiotic program revealed by ribosome profiling. *Science* 335, 552-557.
- Brown, S.D., Audouy, C., and Lorenz, A. (2020). Intragenic meiotic recombination in *Schizosaccharomyces pombe* is sensitive to environmental temperature changes. *Chromosome Res* 28, 195-207.
- Brown, S.D., Jarosinska, O.D., and Lorenz, A. (2018). Genetic interactions between the chromosome axis-associated protein Hop1 and homologous recombination determinants in *Schizosaccharomyces pombe*. *Curr Genet* 64, 1089-1104.
- Brownfield, L., and Kohler, C. (2011). Unreduced gamete formation in plants: mechanisms and prospects. *J Exp Bot* 62, 1659-1668.
- Brownfield, L., Yi, J., Jiang, H., Minina, E.A., Twell, D., and Kohler, C. (2015). Organelles maintain spindle position in plant meiosis. *Nat Commun* 6, 6492.
- Browning, K.S., and Bailey-Serres, J. (2015). Mechanism of cytoplasmic mRNA translation. *Arabidopsis Book* 13, e0176.
- Buchan, J.R., and Parker, R. (2009). Eukaryotic stress granules: the ins and outs of translation. *Mol Cell* 36, 932-941.
- Bulankova, P., Riehs-Kearnan, N., Nowack, M.K., Schnittger, A., and Riha, K. (2010). Meiotic progression in *Arabidopsis* is governed by complex regulatory interactions between SMG7, TDM1, and the meiosis I-specific cyclin TAM. *Plant Cell* 22, 3791-3803.
- Bush, M.S., Hutchins, A.P., Jones, A.M., Naldrett, M.J., Jarmolowski, A., Lloyd, C.W., and Doonan, J.H. (2009). Selective recruitment of proteins to 5' cap complexes during the growth cycle in *Arabidopsis*. *Plant J* 59, 400-412.
- About, S., Leask, M.P., Varghese, S., Yi, J., Peters, B., Conze, L.L., Kohler, C., and Brownfield, L. (2017). The meiotic regulator JASON utilizes alternative translation initiation sites to produce differentially localized forms. *J Exp Bot* 68, 4205-4217.
- Cai, X., Dong, F., Edelman, R.E., and Makaroff, C.A. (2003). The *Arabidopsis* SYN1 cohesin protein is required for sister chromatid arm cohesion and homologous chromosome pairing. *J Cell Sci* 116, 2999-3007.
- Cao, H., Li, X., Wang, Z., Ding, M., Sun, Y., Dong, F., Chen, F., Liu, L., Doughty, J., Li, Y., *et al.* (2015). Histone H2B Monoubiquitination Mediated by HISTONE MONOUBIQUITINATION1 and

HISTONE MONOUBIQUITINATION2 Is Involved in Anther Development by Regulating Tapetum Degradation-Related Genes in Rice. *Plant Physiol* 168, 1389-1405.

Capilla-Perez, L., Durand, S., Hurel, A., Lian, Q., Chambon, A., Taochy, C., Solier, V., Grelon, M., and Mercier, R. (2021). The synaptonemal complex imposes crossover interference and heterochiasmy in Arabidopsis. *Proc Natl Acad Sci U S A* 118.

Carlile, T.M., and Amon, A. (2008). Meiosis I is established through division-specific translational control of a cyclin. *Cell* 133, 280-291.

Carroll, A.J., Heazlewood, J.L., Ito, J., and Millar, A.H. (2008). Analysis of the Arabidopsis cytosolic ribosome proteome provides detailed insights into its components and their post-translational modification. *Mol Cell Proteomics* 7, 347-369.

Caryl, A.P., Armstrong, S.J., Jones, G.H., and Franklin, F.C. (2000). A homologue of the yeast HOP1 gene is inactivated in the Arabidopsis meiotic mutant *asy1*. *Chromosoma* 109, 62-71.

Caryl, A.P., Jones, G.H., and Franklin, F.C. (2003). Dissecting plant meiosis using Arabidopsis thaliana mutants. *J Exp Bot* 54, 25-38.

Cha, R.S., Weiner, B.M., Keeney, S., Dekker, J., and Kleckner, N. (2000). Progression of meiotic DNA replication is modulated by interchromosomal interaction proteins, negatively by Spo11p and positively by Rec8p. *Genes Dev* 14, 493-503.

Chen, C., Farmer, A.D., Langley, R.J., Mudge, J., Crow, J.A., May, G.D., Huntley, J., Smith, A.G., and Retzel, E.F. (2010). Meiosis-specific gene discovery in plants: RNA-Seq applied to isolated Arabidopsis male meiocytes. *BMC Plant Biol* 10, 280.

Chen, J., Tresenrider, A., Chia, M., McSwiggen, D.T., Spedale, G., Jorgensen, V., Liao, H., van Werven, F.J., and Unal, E. (2017). Kinetochores inactivation by expression of a repressive mRNA. *Elife* 6.

Chen, Z.S., Liu, X.F., Wang, D.H., Chen, R., Zhang, X.L., Xu, Z.H., and Bai, S.N. (2018). Transcription Factor OsTGA10 Is a Target of the MADS Protein OsMADS8 and Is Required for Tapetum Development. *Plant Physiol* 176, 819-835.

Cheng, Z., Otto, G.M., Powers, E.N., Keskin, A., Mertins, P., Carr, S.A., Jovanovic, M., and Brar, G.A. (2018). Pervasive, Coordinated Protein-Level Changes Driven by Transcript Isoform Switching during Meiosis. *Cell* 172, 910-923 e916.

Cheong, C.G., and Hall, T.M. (2006). Engineering RNA sequence specificity of Pumilio repeats. *Proc Natl Acad Sci U S A* 103, 13635-13639.

Chia, M., Tresenrider, A., Chen, J., Spedale, G., Jorgensen, V., Unal, E., and van Werven, F.J. (2017). Transcription of a 5' extended mRNA isoform directs dynamic chromatin changes and interference of a downstream promoter. *Elife* 6.

Chodasiewicz, M., Sokolowska, E.M., Nelson-Dittrich, A.C., Masiuk, A., Beltran, J.C.M., Nelson, A.D.L., and Skirycz, A. (2020). Identification and Characterization of the Heat-Induced Plastidial Stress Granules Reveal New Insight Into Arabidopsis Stress Response. *Front Plant Sci* 11, 595792.

Chotewutmontri, P., and Barkan, A. (2016). Dynamics of Chloroplast Translation during Chloroplast Differentiation in Maize. *PLoS Genet* 12, e1006106.

Chung, B.Y., Hardcastle, T.J., Jones, J.D., Irigoyen, N., Firth, A.E., Baulcombe, D.C., and Brierley, I. (2015). The use of duplex-specific nuclease in ribosome profiling and a user-friendly software package for Ribo-seq data analysis. *RNA* 21, 1731-1745.

Ciska, M., and Moreno Diaz de la Espina, S. (2013). NMCP/LINC proteins: putative lamin analogs in plants? *Plant Signal Behav* 8, e26669.

Clift, D., and Marston, A.L. (2011). The role of shugoshin in meiotic chromosome segregation. *Cytogenet Genome Res* 133, 234-242.

Clough, S.J., and Bent, A.F. (1998). Floral dip: a simplified method for Agrobacterium-mediated transformation of Arabidopsis thaliana. *Plant J* 16, 735-743.

-
- Collins, M. (2014). Long-term Climate Change: Projections, Commitments and Irreversibility Pages 1029 to 1076. In *Climate Change 2013 – The Physical Science Basis: Working Group I Contribution to the Fifth Assessment Report of the Intergovernmental Panel on Climate Change*, C. Intergovernmental Panel on Climate, ed. (Cambridge: Cambridge University Press), pp. 1029-1136.
- Couteau, F., Belzile, F., Horlow, C., Grandjean, O., Vezon, D., and Doutriaux, M.P. (1999). Random chromosome segregation without meiotic arrest in both male and female meiocytes of a *dmc1* mutant of *Arabidopsis*. *Plant Cell* 11, 1623-1634.
- Crichton, J.H., Read, D., and Adams, I.R. (2018). Defects in meiotic recombination delay progression through pachytene in *Tex19.1(-/-)* mouse spermatocytes. *Chromosoma* 127, 437-459.
- Crick, F. (1970). Central dogma of molecular biology. *Nature* 227, 561-563.
- d'Erfurth, I., Cromer, L., Jolivet, S., Girard, C., Horlow, C., Sun, Y., To, J.P., Berchowitz, L.E., Copenhaver, G.P., and Mercier, R. (2010). The cyclin-A *CYCA1;2/TAM* is required for the meiosis I to meiosis II transition and cooperates with *OSD1* for the prophase to first meiotic division transition. *PLoS Genet* 6, e1000989.
- de Rooij, D.G., and de Boer, P. (2003). Specific arrests of spermatogenesis in genetically modified and mutant mice. *Cytogenet Genome Res* 103, 267-276.
- De Storme, N., and Geelen, D. (2013a). Cytokinesis in plant male meiosis. *Plant Signal Behav* 8, e23394.
- De Storme, N., and Geelen, D. (2013b). Sexual polyploidization in plants--cytological mechanisms and molecular regulation. *New Phytol* 198, 670-684.
- De Storme, N., and Geelen, D. (2020). High temperatures alter cross-over distribution and induce male meiotic restitution in *Arabidopsis thaliana*. *Commun Biol* 3, 187.
- delCardayre, S.B., and Raines, R.T. (1995). The extent to which ribonucleases cleave ribonucleic acid. *Anal Biochem* 225, 176-178.
- Dissmeyer, N., Nowack, M.K., Pusch, S., Stals, H., Inze, D., Grini, P.E., and Schnittger, A. (2007). T-loop phosphorylation of *Arabidopsis* *CDKA;1* is required for its function and can be partially substituted by an aspartate residue. *Plant Cell* 19, 972-985.
- Dowrick, G.J. (1957). The influence of temperature on meiosis. *Heredity* 11, 37-49.
- Draeger, T., and Moore, G. (2017). Short periods of high temperature during meiosis prevent normal meiotic progression and reduce grain number in hexaploid wheat (*Triticum aestivum* L.). *Theor Appl Genet* 130, 1785-1800.
- Dubiel, M., De Coninck, T., Osterne, V.J.S., Verbeke, I., Van Damme, D., Smaghe, G., and Van Damme, E.J.M. (2020). The *ArathEULS3* Lectin Ends up in Stress Granules and Can Follow an Unconventional Route for Secretion. *Int J Mol Sci* 21.
- Dukowic-Schulze, S., Harris, A., Li, J., Sundararajan, A., Mudge, J., Retzel, E.F., Pawlowski, W.P., and Chen, C. (2014a). Comparative transcriptomics of early meiosis in *Arabidopsis* and maize. *J Genet Genomics* 41, 139-152.
- Dukowic-Schulze, S., Sundararajan, A., Mudge, J., Ramaraj, T., Farmer, A.D., Wang, M., Sun, Q., Pillardy, J., Kianian, S., Retzel, E.F., *et al.* (2014b). The transcriptome landscape of early maize meiosis. *BMC Plant Biol* 14, 118.
- Dukowic-Schulze, S., Sundararajan, A., Ramaraj, T., Kianian, S., Pawlowski, W.P., Mudge, J., and Chen, C. (2016). Novel Meiotic miRNAs and Indications for a Role of PhasiRNAs in Meiosis. *Front Plant Sci* 7, 762.
- Duncan, C.D., and Mata, J. (2014). The translational landscape of fission-yeast meiosis and sporulation. *Nat Struct Mol Biol* 21, 641-647.
- Ferdous, M., Higgins, J.D., Osman, K., Lambing, C., Roitinger, E., Mechtler, K., Armstrong, S.J., Perry, R., Pradillo, M., Cunado, N., *et al.* (2012). Inter-homolog crossing-over and synapsis in

Arabidopsis meiosis are dependent on the chromosome axis protein AtASY3. *PLoS Genet* 8, e1002507.

Fiserova, J., and Goldberg, Martin W. (2010). Relationships at the nuclear envelope: lamins and nuclear pore complexes in animals and plants. *Biochemical Society Transactions* 38, 829-831.

France, M.G., Enderle, J., Rohrig, S., Puchta, H., Franklin, F.C.H., and Higgins, J.D. (2021). ZYP1 is required for obligate cross-over formation and cross-over interference in Arabidopsis. *Proc Natl Acad Sci U S A* 118.

Franklin, A.E., McElver, J., Sunjevaric, I., Rothstein, R., Bowen, B., and Cande, W.Z. (1999). Three-dimensional microscopy of the Rad51 recombination protein during meiotic prophase. *Plant Cell* 11, 809-824.

Garcia, J.F., and Parker, R. (2015). MS2 coat proteins bound to yeast mRNAs block 5' to 3' degradation and trap mRNA decay products: implications for the localization of mRNAs by MS2-MCP system. *RNA* 21, 1393-1395.

Garcia, J.F., and Parker, R. (2016). Ubiquitous accumulation of 3' mRNA decay fragments in *Saccharomyces cerevisiae* mRNAs with chromosomally integrated MS2 arrays. *RNA* 22, 657-659.

Garcia, V., Bruchet, H., Comescaisse, D., Granier, F., Bouchez, D., and Tissier, A. (2003). AtATM is essential for meiosis and the somatic response to DNA damage in plants. *Plant Cell* 15, 119-132.

Ge, F., Qu, J., Liu, P., Pan, L., Zou, C., Yuan, G., Yang, C., Gao, S., Pan, G., Huang, J., *et al.* (2021). Genome assembly of the maize inbred line A188 provides a new reference genome for functional genomics. *bioRxiv*, 2021.2003.2015.435372.

Gerashchenko, M.V., and Gladyshev, V.N. (2017). Ribonuclease selection for ribosome profiling. *Nucleic Acids Res* 45, e6.

Giavalisco, P., Wilson, D., Kreitler, T., Lehrach, H., Klose, J., Gobom, J., and Fucini, P. (2005). High heterogeneity within the ribosomal proteins of the Arabidopsis thaliana 80S ribosome. *Plant Mol Biol* 57, 577-591.

Glaub, A., Huptas, C., Neuhaus, K., and Ardern, Z. (2020). Recommendations for bacterial ribosome profiling experiments based on bioinformatic evaluation of published data. *J Biol Chem* 295, 8999-9011.

Goldberg, R.B., Beals, T.P., and Sanders, P.M. (1993). Anther development: basic principles and practical applications. *Plant Cell* 5, 1217-1229.

Gorbsky, G.J. (2015). The spindle checkpoint and chromosome segregation in meiosis. *FEBS J* 282, 2471-2487.

Grelon, M., Vezon, D., Gendrot, G., and Pelletier, G. (2001). AtSPO11-1 is necessary for efficient meiotic recombination in plants. *EMBO J* 20, 589-600.

Guerrero-Gonzalez, M.L., Ortega-Amaro, M.A., Juarez-Montiel, M., and Jimenez-Bremont, J.F. (2016). Arabidopsis Polyamine oxidase-2 uORF is required for downstream translational regulation. *Plant Physiol Biochem* 108, 381-390.

Haimovich, G., Zabezhinsky, D., Haas, B., Slobodin, B., Purushothaman, P., Fan, L., Levin, J.Z., Nusbaum, C., and Gerst, J.E. (2016). Use of the MS2 aptamer and coat protein for RNA localization in yeast: A response to "MS2 coat proteins bound to yeast mRNAs block 5' to 3' degradation and trap mRNA decay products: implications for the localization of mRNAs by MS2-MCP system". *RNA* 22, 660-666.

Halstead, J.M., Lionnet, T., Wilbertz, J.H., Wippich, F., Ephrussi, A., Singer, R.H., and Chao, J.A. (2015). Translation. An RNA biosensor for imaging the first round of translation from single cells to living animals. *Science* 347, 1367-1671.

Hamada, S., Ishiyama, K., Choi, S.B., Wang, C., Singh, S., Kawai, N., Franceschi, V.R., and Okita, T.W. (2003). The transport of prolamine RNAs to prolamine protein bodies in living rice endosperm cells. *Plant Cell* 15, 2253-2264.

-
- Hamada, T., Yako, M., Minegishi, M., Sato, M., Kamei, Y., Yanagawa, Y., Toyooka, K., Watanabe, Y., and Hara-Nishimura, I. (2018). Stress granule formation is induced by a threshold temperature rather than a temperature difference in *Arabidopsis*. *J Cell Sci* 131.
- Han, Y.H., Moon, H.J., You, B.R., and Park, W.H. (2009). The effect of MG132, a proteasome inhibitor on HeLa cells in relation to cell growth, reactive oxygen species and GSH. *Oncol Rep* 22, 215-221.
- Harrison, C.J., Alvey, E., and Henderson, I.R. (2010). Meiosis in flowering plants and other green organisms. *J Exp Bot* 61, 2863-2875.
- Hartung, F., Wurz-Wildersinn, R., Fuchs, J., Schubert, I., Suer, S., and Puchta, H. (2007). The catalytically active tyrosine residues of both SPO11-1 and SPO11-2 are required for meiotic double-strand break induction in *Arabidopsis*. *Plant Cell* 19, 3090-3099.
- Hatfield, J.L., and Prueger, J.H. (2015). Temperature extremes: Effect on plant growth and development. *Weather and Climate Extremes* 10, 4-10.
- Hedhly, A., Nestorova, A., Herrmann, A., and Grossniklaus, U. (2020). Acute heat stress during stamen development affects both the germline and sporophytic lineages in *Arabidopsis thaliana* (L.) Heynh. *Environmental and Experimental Botany* 173, 103992.
- Heinrich, S., Sidler, C.L., Azzalin, C.M., and Weis, K. (2017). Stem-loop RNA labeling can affect nuclear and cytoplasmic mRNA processing. *RNA* 23, 134-141.
- Henderson, S.A. (1988). Four effects of elevated temperature on chiasma formation in the locust *Schistocerca gregaria*. *Heredity* 60, 387-401.
- Higgins, J.D., Armstrong, S.J., Franklin, F.C., and Jones, G.H. (2004). The *Arabidopsis* MutS homolog AtMSH4 functions at an early step in recombination: evidence for two classes of recombination in *Arabidopsis*. *Genes Dev* 18, 2557-2570.
- Higgins, J.D., Perry, R.M., Barakate, A., Ramsay, L., Waugh, R., Halpin, C., Armstrong, S.J., and Franklin, F.C. (2012). Spatiotemporal asymmetry of the meiotic program underlies the predominantly distal distribution of meiotic crossovers in barley. *Plant Cell* 24, 4096-4109.
- Higgins, J.D., Sanchez-Moran, E., Armstrong, S.J., Jones, G.H., and Franklin, F.C. (2005). The *Arabidopsis* synaptonemal complex protein ZYP1 is required for chromosome synapsis and normal fidelity of crossing over. *Genes Dev* 19, 2488-2500.
- Hillers, K.J., Jantsch, V., Martinez-Perez, E., and Yanowitz, J.L. (2017). Meiosis. *WormBook* 2017, 1-43.
- Hummel, M., Cordewener, J.H., de Groot, J.C., Smeekens, S., America, A.H., and Hanson, J. (2012). Dynamic protein composition of *Arabidopsis thaliana* cytosolic ribosomes in response to sucrose feeding as revealed by label free MSE proteomics. *Proteomics* 12, 1024-1038.
- Igea, A., and Mendez, R. (2010). Meiosis requires a translational positive loop where CPEB1 ensues its replacement by CPEB4. *EMBO J* 29, 2182-2193.
- Ingolia, N.T., Ghaemmaghami, S., Newman, J.R., and Weissman, J.S. (2009). Genome-wide analysis in vivo of translation with nucleotide resolution using ribosome profiling. *Science* 324, 218-223.
- Interthal, H., and Heyer, W.D. (2000). MUS81 encodes a novel helix-hairpin-helix protein involved in the response to UV- and methylation-induced DNA damage in *Saccharomyces cerevisiae*. *Mol Gen Genet* 263, 812-827.
- Ishiguro, K.I. (2019). The cohesin complex in mammalian meiosis. *Genes Cells* 24, 6-30.
- Jachymczyk, W.J., von Borstel, R.C., Mowat, M.R., and Hastings, P.J. (1981). Repair of interstrand cross-links in DNA of *Saccharomyces cerevisiae* requires two systems for DNA repair: the RAD3 system and the RAD51 system. *Mol Gen Genet* 182, 196-205.
- Jackson, N., Sanchez-Moran, E., Buckling, E., Armstrong, S.J., Jones, G.H., and Franklin, F.C. (2006). Reduced meiotic crossovers and delayed prophase I progression in AtMLH3-deficient *Arabidopsis*. *EMBO J* 25, 1315-1323.

-
- Jha, A.K., Wang, Y., Hercyk, B.S., Shin, H.S., Chen, R., and Yang, M. (2014). The role for CYCLIN A1;2/TARDY ASYNCHRONOUS MEIOSIS in differentiated cells in Arabidopsis. *Plant Mol Biol* 85, 81-94.
- Ji, C., Li, H., Chen, L., Xie, M., Wang, F., Chen, Y., and Liu, Y.G. (2013). A novel rice bHLH transcription factor, DTD, acts coordinately with TDR in controlling tapetum function and pollen development. *Mol Plant* 6, 1715-1718.
- Jia, L., Mao, Y., Ji, Q., Dersh, D., Yewdell, J.W., and Qian, S.B. (2020). Decoding mRNA translatability and stability from the 5' UTR. *Nat Struct Mol Biol* 27, 814-821.
- Jiao, K., Bullard, S.A., Salem, L., and Malone, R.E. (1999). Coordination of the initiation of recombination and the reductional division in meiosis in *Saccharomyces cerevisiae*. *Genetics* 152, 117-128.
- Jin, L., Zhang, K., Sternglanz, R., and Neiman, A.M. (2017). Predicted RNA Binding Proteins Pes4 and Mip6 Regulate mRNA Levels, Translation, and Localization during Sporulation in Budding Yeast. *Mol Cell Biol* 37.
- Jin, L., Zhang, K., Xu, Y., Sternglanz, R., and Neiman, A.M. (2015). Sequestration of mRNAs Modulates the Timing of Translation during Meiosis in Budding Yeast. *Mol Cell Biol* 35, 3448-3458.
- Jones, G.H., and Franklin, F.C.H. (2008). Meiosis in *Arabidopsis thaliana*: Recombination, Chromosome Organization and Meiotic Progression. In *Recombination and Meiosis: Crossing-Over and Disjunction*, R. Egel, and D.-H. Lankenau, eds. (Berlin, Heidelberg: Springer Berlin Heidelberg), pp. 279-306.
- Kamalay, J.C., and Goldberg, R.B. (1980). Regulation of structural gene expression in tobacco. *Cell* 19, 935-946.
- Kaur, H., De Muyt, A., and Lichten, M. (2015). Top3-Rmi1 DNA single-strand decatenase is integral to the formation and resolution of meiotic recombination intermediates. *Mol Cell* 57, 583-594.
- Kaur, H., Gn, K., and Lichten, M. (2019). Unresolved Recombination Intermediates Cause a RAD9-Dependent Cell Cycle Arrest in *Saccharomyces cerevisiae*. *Genetics* 213, 805-818.
- Keeney, S., Giroux, C.N., and Kleckner, N. (1997). Meiosis-specific DNA double-strand breaks are catalyzed by Spo11, a member of a widely conserved protein family. *Cell* 88, 375-384.
- Kim, B., Cooke, H.J., and Rhee, K. (2012). DAZL is essential for stress granule formation implicated in germ cell survival upon heat stress. *Development* 139, 568-578.
- King, H.A., and Gerber, A.P. (2016). Translatome profiling: methods for genome-scale analysis of mRNA translation. *Brief Funct Genomics* 15, 22-31.
- Klapholz, S., Waddell, C.S., and Esposito, R.E. (1985). The role of the SPO11 gene in meiotic recombination in yeast. *Genetics* 110, 187-216.
- Komaki, S., and Schnittger, A. (2017). The Spindle Assembly Checkpoint in Arabidopsis Is Rapidly Shut Off during Severe Stress. *Dev Cell* 43, 172-185 e175.
- Kosmacz, M., Gorka, M., Schmidt, S., Luzarowski, M., Moreno, J.C., Szlachetko, J., Leniak, E., Sokolowska, E.M., Sofroni, K., Schnittger, A., *et al.* (2019). Protein and metabolite composition of Arabidopsis stress granules. *New Phytol* 222, 1420-1433.
- Ku, S., Yoon, H., Suh, H.S., and Chung, Y.Y. (2003). Male-sterility of thermosensitive genic male-sterile rice is associated with premature programmed cell death of the tapetum. *Planta* 217, 559-565.
- Kukal, M.S., and Irmak, S. (2018). Climate-Driven Crop Yield and Yield Variability and Climate Change Impacts on the U.S. Great Plains Agricultural Production. *Sci Rep* 8, 3450.
- Kurzbauer, M.T., Janisiw, M.P., Paulin, L.F., Prusen Mota, I., Tomanov, K., Krsicka, O., Haeseler, A.V., Schubert, V., and Schlogelhofer, P. (2021). ATM controls meiotic DNA double-strand break formation and recombination and affects synaptonemal complex organization in plants. *Plant Cell*.

-
- Kurzbauer, M.T., Uanschou, C., Chen, D., and Schlogelhofer, P. (2012). The recombinases DMC1 and RAD51 are functionally and spatially separated during meiosis in Arabidopsis. *Plant Cell* 24, 2058-2070.
- Lamb, B.C. (1969). Related and unrelated changes in conversion and recombination frequencies with temperature in *Sordaria fimicola*, and their relevance to hybrid-DNA models of recombination. *Genetics* 62, 67-78.
- Lambing, C., Osman, K., Nuntasontorn, K., West, A., Higgins, J.D., Copenhaver, G.P., Yang, J., Armstrong, S.J., Mechtler, K., Roitinger, E., *et al.* (2015). Arabidopsis PCH2 Mediates Meiotic Chromosome Remodeling and Maturation of Crossovers. *PLoS Genet* 11, e1005372.
- Lange, J., Pan, J., Cole, F., Thelen, M.P., Jasin, M., and Keeney, S. (2011). ATM controls meiotic double-strand-break formation. *Nature* 479, 237-240.
- Larson, D.R., Zenklusen, D., Wu, B., Chao, J.A., and Singer, R.H. (2011). Real-time observation of transcription initiation and elongation on an endogenous yeast gene. *Science* 332, 475-478.
- Laudencia-Chingcuanco, D., and Hake, S. (2002). The indeterminate floral apex1 gene regulates meristem determinacy and identity in the maize inflorescence. *Development* 129, 2629-2638.
- Lee, D.H., Kao, Y.H., Ku, J.C., Lin, C.Y., Meeley, R., Jan, Y.S., and Wang, C.J. (2015). The Axial Element Protein DESYNAPTIC2 Mediates Meiotic Double-Strand Break Formation and Synaptonemal Complex Assembly in Maize. *Plant Cell* 27, 2516-2529.
- Lee, Y.J., and Liu, B. (2019). Microtubule nucleation for the assembly of acentrosomal microtubule arrays in plant cells. *New Phytol* 222, 1705-1718.
- Lei, L., Shi, J., Chen, J., Zhang, M., Sun, S., Xie, S., Li, X., Zeng, B., Peng, L., Hauck, A., *et al.* (2015). Ribosome profiling reveals dynamic translational landscape in maize seedlings under drought stress. *Plant J* 84, 1206-1218.
- Lei, X., and Liu, B. (2019). Tapetum-Dependent Male Meiosis Progression in Plants: Increasing Evidence Emerges. *Front Plant Sci* 10, 1667.
- Lei, X., Ning, Y., Eid Elesawi, I., Yang, K., Chen, C., Wang, C., and Liu, B. (2020). Heat stress interferes with chromosome segregation and cytokinesis during male meiosis in *Arabidopsis thaliana*. *Plant Signal Behav* 15, 1746985.
- Li, H., Zeng, X., Liu, Z.Q., Meng, Q.T., Yuan, M., and Mao, T.L. (2009a). Arabidopsis microtubule-associated protein AtMAP65-2 acts as a microtubule stabilizer. *Plant Mol Biol* 69, 313-324.
- Li, N., Zhang, D.S., Liu, H.S., Yin, C.S., Li, X.X., Liang, W.Q., Yuan, Z., Xu, B., Chu, H.W., Wang, J., *et al.* (2006). The rice tapetum degeneration retardation gene is required for tapetum degradation and anther development. *Plant Cell* 18, 2999-3014.
- Li, W., Chen, C., Markmann-Mulisch, U., Timofejeva, L., Schmelzer, E., Ma, H., and Reiss, B. (2004). The Arabidopsis AtRAD51 gene is dispensable for vegetative development but required for meiosis. *Proc Natl Acad Sci U S A* 101, 10596-10601.
- Li, X.C., Barringer, B.C., and Barbash, D.A. (2009b). The pachytene checkpoint and its relationship to evolutionary patterns of polyploidization and hybrid sterility. *Heredity (Edinb)* 102, 24-30.
- Libeau, P., Durandet, M., Granier, F., Marquis, C., Berthome, R., Renou, J.P., Taconnat-Soubirou, L., and Horlow, C. (2011). Gene expression profiling of Arabidopsis meiocytes. *Plant Biol (Stuttg)* 13, 784-793.
- Lin, G., He, C., Zheng, J., Koo, D.H., Le, H., Zheng, H., Tamang, T.M., Lin, J., Liu, Y., Zhao, M., *et al.* (2021). Chromosome-level genome assembly of a regenerable maize inbred line A188. *Genome Biol* 22, 175.
- Liu, B., De Storme, N., and Geelen, D. (2017). Cold interferes with male meiotic cytokinesis in *Arabidopsis thaliana* independently of the AHK2/3-AHP2/3/5 cytokinin signaling module. *Cell Biol Int* 41, 879-889.

-
- Liu, H., Yin, J., Xiao, M., Gao, C., Mason, A.S., Zhao, Z., Liu, Y., Li, J., and Fu, D. (2012). Characterization and evolution of 5' and 3' untranslated regions in eukaryotes. *Gene* 507, 106-111.
- Liu, M.J., Wu, S.H., Wu, J.F., Lin, W.D., Wu, Y.C., Tsai, T.Y., Tsai, H.L., and Wu, S.H. (2013). Translational landscape of photomorphogenic Arabidopsis. *Plant Cell* 25, 3699-3710.
- Lloyd, A., Morgan, C., FC, H.F., and Bomblies, K. (2018). Plasticity of Meiotic Recombination Rates in Response to Temperature in Arabidopsis. *Genetics* 208, 1409-1420.
- Loidl, J. (1989). Effects of elevated temperature on meiotic chromosome synapsis in *Allium ursinum*. *Chromosoma* 97, 449-458.
- Long, J., Walker, J., She, W., Aldridge, B., Gao, H., Deans, S., Vickers, M., and Feng, X. (2021). Nurse cell--derived small RNAs define paternal epigenetic inheritance in Arabidopsis. *Science* 373.
- Lukoszek, R., Feist, P., and Ignatova, Z. (2016). Insights into the adaptive response of Arabidopsis thaliana to prolonged thermal stress by ribosomal profiling and RNA-Seq. *BMC Plant Biol* 16, 221.
- Luo, S., and Tong, L. (2018). Structural biology of the separase-securin complex with crucial roles in chromosome segregation. *Curr Opin Struct Biol* 49, 114-122.
- Luong, X.G., Daldello, E.M., Rajkovic, G., Yang, C.R., and Conti, M. (2020). Genome-wide analysis reveals a switch in the translational program upon oocyte meiotic resumption. *Nucleic Acids Res* 48, 3257-3276.
- Lydall, D., Nikolsky, Y., Bishop, D.K., and Weinert, T. (1996). A meiotic recombination checkpoint controlled by mitotic checkpoint genes. *Nature* 383, 840-843.
- Ma, H. (2006). A molecular portrait of Arabidopsis meiosis. *Arabidopsis Book* 4, e0095.
- Makrantonis, V., and Marston, A.L. (2018). Cohesin and chromosome segregation. *Curr Biol* 28, R688-R693.
- Marston, A.L., and Wassmann, K. (2017). Multiple Duties for Spindle Assembly Checkpoint Kinases in Meiosis. *Front Cell Dev Biol* 5, 109.
- McGlinchy, N.J., and Ingolia, N.T. (2017). Transcriptome-wide measurement of translation by ribosome profiling. *Methods* 126, 112-129.
- Mendenhall, M.D., and Hodge, A.E. (1998). Regulation of Cdc28 cyclin-dependent protein kinase activity during the cell cycle of the yeast *Saccharomyces cerevisiae*. *Microbiol Mol Biol Rev* 62, 1191-1243.
- Mercier, R., Mezard, C., Jenczewski, E., Macaisne, N., and Grelon, M. (2015). The molecular biology of meiosis in plants. *Annu Rev Plant Biol* 66, 297-327.
- Mili, S., and Macara, I.G. (2009). RNA localization and polarity: from A(PC) to Z(BP). *Trends Cell Biol* 19, 156-164.
- Modliszewski, J.L., Wang, H., Albright, A.R., Lewis, S.M., Bennett, A.R., Huang, J., Ma, H., Wang, Y., and Copenhaver, G.P. (2018). Elevated temperature increases meiotic crossover frequency via the interfering (Type I) pathway in Arabidopsis thaliana. *PLoS Genet* 14, e1007384.
- Morgan, C.H., Zhang, H., and Bomblies, K. (2017). Are the effects of elevated temperature on meiotic recombination and thermotolerance linked via the axis and synaptonemal complex? *Philos Trans R Soc Lond B Biol Sci* 372.
- Mustroph, A., Juntawong, P., and Bailey-Serres, J. (2009a). Isolation of plant polysomal mRNA by differential centrifugation and ribosome immunopurification methods. *Methods Mol Biol* 553, 109-126.
- Mustroph, A., Zanetti, M.E., Jang, C.J., Holtan, H.E., Repetti, P.P., Galbraith, D.W., Girke, T., and Bailey-Serres, J. (2009b). Profiling translomes of discrete cell populations resolves altered cellular priorities during hypoxia in Arabidopsis. *Proc Natl Acad Sci U S A* 106, 18843-18848.
- Muyt, A., Mercier, R., Mezard, C., and Grelon, M. (2009). Meiotic recombination and crossovers in plants. *Genome Dyn* 5, 14-25.

-
- Nasmyth, K., and Haering, C.H. (2009). Cohesin: its roles and mechanisms. *Annu Rev Genet* 43, 525-558.
- Nebel, B.R., and Hackett, E.M. (1961). Synaptonemal complexes (cores) in primary spermatocytes of mouse under elevated temperature. *Nature* 190, 467-468.
- Nelms, B., and Walbot, V. (2019). Defining the developmental program leading to meiosis in maize. *Science* 364, 52-56.
- Ono, S., Liu, H., Tsuda, K., Fukai, E., Tanaka, K., Sasaki, T., and Nonomura, K.I. (2018). EAT1 transcription factor, a non-cell-autonomous regulator of pollen production, activates meiotic small RNA biogenesis in rice anther tapetum. *PLoS Genet* 14, e1007238.
- Osman, K., Sanchez-Moran, E., Higgins, J.D., Jones, G.H., and Franklin, F.C. (2006). Chromosome synapsis in Arabidopsis: analysis of the transverse filament protein ZYP1 reveals novel functions for the synaptonemal complex. *Chromosoma* 115, 212-219.
- Ozawa, T., Natori, Y., Sato, M., and Umezawa, Y. (2007). Imaging dynamics of endogenous mitochondrial RNA in single living cells. *Nat Methods* 4, 413-419.
- Pacheco, S., Marcet-Ortega, M., Lange, J., Jasin, M., Keeney, S., and Roig, I. (2015). The ATM signaling cascade promotes recombination-dependent pachytene arrest in mouse spermatocytes. *PLoS Genet* 11, e1005017.
- Pacini, E., Franchi, G.G., and Hesse, M. (1985). The tapetum: Its form, function, and possible phylogeny in Embryophyta. *Plant Systematics and Evolution* 149, 155-185.
- Pao, W.K., and Li, H.W. (1948). Desynapsis and other abnormalities induced by high temperature. *J Genet* 48, 297-310.
- Pecrix, Y., Rallo, G., Folzer, H., Cigna, M., Gudín, S., and Le Bris, M. (2011). Polyploidization mechanisms: temperature environment can induce diploid gamete formation in *Rosa* sp. *J Exp Bot* 62, 3587-3597.
- Pendle, A.F., Clark, G.P., Boon, R., Lewandowska, D., Lam, Y.W., Andersen, J., Mann, M., Lamond, A.I., Brown, J.W., and Shaw, P.J. (2005). Proteomic analysis of the Arabidopsis nucleolus suggests novel nucleolar functions. *Mol Biol Cell* 16, 260-269.
- Penedos, A., Johnson, A.L., Strong, E., Goldman, A.S., Carballo, J.A., and Cha, R.S. (2015). Essential and Checkpoint Functions of Budding Yeast ATM and ATR during Meiotic Prophase Are Facilitated by Differential Phosphorylation of a Meiotic Adaptor Protein, Hop1. *PLoS One* 10, e0134297.
- Peterson, R., Slovin, J.P., and Chen, C. (2010). A simplified method for differential staining of aborted and non-aborted pollen grains. *International Journal of Plant Biology* 1, e13.
- Phillips, D., Jenkins, G., Macaulay, M., Nibau, C., Wnetrzak, J., Fallding, D., Colas, I., Oakey, H., Waugh, R., and Ramsay, L. (2015). The effect of temperature on the male and female recombination landscape of barley. *New Phytol* 208, 421-429.
- Phizicky, D.V., and Bell, S.P. (2018). Transcriptional repression of CDC6 and SLD2 during meiosis is associated with production of short heterogeneous RNA isoforms. *Chromosoma* 127, 515-527.
- Prall, W., Sharma, B., and Gregory, B.D. (2019). Transcription Is Just the Beginning of Gene Expression Regulation: The Functional Significance of RNA-Binding Proteins to Post-transcriptional Processes in Plants. *Plant Cell Physiol* 60, 1939-1952.
- Prusicki, M.A., Hamamura, Y., and Schnittger, A. (2020). A Practical Guide to Live-Cell Imaging of Meiosis in Arabidopsis. *Methods Mol Biol* 2061, 3-12.
- Prusicki, M.A., Keizer, E.M., van Rosmalen, R.P., Komaki, S., Seifert, F., Müller, K., Wijnker, E., Fleck, C., and Schnittger, A. (2019). Live cell imaging of meiosis in Arabidopsis thaliana. *Elife* 8.
- Pusch, S., Dissmeyer, N., and Schnittger, A. (2011). Bimolecular-fluorescence complementation assay to monitor kinase-substrate interactions in vivo. *Methods Mol Biol* 779, 245-257.

-
- Rieder, C.L., and Maiato, H. (2004). Stuck in division or passing through: what happens when cells cannot satisfy the spindle assembly checkpoint. *Dev Cell* 7, 637-651.
- Rockmill, B., Sym, M., Scherthan, H., and Roeder, G.S. (1995). Roles for two RecA homologs in promoting meiotic chromosome synapsis. *Genes Dev* 9, 2684-2695.
- Roeder, G.S., and Bailis, J.M. (2000). The pachytene checkpoint. *Trends Genet* 16, 395-403.
- Roig, M.B., Lowe, J., Chan, K.L., Beckouet, F., Metson, J., and Nasmyth, K. (2014). Structure and function of cohesin's Scc3/SA regulatory subunit. *FEBS Lett* 588, 3692-3702.
- Rossio, V., Galati, E., and Piatti, S. (2010). Adapt or die: how eukaryotic cells respond to prolonged activation of the spindle assembly checkpoint. *Biochem Soc Trans* 38, 1645-1649.
- Sabi, R., and Tuller, T. (2019). Novel insights into gene expression regulation during meiosis revealed by translation elongation dynamics. *NPJ Syst Biol Appl* 5, 12.
- Sanchez-Moran, E., Santos, J.L., Jones, G.H., and Franklin, F.C. (2007). ASY1 mediates AtDMC1-dependent interhomolog recombination during meiosis in Arabidopsis. *Genes Dev* 21, 2220-2233.
- Santucci-Darmanin, S., Neyton, S., Lespinasse, F., Saunieres, A., Gaudray, P., and Paquis-Flucklinger, V. (2002). The DNA mismatch-repair MLH3 protein interacts with MSH4 in meiotic cells, supporting a role for this MutL homolog in mammalian meiotic recombination. *Hum Mol Genet* 11, 1697-1706.
- Scarpin, M.R., Sigaut, L., Temprana, S.G., Boccaccio, G.L., Pietrasanta, L.I., and Muschiatti, J.P. (2017). Two Arabidopsis late pollen transcripts are detected in cytoplasmic granules. *Plant Direct* 1, e00012.
- Schindelin, J., Arganda-Carreras, I., Frise, E., Kaynig, V., Longair, M., Pietzsch, T., Preibisch, S., Rueden, C., Saalfeld, S., Schmid, B., *et al.* (2012). Fiji: an open-source platform for biological-image analysis. *Nat Methods* 9, 676-682.
- Schnable, J.C., Springer, N.M., and Freeling, M. (2011). Differentiation of the maize subgenomes by genome dominance and both ancient and ongoing gene loss. *Proc Natl Acad Sci U S A* 108, 4069-4074.
- Schnable, P.S., Ware, D., Fulton, R.S., Stein, J.C., Wei, F., Pasternak, S., Liang, C., Zhang, J., Fulton, L., Graves, T.A., *et al.* (2009). The B73 maize genome: complexity, diversity, and dynamics. *Science* 326, 1112-1115.
- Schneider, C.A., Rasband, W.S., and Eliceiri, K.W. (2012). NIH Image to ImageJ: 25 years of image analysis. *Nat Methods* 9, 671-675.
- Schonberger, J., Hammes, U.Z., and Dresselhaus, T. (2012). In vivo visualization of RNA in plants cells using the lambdaN(2)(2) system and a GATEWAY-compatible vector series for candidate RNAs. *Plant J* 71, 173-181.
- Schubert, V. (2009). SMC proteins and their multiple functions in higher plants. *Cytogenet Genome Res* 124, 202-214.
- Schuller, A.P., and Green, R. (2018). Roadblocks and resolutions in eukaryotic translation. *Nat Rev Mol Cell Biol* 19, 526-541.
- Scott, R.J., Spielman, M., and Dickinson, H.G. (2004). Stamen structure and function. *Plant Cell* 16 *Suppl*, S46-60.
- Sheehan, M.J., and Pawlowski, W.P. (2012). Imaging chromosome dynamics in meiosis in plants. *Methods Enzymol* 505, 125-143.
- Skibbens, R.V. (2019). Condensins and cohesins - one of these things is not like the other! *J Cell Sci* 132.
- Smyth, D.R., Bowman, J.L., and Meyerowitz, E.M. (1990). Early flower development in Arabidopsis. *Plant Cell* 2, 755-767.

-
- Sofroni, K., Takatsuka, H., Yang, C., Dissmeyer, N., Komaki, S., Hamamura, Y., Bottger, L., Umeda, M., and Schnittger, A. (2020). CDKD-dependent activation of CDKA₁ controls microtubule dynamics and cytokinesis during meiosis. *J Cell Biol* 219.
- Song, P., Jia, Q., Chen, L., Jin, X., Xiao, X., Li, L., Chen, H., Qu, Y., Su, Y., Zhang, W., *et al.* (2020). Involvement of Arabidopsis phospholipase D delta in regulation of ROS-mediated microtubule organization and stomatal movement upon heat shock. *J Exp Bot* 71, 6555-6570.
- Stacey, N.J., Kuromori, T., Azumi, Y., Roberts, G., Breuer, C., Wada, T., Maxwell, A., Roberts, K., and Sugimoto-Shirasu, K. (2006). Arabidopsis SPO11-2 functions with SPO11-1 in meiotic recombination. *Plant J* 48, 206-216.
- Stefani, A., and Colonna, N. (1996). The Influence of Temperature on Meiosis and Microspores Development in *Dasyphyrum villosum* (L.) P. Candargy. *CYTOLOGIA* 61, 277-283.
- Steffensen, D.M. (1966). Synthesis of ribosomal RNA during growth and division in *Lilium*. *Exp Cell Res* 44, 1-12.
- Stronghill, P.E., Azimi, W., and Hasenkampf, C.A. (2014). A novel method to follow meiotic progression in Arabidopsis using confocal microscopy and 5-ethynyl-2'-deoxyuridine labeling. *Plant Methods* 10, 33.
- Stuart, D., and Wittenberg, C. (1998). CLB5 and CLB6 are required for premeiotic DNA replication and activation of the meiotic S/M checkpoint. *Genes Dev* 12, 2698-2710.
- Su, S.S., and Modrich, P. (1986). Escherichia coli mutS-encoded protein binds to mismatched DNA base pairs. *Proc Natl Acad Sci U S A* 83, 5057-5061.
- Sugimura, I., and Lilly, M.A. (2006). Bruno inhibits the expression of mitotic cyclins during the prophase I meiotic arrest of *Drosophila* oocytes. *Dev Cell* 10, 127-135.
- Takei, N., Sato, K., Takada, Y., Iyyappan, R., Susor, A., Yamamoto, T., and Kotani, T. (2021). Tdrd3 regulates the progression of meiosis II through translational control of Emi2 mRNA in mouse oocytes. *Current Research in Cell Biology* 2, 100009.
- Tang, S., Wu, M.K.Y., Zhang, R., and Hunter, N. (2015). Pervasive and essential roles of the Top3-Rmi1 decatenase orchestrate recombination and facilitate chromosome segregation in meiosis. *Mol Cell* 57, 607-621.
- Tian, T., Liu, Y., Yan, H., You, Q., Yi, X., Du, Z., Xu, W., and Su, Z. (2017). agriGO v2.0: a GO analysis toolkit for the agricultural community, 2017 update. *Nucleic Acids Res* 45, W122-W129.
- Toca-Herrera, J.L., Kupcu, S., Diederichs, V., Moncayo, G., Pum, D., and Sleytr, U.B. (2006). Fluorescence emission properties of S-Layer enhanced green fluorescent fusion protein as a function of temperature, pH conditions, and guanidine hydrochloride concentration. *Biomacromolecules* 7, 3298-3301.
- Van Der Kelen, K., Beyaert, R., Inze, D., and De Veylder, L. (2009). Translational control of eukaryotic gene expression. *Crit Rev Biochem Mol Biol* 44, 143-168.
- Vizcay-Barrena, G., and Wilson, Z.A. (2006). Altered tapetal PCD and pollen wall development in the Arabidopsis ms1 mutant. *J Exp Bot* 57, 2709-2717.
- Wang, J., Li, D., Shang, F., and Kang, X. (2017). High temperature-induced production of unreduced pollen and its cytological effects in *Populus*. *Sci Rep* 7, 5281.
- Wang, Y., Magnard, J.L., McCormick, S., and Yang, M. (2004). Progression through meiosis I and meiosis II in Arabidopsis anthers is regulated by an A-type cyclin predominately expressed in prophase I. *Plant Physiol* 136, 4127-4135.
- Watanabe, Y. (2005). Sister chromatid cohesion along arms and at centromeres. *Trends Genet* 21, 405-412.
- Wei, T., Huang, T.S., McNeil, J., Laliberte, J.F., Hong, J., Nelson, R.S., and Wang, A. (2010). Sequential recruitment of the endoplasmic reticulum and chloroplasts for plant potyvirus replication. *J Virol* 84, 799-809.

-
- Weill, L., Belloc, E., Bava, F.A., and Mendez, R. (2012). Translational control by changes in poly(A) tail length: recycling mRNAs. *Nat Struct Mol Biol* 19, 577-585.
- Weiss, H., and Maluszynska, J. (2001). Molecular Cytogenetic Analysis of Polyploidization in the Anther Tapetum of Diploid and Autotetraploid *Arabidopsis thaliana* Plants. *Annals of Botany* 87, 729-735.
- Wellmer, F., Alves-Ferreira, M., Dubois, A., Riechmann, J.L., and Meyerowitz, E.M. (2006). Genome-wide analysis of gene expression during early *Arabidopsis* flower development. *PLoS Genet* 2, e117.
- Wethmar, K., Schulz, J., Muro, E.M., Talyan, S., Andrade-Navarro, M.A., and Leutz, A. (2016). Comprehensive translational control of tyrosine kinase expression by upstream open reading frames. *Oncogene* 35, 1736-1742.
- Wijnker, E., Harashima, H., Muller, K., Parra-Nunez, P., de Snoo, C.B., van de Belt, J., Dissmeyer, N., Bayer, M., Pradillo, M., and Schnittger, A. (2019). The Cdk1/Cdk2 homolog CDKA;1 controls the recombination landscape in *Arabidopsis*. *Proc Natl Acad Sci U S A* 116, 12534-12539.
- Wijnker, E., and Schnittger, A. (2013). Control of the meiotic cell division program in plants. *Plant Reprod* 26, 143-158.
- Wilson, J.Y. (1959). Duration of meiosis in relation to temperature. *Heredity* 13, 263-267.
- Wsierska-Gadek, J., and Horvath, M. (2003). How the nucleolar sequestration of p53 protein or its interplayers contributes to its (re)-activation. *Ann N Y Acad Sci* 1010, 266-272.
- Wu, G., Park, M.Y., Conway, S.R., Wang, J.W., Weigel, D., and Poethig, R.S. (2009). The sequential action of miR156 and miR172 regulates developmental timing in *Arabidopsis*. *Cell* 138, 750-759.
- Wu, S., Scheible, W.R., Schindelasch, D., Van Den Daele, H., De Veylder, L., and Baskin, T.I. (2010). A conditional mutation in *Arabidopsis thaliana* separase induces chromosome non-disjunction, aberrant morphogenesis and cyclin B1;1 stability. *Development* 137, 953-961.
- Wu, Z., Ji, J., Tang, D., Wang, H., Shen, Y., Shi, W., Li, Y., Tan, X., Cheng, Z., and Luo, Q. (2015). OsSDS is essential for DSB formation in rice meiosis. *Front Plant Sci* 6, 21.
- Yahya, G., Perez, A.P., Mendoza, M.B., Parisi, E., Moreno, D.F., Artes, M.H., Gallego, C., and Aldea, M. (2021). Stress granules display bistable dynamics modulated by Cdk. *J Cell Biol* 220.
- Yang, C., Hamamura, Y., Sofroni, K., Bower, F., Stolze, S.C., Nakagami, H., and Schnittger, A. (2019). SWITCH 1/DYAD is a WINGS APART-LIKE antagonist that maintains sister chromatid cohesion in meiosis. *Nat Commun* 10, 1755.
- Yang, C., Sofroni, K., Wijnker, E., Hamamura, Y., Carstens, L., Harashima, H., Stolze, S.C., Vezon, D., Chelysheva, L., Orban-Nemeth, Z., *et al.* (2020). The *Arabidopsis* Cdk1/Cdk2 homolog CDKA;1 controls chromosome axis assembly during plant meiosis. *EMBO J* 39, e101625.
- Yang, H., Lu, P., Wang, Y., and Ma, H. (2011). The transcriptome landscape of *Arabidopsis* male meiocytes from high-throughput sequencing: the complexity and evolution of the meiotic process. *Plant J* 65, 503-516.
- Yang, W.C., Ye, D., Xu, J., and Sundaresan, V. (1999). The SPOROCTELESS gene of *Arabidopsis* is required for initiation of sporogenesis and encodes a novel nuclear protein. *Genes Dev* 13, 2108-2117.
- Yang, Y., and Wang, Z. (2019). IRES-mediated cap-independent translation, a path leading to hidden proteome. *J Mol Cell Biol* 11, 911-919.
- Yao, Y., Li, X., Chen, W., Liu, H., Mi, L., Ren, D., Mo, A., and Lu, P. (2020). ATM Promotes RAD51-Mediated Meiotic DSB Repair by Inter-Sister-Chromatid Recombination in *Arabidopsis*. *Front Plant Sci* 11, 839.
- Yi, J., Moon, S., Lee, Y.S., Zhu, L., Liang, W., Zhang, D., Jung, K.H., and An, G. (2016). Defective Tapetum Cell Death 1 (DTC1) Regulates ROS Levels by Binding to Metallothionein during Tapetum Degeneration. *Plant Physiol* 170, 1611-1623.

-
- Yue, Y., Zhang, P., and Shang, Y. (2019). The potential global distribution and dynamics of wheat under multiple climate change scenarios. *Sci Total Environ* 688, 1308-1318.
- Zhai, J., Zhang, H., Arikait, S., Huang, K., Nan, G.L., Walbot, V., and Meyers, B.C. (2015). Spatiotemporally dynamic, cell-type-dependent premeiotic and meiotic phasiRNAs in maize anthers. *Proc Natl Acad Sci U S A* 112, 3146-3151.
- Zhang, T., Wu, A., Yue, Y., and Zhao, Y. (2020). uORFs: Important Cis-Regulatory Elements in Plants. *Int J Mol Sci* 21.
- Zhang, Y., Werling, U., and Edelman, W. (2014). Seamless Ligation Cloning Extract (SLiCE) cloning method. *Methods Mol Biol* 1116, 235-244.
- Zhao, X., Bramsiepe, J., Van Durme, M., Komaki, S., Prusicki, M.A., Maruyama, D., Forner, J., Medzihradzky, A., Wijnker, E., Harashima, H., *et al.* (2017). RETINOBLASTOMA RELATED1 mediates germline entry in Arabidopsis. *Science* 356.
- Zhao, X., Harashima, H., Dissmeyer, N., Pusch, S., Weimer, A.K., Bramsiepe, J., Bouyer, D., Rademacher, S., Nowack, M.K., Novak, B., *et al.* (2012). A general G1/S-phase cell-cycle control module in the flowering plant Arabidopsis thaliana. *PLoS Genet* 8, e1002847.

DECLARATION OF OATH

Eidesstattliche Versicherung

Declaration of oath

Hiermit erkläre ich an Eides statt, dass ich die vorliegende Dissertationsschrift selbst verfasst und keine anderen als die angegebenen Quellen und Hilfsmittel benutzt habe.

I hereby declare, on oath, that I have written the present dissertation on my own and have not used other than the acknowledged resources and aids.

Hamburg, den 21. Oktober 2021

Hamburg, the 21st of October 2021

A handwritten signature in black ink, consisting of several loops and a long horizontal line extending to the right.

CONFIRMATION OF ENGLISH

Stefan Comhaire
1256 Pinecrest Circle
Tarpon Springs, FL34689, USA

Tarpon Springs, 16 October 2021

To whom it may concern,

I, Stefan Comhaire, confirm that to the best of my knowledge the English of the dissertation entitled 'The meiotic progression of Arabidopsis under elevated temperatures and towards an understanding of translational control in plant meiosis' written by Joke De Jaeger-Braet is linguistically correct.

Yours truly,



Stefan Comhaire

ACKNOWLEDGMENT

Writing my dissertation together and slowly coming toward the end of my PhD journey, I realize that this dissertation only includes a fraction of my adventures of the past five years. This is my work, yes, but I did not walk alone. All of it would not have been possible without the contribution, help and support of several people who deserve to be embraced in this thesis.

It all starts with a great mind for science, the one of my supervisor, Prof. Dr. Arp Schnittger, who gave me the opportunity to join his group and work on diverse topics which were not only challenging, but also fascinating to dive into. Our meetings always started with discussing research questions, however we often drifted off talking about the academic system and other aspects, which also became an important part of our meetings for me. Thank you, Arp, for this and so much more.

During my PhD, I also had the chance to join several conferences where I met experts in the field but I also got to work together with some of them. I spend a few months working closely together with Dr. Frauke Adaml and Dr. Robert Rauscher from the group of Prof. Dr. Zoya Ignatova, who taught me everything about their experience with ribosome profiling. I'm very thankful for their help, their patience with the countless optimization rounds, but also for all the fun moments we had together.

And what would science be without collaborations connecting different fields, I would not have made it so far as I reached today. Thanks to Johannes Wagner and Dr. Dermot Harnett for the analysis of the sequencing data, the results might be preliminary for now but their importance will grow in the future. Thank you, Dr. Linda Krause and Dr. Anika Buchholz for your statistical knowledge which led to a fruitful collaboration between developmental biology and statistical modelling.

Credits to Dr. Maren Heese, Dr. Viola Kuttig and Stefan Comhaire for their critical revisions and support, which brought my writing to a higher level and thank you Arp and Prof. Dr. Stefan Hoth for being the examiners of my work.

Finally, the effect of the working environment and the people around me should not be underestimated, not like heat stress affects meiosis, yet in a greater way. Thanks to all current and past members of the Schnittger lab for making the lab a warm and inspiring place to work and your scientific help but also for all the past working time activities, with my favourite of course playing "saboteur" together.

Ending with the best family and friends all around the world who are always there for me, support me in every step I take, go off-road with me and bring me back on track, which led to this unforgettable journey, thank you so much.

Joke De Jaeger-Braet

October 2021